

CARBONATE CLUMPED ISOTOPE THERMOMETRY:
APPLICATION TO CARBONACEOUS CHONDRITES
&
EFFECTS OF KINETIC ISOTOPE FRACTIONATION

Thesis by

Weifu Guo

In Partial Fulfillment of the Requirements
for the Degree of
Doctor of Philosophy

California Institute of Technology

Pasadena, California

2009

(Defended September 30, 2008)

© 2009

Weifu Guo

All Rights Reserved

ACKNOWLEDGEMENTS

I would like to express my gratitude to all those who made it possible for me to complete this thesis. First of all, I am deeply indebted to my thesis advisor, John M. Eiler, whose encouragement, patience and stimulating suggestions helped me throughout my graduate study, shaping my training and interests, and helping to form my appreciation of scientific problems. I want to thank Geoffrey Blake, who kindly acted as my academic advisor and co-advisor for one of my oral projects. It was through that oral project I was first exposed to clumped isotope geochemistry, which now becomes the main theme of this thesis. I thank Edwin Schauble, Jess Adkins and Alex Session, who have been extraordinary generous with their time and thoughts, and are always willing to offer insightful advice. I want to thank Donald Burnett, whose insights on cosmochemistry enlightened me on the meteoritics research. I thank William Goddard, who kindly provided the opportunity for me to use the computation facility at the Material and Process Simulation Center and thus made all my theoretical work possible.

I sincerely appreciate the help and friendships from all the members of the “47” group: Hagit Affek, Magali Bonifacie, Rosemarie Came, Mathieu Daeron, Prosenjit Ghosh, Katharine Huntington, Anna Meckler, Ben Passey, Nithya Thiagarajan, Aradhna Tripati and Laurence Yeung. Their talents and enthusiasm have made the exploration of clumped isotope geochemistry even more interesting and enjoying. I would particularly like to thank Hagit Affek and Prosenjit Ghosh for helping me get started on the clumped isotope lab work and for their generosity with time and expertise.

I would also like to thank the help and friendships of Zhengrong Wang, Charles Verdel, Alexander Gagnon, Robert Kopp, Julie O’Leary, Ying Wang, Jiafang Xiao, Chao

Li, Mao-Chang Liang, Junjun Liu, Yuanbin Guan, Laurent Remusat, Rinat Gabitov, Alon Amrani, Lindsey Hedges, Chi Ma, David Fike, Amy Hoffman, Kaveh PahLevan, Sally Newman, John Beckett, Risheng Chu, Xin Guo, Daoyuan Sun, Zhonghua Yang, Huiyu Li, Yu Huang, Alan Kwan, Seth John. They have made my life at Caltech more fun and colorful.

This thesis greatly benefits from my collaboration with Jed Mosenfelder, Paul Niles, Sang-Tae Kim, Rinat Gabitov, Mike Zolensky, Jan Veizer. I thank John Ferry for sharing unpublished data, Jonathan Erez for kind encouragement and for sharing his insights on biomineralization mechanism.

Lastly, I would like to thank my wife, Wei Zhang, and my parents, Guanlian Zhang & Bixue Guo, who have been always supportive in all aspects of my life. I would not have been able to finish this thesis without them.

To my wife, Wei Zhang

and my parents, Guanlian Zhang & Bixue Guo

for all the support and happiness

ABSTRACT

‘Clumped isotope’ thermometry of carbonates in the carbonaceous chondrites (CM, CI, CR and Tagish Lake) demonstrates that aqueous alteration of their parent bodies occurred from -31 to 71°C and involved reaction with fluids having $\delta^{18}\text{O}_{\text{VSMOW}}$ values of -29.7‰ to 11.8‰ and $\delta^{17}\text{O}_{\text{VSMOW}}$ of -14.9‰ to 7.6‰. Estimated carbonate formation temperatures decrease in the order: calcite > dolomite > breunnerite. Based on independent constraints on the ages of these carbonates and models of the evolution of the oxygen isotope compositions of parent body waters, I estimate that carbonate precipitation during aqueous alteration of the carbonaceous chondrite parent bodies started within 1-2 million years after the accretion of those parent bodies, and that the alteration temperatures decreased from 34°C to 18°C in the first ~4 million years and further to -20°C after a total of ~6.5 million years. Our results provide the first direct measurements of the low-temperature cooling histories of C1 and C2 carbonaceous chondrite parent bodies. Within the CM chondrite group itself, I observe a negative correlation between the $\delta^{13}\text{C}$ values of CM carbonates and the $\delta^{18}\text{O}$ of their formation waters, suggesting formation and escape of ^{13}C -depleted CH_4 during aqueous alteration on the CM chondrite parent bodies.

I apply ab initio transition state and statistical thermodynamics theory to study the kinetic isotope fractionations of clumped isotopologues (i.e., multiply-substituted isotopologues; I also consider singly-substituted isotopologues) associated with phosphoric acid digestion of carbonate minerals and with the degassing of CO_2 from aqueous solutions. Assuming that H_2CO_3 is the reaction intermediate during phosphoric acid digestion of carbonate minerals, I predict at 25°C that CO_2 derived from acid

digestion of carbonate minerals will be 10.72‰ and 0.220‰ higher, respectively, in $^{18}\text{O}/^{16}\text{O}$ ratios and $^{13}\text{C}-^{18}\text{O}$ clumped isotope anomaly than the reactant carbonate. These predicted kinetic isotope fractionations associated with phosphoric acid digestion and their temperature dependences (for both oxygen isotope and clumped isotopologues) compare favorably with independent experimental constraints for phosphoric acid digestion of calcite. I evaluate the effect of carbonate cation compositions on phosphoric acid digestion fractionations using cluster models in which disproportionating H_2CO_3 interacts with adjacent cations. These cluster models underestimate the magnitude of isotope fractionations, but do successfully reproduce the general trend of variations and temperature dependences of oxygen isotope acid digestion fractionations among different carbonate minerals (suggesting I have correctly identified the basic mechanism responsible for a dependence on cation chemistry, but not the exact structural model for cation— H_2CO_3 clusters). I further integrate our acid digestion fractionation model with previous theoretical evaluations of abundances of $^{13}\text{C}-^{18}\text{O}$ bonds in carbonate minerals, and predict the relationship between Δ_{47} values for CO_2 extracted from carbonate minerals and the growth temperatures of those carbonates, including witherite, calcite, aragonite, dolomite and magnesite. I observe reasonable agreement between these predictions and available experimental determinations (e.g., difference of less than 0.05‰ over 0–50°C, for calcite).

Kinetic isotope fractionation associated with HCO_3^- dehydration and HCO_3^- dehydroxylation reactions (the two pathways of CO_2 degassing from aqueous solutions) are estimated with ab initio transition state theory calculations. Coupled with models of isotopic fractionations accompanying carbonate precipitation, I predict that kinetic

isotope fractionation associated with CO₂ degassing reactions will increase the δ¹³C and δ¹⁸O but decrease the relative proportion of ¹³C-¹⁸O bonds in carbonate minerals that precipitate from degassing solutions. Furthermore, these kinetic isotope effects are correlated with each other. For example, I predict the ¹³C/¹²C ratio of carbonate increases by 1.1-3.2‰ and its Δ₄₇ value decreases by 0.017-0.026‰ for every 1‰ kinetic enrichment in its ¹⁸O/¹⁶O at 25°C, with the exact values depending on the pathway for CO₂ degassing (i.e., HCO₃⁻ dehydration vs. HCO₃⁻ dehydroxylation) and on the amount of carbonate formation that accompanies CO₂ degassing. These predictions compare favorably with the experimental constraints from laboratory synthesized cryogenic carbonates and speleothem-like carbonates and with the isotopic compositions of natural modern speleothems.

TABLE OF CONTENTS

ACKNOWLEDGEMENTS.....	iii
ABSTRACT.....	vi
LIST OF FIGURES.....	xiii
LISIT OF TABLES.....	xvii
INTRODUCTION.....	1
PART I: AQUEOUS ALTERTION OF CARBONACEOUS CHONDRITE PARENT BODIES — INSIGHTS FROM CARBOANTE CLUMPED ISOTOPE THERMOMETRY.....	9
CHPATER 1. TEMPERTURES OF AQUEOUS ALTERATION AND EVIDENCE FOR METHANE GENRATION ON THE PARENT BODIES OF CM CHONDRITE.....	10
Abstract.....	11
1.1 Introduction.....	11
1.2 Samples and method.....	13
1.2.1 Samples.....	13
1.2.2 Carbonate clumped isotope thermometry.....	13
1.2.3 Analytical method.....	14
1.3 Results and discussion.....	22
1.3.1 Temperatures of aqueous alteration and isotopic compositions of the alteration fluid.....	22

1.4 Implications.....	37
Acknowledgements.....	39
References.....	39
CHAPTER 2: TEMPERATURES OF AQUEOUS ALTERATION ON	
CARBONACEOUS CHONDRITE PARENT	
BODIES.....	46
Abstract.....	47
2.1 Introduction.....	47
2.2 Samples and method.....	49
2.2.1 Samples.....	49
2.2.2 Phosphoric acid digestion.....	51
2.2.3 Purification of sample CO ₂ and mass spectrometric analysis.....	54
2.2.4 Estimation of carbonate formation temperatures.....	60
2.3 Results and discussion.....	63
2.3.1 Test of stepped phosphoric acid digestion procedure.....	63
2.3.2 Temperatures of carbonate growth in the carbonaceous	
chondrite parent bodies.....	65
2.3.3 Isotopic compositions of the alteration fluid.....	71
2.3.4 Implications for the chemical and thermal evolution	
of the carbonaceous chondrite parent body.....	75
2.4 Summary.....	86
Acknowledgements.....	87
References.....	87

PART II: KINETIC ISOTOPE FRACTIONATIONS OF CLUMPED	
ISOTOPLOGUES ASSOCIATED WITH CHEMICAL REACTIONS	
—IMPLICATIONS FOR CARBONATE CLUMPED ISOTOPE	
THERMOMETRY	93

CHAPTER 3: ISOTOPIC FRACTIONATIONS ASSOCIATED WITH

PHOSPHORIC ACID DIGESTION OF CARBONATE MINREALS.....	94
Abstract.....	95
3.1 Introduction.....	96
3.2 Theoretical and computational methods.....	100
3.2.1 Transition state theory of reaction rates.....	100
3.2.2 Application of transition state theory to phosphoric acid digestion of carbonate minerals.....	103
3.2.3 Computational methods.....	112
3.3 Experimental methods.....	114
3.4 Results and discussion.....	114
3.4.1 Experimentally determined acid-digestion fractionation of Δ_{47}	114
3.4.2 Model results for the oxygen-isotope and clumped-isotope fractionations associated with carbonic acid dissociation.....	116
3.4.3 Dependence of acid digestion fractionations on the isotopic compositions of reactant carbonate minerals?.....	124
3.4.4 Cation effects on acid digestion fractionations.....	131
3.5 Summary.....	146
Acknowledgements.....	147
References.....	147
Appendix.....	151

CHAPTER 4: ISOTOPIC FRACTIONATIONS ASSOCIATED WITH**DEGASSING OF CO₂ FROM AQUEOUS SOLUTIONS AND
IMPLICATIONS FOR CARBONATE CLUMPED ISOTOPE
THERMOMETRY.....**

Abstract.....	158
4.1 Introduction.....	159
4.2 Theoretical and computational methods.....	165
4.2.1 Kinetics of HCO ₃ ⁻ dehydration and dehydroxylation reactions.....	165
4.2.2 Transition state theory and the reaction mechanisms of HCO ₃ ⁻	

dehydration and HCO ₃ ⁻ dehydroxylation.....	168
4.2.3 A model of isotopic fractionations associated with carbonate precipitation induced from CO ₂ degassing.....	172
4.2.4 Computational methods.....	181
4.3 Experimental methods.....	181
4.3.1 Synthesis of cryogenic carbonates.....	181
4.3.2 Mass spectrometric analysis.....	183
4.4 Results and discussion.....	185
4.4.1 Model results for the kinetic isotope fractionations associated with HCO ₃ ⁻ dehydration and HCO ₃ ⁻ dehydroxylation reactions.....	185
4.4.2 Predicted influence of kinetic isotope fractionations on carbonate minerals grown from degassing aqueous solutions.....	199
4.4.3 Isotopic compositions of cryogenic carbonates.....	207
4.4.4 Comparison between model predictions and isotopic compositions of natural and synthetic carbonates.....	210
4.4.5 Implications for isotopic studies in other natural systems.....	217
4.5 Summary.....	221
Acknowledgements.....	222
References.....	223
Appendix.....	228

LIST OF FIGURES

<p>Figure 1-1: Comparison of oxygen isotope compositions of water in equilibrium with CM chondrite carbonates at their known growth temperatures and water calculated by the forward model of aqueous alteration.....</p>	25
Figure 1-2: Comparison of $\delta^{13}\text{C}_{\text{VPDB}}$ values of carbonates in the CM chondrites to the $\delta^{18}\text{O}_{\text{VSMOW}}$ values of the waters from which they grew.....	29
Figure 1-3: Predicted inverse correlation between $\Delta^{17}\text{O}_{\text{VSMOW}}$ of the formation water and $\delta^{13}\text{C}_{\text{VPDB}}$ of the carbonate during aqueous alteration of the CM chondrite parent body at 28°C.....	33
Figure 2-1: Negative correlations between raw Δ_{47} of analyte CO ₂ and their mass voltages during the mass spectrometric analyses.....	57
Figure 2-2: Absence of correlations between Δ_{47} and Δ_{48} of meteoritic sample CO ₂	60
Figure 2-3: Comparison between the experimentally determined Δ_{47} -T calibration line for calcite and the theoretically predicted Δ_{47} -T calibration lines for calcite, dolomite and magnesite.....	62
Figure 2-4: Oxygen isotope compositions of water in equilibrium with carbonaceous chondrite carbonates at their known growth temperatures....	72
Figure 2-5: Comparison between the experimentally estimated oxygen isotope compositions of alteration water with those calculated by the forward model of aqueous alteration.....	80
Figure 2-6: Negative correlation between the carbonate formation temperatures and the oxygen isotope compositions of alteration fluid from which the carbonates grew.....	83
Figure 2-7: Estimated thermal evolution of carbonaceous chondrite parent bodies, based on the formation temperatures of carbonates in different carbonaceous chondrite and the corresponding formation ages of these carbonates.....	83

Figure 2-8: Comparison of our estimated thermal evolution of carbonaceous chondrite parent bodies with the predictions from available thermal models.....	85
Figure 2-9: Agreement of our estimated thermal evolution of carbonaceous chondrite parent bodies with the modeled thermal evolution for a layer 10km from the surface of a 50km radius parent body, when constraints on carbonate formation ages are relaxed.....	85
Figure 3-1: Transition state structures during phosphoric acid digestion of carbonate minerals (H_2CO_3 model).....	105
Figure 3-2: Representative transition state structures during phosphoric acid digestion of carbonate minerals, as in our ‘cluster models’	112
Figure 3-3: Comparison of vibration frequencies of gas-phase carbonic acid (H_2CO_3) obtained in this study using B3LYP/6-31G* ab initio models with a scaling factor of 0.9614 vs. those obtained through more sophisticated higher level calculations and anharmonicity corrections.....	113
Figure 3-4: Comparison of our H_2CO_3 dissociation model predicted acid digestion oxygen isotope fractionations with experimentally determined acid digestion oxygen isotope fractionations for different carbonate minerals.....	120
Figure 3-5: Fractionations of multiply-substituted species (Δ_{47}^* , Δ_{48}^* , Δ_{49}^*) during phosphoric acid digestion predicted by our H_2CO_3 dissociation model....	122
Figure 3-6: Empirically observed correlations between the oxygen isotope fractionations associated with phosphoric acid digestion and the oxygen isotopic composition of reactant carbonates.....	126
Figure 3-7: Comparison of the isotope fractionations associated with phosphoric acid digestion predicted by our ‘cluster models’ with experimentally observed fractionations for various metal carbonates.....	134
Figure 3-8: Correlations between fractionations of oxygen isotopes associated with acid digestion and the ionic radius of the cation in the reactant carbonate.....	137

Figure 3-9: Inverse correlation between the oxygen isotope fractionation and Δ_{47}^* fractionation during phosphoric acid digestion of different carbonate minerals, predicted from our cluster model.....	141
Figure 3-10: Predicted temperature calibration lines for different carbonate clumped isotope thermometers, by combining predicted equilibrium ^{13}C - ^{18}O and ^{18}O - ^{17}O clumping effects inside the carbonate minerals and predicted Δ_{47}^* kinetic fractionations during phosphoric acid digestion of carbonate minerals.....	144
Figure 3-11: Comparison between predicted temperature calibration lines for CaCO_3 (calcite and aragonite) clumped isotope thermometer and the experimental temperature calibration data.....	145
Figure 4-1: Dependence of relative importance of bicarbonate dehydration and dehydroxylation on the solution pH, temperature and salinity.....	167
Figure 4-2: Optimized reactant and transition state structures for HCO_3^- dehydration and HCO_3^- dehydroxylation reactions in aqueous solution.....	171
Figure 4-3: Comparison of our calculated vibration frequencies for dissolved HCO_3^- with the experimentally determined vibration frequencies.....	186
Figure 4-4: Model predicted kinetic isotope fractionation factors associated with HCO_3^- dehydration reaction (0-100°C).....	191
Figure 4-5: Model predicted kinetic isotope fractionation factors associated with HCO_3^- dehydroxylation reaction (0-100°C).....	192
Figure 4-6: Position specificity of kinetic isotope fractionations of oxygen isotope and ^{13}C - ^{18}O clumped isotopologues associated with HCO_3^- dehydration; of oxygen isotope and ^{13}C - ^{18}O clumped isotopologues associated with HCO_3^- dehydroxylation.....	195
Figure 4-7: Model predicted fractionations of carbon isotope, oxygen isotope, ^{13}C - ^{18}O clumped isotopic anomaly and ^{18}C - ^{17}O clumped isotopic anomaly between degassed CO_2 and reactant HCO_3^- during HCO_3^- dehydration and HCO_3^- dehydroxylation.....	198
Figure 4-8: The kinetic fractionations of carbon isotope, oxygen isotope, $\Delta_{^{13}\text{C}^{18}\text{O}^{16}\text{O}_2}$	

and $\Delta_{^{12}\text{C}^{18}\text{O}^{16}\text{O}}$ in the carbonate mineral as a function of the fraction of remaining HCO_3^- (F), predicted by our model.....	201
Figure 4-9: Correlations between kinetic carbon isotope, oxygen isotope and Δ_{47} clumped isotope fractionations expected in the carbonate mineral, based on our predictions of the kinetic isotope fractionation associated with HCO_3^- dehydration and dehydroxylation reactions and our carbonate precipitation model.....	206
Figure 4-10: Comparison of our model predicted correlation between kinetic Δ_{47} clumped isotope fractionation and kinetic oxygen isotope fractionation, with the observed isotopic compositions of cryogenic carbonates, and with natural modern speleothems and speleothem-like carbonates synthesized in the laboratory.....	211
Figure 4-11: Comparison of our model predicted correlation between kinetic carbon isotope fractionation and kinetic oxygen isotope fractionation, with the observed isotopic compositions of cryogenic carbonates and with the observed isotopic variations among different pieces of speleothem Vil-Gal.....	211
Figure 4-12: Depletion of Δ_{47} and $^{18}\text{O}/^{16}\text{O}$ in aragonite during its fast precipitation.....	214

LIST OF TABLES

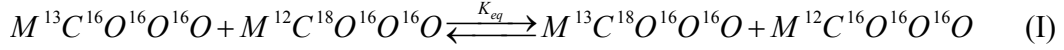
Table 1-1: Isotopic analyses of carbonates in CM chondrites.....	16
Table 1-2: GEM (Gibbs Energy Minimization) simulations of aqueous alteration on CM chondrite parent body.....	36
Table 2-1: Isotopic analyses of carbonates in carbonaceous chondrites.....	50
Table 2-2: Tests and establishment of stepped extraction procedures on synthetic mixtures of calcite and dolomite, and of dolomite and magnesite.....	53
Table 2-3: Effects of voltage correction on the estimations of carbonate formation temperatures and of the oxygen isotope compositions of alteration fluid.....	70
Table 2-4: Forward evolution models for the oxygen isotope compositions of the alteration fluid on CM, CR and CI carbonaceous chondrite parent bodies.....	79
Table 3-1: Evolution of different CO_3^{2-} isotopologues during phosphoric acid digestion of carbonate minerals.....	107
Table 3-2: Fractionation of multiply-substituted isotopologues, Δ_{47}^* , during phosphoric acid digestion of CaCO_3 at 25°C determined through phosphoric acid digestion of high temperature and pressure equilibrated CaCO_3 (calcite) samples.....	116
Table 3-3: Scaled vibration frequencies (unit: cm^{-1}) for different transition state (TS) isotopologues during phosphoric acid digestion of carbonate minerals.....	117
Table 3-4: Comparison of model predicted and experimentally observed phosphoric acid digestion fractionations.....	121
Table 3-5: Dependences of phosphoric acid digestion fractionations on the isotopic compositions and the distributions of multiply-substituted isotopologues in reactant carbonates at 25°C.....	127
Table 3-6: Variations of acid digestion isotope fractionations and their temperature dependencies among different carbonate minerals,	

predicted from our cluster model.....	133
Table 3-A1: Scaled vibration frequencies for different CO_3^{2-} isotopologues (isolated CO_3^{2-} in the gas phase).....	153
Table 3-A2: Estimated abundances of all CO_3^{2-} isotopologues (isolated CO_3^{2-} in the gas phase) at different equilibration temperatures and with different bulk isotopic compositions.....	156
Table 4-1: Isotopic compositions of natural modern speleothem and lab synthesized speleothem-like carbonates.....	163
Table 4-2: Preparation conditions of cryogenic carbonates synthesized in this study.....	183
Table 4-3: Predicted kinetic isotope fractionations associated with HCO_3^- dehydration and HCO_3^- dehydroxylation reactions at 25°C.....	190
Table 4-4: The co-variations of carbon isotope, $\Delta_{^{13}\text{C}^{18}\text{O}^{16}\text{O}_2}$, $\Delta_{^{12}\text{C}^{18}\text{O}^{17}\text{O}^{16}\text{O}}$ and $\Delta_{^{63}}$ fractionations, predicted from our model.....	202
Table 4-5: Isotopic compositions of cryogenic carbonates synthesized in this study.....	207
Table 4-A1: Scaled vibration frequencies for all 54 isotopologues of our modeled reactant during HCO_3^- dehydration reaction in aqueous solution.....	229
Table 4-A2: Scaled vibration frequencies for all 54 isotopologues of our modeled transition state during HCO_3^- dehydration reaction in aqueous solution.....	233
Table 4-A3: Scaled vibration frequencies for all 54 isotopologues of our modeled reactant during HCO_3^- dehydroxylation reaction in aqueous solution.....	237
Table 4-A4: Scaled vibration frequencies for all 54 isotopologues of our modeled transition state during HCO_3^- dehydroxylation reaction in aqueous solution.....	238
Table 4-A5: Model predicted kinetic isotope fractionations for all isotopologues during HCO_3^- dehydration reaction in aqueous solution 25°C.....	240
Table 4-A6: Model predicted kinetic isotope fractionations for all isotopologues during HCO_3^- dehydroxylation reaction in aqueous solution, at 25°C.....	242

INTRODUCTION

This thesis consists of two parts: I. Aqueous alteration of carbonaceous chondrite parent bodies—insights from carbonate clumped isotope thermometry; and II. Kinetic isotope fractionations of clumped isotopologues associated with chemical reaction—implications for carbonate clumped isotope thermometry. Both parts consider a common theme—carbonate clumped isotope thermometry, but focus on different problems. Part I centers on the application of carbonate clumped isotope to novel geoscience problems, and the development of analytical techniques to deal with particularly challenging samples; Part II attempts to develop a quantitative understanding of the physiochemical principles behind carbonate clumped isotope thermometry, particularly for carbonate systems that show signs of isotopic disequilibrium. In Part II, I use both theoretical techniques from ab initio chemical theory, transition state theory and statistical thermodynamics and experimental measurements of natural and lab-synthesized materials.

^{13}C and ^{18}O in thermodynamically equilibrated carbonate minerals preferentially group or ‘clump’ together into the same carbonate ion group to form $^{13}\text{C}^{18}\text{O}^{16}\text{O}^{16}\text{O}^{2-}$ as opposed to being randomly dispersed. This effect leads to abundances of $^{13}\text{C}^{18}\text{O}^{16}\text{O}^{16}\text{O}^{2-}$ higher than that expected for a random distribution of isotopes. This preferential clumping of heavy rare isotopes results from the fact that the doubly-substituted isotopologue of the carbonate ion, $^{13}\text{C}^{18}\text{O}^{16}\text{O}^{16}\text{O}^{2-}$, has a lower zero point energy than its normal and singly-substituted relatives ($^{12}\text{C}^{16}\text{O}^{16}\text{O}^{16}\text{O}^{2-}$, $^{13}\text{C}^{16}\text{O}^{16}\text{O}^{16}\text{O}^{2-}$ and $^{12}\text{C}^{18}\text{O}^{16}\text{O}^{16}\text{O}^{2-}$), and can be expressed through the equilibrium constant for the exchange reaction (Ghosh et al., 2006; Schauble et al., 2006):



The equilibrium constant, K_{eq} , for this reaction varies as a function of the temperature of carbonate growth or equilibration and forms the basis of carbonate clumped isotope thermometry (Ghosh et al., 2006; Schable et al., 2006). This K_{eq} can be determined through the measurements of anomalous enrichment of mass 47 CO_2 (mainly $^{13}\text{C}^{18}\text{O}^{16}\text{O}$) in the CO_2 derived from phosphoric acid digestion of carbonate minerals (Ghosh et al., 2006). The mass 47 anomaly, Δ_{47} , is defined as the difference between the measured value of R^{47} ($=[\text{mass } 47]/[\text{mass } 44]$) and the value of R^{47} expected in that sample if its C and O isotopes are randomly distributed among all isotopologues:

$$\Delta_{47} = \left(\frac{R_{\text{measured}}^{47}}{R_{\text{random}}^{47}} - 1 \right) \times 1000 \text{ (Eiler and Schable, 2004).}$$

Unlike conventional stable isotope thermometry (e.g., the classic carbonate-water oxygen isotope thermometry), which is based on a heterogeneous thermodynamic equilibrium between two different phases (e.g., carbonate and water), the carbonate clumped-isotope thermometer is based on a homogeneous thermodynamic equilibrium that orders ^{13}C and ^{18}O into bonds with each other within the carbonate lattice (i.e., reaction I). Therefore, it is independent of the isotopic composition of any co-existing phases, and lets one determine carbonate formation temperatures based on only the isotopic compositions of carbonate minerals. This provides great advantage for quantitative estimations of carbonate formation temperatures, especially when the oxygen isotope composition of the fluid from which carbonate grew can not be reliably constrained. Furthermore, this temperature information, combined with the known temperature-dependence of carbonate-water oxygen isotope fractionation, allows one to

determine the oxygen isotope compositions of waters from which these carbonates grew. Since its development (Ghosh et al., 2006; Schauble et al., 2006), carbonate clumped isotope thermometry has been successfully applied to a number of geoscience problems, e.g., to reconstruct the uplift history of the Altiplano (Ghosh et al., 2006) and the global surface temperature during the Palaeozoic era (Came et al., 2007).

In Chapter 1 and Chapter 2 I apply carbonate clumped isotope thermometry to carbonates in carbonaceous chondrites (CM chondrite, Chapter 1; CI chondrite, CR chondrite and Tagish Lake, Chapter 2), in order to estimate the temperatures of aqueous alterations on their parent bodies.

Aqueous alteration of primitive meteorites is one of the earliest and most widespread geological processes in the solar system, occurring within the first tens of million of years of solar system history and producing abundant secondary minerals (including carbonates) in the matrix of carbonaceous chondrites (Brearley, 2006). Understanding of these alteration processes, including precise reconstructions of alteration temperatures, will help us constrain the early conditions of the solar system and test models of thermal and chemical evolution of planetesimals. Previous estimates of the alteration temperatures, based on stabilities of constituent phases (e.g., tochilinite; Zolensky, 1984) or the oxygen isotope fractionation between carbonate and phyllosilicate in the matrix (Clayton and Mayeda, 1984), are inconclusive and range from <20°C to <300°C for different types of carbonaceous chondrites (Keil, 2000). Both of these approaches are compromised in certain ways: the first approach provides only upper limits for the alteration temperature; the second requires the assumption that matrix carbonate and phyllosilicate reached isotopic equilibrium with one another. In contrast, carbonate clumped isotope

thermometry is independent of the isotopic composition of any coexisting phases, can provide a precise determination of the carbonate precipitation temperature, and has the added benefit of constraining the oxygen isotope composition of the alteration fluid.

Based on carbonate clumped isotope thermometry, I estimate that the aqueous alteration temperatures on parent bodies of the carbonaceous chondrites ranged from -31°C to 70°C and decreased during the course of aqueous alteration. I further estimate the oxygen isotopic compositions of the alteration fluid and interpret them in the context of aqueous alteration models (Clayton and Mayeda, 1999). I observe a negative correlation between $\delta^{13}\text{C}_{\text{PDB}}$ values of CM carbonates and the $\delta^{18}\text{O}$ of their formation water, and suggest this as evidence of formation and escape of ^{13}C -depleted CH_4 during aqueous alteration on the CM chondrite parent bodies. CI chondrites and Tagish Lake contain several generations of distinct carbonate phases (e.g., calcite, dolomite and breunnerite) that grew at different times. I use techniques of stepped acid digestion to separately determine the clumped isotope formation temperatures of these different carbonates, thereby constraining the thermal evolution of carbonaceous chondrite parent bodies. These results provide the first direct experimental constraints on the low-temperature thermal evolution histories of C1 and C2 carbonaceous chondrite parent bodies.

In Chapters 3 and 4, I employ ab initio transition state statistical thermodynamic theory to study kinetic fractionations of clumped isotopologues associated with two chemical reactions, i.e., the phosphoric acid digestion of carbonate mineral and the degassing of CO_2 from aqueous solutions.

Phosphoric acid digestion has been adopted as a routine analytical technique for oxygen- and carbon-isotope measurements of carbonate minerals since 1950, and was recently extended for use as a method for carbonate ‘clumped isotope’ analysis. The CO₂ derived from phosphoric acid digestion differs significantly in its oxygen isotope composition and clumped isotope composition from reactant carbonate, by an amount that varies with the temperature of digestion and carbonate chemistry. However, so far a quantitative understanding of this fractionation process has been missing. Based on structural arguments, I assume H₂CO₃ as the intermediate during phosphoric acid digestion of carbonate minerals and predict from ab initio transitions state theory the kinetic isotope fractionations between the product CO₂ and reactant carbonate. For example, at 25°C we predict that CO₂ derived from acid digestion of carbonate minerals will be 10.72‰ and 0.220‰ higher, respectively, in ¹⁸O/¹⁶O ratios and ¹³C-¹⁸O clumped isotope anomaly than the reactant carbonate. The predicted kinetic isotope fractionations associated with phosphoric acid digestion and their temperature dependence (for both oxygen isotope and clumped isotopologues) agree reasonably well with independent experimental constraints for phosphoric acid digestion of calcite, including my new experimental data for fractionations of ¹³C-¹⁸O bonds (the measured change in $\Delta_{47}=0.23\text{\textperthousand}$) during phosphoric acid digestion of calcite at 25°C. I evaluate the effect of carbonate cation compositions on phosphoric acid digestion fractionations using cluster models in which disproportionating H₂CO₃ interacts with adjacent cations. These cluster models underestimate the magnitude of isotope fractionations, but do successfully reproduce the general trend of variations and temperature dependences of oxygen isotope acid digestion fractionations among different carbonate minerals (suggesting I have

correctly identified the basic mechanism responsible for a dependence on cation chemistry, but not the exact structural model for cation—H₂CO₃ clusters). I further integrate our acid digestion fractionation model with previous theoretical evaluations of ¹³C-¹⁸O clumping effects in carbonate minerals, and predict the temperature calibration relationship for different carbonate clumped isotope thermometers (witherite, calcite, aragonite, dolomite and magnesite). I observe reasonable agreement between these predictions and the available experimental determinations (e.g., difference of less than 0.05‰ over 0–50°C, for calcite).

CO₂ degassing from aqueous solution occurs in most aqueous environments that contain dissolved inorganic carbon, and is involved in a number of important geologic processes, including speleothem deposition, cryogenic carbonate formation, air-sea CO₂ exchange, etc. Significant kinetic fractionations accompany this process, influencing the isotopic compositions of both the degassed CO₂ and the carbonate minerals that might grow from degassing solutions. In Chapter 4, I focus on quantitatively understanding the influence of these kinetic fractionations on the clumped isotope anomaly in the carbonate minerals grown from degassing solutions, e.g., speleothems. I estimate the kinetic isotope fractionation factors associated with HCO₃⁻ dehydration and dehydroxylation reactions in aqueous solution (the two pathways of CO₂ degassing), using first principle transition state theory calculations. Combining these predicted isotope fractionation factors with models of isotopic fractionations accompanying carbonate formation, I predict kinetic isotope fractionation associated with CO₂ degassing reactions will increase the δ¹³C and δ¹⁸O but decrease the relative proportion of ¹³C-¹⁸O bonds in the carbonate precipitating from the degassing solution. Furthermore, these kinetic isotope effects are correlated with

each other. I test these predictions against the experimental measurements of the lab-synthesized cryogenic carbonates and the available isotopic data of both natural modern speleothems and speleothem-like carbonates synthesized in the laboratory, and observe reasonable agreement. I also predict, based on the ab initio calculations, that CO₂ degassed from aqueous solution will be depleted in the ¹³C-¹⁸O clumped isotope distribution relative to that expected from thermodynamic equilibrium, an effect that might therefore explain the low Δ_{47} observed in terrestrial respiration CO₂ and human breath.

REFERENCE

- Brearley A. J. (2006). The action of water. In *Meteorites and the Early Solar System II*, Arizona University Press. 587-624.
- Cane R. E., Eiler J. M., Veizer J., Azmy K., Brand U. and Weidman C. R. (2007). Coupling of surface temperatures and atmospheric CO₂ concentrations during the Palaeozoic era. *Nature*. **449**: 198-201.
- Clayton R. N. and Mayeda T. K. (1984). The oxygen isotope record in Murchison and other carbonaceous chondrites. *Earth Planet. Sci. Lett.* **67**: 151-161.
- Clayton R. N. and Mayeda T. K. (1999). Oxygen isotope studies of carbonaceous chondrites. *Geochim. Cosmochim. Acta* **63**: 2089-2104.
- Eiler J. M. and Schauble E. A. (2004). ¹⁸O¹³C¹⁶O in Earth's atmosphere. *Geochim. Cosmochim. Acta* **68**: 4767-4777.
- Ghosh P., Adkins J., Affek H., Balta B., Guo W., Schauble E. A., Schrag D. and Eiler J. M. (2006). ¹³C-¹⁸O bonds in carbonate minerals: A new kind of paleothermometer. *Geochim. Cosmochim. Acta* **70**: 1439-1456.
- Ghosh P., Garzione C. N. and Eiler J. M. (2006). Rapid uplift of the Altiplano revealed through ¹³C-¹⁸O bonds in paleosol carbonates. *Science*. **311**: 511-515.
- Keil K. (2000). Thermal alteration of asteroids: evidence from meteorites. *Planet. Space Sci.* **48**: 887-903.

Schauble E. A., Ghosh P. and Eiler J. M. (2006). Preferential formation of ^{13}C - ^{18}O bonds in carbonate minerals, estimated using first-principles lattice dynamics. *Geochim. Cosmochim. Acta.* **70**: 2510-2529.

PART I

**AQUEOUS ALTERATION OF CARBONACEOUS CHONDRITE
PARENT BODIES — INSIGHTS FROM CARBONATE CLUMPED
ISOTOPE THEMOMETRY**

Chapter 1

**TEMPERATURES OF AQUEOUS ALTERATION AND EVIDENCE
FOR METHANE GENERATION ON THE PARENT BODIES OF
THE CM CHONDRITES**

Weifu Guo and John M. Eiler

Division of Geological and Planetary Sciences,
California Institute of Technology, Pasadena, CA 91125

(Published in *Geochimica et Cosmochimica Acta*, **71**, 5565-5575, 2007)

ABSTRACT

Aqueous alteration of primitive meteorites was among the earliest geological process during the evolution of our solar system. ‘Clumped-isotope’ thermometry of carbonates in the CM chondrites Cold Bokkeveld, Murray, and Murchison, demonstrates that they underwent aqueous alteration at 20-71°C from a fluid with $\delta^{18}\text{O}_{\text{VSMOW}}$ of 1.8 to 7.8‰ and $\delta^{17}\text{O}_{\text{VSMOW}}$ of -0.2 to 2.9‰. The $\delta^{13}\text{C}_{\text{PDB}}$ values of these carbonates exhibit a negative correlation with the $\delta^{18}\text{O}$ of their formation waters, consistent with formation and escape of ^{13}C -depleted CH_4 during aqueous alteration. Methane generation under these conditions implies that the alteration fluid was characterized by an $\text{Eh} \leq -0.67$ and $\text{pH} \geq 12.5$ (or lower at the highest alteration temperatures). Our findings suggest that methane generation may have been a widespread consequence of planetesimal and planetary aqueous alteration, perhaps explaining the occurrence of methane on Titan, Triton, Pluto and Kuiper-belt objects.

1. INTRODUCTION

Aqueous alteration occurred on the parent bodies of the carbonaceous chondrites within the first tens of million of years of solar system history (Endress et al., 1996). The conditions of these processes are poorly constrained, both because direct samples of reactant fluids are rarely, if ever, preserved (Zolensky et al., 2004), and because the altered solids consist of complex, fine-grained mixtures of phases that presents challenges to equilibrium thermodynamic approaches to calculating temperature, oxygen fugacity and other relevant variables. Previous estimates of the temperatures of CM chondrite alteration range from <20°C to <170°C (Keil, 2000), based on the stabilities of

constituent phases (e.g. tochilinite; Zolenksy, 1984) or oxygen isotope fractionations between carbonate and phyllosilicate in the matrix (Clayton and Mayeda, 1984). This first approach yields only upper temperature limits; the second is only valid if matrix carbonate and phyllosilicate achieved oxygen-isotope exchange equilibrium. Differences in $\Delta^{17}\text{O}$ between carbonate and matrix in these samples (Benedix et al., 2003) indicate this assumption is not valid. In any event, uncertainties regarding the reduced partition coefficient ratios of the relevant phyllosilicate phases (Sheppard and Gilg, 1996) engender large uncertainties in apparent temperatures based on this approach. Baker et al. (2002) recently determined the oxygen isotopic composition of the structurally bound water released from phyllosilicates in Murchison and suggested an alteration temperature of $\sim 80^\circ\text{C}$ for the CM chondrites based on the oxygen isotopic fractionation between this water and matrix carbonate. However, this estimation also assumes mutual isotopic equilibrium between these two reservoirs of oxygen.

We used the ‘carbonate clumped-isotope thermometer’ (Ghosh et al., 2006; Schauble et al., 2006) to determine the temperatures of carbonate precipitation in the CM chondrites. The carbonate clumped-isotope thermometer is based on a thermodynamic equilibrium that orders ^{13}C and ^{18}O into bonds with each other within the carbonate lattice, and is independent of the isotopic composition of any co-existing phase. Moreover, this temperature information, combined with the known temperature-dependence of carbonate-water oxygen isotope fractionation (Kim and O’Neil, 1997), allows us to determine the oxygen isotope compositions of waters from which these carbonates grew.

2. SAMPLES AND METHOD

2.1. Samples

Carbonate in the CM chondrites is mostly calcite—the basis of previous calibrations of the carbonate clumped isotope thermometer (Ghosh et al., 2006; Ghosh et al., 2007)—and is relatively homogeneous in composition and texture (Brearley and Jones, 1998). We analyzed carbonates from 7 splits of three different CM chondrites: Cold Bokkeveld (3 splits), Murray (1 split) and Murchison (3 splits). Each split was prepared from a separate fragment of a whole rock meteorite sample and ground individually. These samples represent near-extremes to the range of extent of aqueous alteration of CM chondrites: Murchison and Murray retain ca. ~93% and ~87%, respectively, of their original coarse, anhydrous silicate (chondrules and CAIs), whereas Cold Bokkeveld retains only ~45% of this original coarse anhydrous material (i.e., its texture more closely approaches that of the CI chondrites) (Browning et al., 1996).

2.2. Carbonate clumped isotope thermometry

^{13}C and ^{18}O in thermodynamically equilibrated carbonate minerals preferentially group or ‘clump’ together into the same carbonate ion group to form $^{13}\text{C}^{18}\text{O}^{16}\text{O}^{16}\text{O}^{2-}$ as opposed to being randomly dispersed. This preferential clumping can be expressed through the equilibrium constant for the exchange reaction, $^{13}\text{C}^{16}\text{O}^{16}\text{O}^{16}\text{O}^{2-} + ^{12}\text{C}^{18}\text{O}^{16}\text{O}^{16}\text{O}^{2-} = ^{13}\text{C}^{18}\text{O}^{16}\text{O}^{16}\text{O}^{2-} + ^{12}\text{C}^{16}\text{O}^{16}\text{O}^{16}\text{O}^{2-}$. Because the doubly-substituted isotopologue of the carbonate ion ($^{13}\text{C}^{18}\text{O}^{16}\text{O}^{16}\text{O}^{2-}$) has a lower zero point energy than its normal and singly-substituted relatives ($^{12}\text{C}^{16}\text{O}^{16}\text{O}^{16}\text{O}^{2-}$, $^{13}\text{C}^{16}\text{O}^{16}\text{O}^{16}\text{O}^{2-}$ and $^{12}\text{C}^{18}\text{O}^{16}\text{O}^{16}\text{O}^{2-}$), the above reaction is thermodynamically driven to the right, producing

abundances of $^{13}\text{C}^{18}\text{O}^{16}\text{O}^{16}\text{O}^{2-}$ higher than that expected for a random distribution of isotopes. This abundance excess varies as a function of the temperature of carbonate growth or equilibration and forms the basis of a geothermometer (Ghosh et al., 2006; Schauble et al., 2006). The extent of $^{13}\text{C}-^{18}\text{O}$ clumping in a carbonate mineral is determined through the measurements of anomalous enrichment of mass 47 CO_2 (mainly $^{13}\text{C}^{18}\text{O}^{16}\text{O}$) in the CO_2 derived from phosphoric acid digestion of that mineral (Ghosh et al., 2006). We define the mass 47 anomaly, Δ_{47} , as the difference between the measured value of R^{47} ($=[\text{mass } 47]/[\text{mass } 44]$) and the value of R^{47} expected in that sample if its C and O isotopes are randomly distributed among all isotopologues:

$$\Delta_{47} = \left(\frac{R_{\text{measured}}^{47}}{R_{\text{stochastic}}^{47}} - 1 \right) \times 1000 \text{ (Eiler and Schauble, 2004; Affek and Eiler, 2006).}$$

2.3. Analytical method

2.3.1 Sample Digestion

Each sample split consisted of a whole rock fragment weighing between 40 and 250 mg. Each split was ground to a grain size of $\leq 500 \mu\text{m}$ with an agate mortar and pestle into unsieved particles and then reacted with anhydrous phosphoric acid at 25°C for 18–24 hours to extract CO_2 from calcite. Carbonates other than calcite (e.g., dolomite) are rare in CM chondrites (Brearley and Jones, 1998) and do not react actively with phosphoric acid at 25°C (less than 20% reaction of dolomite within 24 hours, compared to 100% reaction of calcite; e.g., Al-Aasm et al., 1990). Therefore cross-contamination from other carbonate components in CM chondrite should be negligible during our extraction.

We examined the contribution of CO₂ from oxidation of organic matter by conducting stepped acid extractions at 25°C (i.e., anticipating that early steps would be dominated by carbonate and later steps by oxidation of organics). CO₂ evolved at an average rate of ~76.2 nmol/mg/day during the first 24 hours, and after that at an average rate of ~0.9 nmol/mg/day, suggesting to us that CO₂ extracted for the first 24 hours contained a negligible contribution from the oxidation of organic matter. We did not attempt to characterize the isotopic compositions of CO₂ fractions collected after the first 24 hrs in this study because their sizes were too small for Δ_{47} analysis and their $\delta^{13}\text{C}$, $\delta^{18}\text{O}$ and $\Delta^{17}\text{O}$ values are well known from previous stepped-extraction studies (Grady et al., 1988; Benedix et al., 2003).

The yield of CO₂ from each split varied between 39.3 $\mu\text{mol/g}$ and 127.6 $\mu\text{mol/g}$. We observe that smaller splits consistently produce higher yields of CO₂ than larger splits (95.5-127.6 $\mu\text{mol/g}$ for 40.5-60.6 mg splits vs. 39.3-61.8 $\mu\text{mol/g}$ for 195.3-253.4 mg splits; Table 1). A similar correlation between CO₂ yield and split size was observed in a previous study of CM chondrites (Murchison splits in Grady et al, 1988), and could be due to either heterogeneity among sample splits (i.e., if carbonate is generally present as widely-separated ‘nuggets’, smaller splits will produce greater maximum CO₂ yields) or that phosphoric acid digestion more effectively attacks carbonate in smaller samples (e.g., if large amounts of ground sample are relatively impermeable).

Table 1-1 Isotopic analyses of carbonates in CM chondrites.

Sample	Murchison (split 1)	Murchison (split 2)	Murchison (split 3)	Murray	Cold Bokkeveld (split 1)	Cold Bokkeveld (split 2)	Cold Bokkeveld (split 3)	Estimated External Precision (1 σ)
Date of Analysis	11/18/05	12/31/05	2/18/06	2/24/06	12/23/05	2/18/06	2/24/06	
Weight (mg)	253.4	241.2	60.6	40.5	195.3	48.0	52.8	
CO ₂ (μmol)	11.3	9.5	6.6	3.9	12.1	4.8	6.7	
yield (μmol/g)	44.6	39.3	108.1	95.5	61.8	100.5	127.6	
MAI*	0.43	0.43	0.43	0.57	1.03	1.03	1.03	
Δ ¹⁷ O** (‰)	-0.55	-0.55	-0.55	-0.49	-1.40	-1.40	-1.40	
δ ¹³ C _{carb} (‰)	60.09	68.88	61.04	37.77	50.63	51.33	45.18	0.14
VPDB								
δ ¹⁸ O _{carb} (‰)	33.18	30.54	32.10	34.13	34.61	28.89	28.21	0.21
VSMOW								
Δ ₁₇ (‰)	0.668	0.651	0.612	0.623	0.642	0.605	0.481	0.041
Temperature (°C)	20	24	33	30	26	35	71	~10
δ ¹⁸ O _{water} (‰)	3.6	1.8	5.1	6.6	6.2	2.3	7.8	~2
VSMOW								

* MAI-Mineralogical Alteration Index (Browning et al., 1996); ** Δ¹⁷O values are averages recalculated from Benedict et al. (2003), with λ=0.5164, and are used in O¹⁷ corrections of this study.

Because of the relatively low abundances of carbonates in CM chondrites and the precious nature of the samples, we generally obtained less CO₂ from our samples (~5 to ~12 μmol) than analyzed in previous studies of the Δ_{47} of CO₂ produced by acid digestion of carbonate (~50 μmol ; e.g., Ghosh et al., 2006).

2.3.2 Purification of sample CO₂

CO₂ produced by phosphoric acid digestion of CM chondrites is exceptionally rich in sulfur and organic contaminants that must be removed prior to isotopic analysis. Therefore, each sample of extracted CO₂ was purified by exposure to dry Ag₃PO₄ (to remove sulfur contaminants, e.g., H₂S), passage through a series of glass traps cooled with ethanol slush (-78°C) and pentane slush (-130°C), and passage through a Supelco Q-Plot GC column held at -20°C (mainly to remove hydrocarbon contaminants; Affek and Eiler, 2006). Samples sized before and after dry Ag₃PO₄ treatment suggest that sulfur contaminants constitute 19-62% of the sample gas derived from phosphoric acid digestion of CM chondrite splits (38-62% for 3 Murchison splits, 58% for 1 Murray split and 19-29% for 3 Cold Bokkeveld splits). The potential for remaining contaminants was monitored by analyses of masses 48 and 49 in the purified CO₂ gas, because these ion beams are less intense than that for mass 47 and can be strongly elevated in gases containing volatile organic contaminants. Previous studies have shown that such contaminants can lead to correlations between relatively small mass 47 excesses and proportionately greater excesses in masses 48 and 49 (Eiler and Schauble, 2004). While we never succeeded in completely removing masses 48 and 49 contaminants from these samples, no such correlations between Δ_{47} values and either mass 48 or 49 excesses were

observed in these purified samples, suggesting that, in this case, the remaining contaminants are not associated with a mass-47 isobar. Consequently, no correction on measured Δ_{47} was made to account for masses 48 and 49 enrichments.

Although the sample purification procedures used in this study resemble those used in previous studies involving Δ_{47} measurements (e.g., Eiler and Schauble, 2004; Affek and Eiler, 2006; Ghosh et al., 2006), we apply them to considerably smaller samples. Therefore, we examined the effect of sample size on analytical fractionations associated with cryogenic purification, sulfide removal on silver phosphate, gas chromatography and mass spectrometric measurements. We observe a systematic effect of sample size on measured Δ_{47} value only for the gas chromatography step. In particular, Δ_{47} values of small samples (less than ca. 15 μ moles) are systematically higher (by up to 0.2‰) in Δ_{47} value as compared to large (i.e., larger than 15 μ mole) samples of that same gas subjected to the same gas chromatographic purification procedure. The magnitude of this Δ_{47} increase in small samples is independent of the isotopic compositions of the CO₂ gas and varies only with the size of the gas (i.e., the smaller the size of CO₂ gas, the bigger is its Δ_{47} increase after GC purification). It is possible that this sample-size effect reflects interaction between CO₂ and adsorbed water in the GC column (although the column is routinely heated to 150°C between samples and the observed Δ_{47} increases are independent of the starting Δ_{47} value—consistent with the effects of CO₂-H₂O exchange). It is unlikely that the effect reflects fractionation associated with partial loss of the sample because we routinely achieved >95% sample recovery of CO₂. Nevertheless, despite the fact that the cause of this effect is unclear, it is a consistently and clearly observed artifact of GC purification. Therefore, we routinely standardized

analyses of samples smaller than 15 μ moles by comparison with standard CO₂ gases of the same size that had been heated them to 1000°C to achieve the stochastic distribution. We tested the validity of this standardization method by measuring ~5 μ mole samples of CO₂ prepared by acid digestion of small aliquots of carbonate standards having known Δ_{47} values (NBS-19 and Sigma carbonate; Ghosh et al., 2006). Values of Δ_{47} determined for these small aliquots of NBS-19 (n=4) and Sigma carbonate (n=4), standardized to heated gas of the same size, average 0.36±0.03 (1 σ , one standard error) and 0.56±0.06 (1 σ), respectively, consistent with their established values (0.35±0.02, 0.55±0.03; Ghosh et al., 2006). Therefore, we believe that small samples can be analyzed with no systematic error provided they are compared to reference gases of the same size processed in the same way. Note, however, that while developing these methods of small sample analyses, some initial tests of NBS19 yielded CO₂ having Δ_{47} values consistent with room-temperature equilibrium of CO₂ gas (~0.98‰). We believe this reflects the great susceptibility of small samples to exchange with water adsorbed on surfaces in the gas-handling apparatus, necessitating unusually aggressive measures to dry the apparatus between samples (i.e., relatively long baking).

It is possible that exposure of CO₂ gas to dry Ag₃PO₄ may also influence the Δ_{47} of CO₂ samples. To evaluate this possibility, we prepared clean CO₂ gas and divided it into 2 splits of approximately equal size. We passed one split only through the GC column and the other split was first exposed to dry Ag₃PO₄ and then passed through the GC column. Values of Δ_{47} for these two splits were within 2 standard errors of each other, suggesting that exposure to dry Ag₃PO₄ does not influence the Δ_{47} value. Purifications on

meteorite samples were performed only after such tests showed that a given batch of Ag_3PO_4 had negligible influences on Δ_{47} values.

2.3.3 Mass spectrometric analysis

Mass spectrometric analyses of purified CO_2 were performed in dual inlet mode on a Finnigan-MAT 253 gas source isotope ratio mass spectrometer, configured to simultaneously measure masses 44, 45, 46, 47, 48, and 49. Detailed descriptions of the mass spectrometer configuration are given by Eiler and Schauble (2004) and Ghosh et al. (2006). Two types of dual inlet measurements were employed in the present study: 1) the 3 analyses made in 2005 were performed at signal intensities of 2V for mass 44 in regular dual inlet mode; 2) the 4 analyses made in 2006 were performed at signal intensities of 3.4-7.4V for mass 44 in microvolume dual inlet mode (i.e., purified sample CO_2 was cryogenically concentrated in a small volume during measurements, instead of being expanded to the sample bellow). Measurements of each sample gas consist of 6-10 analyses, each of which involves 10 cycles of sample-standard comparison with an ion integration time of 8 seconds per cycle. Pressure balance was maintained at mass 44 between sample gas and reference gas for all analyses. Values of Δ_{47} for each sample were established by comparison with same type of analyses of CO_2 gases of similar size and bulk composition that had been heated to 1000°C (establishing the $\Delta_{47}=0\text{\textperthousand}$ reference scale for that sample size and purification procedure; Ghosh et al., 2006).

It has been previously shown that CO_2 derived from acid digestion of CM chondrite carbonates differs in oxygen isotope composition from the terrestrial mass fractionation line (Clayton and Mayeda, 1984; Benedix et al., 2003). We must consider this fact when

performing ion correction calculations associated with our measurements. To compute the $\delta^{13}\text{C}$ and $\delta^{18}\text{O}$ values for these samples from their measured masses 44 45 and 46 abundances, we assumed the average carbonate $\Delta^{17}\text{O}$ (recalculated from Benedix et al., 2003) for samples from the same CM chondrite and a value of $\lambda=0.5164$ for the terrestrial mass fractionation line (Santrock et al., 1985). Values of $\delta^{13}\text{C}$ and $\delta^{18}\text{O}$ were standardized by comparison with CO_2 generated by phosphoric acid digestion of NBS-19 and are reported vs. VPDB and VSMOW, respectively.

Carbonate formation temperatures were estimated from the $\Delta_{47}\text{-T}$ calibration line for calcite and aragonite determined in Ghosh et al. (2006): $\Delta_{47} = \frac{0.0592 \times 10^6}{T^2} - 0.02$, where T is in Kelvin. Note that $\Delta^{17}\text{O}$ values also affect calculated Δ_{47} values since the Δ_{47} value depends on $\delta^{13}\text{C}$, $\delta^{17}\text{O}$ and $\delta^{18}\text{O}$ values, and thus one must know or assume a $\Delta^{17}\text{O}$ value when calculating Δ_{47} (Affek and Eiler, 2006). For example, a 1‰ decrease in $\Delta^{17}\text{O}$, if unrecognized or unaccounted for, would lead to a systematic error of 0.034‰ in Δ_{47} . The $\Delta^{17}\text{O}$ values of carbonates in any given CM chondrite vary by 0.1-0.8‰ (Murchison, n=5; Murray, n=2; Clayton and Mayeda, 1984; Benedix et al., 2003), thus introducing ~1 to ~5°C uncertainty in our temperature estimation.

Because our measurements were made on relatively small samples and required extensive purifications of CO_2 produced by phosphoric acid digestion, they are less precise than previously reported temperatures based on carbonate clumped isotope thermometry (ca. $\pm 10^\circ\text{C}$ 1σ vs. ± 2 to 3°C 1σ). External precisions of individual measurements of $\delta^{13}\text{C}$, $\delta^{18}\text{O}$ and Δ_{47} were estimated based on analyses of ~ 5 μmole samples of CO_2 prepared from small aliquots of carbonate standards and purified as for

gases derived from samples. External precisions for these standard analyses averaged 0.14‰ for $\delta^{13}\text{C}$, 0.21‰ for $\delta^{18}\text{O}$ and 0.041‰ for Δ_{47} (all 1σ ; see section 2.3.2). Similarly, analyses of clean $\sim 5 \mu\text{mole}$ CO_2 gases exposed to dry Ag_3PO_4 and/or GC purification demonstrated external precisions averaging 0.05‰, 0.12‰ and 0.039‰, respectively (all 1σ). We assume the larger of these two sets of external errors (those for small aliquots of carbonate standards) apply to our measurements of CM chondrite carbonates.

3. RESULTS AND DISCUSSION

3.1. Temperatures of aqueous alteration and isotopic compositions of the alteration fluid

Six out of the seven temperatures of carbonate formation determined using the carbonate clumped isotope thermometer are within the range 20 to 35°C—indistinguishable from each other given our analytical precision (Table 1-1). The exception is a split from Cold Bokkeveld, which yielded a significantly higher temperature of 71°C. The similarity in temperatures of aqueous alteration among most splits of Cold Bokkeveld, Murray, and Murchison suggests that they reacted with water at similar depths in and stages of evolution of their respective parent bodies. This result is broadly consistent with previous thermal models for the parent bodies of the carbonaceous chondrites, which suggest that aqueous alteration occurred within a relatively narrow range of locations within their host parent bodies (Young, 2001; McSween et al., 2002). Note, however, that the higher temperature we observe for one split of Cold Bokkeveld indicates that aqueous alteration occurred over a range of temperatures in at least one sample.

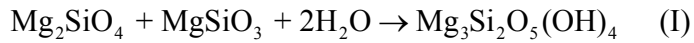
If we interpret our results in the context of the model of Young (2001) that describes the thermal evolution of small planetesimals, water-rock reaction could have occurred within a \sim 250m thick zone, 1.8km from the surface of an assumed 9km radius parent body, although the higher temperature observed in one split requires that alteration occurred in a region, perhaps somewhat deeper, that was heated to well above the melting point of water ice. This compares with the estimate of an alteration zone 100-m-thick, 1km from the surface previously inferred based on oxygen isotope geochemistry and the mineralogical alteration index (Benedix et al., 2003).

Our measurements of the $\delta^{13}\text{C}$ and $\delta^{18}\text{O}$ values of CM chondrite carbonates (in particular the calcite fraction extracted by our acid digestion methods) vary from 37.77‰ to 68.88‰ and from 28.21‰ to 34.61‰, respectively (Table 1). This variation is similar to that previously observed for calcites in CM chondrites ($\delta^{13}\text{C}=23.7\text{\textperthousand}$ to 67.8‰; $\delta^{18}\text{O}=20.0\text{\textperthousand}$ to 37.2‰; Clayton and Mayeda, 1984; Grady et al., 1988; Brearley et al., 1999; Benedix et al., 2003). Note, however, that the $\delta^{13}\text{C}$ values of our samples of Murchison carbonates differ markedly from those in Grady et al. (1988) (60.09-68.88‰ vs. 31.6‰ to 45.1‰, respectively). An inverse correlation exists between $\delta^{13}\text{C}$ and $\delta^{18}\text{O}$ of carbonates considered in this study, in contrast to the weak positive correlation observed for eleven splits of Murchison in Grady et al. (1988). We suspect this difference reflects the fact that CM chondrites are highly heterogeneous breccias and contain alteration phases that may have formed over a range of conditions; thus, it is unsurprising that repeated sampling of small aliquots of such materials can produce divergent results.

Given the temperatures of carbonate growth summarized above and previous experimental calibration of the oxygen isotope fractionation between calcite and water

(Kim and O'Neil, 1997), we can estimate the oxygen isotope compositions of waters from which the carbonates we analyzed grew. These waters varied in $\delta^{18}\text{O}_{\text{SMOW}}$ between values of 1.8‰ and 7.8‰ ($\pm 2\text{\textperthousand}$, 1σ). If we assume that the carbonates we analyzed have $\Delta^{17}\text{O}$ values equal to the averages previously determined by Bendix et al. (2003), our results also indicate that the $\delta^{17}\text{O}$ values of waters from which carbonates grew varied between -0.2‰ and 2.9‰. These $\delta^{18}\text{O}$ and $\delta^{17}\text{O}$ values of carbonate formation water are significantly lower than those estimated for the primary source of water that altered the CM chondrites ($\delta^{18}\text{O}$ ca. $\geq 15.9\text{\textperthousand}$, $\delta^{17}\text{O}$ ca. $\geq 9.2\text{\textperthousand}$; Clayton and Mayeda, 1999). This difference in isotopic composition between model reactant water and the water from which carbonates grew suggests that water evolves toward lower $\delta^{18}\text{O}$, $\delta^{17}\text{O}$ and $\Delta^{17}\text{O}$ as a result of reaction with host rock (Clayton and Mayeda, 1984; Clayton and Mayeda, 1999) (Figure 1-1).

We interpret our results in the context of a quantitative model for the aqueous alteration of CM chondrites. This model simplifies many aspects of this process, but provides a framework for testing the internal consistency of our interpretations. First, we assume, following Clayton and Mayeda (1999) and Eiler and Kitchen (2004), that the most volumetrically important alteration reactions (i.e., silicate hydration) can be represented by:



We define the reaction progress parameter (Clayton and Mayeda, 1999), p , as $p = \frac{f}{x}$,

where f is the fraction of initial olivine and pyroxene that has been converted to serpentine (on a molar oxygen basis) and x is the ratio of moles of O in reactant water to

moles of O in reactant olivine and pyroxene (thus p denotes the ratio of moles of oxygen in the reacted rock to moles of oxygen in initial water). We assume that the initial oxygen isotopic composition of reactant water (i.e., prior to any reaction with anhydrous silicate) was $\delta^{18}\text{O}_{\text{w}, \text{i}} = 28.1\text{\textperthousand}$, $\delta^{17}\text{O}_{\text{w}, \text{i}} = 17.7\text{\textperthousand}$, and that the oxygen isotope composition of reactant silicate was $\delta^{18}\text{O}_{\text{r}, \text{i}} = -4.2\text{\textperthousand}$, $\delta^{17}\text{O}_{\text{r}, \text{i}} = -7.4\text{\textperthousand}$ (Clayton and Mayeda, 1999).

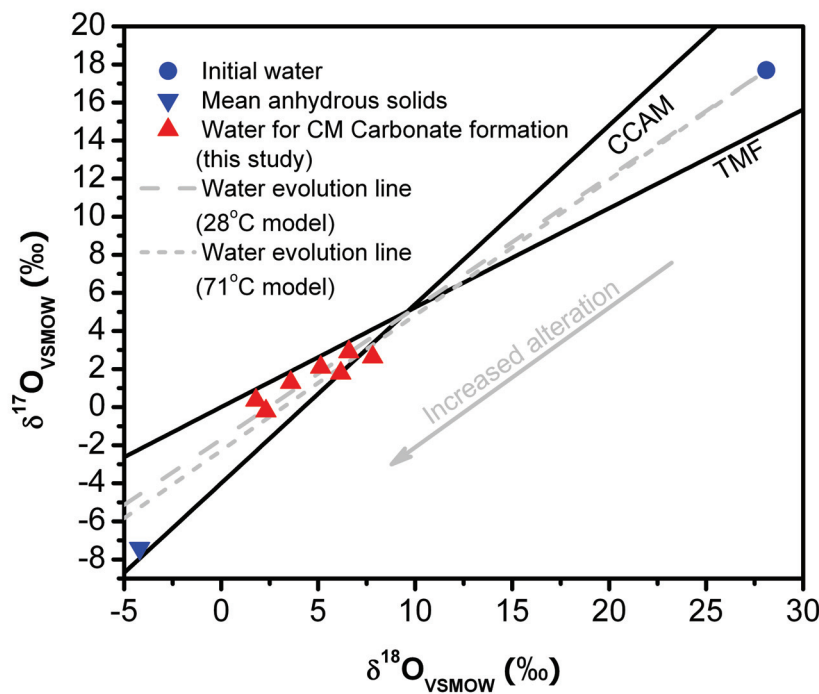


Figure 1-1 Oxygen isotope compositions (all values reported vs. VSMOW) of water in equilibrium with CM chondrite carbonates at their known growth temperatures (triangles) and water calculated by the forward model of aqueous alteration described in the text (circle and dashed lines; note models for two different assumed temperatures of water-rock reaction are shown). The terrestrial mass fractionation line ('TMF') and carbonaceous chondrite anhydrous mineral line ('CCAM') are shown for reference. The inverted triangle shows the location of typical anhydrous solids in CM chondrites. Data are from this study (Table 1-1) and Clayton and Mayeda (1999) (see figure legend for details).

Most of our model calculations adopt a serpentine-water oxygen isotope fractionation of $\Delta^{18}\text{O}_{\text{s-w}}=12.5\text{\textperthousand}$ (Wenner and Taylor, 1971), appropriate for equilibration at 28°C. This corresponds to a $^{17}\text{O}/^{16}\text{O}$ fractionation between serpentine and water of $\Delta^{17}\text{O}_{\text{s-w}}=6.4\text{\textperthousand}$ (assuming a normal mass-dependent fractionation between serpentine and water). We selected a model temperature of 28°C because it is a reasonable approximation of the temperatures of carbonate growth for most of our samples (though silicate hydration need not occur at the same temperatures as carbonate precipitation) and it is similar to temperatures of aqueous alteration assumed by previous models of this kind (e.g., Clayton and Mayeda, 1999). While we are aware of no definitive reports of serpentinization occurring at 28°C in terrestrial rocks, both lab experiments and field observations have been used to suggest that serpentinization (and, important for our further discussion of this model in section 3.2 of this paper, concurrent H₂ generation) occurs at earth-surface temperatures (Neal and Stanger, 1983; Stevens and McKinley, 1995; Stevens and McKinley, 2000). The lowest measured temperature of a serpentinization reaction is 45°C, in the Lost City hydrothermal field, determined using a hydrogen isotope geothermometer (Proskurowski et al., 2006). However, the authors of that study suggested that this low temperature reflects re-equilibration of hydrogen isotopes after serpentinization at 110-150°C. Experimental studies suggest that hydration reactions are generally geologically fast (e.g., at 245°C with a rock/water ratio of 2.5/1, ~28% enstatite converts to serpentine within 6 days; Martin and Fyfe, 1970) and, in most circumstances, the rate limiting step is transport of water to the reaction site rather than the temperature-dependent kinetics of the reaction itself (Martin and Fyfe, 1970). We conclude that it is plausible to imagine silicate hydration on the CM parent bodies

occurring at temperatures as low as 28°C, although a more definitive understanding of this problem will require further experimental studies of the kinetics of silicate hydration at such low temperatures. We also present a version of this model that assumes serpentine-water oxygen isotope fractionations more appropriate for a higher temperature of 71°C — the highest carbonate precipitation temperature observed in this study ($\Delta^{18}\text{O}_{\text{s-w}}=8.5\text{\textperthousand}$, and $\Delta^{17}\text{O}_{\text{s-w}}=4.4\text{\textperthousand}$; Wenner and Taylor, 1971) (Figure 1-1).

Given the parameters summarized above, the oxygen isotope composition of aqueous fluid after reaction is given by Clayton and Mayeda (1999):

$$\delta^{18}\text{O}_{\text{w,f}} = \frac{\delta^{18}\text{O}_{\text{w,i}} + (\delta^{18}\text{O}_{\text{r,i}} - \frac{9}{7}\Delta^{18}\text{O}_{\text{s-w}}) p}{1 + p} \quad (1)$$

$$\delta^{17}\text{O}_{\text{w,f}} = \frac{\delta^{17}\text{O}_{\text{w,i}} + (\delta^{17}\text{O}_{\text{r,i}} - \frac{9}{7}\Delta^{17}\text{O}_{\text{s-w}}) p}{1 + p} \quad (2)$$

$$\Delta^{17}\text{O}_{\text{w,f}} = \left(\frac{1+\delta^{17}\text{O}_{\text{w,f}}/1000}{(1+\delta^{18}\text{O}_{\text{w,f}}/1000)^{0.5164}} - 1 \right) \times 1000 \quad (3)$$

Note that $\Delta^{17}\text{O}_{\text{w,f}}$ values are independent of alteration temperature and vary only as a function of p once the initial isotopic compositions of water and rock (i.e., $\Delta^{17}\text{O}_{\text{w,i}}$ and $\Delta^{17}\text{O}_{\text{r,i}}$) are specified. Therefore $\Delta^{17}\text{O}_{\text{w,f}}$ (i.e., $\Delta^{17}\text{O}_{\text{carbonate}}$, assuming carbonate formed in isotopic equilibrium with its formation water) can be used as an indicator for the extent of alteration. In contrast, the slope of the correlation between $\delta^{18}\text{O}_{\text{w,f}}$ and $\delta^{17}\text{O}_{\text{w,f}}$ is influenced by the alteration temperature (the higher the alteration temperature, the steeper is the line of $\delta^{18}\text{O}_{\text{w,f}}$ vs. $\delta^{17}\text{O}_{\text{w,f}}$).

Our results imply that the water that precipitated carbonate in Cold Bokkeveld varied significantly in oxygen isotope composition over the course of that rock's

alteration history (Table 1-1). In the context of the model trend depicting the expected isotopic evolution of reactant water illustrated in Figure 1-1 (i.e., the higher extent of alteration the lower $\delta^{18}\text{O}$ of the water), this water had experienced less previous reaction when the precipitation temperature was high and more previous reaction when the precipitation temperature was low; i.e., the rock was cooling as alteration proceeded. Previous studies of the minor and trace element (Riciputi et al., 1994) and stable isotope geochemistry (Grady et al., 1988) of carbonates in CM chondrites have also suggested that their parental waters varied in composition both spatially and temporally.

3.2. Correlation between $\delta^{13}\text{C}$ of the carbonates and $\delta^{18}\text{O}$ of their formation waters: evidence for methane generation

The $\delta^{13}\text{C}$ values of carbonates in the CM chondrites exhibit a negative correlation with the oxygen isotope compositions of the waters from which they grew (Figure 1-2). If we interpret this correlation in the context of the model water evolution trend marked in Figure 1-1, it suggests that the pool of dissolved inorganic carbon from which carbonate grew evolved from lower $\delta^{13}\text{C}$ to higher $\delta^{13}\text{C}$ as alteration proceeded. This interpretation is supported by weak correlations previously observed between the alteration index and both oxygen and carbon isotope compositions of CM chondrite carbonates (Grady et al., 1988), which was interpreted by the authors as possible indications that isotopically distinct components were altered and added to the fluid phase over the course of aqueous alteration.

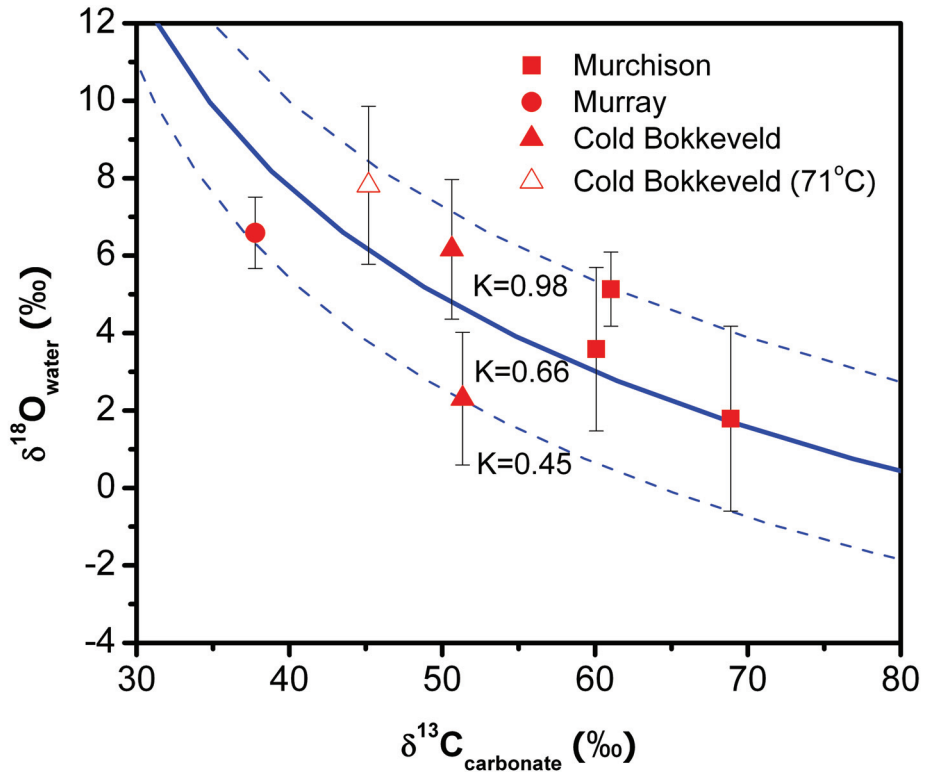


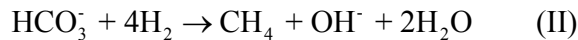
Figure 1-2. Comparison of $\delta^{13}\text{C}_{\text{VPDB}}$ values of carbonates in the CM chondrites to the $\delta^{18}\text{O}_{\text{VSMOW}}$ values of the waters from which they grew (based on the known $\delta^{18}\text{O}$ values and growth temperatures of those carbonates and the temperature-dependent carbonate-water fractionation given by Kim and O'Neil, 1997). Curves indicate trends predicted by our model of coupled serpentinization and reduction of dissolved inorganic carbon to form methane. Values of 'K' for each model trend indicate the relative rates of methane production to silicate hydration (see text for details). Error bars indicate internal standard errors of each analysis; external errors, including contributions from all sources, average ca. 2 ‰ in $\delta^{18}\text{O}$ and ca. 0.2 ‰ in $\delta^{13}\text{C}$. See Table 1-1 for further details.

It is possible that the trend in Figure 1-2 reflects oxidation and dissolution of ^{13}C -enriched carbon in the reactant assemblage. Carbon reservoirs, other than carbonates, in CM chondrites include organics ($\delta^{13}\text{C}_{\text{PDB}}$ of ca. -36 to 41‰ for the major constituents; Sephton and Gilmour, 2001) and presolar grains ($\delta^{13}\text{C}_{\text{PDB}}$ of bulk measurements on some presolar phases vary up to ca. 1500‰; Yang and Epstein, 1984). Organic constituents are

lower in $\delta^{13}\text{C}$ than the highest values observed in CM chondrite carbonates and so they cannot be the sole contributors to observed carbon isotope variations of those carbonates. Most presolar phases are highly resistant to chemical oxidation and dissolution (Yang and Epstein, 1984) and so should have been inert under the relatively mild conditions at which CM chondrites underwent aqueous alteration. Presolar diamond and graphite might be more vulnerable to aqueous alteration, but their average $\delta^{13}\text{C}$ is also lower than that of CM chondrite carbonates (Hoppe et al., 1995). Thus, this hypothesis seems implausible.

Alternatively, ^{13}C enrichment could have accompanied aqueous alteration if it occurred in an open system (Wilson et al., 1999) from which CO_2 vapor was lost by a mechanism that involved a kinetic isotope fractionation. Such processes lead to ^{13}C enrichment of dissolved inorganic carbon in evaporating Dead Sea brines (Stiller et al., 1985), caliches (Knauth et al., 2003) and cryogenic weathering products (Clark and Lauriol, 1992). However, significant CO_2 degassing in evaporating Dead Sea brines is caused by low pH of those brines (3.7-6.0; Stiller et al., 1985). Alteration fluids that reacted with the CM chondrites are inferred to have had far higher pH values (10-12; Zolensky, 1984) and are not expected to have evolved a substantial fraction of their dissolved inorganic carbon as CO_2 . More importantly, kinetic isotope effects associated with evaporation of carbonate-bearing aqueous solutions typically also lead to increases in the $\delta^{18}\text{O}$ value of the residual solution (Stiller et al., 1985; Knauth et al., 2003). There is no evidence for such ^{18}O enrichment in the solutions that altered the CM chondrites—in fact, the opposite trend is observed in Figure 1-2. Therefore, this process also seems like a poor explanation of our observations.

Finally, aqueous alteration of the CM parent body could have led to an increase in $\delta^{13}\text{C}$ of dissolved inorganic carbon in the pore waters of that body if alteration was accompanied by production and escape of low- $\delta^{13}\text{C}$ CH_4 . A terrestrial analogue for this process is serpentinization of ultramafic rocks, during which dissolved inorganic carbon species are converted to CH_4 by the reaction (Horita and Berndt, 1999) :



Palmer and Drummond (1986) and Shock (1988) suggest that reactions like reaction (II) require a condensed phase catalyst to be geologically significant. Chromite, Fe-Ni alloys, and magnetite have been shown to catalyze this reaction (Horita and Berndt, 1999; Foustaoukos and Seyfried, 2004) and these and similar phases are abundant constituents of the CM chondrites (Brearley and Jones, 1998). At 200°C (a temperature at which this reaction occurs over laboratory time scales), the CH_4 produced by this reaction is ca. 60‰ lower in $\delta^{13}\text{C}$ than the residual inorganic carbon (Horita and Berndt, 1999). Based on the temperature dependence of similar reactions (Horita, 2001), we suggest the fractionation at 28°C (assuming the reaction could proceed over geological timescales at such low temperatures) could be as large as 90‰. In this case, the observed range in $\delta^{13}\text{C}$ values for CM chondrite carbonates could be produced by ca. 38% loss of the dissolved inorganic carbon pool through reduction to and loss of CH_4 . If we instead assume the experimentally measured high-temperature fractionation of 60‰, then 51% loss would be required.

The carbon isotope composition of dissolved inorganic carbon varies with the progress of reaction (II), by the relation:

$$\delta^{13}\text{C}_{\text{HCO}_3^-, f} = 1000 \ln \alpha_{\text{HCO}_3^-, f} = 1000 \ln(\alpha_{\text{HCO}_3^-, i} F^{\alpha^{13}\text{C}_{\text{CH}_4-\text{HCO}_3^-} - 1}) \quad (4)$$

where F is the fraction of reactant HCO_3^- that remains and $\alpha^{13}\text{C}_{\text{CH}_4-\text{HCO}_3^-}$ is the kinetic carbon isotope fractionation associated with reaction (II) (i.e., 90‰).

We prescribed that the progress of reaction (II) is a function of the progress of reaction (I), which is reasonable because H_2 is a reactant in reaction I and is produced in Fe-bearing systems as a result of reactions like reaction I (e.g., through olivine oxidation; Oze and Sharma, 2005, or Fe metal oxidation; Zolotov and Shock, 2004). This leads to:

$$F = \frac{[\text{HCO}_3^-]_f}{[\text{HCO}_3^-]_i} = 1 - \frac{\int d[\text{HCO}_3^-]}{[\text{HCO}_3^-]_i} = 1 - \frac{\int -K [\text{HCO}_3^-] p dp}{[\text{HCO}_3^-]_i} , \quad (5)$$

where $[\text{HCO}_3^-]$ is the concentration of HCO_3^- and K is the ratio of the progress of reactions (I) and (II). Equation 5 simplifies to: $F = e^{-\frac{Kp^2}{2}}$. Thus, both the $\delta^{18}\text{O}$ of water and the $\delta^{13}\text{C}$ of inorganic carbon are functions of p , and the position of a sample along the trend in Figure 1-2 depends only on p and K . If we assume that the initial $\delta^{13}\text{C}$ value of dissolved inorganic carbon was 22.8‰, the lowest $\delta^{13}\text{C}$ value observed for carbonates in the CM chondrites (23.7‰; Grady et al., 1988) minus the carbon isotope fractionation between dissolved inorganic carbon and calcite (~0.9‰; Rubinson and Clayton 1969), then the trend in Figure 1-2 is best fit by a value for $K = \frac{-2 \ln F}{p^2}$ of 0.66, with p varying from 0.72 to 1.19 among samples. Because p denotes the ratio of moles of oxygen in the reacted rock to moles of oxygen in initial water, this variation of p among samples indicates that water in some samples underwent ~1.6 times reaction with silicates than water in other samples.

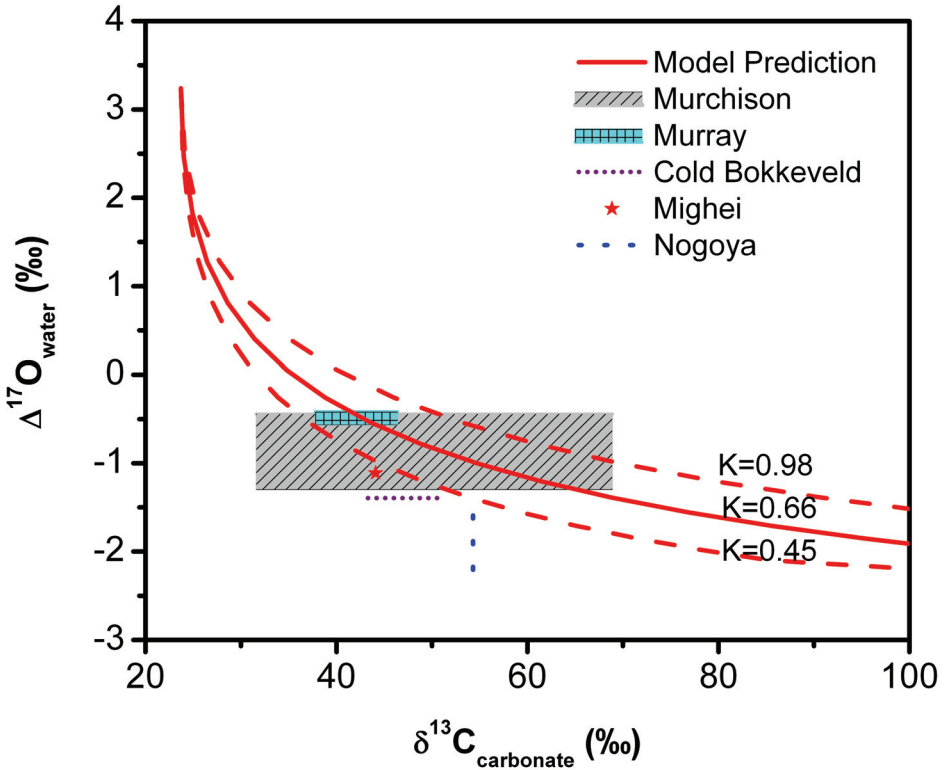


Figure 1-3. Predicted inverse correlation between $\Delta^{17}\text{O}_{\text{VSMOW}}$ of the formation water and $\delta^{13}\text{C}_{\text{VPDB}}$ of the carbonate during aqueous alteration of the CM chondrite parent body at 28°C. Also shown for comparison are reported ranges of $\delta^{13}\text{C}$ and $\Delta^{17}\text{O}$ values of carbonate (calcite portion) in CM chondrites (Clayton and Mayeda 1984; Grady et al. 1988; Benedix et al. 2004; this study). ‘K’ is the same as in Figure 1-2. Note that reported $\delta^{13}\text{C}$ and $\Delta^{17}\text{O}$ values are not from the same aliquots of samples.

Our model also predicts an inverse correlation between $\delta^{17}\text{O}$ and $\Delta^{17}\text{O}$ of the formation water on one hand and $\delta^{13}\text{C}$ of the carbonate on the other (Figure 1-3). Most of the available measurements of $\delta^{13}\text{C}$ (Grady et al., 1988) and $\Delta^{17}\text{O}$ (Clayton and Mayeda, 1984; Benedix et al., 2003) in carbonates from the CM chondrites were made on separate sample aliquots and thus do not clearly test this prediction (although the ranges of their variations are broadly consistent with our predicted trend; Figure 1-3). The only

exception is a recent study on paired Antarctic CM chondrites (Tyra et al., 2007), which observed an inverse correlation between $\delta^{13}\text{C}$ and $\Delta^{17}\text{O}$, as predicted. However, this study also observed that both $\delta^{13}\text{C}$ and $\Delta^{17}\text{O}$ correlate with ^{14}C content in the carbonates, and thus the correlation between $\delta^{13}\text{C}$ and $\Delta^{17}\text{O}$ could be caused or modified by terrestrial weathering (i.e., mixing or replacement of primary carbonate with lower $\delta^{13}\text{C}$, higher $\Delta^{17}\text{O}$ and ^{14}C terrestrial carbonates) (Tyra et al., 2007).

The correlation between $\Delta^{17}\text{O}_{\text{water}}$ and $\delta^{13}\text{C}_{\text{carbonate}}$ predicted by our model (Figure 1-3) implies that carbonates should vary in $\Delta^{17}\text{O}$ between different splits of the same meteorite for both Murchison and Cold Bokkeveld (i.e., because they vary in $\delta^{13}\text{C}$; Table 1-1). Therefore, if our model is correct, then our assumption that $\Delta^{17}\text{O}$ values of carbonates from a given meteorite are uniform and equal to the previously measured average for carbonate from that meteorite introduced errors in Δ_{47} (which is calculated based on a known or assumed $\Delta^{17}\text{O}$ value) and $\delta^{18}\text{O}_{\text{water}}$ (which depends, in part, on Δ_{47}). These errors might potentially influence the correlation in Figure 1-2, which is the primary justification of our methane generation model. A sensitivity analysis suggests that this factor is unlikely to lead to large changes: based on observed $\delta^{13}\text{C}_{\text{carbonate}}$ values and our model trend in Figure 1-3, values of $\Delta^{17}\text{O}$ in carbonates are expected to vary by 0.3‰ or less among different splits from the same meteorite; this would result in variations of only 0.01‰ in ion-corrected Δ_{47} values. These variations would be within our nominal analytical uncertainties. It is possible to calculate an alternate version of Figure 1-2 that assumes the model trend in Figure 1-3 is correct. However, this is an essentially circular exercise (i.e., because the model trend in Figure 1-3 depends, in part, on the fit to data in Figure 1-2) and cannot clarify the issue. We suggest that future

studies should attempt to apply both Δ_{47} and $\Delta^{17}\text{O}$ analyses to aliquots of CO₂ produced by acid digestion of carbonates in each CM chondrite.

3.3. Eh, pH of the alteration fluid estimated through the GEM-Selektor program

Reaction (II) will proceed to the right only under specific Eh conditions. We estimated these conditions using the GEM-Selektor program (Kulik et al. 1997; Kulik et al. 2000), which determines the equilibrium species distribution in a system through Gibbs Energy minimization (Bethke, 1996). This method does not depend on the pre-alteration mineralogy (an uncertainty in previous models of this kind; Zolensky et al., 1989; Rosenberg et al., 2001).

Our model of the chemistry of fluids in equilibrium with the alteration assemblage in the CM chondrites considers Si, Fe, Mg, S and Ca and neglects Al, Cr, K, Ni and other minor elements. Calculations were performed for 28°C, 1 atm, unless stated otherwise, with a bulk chemical composition as estimated by Browning and Bourcier (1998), assuming that aqueous alteration occurred without gain or loss of major cations (Table 1-2). During the simulation, we monitored the redox condition of the system by adding variable amounts of H₂ (0-1 grams) into the system (which typically consisted of ~100 grams of rock and 36 grams of water, and thus corresponds to p=1.023) and observed the concurrent changes of carbon speciation.

Controls were imposed on the final (post-alteration) mineral products to suppress the precipitation of mineral phases that generally do not form at these low temperatures (e.g., andradite, tremolite and troilite etc.) or are kinetically inhibited (e.g., quartz). Chrysotile is the only Mg-phyllosilicate allowed to form in the simulation, consistent with the fact

Table 1-2 GEM (Gibbs Energy Minimization) simulations of aqueous alteration on CM chondrite parent body.

	Temperature (°C)	28	28	28	28	28	28	28
	Pressure (atm)	1	1	1	1	1	10	1
Initial Unaltered Bulk Composition	Rock * (g)	94.91	94.91	94.91	94.91	94.91	94.91	94.91
	Water (g)	36	360	18	36	36	36	36
Simulation Results	p*	1	0.5	2	1	1	1	1
	CO ₂ * (M)	0.1	0.1	0.1	0.01	1	0.1	0.1
	Eh [†]	-0.67	-0.66	-0.69	-0.67	-0.67	-0.69	-0.73
	pH [†]	12.5	12.3	12.7	12.5	12.4	12.6	11.7

* Rock here denotes a bulk composition typical of the fine-grained materials in CM chondrites (Browning and Bourcier, 1998), i.e. 31.15% SiO₂, 30.54% FeO, 21.89% MgO, 9.32 % S, 2.01% CaO, and 5.09% others (wt%). “5.09% others” are not included in the simulations; p is defined as the ratio of moles of oxygen in the reacted rock to moles of oxygen in initial water and is calculated based on the masses of rock and water given in the table; CO₂ denotes the initial concentration of inorganic carbon present in the pre-alteration assemblage, in the unit of moles/L (water).

† Eh and pH here denotes the Eh and pH conditions during the coexistence of calcite and CH₄, determined through GEM simulations (see text for simulation details).

that it is the dominant Mg-rich alteration phase observed in carbonaceous chondrites (Brearley and Jones, 1998; Rosenberg et al., 2001). A typical product assemblage in our simulation included: chrysotile, greenalite, pyrite, pyrrhotite and CH₄ (more reducing conditions); chrysotile, greenalite, pyrite, goethite, gypsum and calcite (less reducing conditions). All the thermodynamic data employed in the calculations are from the Nagra/PSI Chemical Thermodynamic Data Base 01/01 (Hummel et al., 2002) and an updated version of thermodynamic database (slop98.dat) for SUPCRT92 (Johnson et al., 1992), as implemented in the GEM-Selektor Program (Kulik et al., 2000).

Given these constraints, we found that the coexistence of carbonate and CH₄ requires an Eh of -0.67 and pH of 12.5. Both Eh and pH are inversely correlated with the assumed temperature (decreasing to -0.73 and 11.7 at 71°C), but neither of them is strongly dependent on reasonable variations of other model parameters (e.g. water/rock ratios, alteration pressures, and initial CO₂ concentrations etc., Table 2). For a given set of independent constraints, pH of the alteration fluid is inversely correlated with Eh. Note that this calculation (as for similar previous calculations; Zolensky et al., 1989; Rosenberg et al., 2001) assumes equilibrium with respect to redox reactions in the alteration assemblage, which might not apply (Bethke, 1996).

4. IMPLICATIONS

The temperatures of carbonate precipitation in representative CM chondrites, as constrained by carbonate clumped isotope thermometry, are within the range of (though more specific than) previous estimates based on mineral stability and oxygen isotope fractionation between different matrix phases. We observe a negative correlation between

$\delta^{13}\text{C}_{\text{PDB}}$ of carbonates and $\delta^{18}\text{O}_{\text{SMOW}}$ of the water from which those carbonates grew.

This correlation can be explained if carbonate growth was accompanied by the formation and escape of ^{13}C -depleted methane during aqueous alteration on the CM chondrite parent bodies.

Our conclusion that aqueous alteration of the CM chondrites was accompanied by formation and loss of methane implies that methane generation in the interiors of planets and planetessimals may have been a widespread phenomenon in the evolutionary history of the solar system. Several recent studies (Formisano et al. 2004; Lyons et al. 2005; Oze and Sharma 2005) invoked serpentinization and hydrothermal alteration sources of atmospheric methane detected on Mars, and analogous processes could be considered to explain methane found on other solar system objects, such as Titan (Niemann et al., 2005), Triton (Cruikshank et al., 1993), Pluto (Owen et al., 1993) and Kuiper belt objects (Brown et al. 1997; Barucci et al. 2005; Brown et al. 2005; Licandro et al. 2006). It is unclear whether the details of the alteration model we propose (i.e., reactants, temperatures, Eh, pH, stoichiometries) could have any direct relevance for Mars, which has undergone extensive magmatic differentiation and thus consists of relatively volatile-poor igneous rocks that differ in many respects from the carbonaceous chondrites. However, the model we suggest for methane generation in the CM chondrite parent bodies plausibly applies to at least some portions of the interiors of Titan and other outer solar system bodies, especially early during their histories. For example, it is possible that the sub-surface of Titan contains abundant liquid water-ammonia solution with temperatures up to 0°C (Grasset and Pargamin, 2005) and possibly higher early in Titan's history (Atreya et al., 2006; Tobie et al., 2006). This reduced, water-rich interior provides

an environment where silicate alteration reactions such as those we consider in our model could take place. Currently, methane in the atmosphere of Titan is destroyed through photochemical reactions at a rate of 2.5×10^{-14} mol cm $^{-2}$ s $^{-1}$ (Yung et al., 1984). If Titan's atmosphere is in steady state, this loss could be supported by methane produced by serpentinization of silicates in the presence of carbonate-bearing fluids at a rate of $\sim 3.2 \times 10^{12}$ kg of silicate consumed per year. If this rate is typical of the history of Titan, it would lead to time-integrated hydration of a ~ 39 km-thick layer of reactant rock. Similarly, the methane on Pluto is hydro-dynamically escaping with a flux of $2.2 \sim 10.1 \times 10^{-14}$ mol cm $^{-2}$ s $^{-1}$ (Trafton et al., 1997). This flux could have been supported throughout the history of Pluto by gradual aqueous alteration of a 34 to 157 km-thick global layer of reactant silicate rock. In both cases, the layer of reactant rock could be several times thinner if it is rich in metallic iron (because metallic iron is a more efficient source of H₂ during aqueous alteration than Fe^(II)-silicates; Zolotov and Shock, 2004; Oze and Sharma, 2005).

ACKNOWLEDGEMENTS

This research was supported by a grant to J.M.E. from the NASA Cosmochemistry Program. We thank Sara Russell for her editorial handling of this manuscript, and Chris Romanek and two anonymous reviewers for thoughtful and constructive comments.

REFERENCES

- Affek H. P. and Eiler J. M. (2006). Abundance of mass 47 CO₂ in urban air, car exhaust, and human breath. *Geochim. Cosmochim. Acta* **70**: 1-12.

- Al-Aasm I. S., Taylor B. E. and South B. (1990). Stable isotope analysis of multiple carbonate samples using selective acid extraction. *Chem. Geol.* **80**: 119-25.
- Atreya S. K., Adams E. Y., Niemann H. B., Demick-Montelara J. E., Owen T. C., Fulchignoni M., Ferri F. and Wilson E. H. (2006). Titan's methane cycle. *Planet. Space Sci.* **54**: 1177-1187.
- Baker L., Franchi I. A., Wright I. P. and Pillinger C. T. (2002). The oxygen isotopic composition of water from Tagish Lake: Its relationship to low-temperature phases and to other carbonaceous chondrites. *Meteorit. Planet. Sci.* **37**: 977-985.
- Benedix G. K., Leshin L. A., Farquhar J., Jackson T. and Thiemens M. H. (2003). Carbonates in CM2 chondrites: Constraints on alteration conditions from oxygen isotopic compositions and petrographic observations. *Geochim. Cosmochim. Acta* **67**: 1577-1588.
- Bethke C. M. (1996). Geochemical Reaction Modeling: Concepts and Applications. Oxford University Press.
- Brearley A. J. and Jones R. H. (1998). Chondritic meteorites. In *Planetary Materials*. 3-1 to 3-398.
- Brearley A. J., Saxton J. M., Lyon I. C. and Turner G. (1999). Carbonates in the Murchison CM chondrite: CL characteristics and oxygen isotopic compositions. *30th Lun. and Planet. Sci. Conf.* Abstract #1301.
- Browning L. and Bourcier W. (1998). Constraints on the anhydrous precursor mineralogy of fine-grained materials in CM carbonaceous chondrites. *Meteorit. Planet. Sci.* **33**: 1213-1220.
- Browning L. B., McSween H. Y. and Zolensky M. E. (1996). Correlated alteration effects in CM carbonaceous chondrites. *Geochim. Cosmochim. Acta* **60**: 2621-2633.
- Clark I. D. and Lauriol B. (1992). Kinetic enrichment of stable isotopes in cryogenic calcites. *Chem. Geol.* **102**: 217-228.
- Clayton R. N. and Mayeda T. K. (1984). The oxygen isotope record in Murchison and other carbonaceous chondrites. *Earth Planet. Sci. Lett.* **67**: 151-161.
- Clayton R. N. and Mayeda T. K. (1999). Oxygen isotope studies of carbonaceous chondrites. *Geochim. Cosmochim. Acta* **63**: 2089-2104.

- Cruikshank D. P., Roush T. L., Owen T. C., Geballe T. R., Debergh C., Schmitt B., Brown R. H. and Bartholomew M. J. (1993). Ices on the surface of Triton. *Science* **261**: 742-745.
- Eiler J. M. and Kitchen N. (2004). Hydrogen isotope evidence for the origin and evolution of the carbonaceous chondrites. *Geochim. Cosmochim. Acta* **68**: 1395-1411.
- Eiler J. M. and Schauble E. A. (2004). $^{18}\text{O}^{13}\text{C}^{16}\text{O}$ in Earth's atmosphere. *Geochim. Cosmochim. Acta* **68**: 4767-4777.
- Endress M., Zinner E. and Bischoff A. (1996). Early aqueous activity on primitive meteorite parent bodies. *Nature* **379**: 701-703.
- Foustoukos D. I. and Seyfried W. E. (2004). Hydrocarbons in hydrothermal vent fluids: The role of chromium-bearing catalysts. *Science* **304**: 1002-1005.
- Ghosh P., Adkins J., Affek H. P., Balta B., Guo W., Schauble E. A., Schrag D. and Eiler J. M. (2006). $^{13}\text{C}-^{18}\text{O}$ bonds in carbonate minerals: A new kind of paleothermometer. *Geochim. Cosmochim. Acta* **70**: 1439-1456.
- Ghosh P., Eiler J., Campana S. E. and Feeney R. F. (2007). Calibration of the carbonate 'clumped isotope' paleothermometer for otoliths. *Geochim. Cosmochim. Acta* **71**: 2736-2744.
- Grady M. M., Wright I. P., Swart P. K. and Pillinger C. T. (1988). The carbon and oxygen isotopic composition of meteoritic carbonates. *Geochim. Cosmochim. Acta* **52**: 2855-2866.
- Grasset O. and Pargamin J. (2005). The ammonia-water system at high pressures: Implications for the methane of Titan. *Planet. Space Sci.* **53**: 371-384.
- Hoppe P., Amari S., Zinner E. and Lewis R. S. (1995). Isotopic compositions of C, N, O, Mg, and Si, trace element abundances, and morphologies of single circumstellar graphite grains in four density fractions from the Murchison meteorite. *Geochim. Cosmochim. Acta* **59**: 4029-56.
- Horita J. (2001). Carbon isotope exchange in the system $\text{CO}_2\text{-CH}_4$ at elevated temperatures. *Geochim. Cosmochim. Acta* **65**: 1907-1919.
- Horita J. and Berndt M. E. (1999). Abiogenic methane formation and isotopic fractionation under hydrothermal conditions. *Science* **285**: 1055-1057.

- Hummel W., Berner U., Curti E., Pearson F. J. and T T. (2002). Nagra/PSI Chemical Thermodynamic Data Base 01/01. Universal Publishers.
- Johnson J. W., Oelkers E. H. and Helgeson H. C. (1992). SUPCRT92 - A software package for calculating the standard molal thermodynamic properties of minerals, gases, aqueous species, and reactions from 1-bar to 5000 bar and 0°C to 1000°C. *Comput. Geosci.* **18**: 899-947.
- Keil K. (2000). Thermal alteration of asteroids: evidence from meteorites. *Planet. Space Sci.* **48**: 887-903.
- Kim S. T. and O'Neil J. R. (1997). Equilibrium and nonequilibrium oxygen isotope effects in synthetic carbonates. *Geochim. Cosmochim. Acta* **61**: 3461-3475.
- Knauth L. P., Brilli M. and Klonowski S. (2003). Isotope geochemistry of caliche developed on basalt. *Geochim. Cosmochim. Acta* **67**: 185-195.
- Kulik D. A., Aja S. U., Sinitsyn V. A. and Wood S. A. (2000). Acid-base surface chemistry and sorption of some lanthanides on K⁺-saturated marblehead illite: II. A multisite-surface complexation modeling. *Geochim. Cosmochim. Acta* **64**: 195-213.
- Martin B. and Fyfe W. S. (1970). Experimental and theoretical observations on the kinetics of hydration reactions with particular reference to serpentinization. *Chem. Geol.* **6**: 185-202.
- McSween H. Y., Ghosh A., Grimm R. E., Wilson L. and Young E. (2002). Thermal evolution models of asteroids. In *Asteroids III*, The University of Arizona Press. 559-571.
- Neal C. and Stanger G. (1983). Hydrogen generation from mantle source rocks in Oman. *Earth Planet. Sci. Lett.* **66**: 315-20.
- Niemann H. B., Atreya S. K., Bauer S. J., Carignan G. R., Demick J. E., Frost R. L., Gautier D., Haberman J. A., Harpold D. N., Hunten D. M., Israel G., Lunine J. I., Kasprzak W. T., Owen T. C., Paulkovich M., Raulin F., Raaen E. and Way S. H. (2005). The abundances of constituents of Titan's atmosphere from the GCMS instrument on the Huygens probe. *Nature* **438**: 779-784.

- Owen T. C., Roush T. L., Cruikshank D. P., Elliot J. L., Young L. A., Debergh C., Schmitt B., Geballe T. R., Brown R. H. and Bartholomew M. J. (1993). Surface ices and the atmospheric composition of Pluto. *Science* **261**: 745-748.
- Oze C. and Sharma M. (2005). Have olivine, will gas: Serpentinitization and the abiogenic production of methane on Mars. *Geophys. Res. Lett.* **32**: L10203/1-L10203/4.
- Palmer D. A. and Drummond S. E. (1986). Thermal decarboxylation of acetate. Part I. The kinetics and mechanism of reaction in aqueous solution. *Geochim. Cosmochim. Acta* **50**: 813-23.
- Proskurowski G., Lilley M. D., Kelley D. S. and Olson E. J. (2006). Low temperature volatile production at the Lost City Hydrothermal Field, evidence from a hydrogen stable isotope geothermometer. *Chem. Geol.* **229**: 331-343.
- Riciputi L. R., McSween H. Y., Johnson C. A. and Prinz M. (1994). Minor and trace-element concentrations in carbonates of carbonaceous chondrites, and implications for the compositions of coexisting fluids. *Geochim. Cosmochim. Acta* **58**: 1343-1351.
- Rosenberg N. D., Browning L. and Bourcier W. L. (2001). Modeling aqueous alteration of CM carbonaceous chondrites. *Meteorit. Planet. Sci.* **36**: 239-244.
- Rubinson M. and Clayton R. N. (1969). Carbon-13 fractionation between aragonite and calcite. *Geochim. Cosmochim. Acta* **33**: 997-1002.
- Santrock J., Studley S. A. and Hayes J. M. (1985). Isotopic analyses based on the mass spectrum of carbon dioxide. *Anal. Chem.* **57**: 1444-1448.
- Schauble E. A., Ghosh P. and Eiler J. M. (2006). Preferential formation of ^{13}C - ^{18}O bonds in carbonate minerals, estimated using first-principles lattice dynamics. *Geochim. Cosmochim. Acta* **70**: 2510-2529.
- Sephton M. A. and Gilmour I. (2001). Compound-specific isotope analysis of the organic constituents in carbonaceous chondrites. *Mass Spectrom. Rev.* **20**: 111-120.
- Sheppard S. M. F. and Gilg H. A. (1996). Stable isotope geochemistry of clay minerals. *Clay Mineral.* **31**: 1-24.
- Shock E. L. (1988). Organic-acid metastability in sedimentary basins. *Geology* **16**: 886-890.

- Stevens T. O. and McKinley J. P. (1995). Lithoautotrophic microbial ecosystems in deep basalt aquifers. *Science*. **270**: 450-454.
- Stevens T. O. and McKinley J. P. (2000). Abiotic controls on H₂ production from basalt-water reactions and implications for aquifer biogeochemistry. *Environ. Sci. Technol.* **34**: 826-831.
- Stiller M., Rounick J. S. and Shasha S. (1985). Extreme carbon-isotope enrichments in evaporating brines. *Nature* **316**: 434-435.
- Tobie G., Lunine J. I. and Sotin C. (2006). Episodic outgassing as the origin of atmospheric methane on Titan. *Nature* **440**: 61-64.
- Trafton L. M., Hunten D. M., Zahnle K. J. and McNutt R. L. J. (1997). Escape processes at Pluto and Charon In *Pluto and Charon*, The University of Arizona Press. 475-522.
- Tyra M. A., Farquhar J., Wing B. A., Benedix G. K., Jull A. J. T., Jackson T. and Thiemens M. H. (2007). Terrestrial alteration of carbonate in a suite of Antarctic CM chondrites: Evidence from oxygen and carbon isotopes. *Geochim. Cosmochim. Acta*. **71**: 782-795.
- Wenner D. B. and Taylor H. P. (1971). Temperatures of serpentinization of ultramafic rocks based on ¹⁸O/¹⁶O fractionation between coexisting serpentine and magnetite. *Contrib. Mineral. Petrol.* **32**: 165-185.
- Wilson L., Keil K., Browning L. B., Krot A. N. and Bourcier W. (1999). Early aqueous alteration, explosive disruption, and reprocessing of asteroids. *Meteorit. Planet. Sci.* **34**: 541-557.
- Yang J. M. and Epstein S. (1984). Relic interstellar grains in Murchison meteorite. *Nature* **311**: 544-547.
- Young E. D. (2001). The hydrology of carbonaceous chondrite parent bodies and the evolution of planet progenitors. *Phil. Trans. R. Soc. Lond. A* **359**: 2095-2109.
- Yung Y. L., Allen M. and Pinto J. P. (1984). Photochemistry of the atmosphere of Titan: Comparison between model and observations. *Astrophys. J. Suppl. Ser.* **55**: 465-506.

- Zolensky M., Bodnar R., Tsuchiyama A., Okudaira K., Noguchi T., Uesugi K. and Nakano T. (2004). Fluid inclusions in chondrites. *Meteorit. Planet. Sci.* **39**: A118-A118.
- Zolensky M. E. (1984). Hydrothermal alteration of CM carbonaceous chondrites: Implications of the identification of tochilinite as one type of meteoritic PCP. *Meteoritics* **19**: 346-347.
- Zolotov M. Y. and Shock E. L. (2004). Pathways of hydrogen generation during aqueous alteration of chondrites. *Meteorit. Planet. Sci.* **39**: A119-A119.

Chapter 2**TEMPERATURES OF AQUEOUS ALTERATION ON
CARBONACEOUS CHONDRITE PARENT BODIES**

Weifu Guo ¹, Michael Zolensky ² and John M. Eiler ¹

1. Division of Geological and Planetary Sciences, California Institute of Technology,
Pasadena, CA, 91125, USA

2. NASA Johnson Space Center, Houston, TX, USA

ABSTRACT

Application of stepped phosphoric acid digestion and carbonate clumped isotope thermometry to carbonates in carbonaceous chondrites — GRO 95577 (CR1), Orgueil (CI) and Tagish Lake (ungrouped C2) — indicates that aqueous alterations on carbonaceous chondrite parent bodies occurred from -31 to 65°C from fluids with $\delta^{18}\text{O}_{\text{VSMOW}}$ values of -29.7‰ to 11.8‰ and $\delta^{17}\text{O}_{\text{VSMOW}}$ of -14.9‰ to 7.6‰. The estimated carbonate formation temperatures decrease in the order: calcite > dolomite > breunnerite. Based on independent constraints on the ages of these carbonates and models of the evolution of the oxygen isotope compositions of parent body waters, this trend indicates that the parent bodies were cooling as the aqueous alteration proceeded. We estimate that aqueous alteration on the carbonaceous chondrite parent bodies started within 1-2 million years after the accretion of those parent bodies, and that the alteration temperatures decreased from 34°C to 18°C in the first ~4 million years and further to -20°C after a total of ~6.5 million years. Our results provide the first direct measurements of the low-temperature cooling histories of C1 and C2 carbonaceous chondrite parent bodies.

1. INTRODUCTION

Aqueous alteration of primitive meteorites is among the earliest and most widespread geological processes in the solar system, occurring within the first tens of million of years of solar system history (Brearley, 2006). A better understanding of these processes, including precise reconstructions of alteration temperatures, would help us

constrain the early conditions of the solar system and test models of thermal and chemical evolution of planetesimals.

Previous estimates of the alteration temperatures on the carbonaceous chondrite parent bodies, mostly based on the maximum thermal stabilities of matrix phases and oxygen isotope fractionations between the constituent phases in the matrix, range from <20°C to <300°C (Keil 2000 and references therein). As discussed before (Guo and Eiler, 2007), these two approaches either yield only upper temperature limits or require the assumption that phases in the matrix achieved mutual oxygen isotope equilibrium. In a recent study, we apply carbonate clumped isotope thermometry (Ghosh et al., 2006; Schauble et al., 2006) to carbonates in CM chondrites, showing that the aqueous alteration temperatures on the CM chondrite parent body (or bodies) ranged between 20 and 71°C (Guo and Eiler, 2007). Carbonate clumped isotope thermometry is based on a thermodynamic homogeneous equilibrium within the carbonate lattice that orders ^{13}C and ^{18}O into the same carbonate ion. This thermometer is independent of the isotopic compositions of any coexisting phases and makes no assumptions regarding equilibration of carbonates with other phases. Therefore, our approach circumvents some assumption made by previous studies and provides precise ($\pm 10^\circ\text{C}$) constraints on the temperature of aqueous alteration of the carbonaceous chondrite parent bodies.

In this study, we extended our previous work on CM chondrites by further applying carbonate clumped isotope thermometry to carbonates in other types of carbonaceous chondrites, including the CR1 chondrite, GRO 95577, the CI chondrite, Orgueil; and the ungrouped C2 chondrite, Tagish Lake. These samples contain two or more generations of distinct carbonate phases, which previous studies have established grew at different times

and possibly under different conditions and from waters of different isotopic compositions. We used techniques of stepped acid digestion to separately determine the clumped isotope formation temperatures of these diverse carbonates, thereby constraining multiple points on the temperature-time path followed by each of these rocks.

2. SAMPLES AND METHOD

2.1 Samples

We analyzed carbonates from 4 splits of 3 different carbonaceous chondrites: GRO 95577 (CR1, 2 splits), Orgueil (CI, 1 split) and Tagish Lake (ungrouped C2, 1 split). Each sample split (weighing between 26 and 96 mg) was prepared from a separate fragment of a whole rock meteorite sample and ground individually into unsieved particles (grain size of $\leq 500 \mu\text{m}$) with an agate mortar and pestle (Table 2-1).

Each of the three analyzed meteorites is a representative and well-studied member of their respective groups. All experienced extensive aqueous alterations as evidenced by the occurrence of abundant secondary minerals (such as phyllosilicates, carbonates, and magnetite) in their matrix, though Tagish Lake (petrologic type 2) is less altered than GRO 95577 and Orgueil (both petrologic type 1) (Weisberg and Prinz, 2000; Zolensky et al., 2002; Weisberg et al., 2006). Carbonate minerals are abundant in all three of these carbonaceous chondrites (average modal abundances of 5 vol% and 6.4 vol% in Orgueil and GRO95577 respectively, and 7-8 wt% in Tagish Lake), occurring mostly in the form of veins and isolated grains or fragments in the matrix (Endress and Bischoff, 1996; Leshin et al., 2001; Zolensky et al., 2002; Perronnet et al., 2007). However, carbonate mineralogies are significantly different among these three samples: carbonates in GRO

Table 2-1 Isotopic analyses of carbonates in carbonaceous chondrites.

Sample	GRO 95577 (split 2006)	GRO 95577 (split 2007)	Orgueil [†]	Tagish Lake	Estimated External Precision (1 σ)
Petrology Type	CR1	CR1	CI	Ungrouped C2	
Weight (mg)	24.9	30.2	96.18	79.05	
Date of Analysis	8/11/06	4/5/07	12/14/06-1/1/06	1/25/07-2/11/07	
Carbonate Mineralogy	Calcite	Calcite	Dolomite ^ξ	Breunnerite	
CO ₂ yield	(μ mol)	5.7	18.7	8.4	4.6
	(μ mol/g)	229.1	618.9	87.8	48.4
$\Delta^{17}\text{O}^*$ (‰)	-0.93	-0.93	0.50	0.55	1.49
$\delta^{13}\text{C}_{\text{Carbonate}}\text{(‰)}$	69.91	70.79	67.28	67.77	40.42
V PDB					
$\delta^{18}\text{O}_{\text{Carbonate}}\text{(‰)}$	19.62	17.82	28.99	28.91	21.08
VSMOW					
Δ_{47} (‰)	0.726	0.571	0.709	0.650	0.887
Temperature (°C)	8	43	12	24	-20
$\delta^{18}\text{O}_{\text{water}}\text{(‰)}$	-12.3	-7.1	-5.3	-2.7	-29.7
VSMOW					
$\delta^{17}\text{O}_{\text{water}}\text{(‰)}$	-7.3	-4.6	-2.2	-0.9	-14.9
VSMOW					

[†] No CO₂ was yielded during our stepped extraction of calcite from Orgueil, consistent with the rare occurrence of calcite in Orgueil (Brearley and Jones 1998).

* $\Delta^{17}\text{O}$ values are averages recalculated from Leshin et al. (2001) and Clayton and Mayeda (1999) with $\lambda=0.5164$, and are used in ¹⁷O corrections of this study (see texts for details).

^ξ The two splits of CO₂ for Orgueil dolomite were derived from a single extraction. The extracted CO₂ were divided into two splits after exposure to dry Ag_3PO_4 , and these two splits were then analyzed at different time on the mass spectrometer.

95577 are almost exclusively calcite [CaCO_3] (Perronnet et al., 2007); carbonates in Orgueil and Tagish Lake vary in compositions from calcite to dolomite [$\text{CaMg}(\text{CO}_3)_2$] (or siderite [FeCO_3]) and to breunnerite [$\text{Mg}(\text{Fe,Mn})(\text{CO}_3)_2$], with their abundances decreasing in the order of dolomite > breunnerite > calcite (very rare) in Orgueil (Brearley and Jones, 1998; Brown et al., 2000; Zolensky et al., 2002).

2.2 Phosphoric acid digestion

Depending on their respective carbonate mineralogy, each ground meteorite sample was either reacted with anhydrous phosphoric acid at 25°C for 18-24 hours (for GRO 95577) or subjected to a stepped phosphoric acid digestion procedure (for Orgueil and Tagish Lake) to separately measure the isotopic compositions of their constituent carbonate mineral phases — calcite, dolomite and brunnerite. Stepped phosphoric acid digestion is an experimental technique, widely applied in studies of terrestrial carbonate samples, to separately extract and determine the isotopic compositions of two or more carbonate constituents in mixtures that are too finely intermixed to physically separate. It is based on the fact that different carbonate minerals react with anhydrous phosphoric acid at different rates at any given temperature, decreasing in the order of calcite, dolomite and breunnerite/magnesite (Al-Aasm et al., 1990). These techniques have also been previously applied to meteoritic carbonates (Grady et al., 1988; Leshin et al., 2001; Benedix et al., 2003). In this study, we employed a 3-step stepped phosphoric acid digestion and extraction method, designed to release CO_2 from calcite, dolomite and breunnerite/magnesite during steps 1, 2 and 3 respectively: Step 1) the ground sample was first reacted with anhydrous phosphoric acid at 50°C, and the CO_2 released during

the first 3 minutes was collected and assumed to represent the calcite contained in the sample; Step 2) the sample was left reacting further at 50°C, and the CO₂ released between 3 minutes and 24 hours was collected and assumed to represent the dolomite contained in the sample; and Step 3) the reaction vessel was then transferred to a oil bath with a set temperature of 80°C for 2-3 days. The CO₂ released during the third step was collected and assumed to represent the breunnerite/magnesite contained in the sample. The temperatures of phosphoric acid digestions at each step were controlled within ±2°C of the desired temperatures.

The stepped phosphoric acid digestion and extraction method described above was established by experiments on synthetic mixtures of calcite and dolomite and of dolomite and magnesite (magnesite here is assumed to simulate brunnertie in the carbonaceous chondrites; both siderite and magnesite, the two composition-end-members of breunnerite, react with phosphoric acid orders of magnitude much more slowly than dolomite at given temperature, with magnesite being the slowest; Al-Aasm et al., 1990). In both cases we prepared physical mixtures having carbon equivalent molar ratios of ~1:1 between the two constituent phases (Table 2-2). The isotopic compositions of carbonate end members (calcite and dolomite) used in the test were also determined separately by complete reaction of pure end members to compare with those derived from the stepped phosphoric acid digestion. Calcite used in the synthetic mixture was purchased from Sigma-Aldrich Co. as powder; dolomite and magnesite were obtained from the mineral collection of the Division of Geological and Planetary Sciences at Caltech and then ground into powders. The phase identity of each mineral was verified using X-ray diffraction. The results of these methodological tests are presented in section 3.1.

Table 2-2 Tests and establishment of stepped extraction procedures on synthetic mixtures of calcite and dolomite, and of dolomite and magnesite (carbon equivalent molar ratio ~1:1 for both).

Sample	Carbonate Endmembers			Stepped Phosphoric Acid Digestion			Estimated External Precision (1σ)
	Calcite	Dolomite	Calcite + Dolomite ~1:1 Mixture	Dolomite + Magnesite ~1:1 Mixture	Step I (Calcite)	Step II (Dolomite)	
Digestion Temperature (°C)	50	50	50	50	50	50	80
Digestion Time	24hr	24hr	24hr	3min	24hr	24hr	56hr
$\delta^{13}\text{C}_{\text{Carbonate}} (\text{\textperthousand})$	-42.37	-0.20	-0.16	-41.54	-2.38	-0.10	1.60
VPDB							0.001
$\delta^{18}\text{O}_{\text{Carbonate}} (\text{\textperthousand})$	10.00	18.86	18.87	10.11	18.36	18.74	14.59
VSMOW							0.002
$\Delta_{47} (\text{\textperthousand})$	0.395	0.470	0.495	0.400	0.481	0.462	0.319
Components Estimated &	N/A	N/A	N/A	98% Calcite + 2% Dolomite	95% Calcite + 5% Dolomite	96% Calcite + 4% Dolomite	N/A

& The actual compositions of the stepped-extraction products estimated from their carbon isotope compositions (see section 3.1 for details).

The total yield of CO₂ from each meteorite sample split varied from 136.1 μmol/g to 618.9 μmol/g, increasing in the order of Orgueil > GRO 95577 (split 2006) > Tagish Lake > GRO 95577 (split 2007) (Table 1). The difference in CO₂ yields between the two splits of GRO 95577 samples (229.1 μmol/g vs. 618.9 μmol/g) reflects the heterogeneous distribution of carbonates inside the sample. All of these CO₂ yields are higher than those observed from phosphoric acid digestion of CM chondrites (39.3-127.6 μmol/g; Guo and Eiler 2007), and generally agree with the estimations of carbonate abundances from petrographic observations of the samples we've studied (Endress and Bischoff, 1996; Brearley and Jones, 1998; Zolensky et al., 2002; Perronnet et al., 2007) and a previous phosphoric acid digestion study (Leshin et al., 2001). The yields of CO₂ from different steps of our stepped extractions (of Orgueil and Tagish Lake) are also consistent with dolomite being the most abundant carbonate phase in both Orgueil and Tagish Lake, followed by breunnerite and then calcite. Note, no CO₂ was evolved during the calcite extraction step for Orgueil, consistent with the rare occurrence of calcite in the Orgueil matrix (Brearley and Jones, 1998).

2.3 Purification of sample CO₂ and mass spectrometric analysis

CO₂ derived from phosphoric acid digestion of carbonaceous chondrites is rich in sulfur and organic contaminants and requires careful purification before isotopic analyses (Clayton and Mayeda, 1984; Grady et al., 1988; Benedix et al., 2003; Guo and Eiler, 2007). Following the procedures outlined in Guo and Eiler (2007), we exposed the CO₂ produced by acid digestion of chondritic samples to dry Ag₃PO₄, passed it through a series of glass traps cooled with an ethanol slush (-78°C) and a pentane slush (-130°C)

and through a Supelco Q-Plot GC column held at -20°C . CO_2 released from GRO 95577, Orgueil and Tagish Lake were generally poor in contaminants (0.6-2.9% for all sample extractions, except the 80°C extraction for breunnerite in Tagish Lake—30.2%), based on the sample sizes before and after dry Ag_3PO_4 treatment. This contrasts with the consistently high (19-62%) abundances of sulfur and other contaminants in the CO_2 derived from phosphoric acid digestion of CM chondrites (Guo and Eiler, 2007).

The purified CO_2 was then analyzed in micro-volume dual inlet mode on a Finnigan-MAT 253 gas source isotope ratio mass spectrometer, at signal intensities of 2.2-9.5V for mass 44. Note that the CO_2 yields from different sample extractions and extraction steps ranged from $3.9\mu\text{mol}$ to $28.1\mu\text{mol}$. To ensure that all sample CO_2 was processed and analyzed under similar conditions (e.g., similar gas sizes and mass 44 voltages), we divided the extracted CO_2 on the vacuum line for extractions yielding CO_2 gases more than $6\ \mu\text{mol}$, and used only a portion of the extracted CO_2 ($3.8\mu\text{mol}$ to $5.7\mu\text{mol}$) in the sample purification and mass spectrometric analyses. The rest of the extracted sample CO_2 was sealed in pre-evacuated Pyrex tubes for future analyses. One exception is for CO_2 derived from dolomite extraction of Orgueil, which we divided into two splits after exposure to dry Ag_3PO_4 . Both of these two splits of CO_2 were then further purified and analyzed on the mass spectrometer (Table 1). A more detailed description on the sample purification and mass spectrometric analysis can be found in our recent study of carbonates in CM chondrites (Guo and Eiler, 2007).

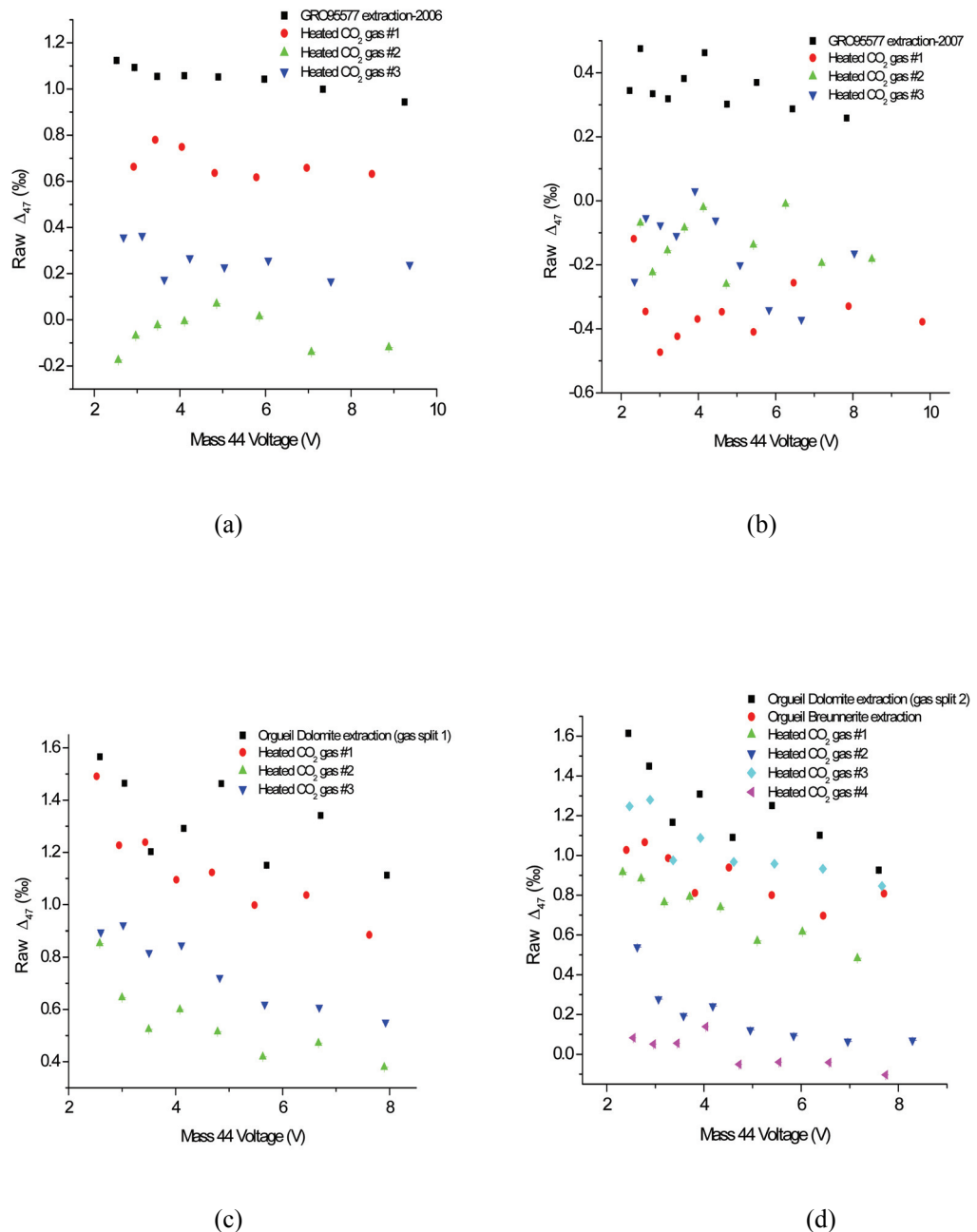
The isotopic compositions of the purified sample CO_2 ($\delta^{13}\text{C}$, $\delta^{18}\text{O}$ and Δ_{47}) obtained from the mass spectrometric analyses were corrected for their $\Delta^{17}\text{O}$ values (Guo and Eiler, 2007). We assume average carbonate $\Delta^{17}\text{O}$ of Orgueil and Tagish Lake (recalculated

from Leshin et al. 2001) and average matrix $\Delta^{17}\text{O}$ of CR chondrites (recalculated from Clayton and Mayeda 1999) in our corrections for samples from the respective carbonaceous chondrites (Table 1). 1‰ decrease in $\Delta^{17}\text{O}$, if unrecognized or unaccounted for, would lead to a systematic error of ~0.034‰ in sample Δ_{47} (Eiler and Schauble, 2004).

The oxygen isotope fractionation factors (α values) associated with phosphoric acid digestion were assumed to be 1.01025, 1.00930, 1.01038 and 1.00976 (Beukes et al., 1990; Das Sharma et al., 2002) for, respectively, CO_2 derived from 25°C calcite extraction, 50°C calcite extraction, 50°C dolomite extraction and 80°C breunnerite extraction. All reported oxygen isotope compositions of carbonates have been corrected for these analytical fractionations.

Values of $\delta^{13}\text{C}$ and $\delta^{18}\text{O}$ were standardized by comparison with CO_2 generated by phosphoric acid digestion of NBS-19 and are reported vs. VPDB and VSMOW, respectively. The external precision of our isotope analyses are estimated to be 0.14‰, 0.21‰, 0.04‰ (1 σ) for $\delta^{13}\text{C}$, $\delta^{18}\text{O}$ and Δ_{47} , respectively, based on measurements of carbonate standards with the same experimental procedures (Guo and Eiler, 2007). Note that these errors are larger than typical of carbonate clumped isotope analyses and reflect the smaller sizes and greater contamination of the samples examined in this study.

During the mass spectrometric analyses, we observed negative correlations between the raw Δ_{47} value of sample CO_2 (relative to the reference CO_2 gas) and the mass 44 voltages at which the raw Δ_{47} was obtained (Fig. 1). Similar correlations were also observed in the mass spectrometric analyses of heated CO_2 gases that accompany the analyses of sample CO_2 (all made within 1-2 days of the analyses of sample CO_2 for



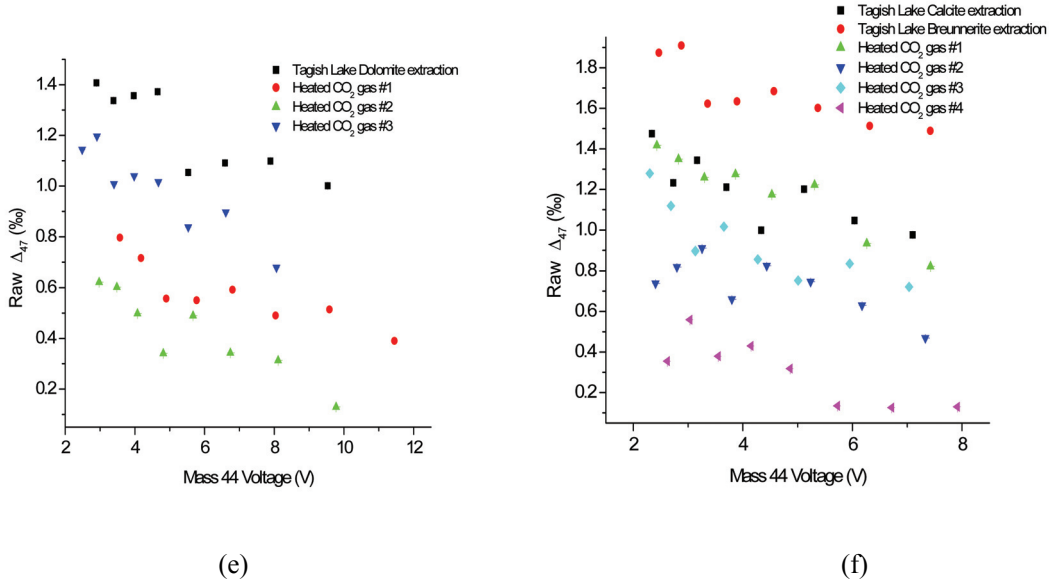


Figure 2-1 Negative correlations between raw Δ_{47} of analyte CO₂ (both meteoritic sample CO₂ and their accompanying heated CO₂ gases) and their mass 44 voltages during the mass spectrometric analyses: (a) GRO 95577 split 2006 extraction; (b) GRO 95577 split 2007 extraction; (c) Orgueil dolomite extraction (gas split 1); (d) Orgueil dolomite extraction (gas split 2); (e) Tagish Lake calcite and breunnerite extractions; (f) Tagish Lake breunnerite extraction. These negative correlations were suspected to be related to a drift in the linearity of the mass spectrometer, and were corrected through a voltage correction procedure before deriving the sample Δ_{47} (section 2.3). Each data point in the figures represents one acquisition (consisting of 10 cycles of sample-standard comparisons) of the mass spectrometric analyses.

which that heated gas was used as a standard). These heated CO₂ gases are used to standardize measurements of the Δ₄₇ value of sample CO₂; they were prepared by heating CO₂ gas of bulk isotopic compositions similar to sample CO₂ at 1000°C to achieve stochastic distribution of all isotopes among all isotopologues (i.e., Δ₄₇=0‰) (see Eiler and Schauble 2004 and Ghosh et al. 2006 for more details). These correlations were not observed in our previous study of carbonates in CM chondrites (Guo and Eiler, 2007), and we suspect they reflect an instrument non-linearity (the appearance of this artifact

coincides with related phenomena, like a dependence of measured Δ_{47} values on the difference in δ^{47} between sample and standard). To correct for these effects, we normalized the raw Δ_{47} of analyte CO₂ to a heated gas standard run at the same sample voltage. The normalization was achieved by first least-squares fitting the observed ‘raw Δ_{47} ’~‘voltage’ correlations with linear functions, and then deriving the normalized Δ_{47} (at 5V) based on the obtained linear functions. We chose 5V as the normalization voltage in our correction because the statistical errors from the least-squares fitting of the “raw Δ_{47} ”~“voltage” correlations near their minimum at this voltage (i.e., because 5V lies in the middle of the voltage range of our analyses, 2.2-9.5V). We evaluated the effects of this voltage correction on the accuracy and precision of our results in section 3.2.

It is also noted that even after our most stringent purification procedures, all samples of CO₂ extracted from the chondrite samples contained detectable levels of contaminants, as monitored by the intensity of the mass-48 ion beam during mass spectrometric analysis.

Values of Δ_{48} for sample gases, defined as $\Delta_{48} = \left(\frac{R_{\text{measured}}^{48}}{R_{\text{stochastic}}^{48}} - 1 \right) \times 1000$, varied up to 4000‰. Past studies of the clumped isotope composition of CO₂ have shown that isobaric interferences at masses 48 and/or 49 can be correlated with isobaric interferences at mass 47, and therefore provide a basis for recognizing samples that are too contaminated for accurate analysis (Eiler and Schauble, 2004). However, we did not observe any consistent correlations between Δ_{47} and Δ_{48} among different samples of CO₂ extracted from carbonaceous chondrites (Fig. 2-2). This suggests that the particular contaminants that are present in these samples are not associated with a significant isobaric interference at masses 44 through 47 and thus do not affect our determination of

sample Δ_{47} . While this conclusion seems supported from our results to-date (figure 2), future measurements of this kind should explore additional methods of sample purification to remove the remaining trace contaminants.

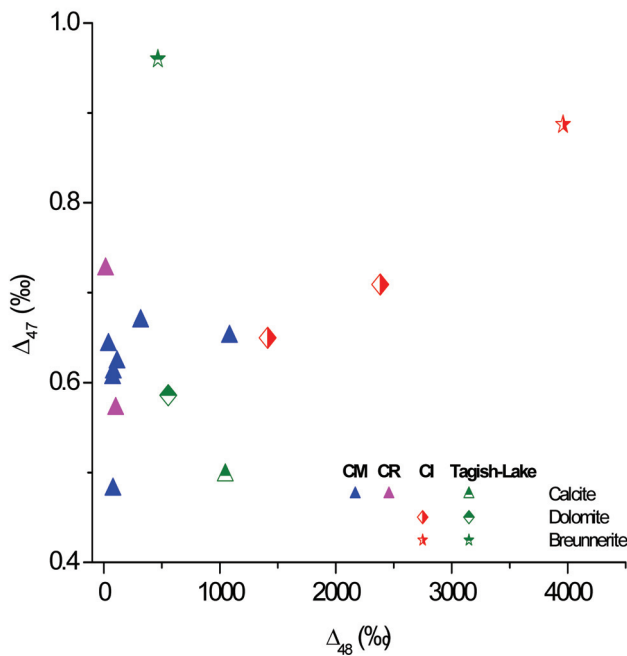


Figure 2-2 Absence of correlations between Δ_{47} and Δ_{48} of meteoritic sample CO₂. Δ_{48} here is an index for the amount of contaminants remaining in the sample CO₂ after extensive purification. The absence of correlation indicates negligible influences of the remaining contaminants on the sample Δ_{47} (see texts for details). Also shown are the Δ_{47} and Δ_{48} of CO₂ derived from phosphoric acid digestion of carbonates in CM chondrites (Guo and Eiler 2007).

2.4 Estimation of carbonate formation temperatures

Determinations of Δ_{47} values of CO₂ derived from phosphoric acid digestion of carbonaceous chondrites enable us to use carbonate clumped isotope thermometry (Ghosh et al., 2006) to estimate the formation temperatures of the carbonate minerals contained within them, and thus the temperatures of at least one stage of the aqueous

alteration of their respective parent bodies (Guo and Eiler, 2007). This approach requires that we know the temperature calibration of the clumped isotope thermometer for each carbonate mineral. This calibration is constrained by experiments and measurements of natural and synthetic materials only for biogenic and inorganic calcite and biogenic aragonite between temperatures of 0 and 50°C (Ghosh et al., 2006; Came et al., 2007; Ghosh et al., 2007). In a recent theoretical study, Guo et al. (2008) predict the temperature dependence of the clumped isotope thermometer for a variety of carbonate minerals (calcite, aragonite, dolomite, magnesite and witherite), by combining previously published theoretical estimations of the ^{13}C - ^{18}O and ^{18}O - ^{17}O clumping effects (representing the two most abundant isotopologues responsible for Δ_{47} anomaly, $^{13}\text{C}^{18}\text{O}^{16}\text{O}^{16}\text{O}^{2-}$ and $^{12}\text{C}^{18}\text{O}^{17}\text{O}^{16}\text{O}^{2-}$) in the carbonate minerals (Schauble et al., 2006) with the estimated fractionations of multiply-substituted isotopologues associated with phosphoric acid digestion of each of these carbonate minerals. The theoretically predicted calibration for calcite exhibits weaker temperature dependence than the experimentally determined calibration, but intersects the experimental calibration line at ~30°C and approximates the trend of experimental data (there is a less than 0.03‰ difference between the two over the temperature range of 10-50°C; Fig. 2-3). This level of disagreement is to be expected when considering the approximations one must make in a purely theoretical treatment, and suggests that the model of Guo et al. (2008) provides a good first-order reference frame for the behavior of isotopic clumping in CO₂ extracted from carbonates by phosphoric acid digestion. Guo et al. (2008) predict that the calibration lines for the calcite, dolomite and magnesite clumped isotope thermometers (i.e., the relationships between Δ_{47} of CO₂ extracted from these minerals and their growth

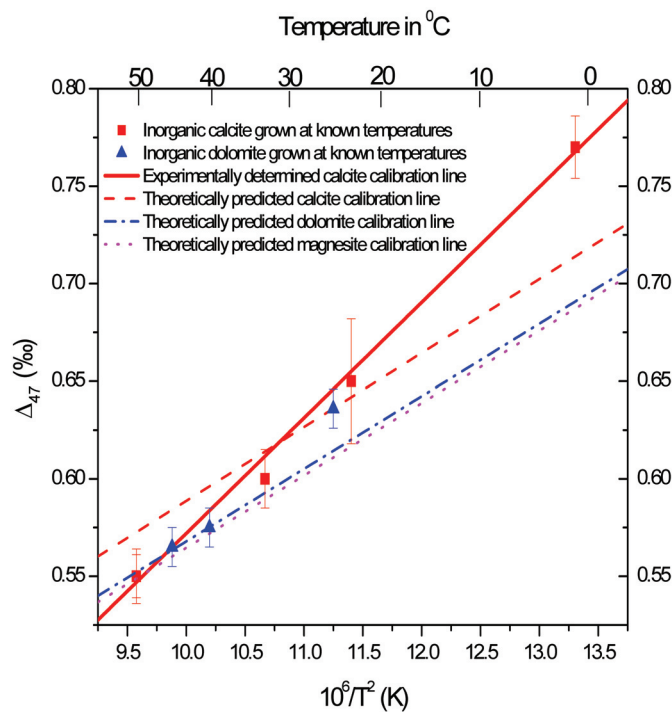


Figure 2-3 Comparison between the experimentally determined Δ_{47} -T calibration line for calcite (Ghosh et al., 2006) and the theoretically predicted Δ_{47} -T calibration lines for calcite, dolomite and magnesite (Guo et al., 2008). Also shown for comparison are the preliminary dolomite Δ_{47} -T calibration data from samples grown and synthesized at known temperatures (triangles; Eiler et al. 2008 and J. Ferry, personal communications).

temperatures) should be similar to each other, with differences less than 0.025‰ among the three at any given temperature. This variation is significant compared to the most precise measurements of Δ_{47} values of CO₂ from carbonates (e.g., Came et al., 2007), but is smaller than the estimated external precision of our measurements of carbonates in carbonaceous chondrites (0.04‰). This predicted similarity among different carbonate minerals is supported by the preliminary data from a recent attempt to experimentally determine the Δ_{47} -T calibration line for dolomite (Eiler et al. 2008 and J. Ferry personal communication). The Δ_{47} derived from inorganic dolomite grown at known temperatures

(45°C, 40°C and 25°C) is almost indistinguishable from the experimentally determined calcite calibration line (Fig. 2-3). Based on these theoretical models and empirical evidence, we therefore adopt the experimentally determined $\Delta_{47}\text{-T}$ calcite calibration line,

$$\Delta_{47} = \frac{0.0592 \times 10^6}{T^2} - 0.02 \quad (\text{T in Kelvin, Ghosh et al. 2006}),$$

to estimate the formation

temperatures for all the carbonate minerals (calcite, dolomite and breunnerite) in the carbonaceous chondrites. Nevertheless, we recognize that future refinements of calibrations for these materials could lead to modest (~5-10°C) changes in the inferred temperatures of dolomite and magnesite growth.

According to the above $\Delta_{47}\text{-T}$ calibration line, the analytical precision from our Δ_{47} analyses (0.04‰, 1 σ ; section 2.3) translates to about $\pm 10^\circ\text{C}$ (1 σ) precision in our estimated carbonate formation temperatures. This is significantly worse than the external precision and calibration accuracy for large, pure samples of calcite and aragonite, but is sufficient for improving our understanding of the thermal histories of carbonaceous chondrites.

3. RESULTS AND DISCUSSION

3.1 Test of the stepped phosphoric acid digestion procedure

Tests of our method of stepped phosphoric acid digestion were conducted on synthetic mixtures of known proportions of calcite and dolomite and of dolomite and magnesite (Table 2-2). The results of these analyses show that this method successfully reproduced the isotopic compositions (including $\delta^{13}\text{C}$, $\delta^{18}\text{O}$ and Δ_{47} values) of the end members, as independently constrained through analyses of pure aliquots of them. In

particular, the differences in Δ_{47} between the calcite and dolomite portions extracted from stepped digestion and their corresponding pure end members are less than 0.02‰ (Table 2-2).

We further evaluate the effectiveness of our stepped extraction method in separating different carbonate end members by calculating the contributions of undesired end members in the stepped-extraction products. For example, the fraction of dolomite that reacted with phosphoric acid during our intended stepped-extraction of calcite from a mixture of calcite and dolomite, $f_{\text{StepCal-Dol}}$, can be computed as:

$$f_{\text{StepCal-Dol}} = \frac{\delta^{13}\text{C}_{\text{StepCal}} - \delta^{13}\text{C}_{\text{Cal}}}{\delta^{13}\text{C}_{\text{Dol}} - \delta^{13}\text{C}_{\text{Cal}}} = \frac{(-41.54) - (-42.37)}{(-0.18) - (-42.37)} = 0.02 ,$$

where $\delta^{13}\text{C}_{\text{StepCal}}$, $\delta^{13}\text{C}_{\text{Cal}}$ and $\delta^{13}\text{C}_{\text{Dol}}$ are the carbon isotopic compositions of the nominal calcite portion of our stepped-extraction, of the pure calcite end member, and of the pure dolomite end member, respectively. Similarly, we can estimate the fraction of calcite that remained in the sample after the ‘calcite’ step and reacted during our intended stepped-extraction of dolomite in a calcite-dolomite mixture mixture ($f_{\text{StepDol1-Cal}}$), or the fraction of magnesite reacted during our intended stepped-extraction of dolomite from a mixture of dolomite and magnesite mixture, $f_{\text{StepDol2-Mag}}$:

$$f_{\text{StepDol1-Cal}} = \frac{\delta^{13}\text{C}_{\text{StepDol1}} - \delta^{13}\text{C}_{\text{Dol}}}{\delta^{13}\text{C}_{\text{Cal}} - \delta^{13}\text{C}_{\text{Dol}}} = \frac{(-2.38) - (-0.18)}{(-42.37) - (-0.18)} = 0.05$$

$$f_{\text{StepDol2-Mag}} = \frac{\delta^{13}\text{C}_{\text{StepDol2}} - \delta^{13}\text{C}_{\text{Dol}}}{\delta^{13}\text{C}_{\text{Mag}} - \delta^{13}\text{C}_{\text{Dol}}} = \frac{(-0.10) - (-0.18)}{(1.60) - (-0.18)} = 0.04 ,$$

where $\delta^{13}\text{C}_{\text{StepDol1}}$ and $\delta^{13}\text{C}_{\text{StepDol2}}$ are the carbon isotopic compositions of the nominal dolomite portion from our stepped-extraction of a mixture of calcite and dolomite, and of the nominal dolomite portion from our stepped-extraction of a mixture of dolomite and

magnesite, respectively. $\delta^{13}\text{C}_{\text{Mag}}$ is the carbon isotopic compositions of the pure magnesite end member; this is assumed to be the same as the carbon isotopic composition of nominal magnesite portion from our stepped-extraction of the mixture of dolomite and magnesite since we didn't determine the isotopic composition of the pure magnesite end member directly due to limited available amounts of magnesite powders. This is an obvious weakness in our tests of the stepped extraction methodology, and should be addressed by repeating the stepped extraction procedure on synthetic mixtures that include well characterized magnesite. Nevertheless, the results of these experiments on synthetic mixtures of carbonates are consistent with the conclusion that our stepped-extraction method is $\geq 95\%$ efficient at isolating each target carbonate phase.

Finally, one more constraint on the effectiveness of our stepped-extraction method comes from the yields of CO_2 at each extraction step. For example, the first step of our stepped-extraction of the calcite-dolomite mixture yielded 1.08 times the amount of CO_2 as the second step. This difference is very nearly equal to the ratio of the amounts of calcite and dolomite present within the mixture (7.06 mg of calcite vs. 6.94 mg of dolomite, corresponding to a carbon equivalent molar ratio of 1.07).

3.2 Temperature of carbonate growth in the carbonaceous chondrites

The apparent temperatures of carbonate formation ($\pm 10^\circ\text{C}$, 1σ) implied by our measurements of carbonaceous chondrites are: 8 to 43°C for calcite in GRO 95577; 18°C for dolomite and -20°C for breunnerite in Orgueil; 65°C for calcite, 39°C for dolomite and -31°C for breunnerite in Tagish Lake (Table 2-1). Our estimated formation temperatures for breunnerite in Orgueil and calcite and breunnerite in Tagish Lake are

beyond the temperature range of experimental calibration of the carbonate clumped isotope thermometer (0-50°C; Gosh et al., 2006). However, theoretical calculations (as those employed in Schauble et al. 2006) indicate the temperature dependences of Δ_{47} in carbonate systems remain almost the same over the temperature range of our interest, -30 to 70°C; therefore, we estimate that extrapolation of the experimentally determined predicted relationship between ^{13}C - ^{18}O clumping effects in carbonate minerals and temperature from the constrained range of 0-50°C to the wider range of -30°C and 70°C leads to less than 0.02‰ errors in Δ_{47} (E. Schauble, personal communications). Therefore our extrapolation of experimentally determined Δ_{47} -T calibration line does not introduce a significant additional error in our temperature estimates.

Our estimated alteration temperatures, though consistent with previous estimations of alteration temperatures on the parent bodies of CR chondrite (<150°C, Zolensky et al. 1993), CI chondrite (<50°C, Leshin et al. 1997; 50-150°C, Zolensky et al. 1993; 150°C, Clayton and Mayeda 1984, 1999) and Tagish Lake (50-100°C, Leshin et al., 2001), lie mostly at the low temperature ends of previous estimations. We suspect this reflects the inaccuracy of some of the assumptions made in previous studies,. For example, Clayton and Mayeda (1984) extrapolated their aqueous alteration model for CM chondrites to CI chondrites, assuming the anhydrous minerals (olivines and pyroxenes, precursor to aqueous alteration) in CI chondrites have the same oxygen isotope compositions as those in CM chondrite, and suggested that CI chondrite parent bodies have experienced aqueous alterations of higher temperatures than CM chondrite parent bodies (150°C vs. <20°C; Clayton and Mayeda 1984, 1999). However, later ion microprobe analyses of oxygen isotopes in single olivine and pyroxene grains separated from CI chondrites

(Orgueil and Ivuna) demonstrated the above assumption was invalid; the anhydrous minerals in CI chondrites are instead more ^{16}O -depleted than those in CM chondrites (Murchison) (Leshin et al., 1997). With the newly determined oxygen isotope compositions of anhydrous minerals in CI chondrites, Leshin et al. (1997) revised the Clayton and Mayeda (1984)'s aqueous alteration model, and estimated the alteration temperature on CI chondrite parent bodies to be less than 50°C. This revised estimation on alteration temperatures for CI chondrites agrees well with our estimated formation temperatures for dolomite in Orgueil ($18\pm10^\circ\text{C}$, 1σ).

Overall, our estimated alteration temperatures for GRO 95577, Orgueil and Tagish Lake, are within or below those estimated for CM chondrites (20 to 71°C, also based on carbonate clumped isotope thermometry; Guo and Eiler 2007). The similarity of alteration temperatures among different groups of carbonaceous chondrites precludes alteration temperature variations as the principle cause of differences in their extents of alteration, and suggests instead other factors such as water/rock ratio and/or duration of aqueous alteration exerting greater control. This suggestion is consistent with results from recent aqueous alteration model on carbonaceous chondrite parent bodies (Young, 2001; J. Palguta, 2007), where regions with high flux of fluid flow on the carbonaceous parent bodies demonstrate most intense alterations.

One surprising finding from this study is the sub-zero formation temperatures (-20°C and -31°C respectively, $\pm10^\circ\text{C}$, 1σ) we estimated for breunnerite in Orgueil and Tagish Lake. This is in contrast with the common belief that all carbonates in carbonaceous chondrites precipitated from liquid water at temperatures above 0°C, and suggests the existence of low temperature brines on the parent bodies of the carbonaceous chondrites.

The eutectic temperatures for the NaCl-H₂O, NaCl-KCl-H₂O, NaCl-MgCl₂-H₂O and NaCl-CaCl₂-H₂O systems are -21.2°C, -22.9°C, -35°C, and -52°C, respectively (Spencer et al. 1990) or ammonia–water mixtures (eutectic temperatures of -97°C; Gaspatrik 2003). Thus, our data suggest that the pore fluids present during the very last stages of aqueous alteration of the carbonaceous chondrites were rich in salt and/or ammonia. Note that, although increases of pressures (e.g., through impact) could also permit the existence of pure liquid water at these low temperatures (as low as -22°C at pressure of 209.9MPa; IAPWS 1993), the sustained presence of water in the liquid form as required by the formation of breunnerite make this a less likely possibility.

Formation of brine-like fluid on carbonaceous chondrite parent bodies has previously been proposed, based on the very high Na/Ca ratios (and possibly high absolute concentrations of Na) inferred for the carbonate-forming fluid (Riciputi et al., 1994). Recent discoveries of fluid inclusions bearing halite [NaCl] and sylvite [KCl] in Monahans 1998 and Zag regolith breccias (two metamorphosed H5 chondrites; Zolensky et al. 1999, Rubin et al. 2002) provides more direct evidence for the presence of brines on chondrite parent bodies. These halides are found in highly metamorphosed meteorites, but are thought to have formed on other bodies at low temperature (<100°C and <70°C respectively) and became incorporated into these H5 chondrite parent bodies as part of petrographically distinct clasts, e.g., the CI clast in Zag (Zolensky et al., 1999; Bridges et al., 2004; Zolensky et al., 2008). Furthermore, Zolenky et al. (1999) demonstrated that the fluid inclusions in Monahans 1998 have eutectic temperatures of ~ -40°C, indicating they may contain divalent cations such as Fe²⁺, Ca²⁺, Mg²⁺, in addition to Na⁺ and K⁺. This is consistent with our above proposal that the parent fluid from which the last

generations carbonates in carbonaceous chondrite precipitated was a brine. Detailed examination of CI clasts in Zag (the potential sources of halite) did reveal the presence of aggregates of Ca-Mn-Mg-Na carbonates inside the clast, along with other secondary minerals such as magnetite, pyrrhotite and phyllosilicates (Zolensky et al., 2003). Future studies should aim to characterize the isotopic and trace element compositions of these carbonates and test them further against our hypothesis of that breunnerite in these meteorites formed from low temperature brines.

The fact that breunnerite in the carbonaceous chondrites formed at temperatures as low as -31°C doesn't necessarily imply the aqueous alteration of silicate minerals on the carbonaceous chondrite parent bodies was active at these temperatures. It is also possible (and perhaps more likely) that breunnerites precipitated from brines after the silicate-alteration reaction had already ceased (due to the slow kinetics under such low temperatures).

As discussion in section 2.3, the sample Δ_{47} used in the above temperature estimations were derived after a voltage correction, to account for the observed negative correlations between the raw Δ_{47} of sample CO₂ and the mass 44 voltages at which the raw Δ_{47} was obtained during our mass spectrometric analyses. Here, we evaluate the effects of the voltage correction on our results by recalculating the carbonate formation temperatures, 1) without any voltage correction (i.e., using the average raw Δ_{47} of analyte CO₂ in the standardization of the Δ_{47} of sample CO₂); 2) with voltage correction at the mass 44 voltage of 7V (Table 2-3). For all the meteorite samples we analyzed, the above two approaches yielded carbonate formation temperatures only 2-26°C different from our

Table 2-3 Effects of voltage correction on the estimations of carbonate formation temperatures and of the oxygen isotope compositions of alteration fluid.

Sample		GRO 95577 (split 2006)		GRO 95577 (split 2007)		Orgueil		Tagish Lake	
Petrology	Type	CR1	CR1	Calcite	Dolomite	Breunnerite	Calcite	Dolomite	Breunnerite
Carbonate Mineralogy									
$\Delta_{47}(\text{\textperthousand})$	0.726	0.571	0.709	0.650	0.887	0.497	0.586	0.960	
Voltage Correction at 5V	Temperature (°C)	8	43	12	24	-20	65	39	-31
	$\delta^{18}\text{O}_{\text{water}}(\text{\textperthousand})$	-12.3	-7.1	-5.3	-2.7	-29.7	11.8	5.8	-18.6
	$\delta^{17}\text{O}_{\text{water}}(\text{\textperthousand})$	-7.3	-4.6	-2.2	-0.9	-14.9	7.6	4.8	-7.6
No Voltage Correction	$\Delta_{47}(\text{\textperthousand})$	0.739	0.583	0.699	0.662	0.899	0.589	0.648	1.036
	Temperature (°C)	6	40	14	21	-19	39	25	-36
	$\delta^{18}\text{O}_{\text{water}}(\text{\textperthousand})$	-12.9	-7.7	-4.8	-3.2	-29.5	7.3	2.9	-20.2
	$\delta^{17}\text{O}_{\text{water}}(\text{\textperthousand})$	-7.6	-4.9	-2.0	-1.2	-14.8	5.2	3.4	-8.4
Voltage Correction at 7V	$\Delta_{47}(\text{\textperthousand})$	0.720	0.555	0.737	0.583	0.876	0.492	0.584	0.982
	Temperature (°C)	10	48	6	40	-18	67	40	-34
	$\delta^{18}\text{O}_{\text{water}}(\text{\textperthousand})$	-12.1	-6.3	-6.6	0.4	-29.1	12.1	5.8	-19.6
	$\delta^{17}\text{O}_{\text{water}}(\text{\textperthousand})$	-7.2	-4.2	-2.9	0.7	-14.6	7.7	4.9	-8.1

preferred approach (i.e., voltage normalization at 5V). The difference is the biggest for calcite in Tagish Lake: its formation temperature estimated without any voltage correction is 26°C lower than what estimated from our preferred approach (39°C v.s. 65°C). For all the other samples, the differences in estimated formation temperatures from different approaches are less than 16°C without any systematic trends. These differences in temperature estimations are within or close to the external errors typical of our analyses ($\pm 10^\circ\text{C}$, 1σ).

3.3 Isotopic compositions of the alteration fluid

$\delta^{13}\text{C}_{\text{VPDB}}$ and $\delta^{18}\text{O}_{\text{VSMOW}}$ values of carbonates in the carbonaceous chondrites we examined vary from 40.42‰ to 73.37‰ and 17.82‰ to 36.70‰ respectively (Table 2-1), and fall within or close to the values from previous isotopic studies of carbonates in Orgueil and Tagish Lake (phosphoric acid digestion, Grady et al., 1998 and Leshin et al., 2001; ion microprobe, Zito et al., 1998, Engrand et al., 2001a and Engrand et al., 2001b). Our results are consistent with previous ion microprobe observations by Zito et al. (1998), which revealed that isotopic compositions (both $\delta^{13}\text{C}_{\text{VPDB}}$ and $\delta^{18}\text{O}_{\text{VSMOW}}$) of carbonates in Orgueil decrease in the order of dolomite and breunnerite (67.52‰ vs. 40.42‰ in $\delta^{13}\text{C}_{\text{VPDB}}$, and 28.95‰ vs. 21.08‰ in $\delta^{18}\text{O}_{\text{VSMOW}}$). This study constitutes the first isotopic study of carbonates in GRO 95577, showing $\delta^{13}\text{C}_{\text{VPDB}}$ of 69.91‰ and 70.91‰ and $\delta^{18}\text{O}_{\text{VSMOW}}$ of 17.82‰ and 19.62‰, respectively for the two GRO 95577 splits we analyzed. Note that $\delta^{13}\text{C}_{\text{VPDB}}$ values of most carbonates studied here cluster around 70‰ (ranging from 67.52‰ to 73.37‰), except for the breunnerite in Orgueil which has a significantly lower $\delta^{13}\text{C}_{\text{VPDB}}$ of 40.42‰.

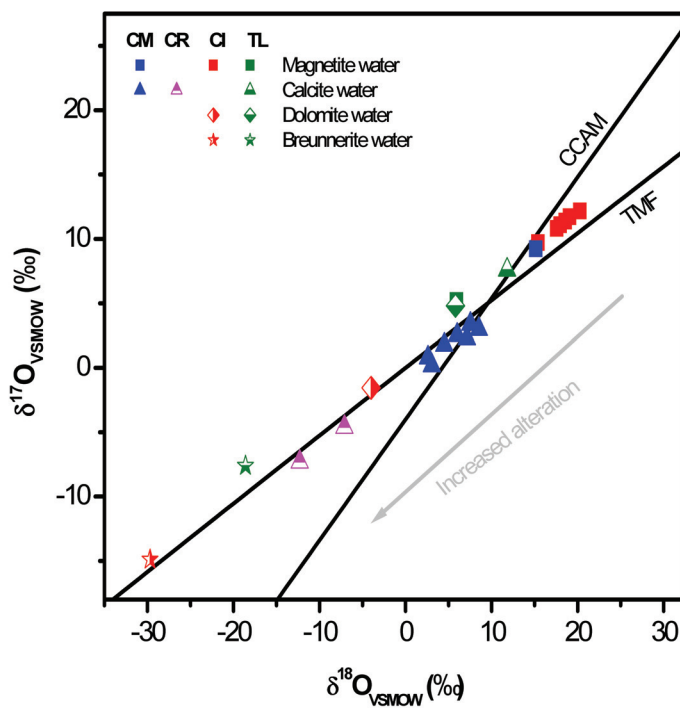


Figure 2-4 Oxygen isotope compositions (all values reported vs. VSMOW) of water in equilibrium with carbonaceous chondrite carbonates at their known growth temperatures (Guo and Eiler 2007 and this study). Also shown for comparison are the oxygen isotope compositions of the water in equilibrium with magnetites in CM and CI chondrites and in Tagish Lake (TL) (squares, estimated from $\delta^{18}\text{O}_{\text{VSMOW}}$ of magnetites reported in Rowe et al. 1994 and Engrand et al. 2001b, with an equilibrium fractionation factor of $-13\text{\textperthousand}$ between magnetite and water). The terrestrial mass fractionation line ('TMF') and carbonaceous chondrite anhydrous mineral line ('CCAM') are shown for reference.

We estimated $\delta^{18}\text{O}_{\text{VSMOW}}$ values of the fluids from which these carbonates grew by combining the carbonate formation temperatures established by clumped isotope thermometry with the temperature-dependent carbonate-water oxygen isotope fractionations established by previous studies—either experimental (for calcite, Kim and O’Neil 1997; and dolomite, Vasconcelos et al. 2005) or theoretical (for magnesite,

Rosenbaum 1997 and Schable et al. 2006). These data and experiments constrain the water from which carbonates grew to have $\delta^{18}\text{O}_{\text{SMOW}}$ values of: -12.3‰ to -7.1‰ for calcite in GRO 95577; -4.0‰ for dolomite and -29.7‰ for breunnerite in Orgueil; and 11.8‰ for calcite, 5.8‰ for dolomite and -18.6‰ for breunnerite in Tagish Lake ($\pm 2\%$, 1σ ; Table 2-1, Fig. 2-4). Assuming that the carbonates we analyzed have $\Delta^{17}\text{O}$ values equal to the averages previously determined by Leshin et al. (2001) and Clayton and Mayeda (1999), our results indicate that the $\delta^{17}\text{O}$ values of waters from which carbonates grew varied between -14.9‰ and 7.6‰.

Again, our estimated formation temperatures for breunnerite in Orgueil and Tagish Lake (-20°C and -31°C, respectively) is beyond the temperature range of theoretically estimated magnesite-water oxygen isotope fractionation relationship (valid $\geq 0^\circ\text{C}$; Rosenbaum 1997 and Schable et al., 2006), forcing us to extrapolate that trend to arrive at an estimated $\delta^{18}\text{O}$ value for water. This extrapolation is justified by the general invariance of temperature-dependence of oxygen isotope fractionations over this temperature range. In addition, our suggestion that breunnerite precipitated from low temperature brines containing divalent cations such as Ca^{2+} and Mg^{2+} (section 3.2), raises the possibility of an oxygen isotope ‘salt effect’ (Horita, 2005) during carbonate precipitation (that is, a dependence of the carbonate-water oxygen isotope fractionation on the salinity of the solution). Consideration of these isotope salt effects would tend to increase our estimated oxygen isotope compositions of alteration fluids (Horita, 2005). The exact magnitude of the effect depends on the cation compositions of the brine (especially concentrations of Ca^{2+} and Mg^{2+}), and could be as much as several per mil (Horita, 2005). For example, for brines with the same cation composition as the eutectic

point of NaCl-MgCl₂-H₂O system (1.10mol NaCl and 2.48mol MgCl₂ per kg H₂O; Spencer et al., 1990), an oxygen isotope salt effect of -2.7‰ is expected at 25°C (Horita, 2005).

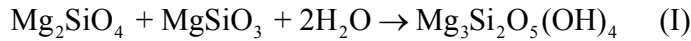
The matrices of carbonaceous chondrites are also rich in a variety of secondary phases (i.e., aqueous alteration products) other than carbonates, such as magnetite and phyllosilicates (Brearley and Jones, 1998). The oxygen isotope compositions of these phases must also reflect the conditions of aqueous alterations and the $\delta^{18}\text{O}$ values of alteration fluid, though they may have grown at temperatures different from those of carbonate precipitation, and these phases are less likely than carbonates to fully equilibrate with co-existing fluid. Nevertheless, we can examine the plausibility of the fluid $\delta^{18}\text{O}$ values we established through carbonate clumped isotope measurements by estimating the oxygen isotope compositions of alteration fluids from which magnetite formed. We adopt previously measured oxygen isotope compositions of magnetites in CI and CM chondrites (Rowe et al., 1994) and in Tagish Lake (Engrand et al., 2001b), and assume an oxygen isotope fractionation of -13‰ between magnetite and water (Rowe et al., 1994). We didn't include in our discussion the oxygen isotope compositions of meteorite matrix water (extracted through stepped pyrolysis of bulk meteorite samples), due to the large uncertainties associated with the nature of the extracted water and thus with the quantitative interpretations of their isotopic compositions (Baker et al., 2002).

Over all, these estimated $\delta^{18}\text{O}$ and $\delta^{17}\text{O}$ for the alteration fluids within each carbonaceous chondrite group are all significantly lower than those estimated for their respective primary water (Clayton and Mayeda, 1999), and decrease in the order of magnetite > calcite > dolomite > breunnerite in CI and CM chondrites and in the order of

calcite > dolomite ~magnetite > breunnerite in Tagish Lake (Fig. 4). The differences in isotopic composition between the model reactant water and that water from which secondary mineral phases grew are consistent with the expectation that water evolves toward lower $\delta^{18}\text{O}$, $\delta^{17}\text{O}$, and $\Delta^{17}\text{O}$ as a result of reaction with host rock (Clayton and Mayeda, 1999; Guo and Eiler, 2007).

3.4 Implications for the chemical and thermal evolution of the carbonaceous chondrite parent bodies

In this section, we develop a general interpretation of our results in the context of a quantitative model for the aqueous alteration of carbonaceous chondrites that was previously developed for CM chondrites (Guo and Eiler, 2007). This model approximates aqueous alteration of the carbonaceous chondrite parent bodies as a serpentinization reaction (Clayton and Mayeda, 1999; Eiler and Kitchen, 2004; Guo and Eiler, 2007):



The oxygen isotopic composition of the alteration fluid is influenced by the progress of this reaction, evolving toward lower $\delta^{18}\text{O}$ and $\delta^{17}\text{O}$ as the reaction proceeds. The isotopic evolution of alteration fluid can be evaluated through the relations (Clayton and Mayeda, 1999; Guo and Eiler, 2007):

$$\delta^{18}\text{O}_{w,f} = \frac{\delta^{18}\text{O}_{w,i} + (\delta^{18}\text{O}_{r,i} - \frac{9}{7}\Delta^{18}\text{O}_{s-w}) p}{1 + p} \quad (1)$$

$$\delta^{17}\text{O}_{w,f} = \frac{\delta^{17}\text{O}_{w,i} + (\delta^{17}\text{O}_{r,i} - \frac{9}{7}\Delta^{17}\text{O}_{s-w}) p}{1 + p} \quad (2)$$

$$\Delta^{17}\text{O}_{w,f} = \left(\frac{1 + \delta^{17}\text{O}_{w,f}/1000}{(1 + \delta^{18}\text{O}_{w,f}/1000)^{0.5164}} - 1 \right) \times 1000 \quad (3)$$

where $\delta^{18}\text{O}_{w,f}$, $\delta^{17}\text{O}_{w,f}$ and $\Delta^{17}\text{O}_{w,f}$ denote the oxygen isotopic composition of the aqueous fluid; $\delta^{18}\text{O}_{w,i}$, $\delta^{17}\text{O}_{w,i}$ and $\delta^{18}\text{O}_{r,i}$, $\delta^{17}\text{O}_{r,i}$ denote the initial (i.e., before the aqueous alteration) oxygen isotopic compositions of the aqueous fluid and the anhydrous reactant minerals; $\Delta^{18}\text{O}_{s-w}$ and $\Delta^{17}\text{O}_{s-w}$ are the oxygen isotope fractionations between serpentine and water at the temperatures of alteration (Wenner and Taylor, 1971); ‘p’ is the reaction progress parameter (Clayton and Mayeda, 1999; Guo and Eiler, 2007), denoting the ratio of moles of oxygen in the reacted rock to moles of oxygen in initial water. ‘p’ ranges from 0 to 3.5; a value of 0 corresponds to the absence of alteration reaction, and a value of 3.5 corresponds to the maximum extent of alteration (i.e., all water has been consumed in the alteration reaction I).

The initial oxygen isotope compositions of the anhydrous minerals in the evolution models (i.e., $\delta^{18}\text{O}_{r,i}$ and $\delta^{17}\text{O}_{r,i}$) were taken as the averages determined from previous studies (CM chondrite, Clayton and Mayeda 1999; CR chondrite, Clayton and Mayeda 1999; CI chondrite, Leshin 1997). The initial oxygen isotope compositions of the alteration fluid (i.e., $\delta^{18}\text{O}_{w,i}$, $\delta^{17}\text{O}_{w,i}$), for CM, CI and CR chondrites were adopted from the values estimated in Clayton and Mayeda (1999) following a two-stage exchange model (Clayton and Mayeda, 1984). Note that, there are no available estimations of the initial oxygen isotope compositions of the alteration fluid for Tagish Lake. Our attempts to derive the value ourselves, following the same aqueous alteration model as in Clayton and Mayeda (1984, 1999) and using the experimentally determined isotopic compositions of different phases in Tagish Lake (anhydrous minerals, Leshin et al., 2001, Engrand et

al., 2001a; matrix, Engrand et al., 2001a; carbonate formation water, this study), yielded a water/rock ratio that exceeds the limit of Clayton and Mayeda (1984) model (4.64 v.s. limit of 3.76). We suspect two factors might have contributed to this complication: (1) the experimental uncertainties associated with the oxygen isotope compositions of anhydrous minerals and matrix in Tagish Lake, both of which were determined with ion microprobe with 1~2‰ uncertainties in $\delta^{17}\text{O}$ and $\delta^{18}\text{O}$; and, (2) the complex lithologies present in Tagish Lake — the dominant carbonate poor lithology vs. the less abundant carbonate-rich lithology (Zolensky et al., 2002). It is not certain whether these two lithologies are genetically related to each other (Zolensky et al., 2002) and whether they went through aqueous alterations from the same water reservoirs (Baker et al., 2002). Therefore, an accurate modeling of the alteration reaction on Tagish Lake parent body should make sure the isotopic compositions of the anhydrous minerals, of matrix and carbonate formation water employed in the model come all from the same lithology. This however seems impossible at this moment due to absence of such complete dataset for Tagish Lake. We therefore focus on the discussion of forward models for CM CR and CI chondrite parent bodies in this study.

The temperatures of aqueous alteration on the carbonaceous chondrite parent bodies changed over the course of alterations, as evidenced by the variations of carbonate formation temperatures within the same chondrite sample (section 3.2). Ideally, we should quantitatively incorporate these temperature changes into our model (e.g., as functions of reaction progress). However, given the absence of any independent quantitative constraints on the co-variations of alteration temperature and reaction progress, such a treatment is out of the range of this study. Instead, in our current model

we assume the alteration temperature to be the average of our estimated carbonate formation temperatures for each chondrite (or chondrite group), and remain constant throughout the aqueous alteration. For the purpose of comparison, we also ran our models at different alteration temperatures, covering the full range of carbonate formation temperatures observed in each chondrite group (dotted lines in Fig. 2-5). Fortunately, the general evolution trends of oxygen isotope composition of the alteration fluid are not sensitive to alteration temperatures (Fig. 2-5), and thus our model results are not systematically biased by the above simplification. We summarize all the parameters employed in our model in Table 2-4.

We observe good agreement between most of experimentally estimated isotopic compositions of alteration fluids (including those estimated based on magnetite $\delta^{18}\text{O}$, carbonate $\delta^{18}\text{O}$ and growth temperature) and those predicted by the forward models (Fig. 2-5): the experimentally estimated oxygen isotopic compositions of alteration fluids lie on or very close to the predicted trend of evolving water oxygen isotope composition. However, our estimated oxygen isotopic compositions of alteration fluids for calcite formation in one split of GRO9557 (split 2006) and breunnerite formation in Orgueil fall beyond the total range of $\delta^{18}\text{O}$ expected from the forward model of aqueous alteration (i.e., requiring $p>3.5$). This implies that the aqueous alteration had reached the maximum extent on the parent bodies of GRO 95577 and Orgueil, consistent with previous petrographic studies on these two meteorites and their classification as petrographic type 1 carbonaceous chondrites (Brearley and Jones, 1998; Weisberg and Prinz, 2000). At the same time, this observation also suggests processes other than alteration reactions affected the oxygen isotopic compositions of the alteration fluids. Given that the

Table 2-4 Forward evolution models for the oxygen isotope compositions of the alteration fluid on CM, CR and CI carbonaceous chondrite parent bodies.

		CM chondrite	CR chondrite	CI chondrite
Initial Water ^{&}	$\delta^{18}\text{O}_{\text{water}} (\text{\textperthousand})$	28.1	28.1	23.4
	$\delta^{18}\text{O}_{\text{water}} (\text{\textperthousand})$	17.7	17.7	13.9
	$\Delta^{17}\text{O}_{\text{water}} (\text{\textperthousand})$	3.2	3.2	1.9
Mean	$\delta^{18}\text{O}_{\text{water}} (\text{\textperthousand})$	-4.2	-1	4.8
Anhydrous Solids ^{&}	$\delta^{18}\text{O}_{\text{water}} (\text{\textperthousand})$	-7.4	-2.8	1.8
	$\Delta^{17}\text{O}_{\text{water}} (\text{\textperthousand})$	-5.2	-2.3	-0.7
Alteration Temperature [◊] (°C)		28	25	5
Serpentine/water fractionation ^{&}	$\Delta^{18}\text{O}_{\text{s-w}} (\text{\textperthousand})$	12.5	12.8	15.5
	$\Delta^{17}\text{O}_{\text{s-w}} (\text{\textperthousand})$	6.4	6.6	8.0
Alteration fluid ^ξ	Essebi Magnetite (average)	CM Calcite Split 2006	GRO 95577 Calcite Split 2007	CI Magnetite (average)
Reaction progress ^ξ (p)	0.4	0.96	N/A	0.2
				2.5
				N/A

[&] The oxygen isotope compositions of the initial water and anhydrous solids are derived from previous studies of carbonaceous chondrites (Clayton and Mayeda 1999, Leshin et al. 1997, Engrand et al. 2001a, Leshin et al. 2001 and this study; see text and Appendix for details); The oxygen isotope fractionations between serpentine and water at the selected alteration temperatures are derived from (Wenner and Taylor 1971).

[◊] Alteration temperatures are assumed to be the average formation temperatures of carbonate minerals in carbonaceous chondrites (Guo and Eiler 2007, and this study)

^ξ The progress of alteration reactions at the formation of different secondary phases in the carbonaceous chondrite matrix, estimated from experimentally determined oxygen isotope compositions of the corresponding alteration fluids. 'N/A' denotes cases where the experimentally determined oxygen isotope compositions of the alteration fluid fall out of the predictions from our forward evolution models (see text for details).

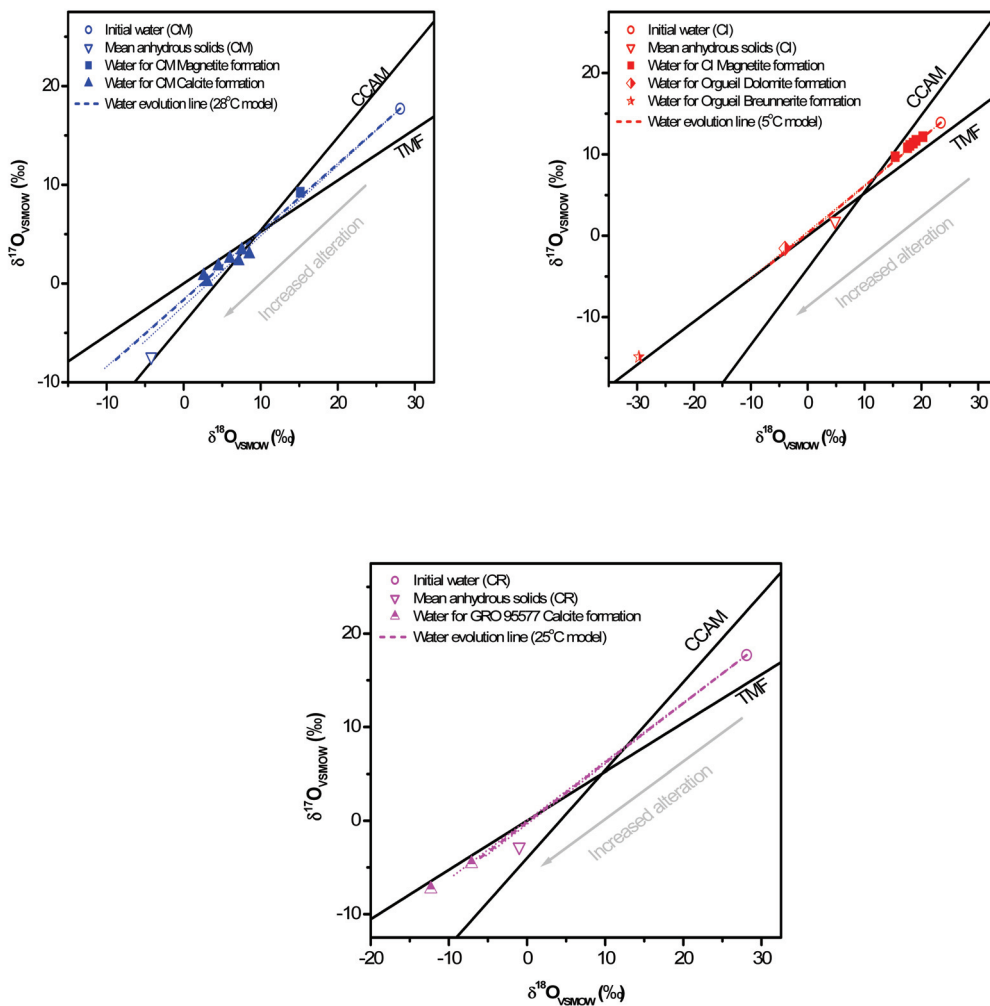


Figure 2-5 Comparison between the experimentally estimated oxygen isotope compositions of alteration water with those calculated by the forward model of aqueous alteration: (a) CM chondrite; (b) CI chondrite; (c) CR chondrite. The temperatures of water-rock reaction are assumed to be the average formation temperatures of carbonate minerals in carbonaceous chondrites. The open squares and inverted triangles shows the location of estimated initial water and typical anhydrous solids for each group of carbonaceous chondrites (Table 2-4). Dotted lines represent the model results with temperatures of water-rock reactions set at the lowest (upper dotted line) and highest (lower dotted line) formation temperatures observed for carbonates in each chondrite group. Model results with different alteration temperatures (dashed lines and dotted lines) closely resemble each other, suggesting the general evolution trend of oxygen isotope compositions of the alteration fluid is not very sensitive to the alteration temperatures. The terrestrial mass fractionation line ('TMF') and carbonaceous chondrite anhydrous mineral line ('CCAM') are shown for reference.

estimated formation temperatures for calcite in GRO 95577 (split 2006) and breunnerite in Orgueil ($6\pm10^{\circ}\text{C}$ and $-20\pm10^{\circ}\text{C}$, 1σ , respectively) are either very close to or below the freezing point of water, we propose partial freezing of the alteration fluids during late stages of aqueous alteration lead to further depletion in their $\delta^{18}\text{O}$. For example, with Rayleigh distillation isotope fractionation during ice formation (i.e., gradual freezing with isotopic equilibrium maintained between the newly formed ice and residual water at all times), depletions as much as $7.1\text{\textperthousand}$ in the $\delta^{18}\text{O}$ of the residual water can be expected when 90% of water freezes into water ice (O’Neil, 1968). The freezing induced reduction in the $\delta^{18}\text{O}$ value of alteration fluids is also consistent with the observation that the relatively large changes in $\delta^{18}\text{O}$ at the end of the alteration process (i.e., at low T and $\delta^{18}\text{O}$ of water) were accompanied by smaller changes in fluid $\Delta^{17}\text{O}$ than those expected to result from reactions with host rock, e.g., $0.05\text{\textperthousand}$ and $0.22\text{\textperthousand}$ variations in $\Delta^{17}\text{O}$ vs. $26\text{\textperthousand}$ and $24.4\text{\textperthousand}$ variations in $\delta^{18}\text{O}$ between dolomite and breunnerite in Orgueil and Tagish Lake respectively (Leshin et al. 2001 and this study).

In the context of the aqueous alteration model we presented above (i.e., higher extents of alteration correspond to lower $\delta^{18}\text{O}$ values of the fluid), our results imply that magnetite and carbonates formed in the order of magnetite > calcite > dolomite > breunnerite during aqueous alteration of carbonaceous chondrites parent bodies. This is consistent with previous studies of $\Delta^{17}\text{O}$ for magnetite and carbonates in carbonaceous chondrites (magnetites have higher $\Delta^{17}\text{O}$ than carbonates inside CM and CI chondrites; Rowe et al., 1994 and Engrand et al. 2001b), and with the formation sequences determined for magnetite and different types of carbonates in CM chondrites (carbonate Mn/Cr chronometry, Brearley and Hutcheon 2000, Brearley et al. 2001) and CI

chondrites (magnetite Xe-I chronometry, Pravdivtseva et al. 2003; carbonate cation chemistry, Endress and Bischoff 1996; carbonate Mn/Cr chronometry, Hoppe et al. 2007; carbonate Rb/Sr chronometry, Macdougall 2000). In addition, based on Xe-I chronometry halites in Monahans 1998 and Zag regolith breccias were estimated to formed at ~4559Ma (i.e., 8.2 Myrs after formation of CAIs in CV chondrites; Busfield et al. 2004). These halite formation ages are significantly older than most secondary mineral phases in carbonaceous chondrite (Fig. 2-7), consistent with our proposition that they formed at late stages of aqueous alteration from aqueous brines.

The reaction progress ('p') corresponding to different alteration fluids range from 0.2 to 3.4, respectively for magnetite and carbonate formation in different carbonaceous chondrites (Table 2-4). In particular, the reaction progresses estimated for calcite in GRO 95577 ($p=3.4$) lies almost at the maximum value plausible for p in our model ($p=3.5$). This suggests, calcite in GRO95577 formed at the very last stages of the aqueous alteration on its parent body.

Combined with our estimated carbonate formation temperatures (Guo and Eiler 2007 and this study), these observations suggest that the carbonaceous chondrite parent bodies were cooling as aqueous alteration proceeded (Fig. 2-6). This conclusion is consistent with Guo and Eiler (2007)'s previous inference based on the variations of carbonate formation temperatures and $\delta^{18}\text{O}$ of the alteration fluid among different splits of Cold Bokkeveld. We quantify the rate of cooling on the carbonaceous chondrite parent bodies by combining our estimated carbonate formation temperatures with their formation ages determined in previous Mn-Cr chronometry studies (Brearley et al., 2001; Krot et al., 2006; Hoppe et al., 2007). All the Mn-Cr chronometric ages were

(re)normalized with the angrite Lewis Cliff (LEW) 86010 as the time anchor ($^{53}\text{Mn}/^{55}\text{Mn}$ ratio of $1.25 \pm 0.07 \times 10^{-6}$ and absolute Pb-Pb age of $4557.8 \pm 0.5\text{ Ma}$; Lugmair and Galer 1992), following conventions from previous studies (Lugmair and Shukolyukov, 1998; Krot et al., 2006; Hoppe et al., 2007). A half-life time of 3.7 Myr has been assumed for

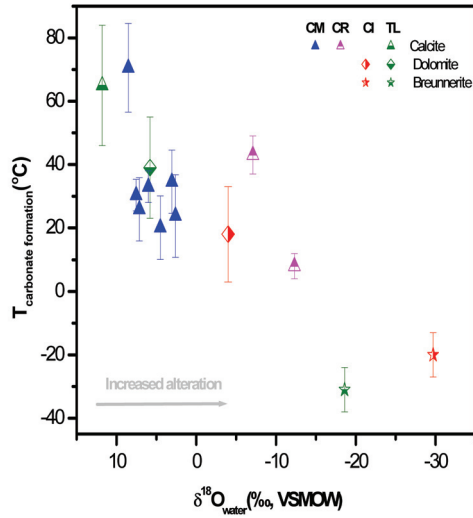


Fig. 2-6

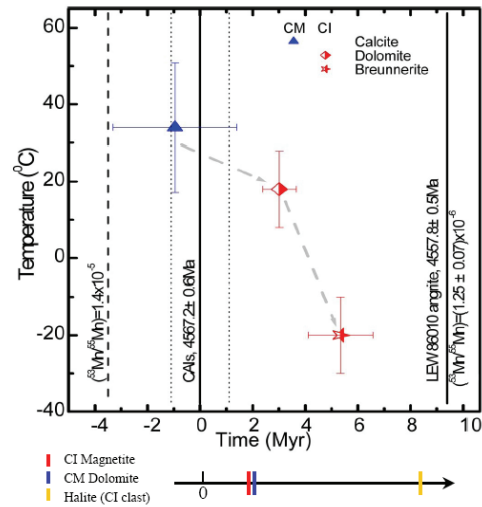


Fig. 2-7

Figure 2-6 Negative correlation between the carbonate formation temperatures and the oxygen isotope compositions of alteration fluid from which the carbonates grew. This negative correlation indicates the carbonaceous chondrite parent bodies were cooling as the aqueous alterations proceeded. Error bars denote 1 standard error (1σ).

Figure 2-7 Estimated thermal evolution of carbonaceous chondrite parent bodies, based on the formation temperatures of carbonates in different carbonaceous chondrite (Guo and Eiler 2007 and this study) and the corresponding formation ages of these carbonates (Brearley et al. 2001; Krot et al. 2006; Hoppe et al. 2007). The absolute ages of CAIs from CV chondrites, ages of angrite LEW 86010 and ages calculated with initial $^{53}\text{Mn}/^{55}\text{Mn}$ ratio of 1.4×10^{-5} are shown for reference (Krot et al. 2003). Also shown for comparison (at the bottom) are the formation ages of magnetite in CI chondrite, of dolomite in CM chondrite and halite in Monahans 1998 and Zag (H6 chondrite) (Brearley and Hutcheon, 2000; Pravdivtseva et al., 2003; Busfield et al., 2004). The estimated formation age for magnetite in Tagish Lake (at least 50 Myrs later than the ages of CI magnetite; Busfield et al. 2001) falls outside the range of this plot. Error bars denote 1 standard error (1σ).

^{53}Mn decay (McKeegan and Davis, 2003). Combination of these data (available for CM calcite, CI dolomite and CI breunnerite) implies aqueous alteration on the carbonaceous chondrite parent bodies started within 1-2 million years after formation of the CAIs in CV chondrites ($4567.2 \pm 0.6\text{ Ma}$) (Krot et al., 2006), with the alteration temperatures decreasing from 34°C to 18°C in the first 4 million years and further to -20°C after ~ 6.5 million years (Fig. 2-7).

Several theoretical studies have attempted to model the thermal evolution of small planetesimals similar in size to the carbonaceous chondrite parent bodies (Grimm and McSween, 1989; Cohen and Coker, 2000; Young, 2001; Travis and Schubert, 2005). Unfortunately, these studies either didn't document in detail the thermal evolutions at different depths inside the parent bodies (Grimm and McSween, 1989; Cohen and Coker, 2000), assumed a relative late accretion of the parent bodies (i.e., relatively low initial $^{26}\text{Al}/^{27}\text{Al}$; Grim and McSween 1989, Young 2001, Travis and Schubert, 2005), and/or focused on only a very short time span of the thermal evolution of the parent body (e.g., the first million year after parent body accretion; Young 2001). These gaps in previous modeling studies preclude a detailed comparison between our experimental results and the predictions from available thermal models (Fig 2-8). However, if we assume the first chondritic carbonate (i.e., CM calcite) formed shortly after the accretion of the carbonaceous chondrite parent body (e.g., within 1 million years) while the formation age differences between different chondritic carbonates are unchanged (in other words, shifting the formation ages of all chondritic carbonates behind by the same amount of ~ 4.8 Myrs), our experimentally estimated alteration temperatures agree almost perfectly with the thermal evolution of a layer 10km from the surface of a 50km radius parent

bodies as modeled by Travis and Schubert (2005) (Fig. 2-9). The exact implication of this agreement needs to be investigated further in the future with more thorough and detailed thermal modeling (e.g., models with earlier accretion of carbonaceous chondrite parent bodies, and variable sizes of parent bodies).

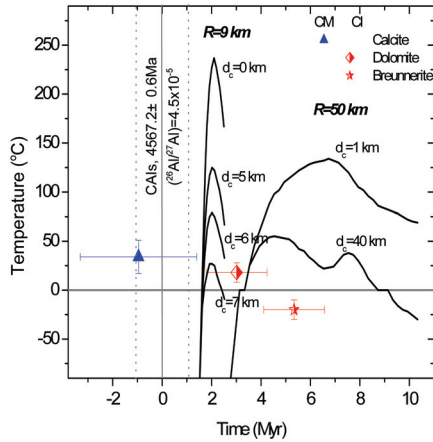


Fig. 2-8

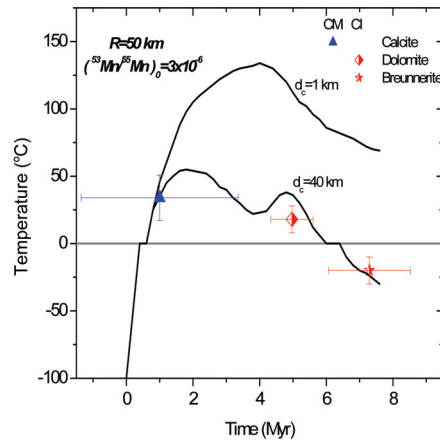


Fig. 2-9

Figure 2-8 Comparison of our estimated thermal evolution of carbonaceous chondrite parent bodies with the predictions from available thermal models. The model predictions, for the 9km radius parent body and 50km radius parent body, are reproduced from Young et al. (2001) and Travis and Schubert (2005) respectively. Different lines represent layers with different distances (' d_c ') from the center of the modeled parent bodies. The start time for each model was calibrated relative to the formation age of CAIs in CV chondrites ($^{26}\text{Al}/^{27}\text{Al}$ ratio of 4.5×10^{-5} and absolute Pb-Pb age of $4567.2 \pm 0.6\text{ Ma}$; Amelin et al. 2002, McKeegan and Davis 2003), based on their initial $^{26}\text{Al}/^{27}\text{Al}$ ratios (1×10^{-5} and 3×10^{-6} respectively) assumed in the modeled parent bodies. The decay of ^{26}Al has a half-life time of 0.7Myr (McKeegan and Davis, 2003). Error bars denote 1 standard error (1σ).

Figure 2-9 Agreement of our estimated thermal evolution of carbonaceous chondrite parent bodies with the modeled thermal evolution for a layer 10km from the surface of a 50km radius parent body (Travis and Schubert 2005), when constraints on carbonate formation ages are relaxed (see text for details). The implication of this agreement needs to be investigated further by future modeling studies. Different lines represent layers with different distances (' d_c ') from the center of the modeled parent bodies. Error bars denote 1 standard error (1σ).

4. SUMMARY

Despite their differences in the extent of aqueous alteration, we show that temperatures of aqueous alteration on different carbonaceous chondrite parent bodies were all relatively low (-31 to 71°C ; $\pm 10^{\circ}\text{C}$, 1σ) and varied significantly (as much as 96°C ; Tagish Lake) during the course of alteration. This similarity in alteration temperatures among different groups of carbonaceous chondrites implies factors other than alteration temperature (e.g., water/rock ratio or duration of aqueous alteration) as the primary causes for their differences in the extents of aqueous alteration. The sub-zero formation temperatures ($-20^{\circ}\text{C} \pm 10^{\circ}\text{C}$ and $-31^{\circ}\text{C} \pm 10^{\circ}\text{C}$ respectively, 1σ) we estimated for breunnerite in Orgueil and Tagish Lake, indicate formation of the low temperatures brines or ammonia–water mixtures during the late stages of aqueous alteration on the carbonaceous chondrite parent bodies. The formation of water ice at these sub-zero temperatures is suspected to have led to further reductions in $\delta^{18}\text{O}$ of the alteration fluid.

Different types of carbonates within the carbonaceous chondrites formed at different stages of the aqueous alteration on their parent bodies, with calcite earlier than dolomite than breunnerite. Our determination of the respective formation temperatures for different carbonates (through stepped phosphoric acid digestions) demonstrates the carbonaceous chondrite parent bodies were cooling as the aqueous alteration proceeded, and furthermore enables us to quantitatively constrain the cooling rate. To the best of our knowledge, this study provides the first quantitative experimental constraints on the thermal evolution of small planetesimals typical of petrology type 1 and 2 carbonaceous chondrite parent bodies.

ACKNOWLEDGEMENTS

This research was supported by a grant to J. M. E from the NASA Cosmochemistry Program. We would like to thank John Ferry and Benjamin Passey for sharing the unpublished data on the dolomite $\Delta_{47}\text{T}$ calibration, Edwin Schauble for checking into the extrapolation of their predicted ^{13}C - ^{18}O clumped isotope effects in carbonate minerals to subzero temperatures, and Murielle Perronnet for providing the GRO 95577 sample for analysis.

REFERENCES

- Al-Aasm I. S., Taylor B. E. and South B. (1990). Stable isotope analysis of multiple carbonate samples using selective acid extraction. *Chem. Geol.* **80**: 119-25.
- Amelin Y., Krot A. N., Hutcheon I. D. and Ulyanov A. A. (2002). Lead isotopic ages of chondrules and calcium-aluminum-rich inclusions. *Science* **297**: 1678 - 1683.
- Baker L., Franchi I. A., Wright I. P. and Pillinger C. T. (2002). The oxygen isotopic composition of water from Tagish Lake: Its relationship to low-temperature phases and to other carbonaceous chondrites. *Meteorit. Planet. Sci.* **37**: 977-985.
- Benedix G. K., Leshin L. A., Farquhar J., Jackson T. and Thiemens M. H. (2003). Carbonates in CM2 chondrites: Constraints on alteration conditions from oxygen isotopic compositions and petrographic observations. *Geochim. Cosmochim. Acta* **67**: 1577-1588.
- Beukes N. J., Klein C., Kaufman A. J. and Hayes J. M. (1990). Carbonate petrography, kerogen distribution, and carbon and oxygen isotope variations in an Early Proterozoic transition from limestone to iron-formation deposition, Traansvaal Supergroup, South Africa. *Econ. Geol.* **85**: 663-690.
- Brearley A. J. (2006). The action of water. In *Meteorites and the Early Solar System II*, Arizona University Press. 587-624.

- Brearley A. J. and Hutcheon I. D. (2000). Carbonates in the CM1 Chondrite ALH84034: Mineral Chemistry, Zoning and Mn-Cr Systematics. *31st Lunar Planet. Sci. Conf.*: Abstract #1407.
- Brearley A. J., Hutcheon I. D. and Browning L. (2001). Compositional zoning and Mn-Cr systematics in carbonates from the Y791198 CM2 carbonaceous chondrite. *32nd Lunar Planet. Sci. Conf.*: Abstract #1458.
- Brearley A. J. and Jones R. H. (1998). Chondritic meteorites. *Rev. Mineral. Geochem.* **36**: 3-1 to 3-398.
- Bridges J. C., Banks D. A., Smith M. and Grady M. M. (2004). Halite and stable chlorine isotopes in the Zag H3-6 breccia. *Meteorit. Planet. Sci.* **39**: 657-666.
- Brown P. G., Hildebrand A. R., Zolensky M. E., Grady M., Clayton R. N., Mayeda T. K., Tagliaferri E., Spalding R., MacRae N. D., Hoffman E. L., Mittlefehldt D. W., Wacker J. F., Bird J. A., Campbell M. D., Carpenter R., Gingerich H., Glatiotis M., Greiner E., Mazur M. J., McCausland P. J., Plotkin H. and Rubak Mazur T. (2000). The fall, recovery, orbit, and composition of the Tagish Lake meteorite: a new type of carbonaceous chondrite. *Science* **290**: 320-325.
- Busfield A., Gilmour J. D., Whitby J. A., Simon S. B., Grossman L., Tang C. C. and Turner G. (2001). I-Xe Analyses of Tagish Lake Magnetite and Monahans Halite. *Meteorit. Planet. Sci.* **36**: A34.
- Busfield A., Gilmour J. D., Whitby J. A. and Turner G. (2004). Iodine-xenon analysis of ordinary chondrite halide: Implications for early solar system water. *Geochim. Cosmochim. Acta* **68**: 195-202.
- Came R. E., Eiler J. M., Veizer J., Azmy K., Brand U. and Weidman C. R. (2007). Coupling of surface temperatures and atmospheric CO₂ concentrations during the paleozoic era. *Nature* **449**: 198-201.
- Clayton R. N. and Mayeda T. K. (1984). The oxygen isotope record in Murchison and other carbonaceous chondrites. *Earth Planet. Sci. Lett.* **67**: 151-161.
- Clayton R. N. and Mayeda T. K. (1999). Oxygen isotope studies of carbonaceous chondrites. *Geochim. Cosmochim. Acta* **63**: 2089-2104.
- Cohen B. A. and Coker R. F. (2000). Modeling of liquid water on CM meteorite parent bodies and implications for amino acid racemization. *Icarus* **145**: 369-381.

- Das Sharma S., Patil D. J. and Gopalan K. (2002). Temperature dependence of oxygen isotope fractionation of CO₂ from magnesite-phosphoric acid reaction. *Geochim. Cosmochim. Acta* **66**: 589-593.
- Eiler J., Affek H., Daeron M., Ferry J., Guo W., Huntington K., Thiagarajan N. and Tripati A. (2008). Carbonate 'clumped isotope' thermometry: A status report. *Geochim. Cosmochim. Acta* **72**: A239.
- Eiler J. M. and Kitchen N. (2004). Hydrogen isotope evidence for the origin and evolution of the carbonaceous chondrites. *Geochim. Cosmochim. Acta* **68**: 1395-1411.
- Eiler J. M. and Schauble E. A. (2004). ¹⁸O¹³C¹⁶O in Earth's atmosphere. *Geochim. Cosmochim. Acta* **68**: 4767-4777.
- Endress M. and Bischoff A. (1996). Carbonates in CI chondrites: Clues to parent body evolution. *Geochim. Cosmochim. Acta* **60**: 489-507.
- Engrand C., Gounelle M., Duprat J. and Zolensky M. E. (2001a). In-Situ Oxygen Isotopic Composition of Individual Minerals in Tagish Lake, a Unique Type 2 Carbonaceous Meteorite. *32nd Lunar Planet. Sci. Conf.*: Abstract #1568.
- Engrand C., Gounelle M. and Zolensky M. E. (2001b). Oxygen isotopic compositions of Tagish Lake. *Meteorit. Planet. Sci.* **36**: A54.
- Gasparik T. (2003). Phase diagrams for geoscientists: an atlas of the earth's interior. New York: Springer.,
- Ghosh P., Adkins J., Affek H. P., Balta B., Guo W., Schauble E. A., Schrag D. and Eiler J. M. (2006). ¹³C-¹⁸O bonds in carbonate minerals: A new kind of paleothermometer. *Geochim. Cosmochim. Acta* **70**: 1439-1456.
- Ghosh P., Eiler J., Campana S. E. and Feeney R. F. (2007). Calibration of the carbonate 'clumped isotope' paleothermometer for otoliths. *Geochim. Cosmochim. Acta* **71**: 2736-2744.
- Grady M. M., Wright I. P., Swart P. K. and Pillinger C. T. (1988). The carbon and oxygen isotopic composition of meteoritic carbonates. *Geochim. Cosmochim. Acta* **52**: 2855-2866.
- Grimm R. E. and McSween H. Y. (1989). Water and the thermal evolution of carbonaceous chondrite parent bodies. *Icarus* **82**: 244-280.

- Guo W. and Eiler J. M. (2007). Temperatures of aqueous alteration and evidence for methane generation on the parent bodies of the CM chondrites. *Geochim. Cosmochim. Acta.* **71**: 5565-5575.
- Guo W., Mosenfelder J. L., Goddard W. A. and Eiler J. M. (2008). Isotopic fractionations associated with phosphoric acid digestion of carbonate minerals. *Geochim. Cosmochim. Acta* **in review**.
- Hoppe P., MacDougall D. and Lugmair G. W. (2007). High spatial resolution ion microprobe measurements refine chronology of carbonate formation in Orgueil. *Meteorit. Planet. Sci.* **42**: 1309-1320.
- Horita J. (2005). Stable isotope thermometry: There is more to it than temperature. *Geochem. J.* **39**: 481-496.
- Keil K. (2000). Thermal alteration of asteroids: evidence from meteorites. *Planet. Space Sci.* **48**: 887-903.
- Krot A. N., Hutcheon I. D., Brearley A. J., Pravdivtseva O. V., Petaev M. I. and Hohenberg C. M. (2006). Timescales and setting for alteration of chondritic meteorites. In *Meteorites and the Early Solar System II*, Arizona University Press. 525-553.
- Leshin L. A., Farquhar J., Guan Y., Pizzarello S., Jackson T. L. and Thiemens M. H. (2001). Oxygen isotopic anatomy of Tagish Lake: relationship to primary and secondary minerals in CI and CM chondrites. *32nd Lunar. Planet. Sci. Conf.*: abstract #1842
- Lugmair G. W. and Galer S. J. G. (1992). Age and isotopic relationships among the angrites Lewis Cliff 86010 and Angra dos Reis. *Geochim. Cosmochim. Acta* **56**: 1673-1694.
- Lugmair G. W. and Shukolyukov A. (1998). Early solar system timescales according to Mn-53-Cr-53 systematics. *Geochim. Cosmochim. Acta* **62**: 2863-2886.
- Macdougall J. D. (2000). Sr isotopes in the Orgueil CI meteorite: Chronology of early solar system hydrothermal activity *Proc. Indian Acad. Sci.-Earth Planet. Sci.* **109**: 187-193.
- McKeegan K. D. and Davis A. M. (2003). Early solar system chronology. In *Treatise on Geochemistry v1: Meteorites, Planets, and Comets*.

- Palguta J., Travis B. J. and Schubert G. (2007). Hydrothermal convection and aqueous alteration in chondritic parent bodies. *38th Lunar Planet. Sci. Conf.*: abstract #1370.
- Perronnet M., Berger G., Zolensky M. E., Toplis M. J., Kolb V. M. and Bajagic M. (2007). The aqueous alteration of CR chondrites: experiments and geochemical modeling. *38th Lunar. Plant. Sci. Conf.*: Abstract #1110.
- Pravdivtseva O. V., Hohenberg C. M. and Meshik A. P. (2003). The I-Xe Age of Orgueil magnetite: new results. *34th Lunar Planet. Sci. Conf.* : abstract #1863.
- Riciputi L. R., McSween H. Y., Johnson C. A. and Prinz M. (1994). Minor and trace-element concentrations in carbonates of carbonaceous chondrites, and implications for the compositions of coexisting fluids. *Geochim. Cosmochim. Acta* **58**: 1343-1351.
- Rosenbaum J. M. (1997). Gaseous, liquid, and supercritical fluid H₂O and CO₂: Oxygen isotope fractionation behavior. *Geochim. Cosmochim. Acta*. **61**: 4993-5003.
- Rowe M. W., Clayton R. N. and Mayeda T. K. (1994). Oxygen isotopes in separated components of CI and CM meteorites. *Geochim. Cosmochim. Acta* **58**: 5341-5347.
- Schauble E. A., Ghosh P. and Eiler J. M. (2006). Preferential formation of ¹³C-¹⁸O bonds in carbonate minerals, estimated using first-principles lattice dynamics. *Geochim. Cosmochim. Acta* **70**: 2510-2529.
- Spencer R. J., Møller N. and Weare J. H. (1990). The prediction of mineral solubilities in natural waters: A chemical equilibrium model for the Na---K---Ca---Mg---Cl---SO₄---H₂O system at temperatures below 25°C. *Geochim. Cosmochim. Acta* **54**: 575-590.
- Travis B. J. and Schubert G. (2005). Hydrothermal convection in carbonaceous chondrite parent bodies. *Earth Planet. Sci. Lett.* **240**: 234-250.
- Weisberg M. K., McCoy T. J. and Krot A. N. (2006). Systematics and Evaluation of Meteorite Classification.In *Meteorites and the Early Solar System II*, Univ. Arizona press. 19-52.
- Weisberg M. K. and Prinz M. (2000). The Grosvenor Mountains 9557 CR1 chondrite and hydration of the CR chondrites. *Meteorit. Planet. Sci.* **35**: A168.

- Wenner D. B. and Taylor H. P. (1971). Temperatures of serpentinization of ultramafic rocks based on $^{18}\text{O}/^{16}\text{O}$ fractionation between coexisting serpentine and magnetite. *Contrib. Mineral. Petrol.* **32**: 165-185.
- Young E. D. (2001). The hydrology of carbonaceous chondrite parent bodies and the evolution of planet progenitors. *Phil. Trans. R. Soc. Lond. A* **359**: 2095-2109.
- Zolensky M. E., Bodnar R. J., Gibson E. K., Nyquist L. E., Reese Y., Shih C. Y. and Wiesmann H. (1999). Asteroidal water within fluid inclusion-bearing halite in an H5 chondrite, Monahans (1998). *Science* **285**: 1377-1379.
- Zolensky M. E., Clayton R. N., Mayeda T., Chokai J. and Norton O. R. (2003). Carbonaceous Chondrite Clasts in the Halite-bearing H5 Chondrite Zag. *Meteorit. Planet. Sci.* **38**: A114.
- Zolensky M. E., Krot A. N. and Benedix G. (2008). Record of low-temperature alterations in asteroids. *Rev. Mineral. Geochem.* **68**: 429-462.
- Zolensky M. E., Nakamura K., Gounelle M., Mikouchi T., Kasama T., Tachikawa O. and Tonui E. (2002). Mineralogy of Tagish Lake: an ungrouped type 2 carbonaceous chondrite. *Meteor. Planet. Sci.* **37**: 737-761.

PART II

**KINETIC ISOTOPE FRACTIONATIONS OF CLUMPED
ISOTOPES ASSOCIATED WITH CHEMICAL REACTIONS
— IMPLICATIONS FOR CARBONATE CLUMPED ISOTOPE
THERMOMETRY**

Chapter 3**ISOTOPIC FRACTIONATIONS ASSOCIATED WITH PHOSPHORIC
ACID DIGESTION OF CARBONATE MINERALS**

Weifu Guo¹, Jed L. Mosenfelder¹, William A. Goddard III² and John M. Eiler¹

¹ Division of Geological and Planetary Sciences,

² Materials and Process Simulation Center,

California Institute of Technology, Pasadena, CA, 91125

(Submitted to *Geochimica et Cosmochimica Acta*, August, 2008)

ABSTRACT

Phosphoric acid digestion has been used for oxygen- and carbon-isotope analysis of carbonate minerals since 1950, and was recently established as a method for carbonate ‘clumped isotope’ analysis. The CO₂ recovered from this reaction has an oxygen isotope composition substantially different from reactant carbonate, by an amount that varies with temperature of reaction and carbonate chemistry. Here, we present a theoretical model of the kinetic isotope effects associated with phosphoric acid digestion of carbonates, based on structural arguments that the key step in the reaction is disproportionation of H₂CO₃ reaction intermediary. We test that model against previous experimental constraints on the magnitudes and temperature dependences of these oxygen isotope fractionations, and against new experimental determinations of the fractionation of ¹³C-¹⁸O-containing isotopologues. Our model predicts that the isotope fractionations associated with phosphoric acid digestion of carbonates at 25°C are 10.72‰, 0.220‰, 0.137‰, 0.593‰ for, respectively, ¹⁸O/¹⁶O ratios (1000lnα*) and three indices that measure proportions of multiply-substituted isotopologues (Δ₄₇*, Δ₄₈*, Δ₄₉*). We also predict that oxygen isotope fractionations follow the mass dependence exponent, λ of 0.5281 (where α_{17O}=α_{18O}^λ). These predictions compare favorably to independent experimental constraints for phosphoric acid digestion of calcite, including our new data for fractionations of ¹³C-¹⁸O bonds (the measured change in Δ₄₇=0.23‰) during phosphoric acid digestion of calcite at 25°C.

We have also attempted to evaluate the effect of carbonate cation compositions on phosphoric acid digestion fractionations using cluster models in which disproportionating H₂CO₃ interacts with adjacent cations. These models underestimate the magnitude of

isotope fractionations (suggesting we have not identified an appropriate structural model for cation—H₂CO₃ clusters), but they do successfully reproduce the general trend of variations and temperature dependences of oxygen isotope acid digestion fractionations among different carbonate minerals (suggesting we have correctly identified the basic mechanism responsible for a dependence on cation chemistry). Examinations of these theoretical predictions and available experimental data suggest cation radius is the most important factor governing the variations of isotope fractionation among different carbonate minerals. Moreover, we predict a negative correlation between acid digestion fractionation of oxygen isotopes and of ¹³C-¹⁸O doubly-substituted isotopologues, and estimate the acid digestion fractionation of Δ₄₇^{*} for different carbonate minerals. Combined with previous theoretical evaluations of ¹³C-¹⁸O clumping effects in carbonate minerals, this enables us to predict the temperature calibration relationship for different carbonate clumped isotope thermometers (witherite, calcite, aragonite, dolomite and magnesite), and to compare these predictions with available experimental determinations. The general success of our models in capturing the major features of isotope fractionation during acid digestion suggests that phosphoric acid digestion of carbonate minerals involves disproportionation of transition state structures containing H₂CO₃.

1. INTRODUCTION

Analysis of the stable oxygen and carbon isotope composition of carbonate minerals is among the most common and useful measurements in isotope geochemistry. For example, much of paleoclimatology is based on carbonate-water oxygen isotope thermometry (Urey, 1947) and most records of the global carbon cycle through time

depend on measuring the carbon isotope compositions of sedimentary carbonates. More recently, Ghosh et al. (2006) and Schauble et al. (2006) developed a carbonate ‘clumped isotope’ thermometer based on the ordering of ^{13}C and ^{18}O into bonds with each other within the carbonate mineral lattice.

In practice, stable isotope measurements of carbonates are generally performed indirectly by reacting the sample carbonate with anhydrous phosphoric acid and then analyzing the product CO_2 on a gas source isotope ratio mass spectrometer (McCrea, 1950). This method is relatively straightforward to perform, is applicable to a wide range of sample sizes, has been automated in several different ways, and is exceptionally precise; these features make this approach preferable to alternative methods for most applications (e.g., fluorination, Sharma and Clayton, 1965; secondary ion mass spectrometry, Rollion-Bard et al., 2007; laser ablation, Sharp and Cerling, 1996). However because only two out of three oxygen atoms in carbonate are released as CO_2 during phosphoric acid digestion, this method involves an oxygen isotope fractionation; i.e., product CO_2 is $\sim 10\text{\textperthousand}$ higher in $\delta^{18}\text{O}$ than reactant carbonate (Gilg et al., 2003 and reference therein). The exact magnitude of this fractionation varies with acid digestion temperature and differs among different carbonate minerals (Sharma and Clayton, 1965; Kim and O’Neil, 1997; Gilg et al., 2003). Similarly, preliminary evidence suggests that values of Δ_{47} (a measure of the abundance anomaly of ^{13}C - ^{18}O bonds in CO_2 ; defined as

$$\Delta_{47} = \left(\frac{R_{actual}^{47}}{R_{stochastic}^{47}} - 1 \right) \times 1000 ; \text{ Eiler and Schauble, 2004} \right)$$

are enriched in CO_2 produced by acid

digestion of calcite and aragonite relative to values one expects in the absence of any associated fractionation (Ghosh et al., 2006). Below, we present new data that confirm

and precisely quantify this effect. These analytical fractionations must be corrected for in any study of the oxygen isotope or ‘clumped isotope’ compositions of carbonate minerals.

The oxygen isotope fractionations associated with phosphoric acid digestion of different carbonate minerals have been experimentally studied over a range of temperatures (Sharma and Clayton, 1965; Sharma and Sharma, 1969a; Sharma and Sharma, 1969b; Rosenbaum and Sheppard, 1986; Swart et al., 1991; Bottcher, 1996; Kim and O’Neil, 1997; Gilg et al., 2003; Kim et al., 2007). However, there are significant discrepancies among acid digestion fractionations of oxygen isotopes determined in different studies (Kim et al., 2007 and reference therein). For example, reported acid digestion fractionations at 25°C range from 10.10‰ (Das Sharma et al., 2002) to 10.52‰ (Land, 1980) for calcite, and from 10.29‰ (Sharma and Clayton, 1965) to 11.01‰ (Kim and O’Neil, 1997) for aragonite. Even within a single study, the measured acid digestion fractionation factors for the same type of carbonate minerals can vary depending on the exact carbonate materials used (as much as ~2‰ for octavite, ~0.6‰ for witherite, and ~0.5‰ for calcite at 25°C; Kim and O’Neil, 1997). More generally, our understanding of this phenomenon is entirely empirical, and thus provides little basis for extrapolation to new materials or conditions of acid digestion.

Our understanding of acid digestion fractionations is particularly poor in relation to the carbonate ‘clumped isotope’ thermometer (Ghosh et al., 2006). It has been shown that the abundance anomaly of ^{13}C - ^{18}O bonds in CO_2 produced by acid digestion of carbonate differs from that in reactant carbonate (Ghosh et al., 2006), but the exact magnitude of this fractionation was poorly constrained and its variation among different carbonate minerals is unexplored. These gaps in our understanding limit the use of the carbonate

clumped isotope thermometer for minerals other than calcite and aragonite, e.g., dolomite or magnesite. Because these carbonates are difficult to synthesize in isotopic equilibrium, theoretical understandings of both ^{13}C - ^{18}O clumping within minerals and clumped isotope fractionations during acid digestion are important guides to interpreting observations on natural samples.

Schauble et al. (2006) previously presented theoretical models of equilibrium ^{13}C - ^{18}O clumping in carbonate minerals other than calcite and aragonite. However, to the best of our knowledge, no detailed theoretical model has been proposed to explain the isotope fractionations that accompany phosphoric acid digestion of carbonate minerals. Sharma and Sharma (1969b) determined the oxygen isotope acid digestion fractionation factors for several different carbonate minerals, and explained them as a result of two factors: a temperature-dependent factor and a temperature-independent factor, with the latter varying as a function of the atomic mass of the cations in carbonate minerals. Sharma and Sharma's data suggest that temperature-independent factors can be explained by their proposed structure for the transition state through which the acid digestion reaction proceeds (Fig. 3-1a). However; their model does not quantitatively describe the temperature-dependent factor, and subsequent experimental results (Bottcher, 1996; Gilg et al., 2003) are inconsistent with their model.

In this study, we present a quantitative model of the phosphoric acid digestion reaction based on transition state theory and statistical thermodynamics. We use this model to predict isotopic fractionations among all isotopologues (including multiply substituted isotopologues) of reactant carbonate ions, and thus the isotopic composition (including ‘clumped isotope’ composition; i.e., abundances of multiply-substituted

isotopologues) of CO₂ produced by phosphoric acid digestion of carbonate minerals. Finally, we test the accuracy of our model by comparison with previous data documenting the oxygen isotope fractionation associated with this reaction, and with new data we have generated documenting the fractionation of ¹³C-¹⁸O bearing isotopologues during acid digestion (which controls the Δ_{47} value of product CO₂). We observe quantitative agreements between our model predictions and available experimental data on the magnitude and temperature dependence of isotope fractionations associated with phosphoric acid digestion for calcite, and on the general trend of variations of oxygen isotope fractionations among different carbonate minerals.

This study provides a framework for understanding fractionations accompanying acid digestion, and applying them to conditions or materials that are not yet understood through experimental work. Furthermore, this study demonstrates a technique of first-principles modeling of kinetic isotope effects associated with irreversible reactions, and illustrates the utility of this technique by application to one of the more extensively studied inorganic reactions in stable isotope geochemistry, taking advantage of new constraints provided by clumped isotope measurements. This approach therefore serves as a model for future work of similar but less well known kinetically-controlled fractionations.

2. THEORETICAL AND COMPUTATIONAL METHODS

2.1 Transition state theory of reaction rates

Transition state theory is long established as a tool for studying chemical kinetics (Eyring, 1935a; Eyring, 1935b) and has been used previously to understand irreversible

reactions in geoscience problems (Lasaga 1998; Felipe et al., 2001). Classical transition state theory is based on two key assumptions (Felipe et al., 2001): 1) instead of transforming directly into products, reactants in a chemical reaction first proceed through an unstable chemical state called the ‘transition state’, which has a higher chemical potential energy than reactants or products; 2) the transition state may only form from the reactants (i.e., the conversion of the transition state to products is irreversible), and any transition state that proceeds in the reaction coordinate past its potential energy maximum must eventually form products. This second assumption is also called the “non-recrossing rule”. For example, transition state theory would describe $A + B \longrightarrow C + D$ as proceeding through two steps: reversible transformation of reactants A and B into a transition state, M^\ddagger , after which M^\ddagger transforms irreversibly into products C and D (i.e. $A + B \xrightleftharpoons[1]{\text{ }} M^\ddagger \xrightarrow[2]{\text{ }} C + D$). The rate of the overall reaction (i.e. the production rate of C and D), R, equals the decomposition rate of the transition state, M^\ddagger and can be described through the relation:

$$R = \frac{[M^\ddagger]}{\tau} = |\nu_L^\ddagger| [M^\ddagger] , \quad (1)$$

where $[M^\ddagger]$ is the concentration of transition state M^\ddagger , τ is the average lifetime of transition state M^\ddagger , and ν_L^\ddagger is the ‘decomposition frequency’ (defined as the reciprocal of the average life time) of M^\ddagger (Melander and Saunders 1987; Felipe et al., 2001). The concentration of the transition state, $[M^\ddagger]$, can be estimated by assuming that the reversible reaction, $A + B \xrightleftharpoons[1]{\text{ }} M^\ddagger$, is at equilibrium (Melander and Saunders, 1987):

$$[M^\ddagger] = K[A][B] , \quad (2)$$

where [A] and [B] are the concentrations of reactant A and B respectively, and K is the equilibrium constant for reaction 1 and can be evaluated using statistical thermodynamics (Urey, 1947):

$$K = \frac{Q^\dagger}{Q_A \times Q_B} = \frac{s_A \times s_B}{s^\dagger} \frac{\prod_i^{3N^\dagger - 7} (u_i^\dagger \times \frac{1}{e^{\frac{1}{2}u_i^\dagger}} \times \frac{1}{1-e^{-u_i^\dagger}})}{\prod_{j_A}^{3N_A - 6} (u_{j_A} \times \frac{1}{e^{\frac{1}{2}u_{j_A}}} \times \frac{1}{1-e^{-u_{j_A}}}) \times \prod_{j_B}^{3N_B - 6} (u_{j_B} \times \frac{1}{e^{\frac{1}{2}u_{j_B}}} \times \frac{1}{1-e^{-u_{j_B}}})} \quad (3)$$

$$u_i^\dagger = \frac{hc\varpi_i^\dagger}{kT}, u_{j_A} = \frac{hc\varpi_{j_A}}{kT}, u_{j_B} = \frac{hc\varpi_{j_B}}{kT},$$

where Q^\dagger, Q_A, Q_B are the partition functions of transition state M^\dagger and reactants A and B, respectively; $\varpi_i^\dagger, \varpi_{j_A}, \varpi_{j_B}$ are the vibration frequencies, in wave numbers, for the transition state M^\dagger and reactants A and B, respectively (one such term is required for each mode of vibration of each species); s^\dagger, s_A, s_B are the symmetry numbers for transition state M^\dagger and reactants A and B respectively; N^\dagger, N_A, N_B are the numbers of atoms within transition state M^\dagger and reactants A and B respectively; h is Plank's constant; c is the velocity of light; k is the Boltzmann constant; and T is the reaction temperature in Kelvin.

When one is interested in kinetic isotope effects, *relative* reaction rates (i.e., the ratios of reaction rates of different isotopologues) are of greatest importance:

$$\frac{R_{(1)}}{R_{(2)}} = \frac{|\nu_L^\dagger|_{(1)} [M^\dagger]_{(1)}}{|\nu_L^\dagger|_{(2)} [M^\dagger]_{(2)}}, \quad (4)$$

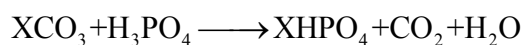
where subscript, (1) and (2) denote different isotopologues of the transition state.

2.2 Application of transition state theory to phosphoric acid digestion of carbonate minerals

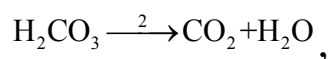
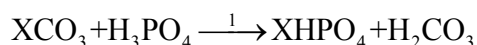
2.2.1 Structure of the transition state relevant to phosphoric acid digestion of carbonate minerals

In order to calculate the partition function of the transition state, we must first determine or assume the transition state structure. This is commonly done by initially guessing the structure of transition state and then refining on that guess using ab initio calculations (Felipe et al., 2001). Sharma and Sharma (1969b) suggested an intuitively appealing structure for the transition state during phosphoric acid digestion of carbonate minerals (Figure 3-1a), but there is no evidence to date that supports it. Instead, recent spectroscopic studies of calcium carbonate undergoing reactions with anhydrous acidic gases (e.g., HNO₃, SO₂, HCOOH and CH₃COOH) suggest that carbonic acid is the important intermediate species (Al-Hosney and Grassian 2004; Al-Hosney and Grassian 2005). We suggest that these experiments are analogous to the local environment at the surface of a carbonate mineral during reaction with anhydrous phosphoric acid (i.e., the 105% concentrated phosphoric acid used in stable isotope analyses of carbonates; Coplen et al., 1983).

We therefore propose that H₂CO₃ is also an intermediate during phosphoric acid digestion of carbonate minerals, i.e. this reaction



proceeds through two steps:



where X is a cation, such as Ca, contained in the carbonate mineral. There are two reasons why we infer that the first of these two reaction steps should be associated with little or no net isotopic fractionation: (1) in practice, phosphoric acid digestion is always driven to completion before collecting and analyzing product CO₂. Because CO₃²⁻ ionic units in the reactant carbonate are quantitatively converted into H₂CO₃ during step 1, it is not possible to express a net isotopic fractionation of C or O isotopes during that step, even if that reaction has some intrinsic kinetic isotope effect. (2) any kinetic isotope effect that might accompany step 1 could only be expressed if the site at which the reaction occurs (i.e., a mineral surface) can undergo isotopic exchange with the unreacted mineral interior, which we consider unlikely at the low temperatures and anhydrous conditions of phosphoric acid digestion. That is, we infer that step 1 is analogous to sublimation of ice, which generally fails to express a vapor pressure isotope effect because the reaction effectively ‘peels’ away layers of the solid without leaving an isotopically modified residue. For these reasons, we focus on step 2 — the dissociation of carbonic acid in this study. We do so by first assuming a previously determined transition state structure for carbonic acid decomposition (Loerting et al., 2000) as our ‘initial guess’ (Figure 3-1c), and then optimizing that structure through further ab initio calculations.

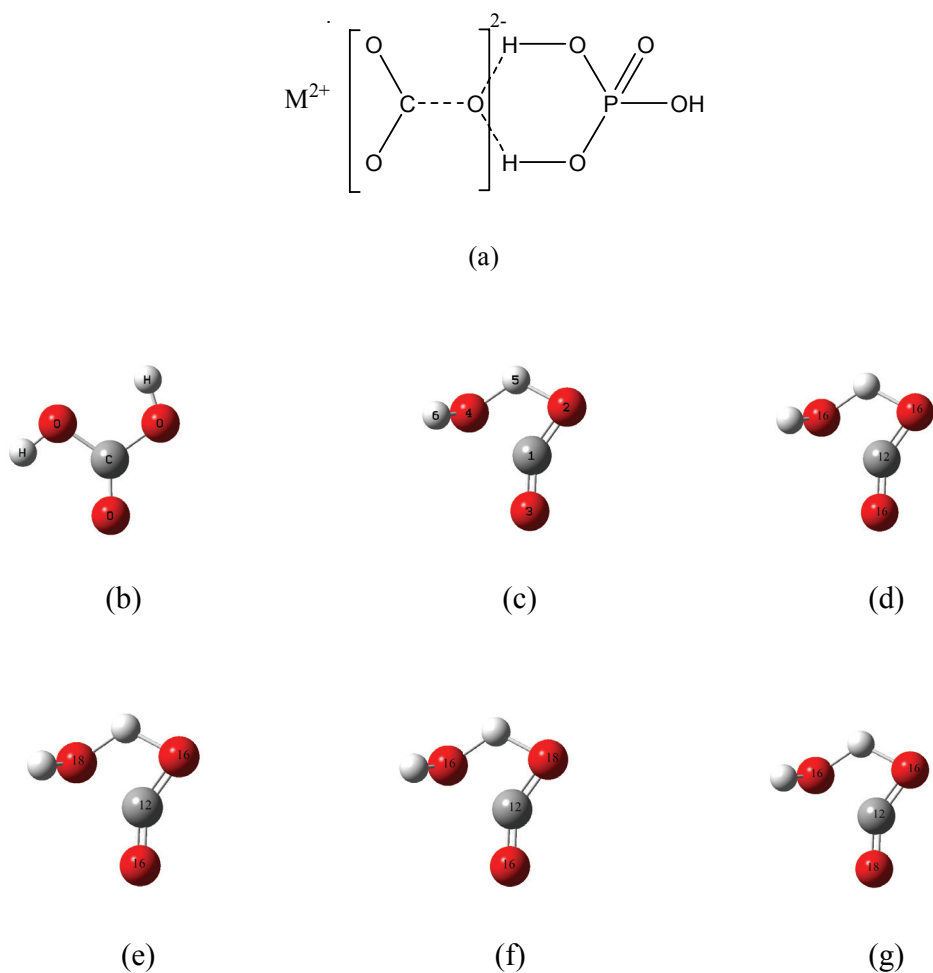


Figure 3-1: Transition state structures during phosphoric acid digestion of carbonate minerals (H_2CO_3 model): **(a)** The transition state structure proposed by Sharma and Sharma, 1969b; **(b)** an optimized stable structure of carbonic acid (i.e., the stable species, not the transition state structure we employ in our models); **(c)** the optimized transition state structure employed in the ab initio calculations of this study (see also Loerting et al., 2000). Numbers refer to atomic positions within the structure. Oxygen atom 4 is the one that is abstracted from the reactant carbonate ion during acid digestion (i.e., oxygen atoms 2 and 3 remain bound to carbon atom 1); **(d)** the only transition state structure isotopologue during the phosphoric acid digestion of $^{12}\text{C}^{16}\text{O}^{16}\text{O}^{16}\text{O}^{2-}$. Numbers refer to the isotopic mass, in AMU, of the atom; **(e-g)** three possible transition state structure isotopomers during the phosphoric acid digestion of $^{12}\text{C}^{18}\text{O}^{16}\text{O}^{16}\text{O}^{2-}$. Numbers again refer to isotopic mass of the atom.

2.2 Fractionation of CO_3^{2-} isotopologues during dissociation of carbonic acid

Carbonic acid, H_2CO_3 , has 20 naturally occurring isotopologues, not counting those containing D or ^{14}C , which can dissociate to produce 12 different isotopologues of product CO_2 (Table 3-1). Furthermore, many of the isotopologues of H_2CO_3 have more than one isotopomer because the various O sites are not structurally equivalent to one another (see Fig. 3-1). Isotopic fractionations during the dissociation of carbonic acid arise for two reasons: (1) the various isotopologues of carbonic acid differ from one another in their rates of dissociation; and (2) when an isotopologue has more than one isotopomer (e.g., Fig. 3-1), the relative rates of dissociation of those isotopomers differ from one another. However, since phosphoric acid digestion is always driven to completion before collecting and analyzing product CO_2 (i.e., all isotopologues of carbonic acid eventually decompose) the first type of isotope effects (e.g., the rate of dissociation of $\text{H}_2^{12}\text{C}^{16}\text{O}_3$ is faster than the weighted average dissociation rate of the three isotopomers of $\text{H}_2^{12}\text{C}^{18}\text{O}^{16}\text{O}_2$; Fig. 3-1d, 3-1e, 3-1f and 3-1g) will not be expressed in the final isotopic composition of product CO_2 , though they might influence the temporal evolution of the isotopic composition of product CO_2 . Only the second type of isotope effects contributes to the fact that final product CO_2 is expected to be lower in $^{18}\text{O}/^{16}\text{O}$ ratio than the reactant H_2CO_3 . For example, differences between the rates of dissociation of the three isotopomers of $\text{H}_2^{12}\text{C}^{18}\text{O}^{16}\text{O}_2$ promote $^{12}\text{C}^{16}\text{O}^{16}\text{O}$ relative to $^{12}\text{C}^{18}\text{O}^{16}\text{O}$ (i.e., those isotopomers that must break a $^{12}\text{C}-^{18}\text{O}$ bond in order to dissociate [Fig. 3-1e] do so more slowly than those isotopomers that must break a $^{12}\text{C}-^{16}\text{O}$ bond [Fig. 3-1f and 3-1g]).

Table 3-1 Evolution of different CO_3^{2-} isotopologues during phosphoric acid digestion of carbonate minerals.

Isotopologue of CO_3^{2-} Reactant	Mass [‡]	Abundance [§] of CO_3^{2-} Isotopologues	Isotopologue of H_2CO_3 Intermediate [¶]	Isotopologue of CO_2 Product	Mass [‡]	Fraction [¥]
$^{12}\text{C}^{16}\text{O}^{16}\text{O}^{16}\text{O}$	60	0.981845503	$\text{H}_2^{12}\text{C}^{16}\text{O}^{16}\text{O}^{16}\text{O}$	$^{12}\text{C}^{16}\text{O}^{16}\text{O}$	44	1
$^{13}\text{C}^{16}\text{O}^{16}\text{O}^{16}\text{O}$	61	0.011033194	$\text{H}_2^{13}\text{C}^{16}\text{O}^{16}\text{O}^{16}\text{O}$	$^{13}\text{C}^{16}\text{O}^{16}\text{O}$	45	1
$^{12}\text{C}^{17}\text{O}^{16}\text{O}^{16}\text{O}$	61	0.000373003	$\text{H}_2^{12}\text{C}^{17}\text{O}^{16}\text{O}^{16}\text{O}$ $\text{H}_2^{12}\text{C}^{16}\text{O}^{17}\text{O}^{16}\text{O}$ $\text{H}_2^{12}\text{C}^{16}\text{O}^{16}\text{O}^{17}\text{O}$	$^{12}\text{C}^{17}\text{O}^{16}\text{O}$ $^{12}\text{C}^{16}\text{O}^{17}\text{O}$ $^{12}\text{C}^{16}\text{O}^{16}\text{O}$	45 45 44	0.3345939 0.3358595 0.3295466
$^{12}\text{C}^{18}\text{O}^{16}\text{O}^{16}\text{O}$	62	0.001968797	$\text{H}_2^{12}\text{C}^{18}\text{O}^{16}\text{O}^{16}\text{O}$ $\text{H}_2^{12}\text{C}^{16}\text{O}^{18}\text{O}^{16}\text{O}$ $\text{H}_2^{12}\text{C}^{16}\text{O}^{16}\text{O}^{18}\text{O}$	$^{12}\text{C}^{18}\text{O}^{16}\text{O}$ $^{12}\text{C}^{16}\text{O}^{18}\text{O}$ $^{12}\text{C}^{16}\text{O}^{16}\text{O}$	46 46 44	0.3357121 0.3381400 0.3261479
$^{13}\text{C}^{17}\text{O}^{16}\text{O}^{16}\text{O}$	62	4.19151E-06	$\text{H}_2^{13}\text{C}^{17}\text{O}^{16}\text{O}^{16}\text{O}$ $\text{H}_2^{13}\text{C}^{16}\text{O}^{17}\text{O}^{16}\text{O}$ $\text{H}_2^{13}\text{C}^{16}\text{O}^{16}\text{O}^{17}\text{O}$	$^{13}\text{C}^{17}\text{O}^{16}\text{O}$ $^{13}\text{C}^{16}\text{O}^{17}\text{O}$ $^{13}\text{C}^{16}\text{O}^{16}\text{O}$	46 46 45	0.3345930 0.3359415 0.3359415
$^{12}\text{C}^{17}\text{O}^{17}\text{O}^{16}\text{O}$	62	1.41704E-07	$\text{H}_2^{12}\text{C}^{17}\text{O}^{17}\text{O}^{16}\text{O}$ $\text{H}_2^{12}\text{C}^{17}\text{O}^{16}\text{O}^{17}\text{O}$ $\text{H}_2^{12}\text{C}^{16}\text{O}^{17}\text{O}^{17}\text{O}$	$^{12}\text{C}^{17}\text{O}^{17}\text{O}$ $^{12}\text{C}^{17}\text{O}^{16}\text{O}$ $^{12}\text{C}^{16}\text{O}^{17}\text{O}$	46 45 45	0.3371440 0.3308090 0.3320470
$^{13}\text{C}^{18}\text{O}^{16}\text{O}^{16}\text{O}$	63	2.21238E-05	$\text{H}_2^{13}\text{C}^{18}\text{O}^{16}\text{O}^{16}\text{O}$ $\text{H}_2^{13}\text{C}^{16}\text{O}^{18}\text{O}^{16}\text{O}$ $\text{H}_2^{13}\text{C}^{16}\text{O}^{16}\text{O}^{18}\text{O}$	$^{13}\text{C}^{18}\text{O}^{16}\text{O}$ $^{13}\text{C}^{16}\text{O}^{18}\text{O}$ $^{13}\text{C}^{16}\text{O}^{16}\text{O}$	47 47 45	0.3357094 0.3382969 0.3259937
$^{12}\text{C}^{18}\text{O}^{17}\text{O}^{16}\text{O}$	63	7.47946E-07	$\text{H}_2^{12}\text{C}^{18}\text{O}^{17}\text{O}^{16}\text{O}$ $\text{H}_2^{12}\text{C}^{18}\text{O}^{16}\text{O}^{17}\text{O}$ $\text{H}_2^{12}\text{C}^{17}\text{O}^{18}\text{O}^{16}\text{O}$ $\text{H}_2^{12}\text{C}^{17}\text{O}^{16}\text{O}^{18}\text{O}$ $\text{H}_2^{12}\text{C}^{16}\text{O}^{18}\text{O}^{17}\text{O}$ $\text{H}_2^{12}\text{C}^{16}\text{O}^{17}\text{O}^{18}\text{O}$	$^{12}\text{C}^{18}\text{O}^{17}\text{O}$ $^{12}\text{C}^{18}\text{O}^{16}\text{O}$ $^{12}\text{C}^{17}\text{O}^{18}\text{O}$ $^{12}\text{C}^{17}\text{O}^{16}\text{O}$ $^{12}\text{C}^{16}\text{O}^{18}\text{O}$ $^{12}\text{C}^{16}\text{O}^{17}\text{O}$	47 46 47 45 46 47	0.1691418 0.1659645 0.1697232 0.1637057 0.1671522 0.1643126
$^{13}\text{C}^{17}\text{O}^{17}\text{O}^{16}\text{O}$	63	1.59235E-09	$\text{H}_2^{13}\text{C}^{17}\text{O}^{17}\text{O}^{16}\text{O}$ $\text{H}_2^{13}\text{C}^{17}\text{O}^{16}\text{O}^{17}\text{O}$ $\text{H}_2^{13}\text{C}^{16}\text{O}^{17}\text{O}^{17}\text{O}$	$^{13}\text{C}^{17}\text{O}^{17}\text{O}$ $^{13}\text{C}^{17}\text{O}^{16}\text{O}$ $^{13}\text{C}^{16}\text{O}^{17}\text{O}$	47 46 46	0.3372255 0.3307273 0.3320472
$^{12}\text{C}^{17}\text{O}^{17}\text{O}^{17}\text{O}$	63	5.38333E-11	$\text{H}_2^{12}\text{C}^{17}\text{O}^{17}\text{O}^{17}\text{O}$	$^{12}\text{C}^{17}\text{O}^{17}\text{O}$	46	1
$^{12}\text{C}^{18}\text{O}^{18}\text{O}^{16}\text{O}$	64	3.94783E-06	$\text{H}_2^{12}\text{C}^{18}\text{O}^{18}\text{O}^{16}\text{O}$ $\text{H}_2^{12}\text{C}^{18}\text{O}^{16}\text{O}^{18}\text{O}$ $\text{H}_2^{12}\text{C}^{16}\text{O}^{18}\text{O}^{18}\text{O}$	$^{12}\text{C}^{18}\text{O}^{18}\text{O}$ $^{12}\text{C}^{18}\text{O}^{16}\text{O}$ $^{12}\text{C}^{16}\text{O}^{18}\text{O}$	48 46 46	0.3406058 0.3285328 0.3308614
$^{13}\text{C}^{18}\text{O}^{17}\text{O}^{16}\text{O}$	64	8.40482E-09	$\text{H}_2^{13}\text{C}^{18}\text{O}^{17}\text{O}^{16}\text{O}$ $\text{H}_2^{13}\text{C}^{18}\text{O}^{16}\text{O}^{17}\text{O}$ $\text{H}_2^{13}\text{C}^{17}\text{O}^{18}\text{O}^{16}\text{O}$ $\text{H}_2^{13}\text{C}^{17}\text{O}^{16}\text{O}^{18}\text{O}$ $\text{H}_2^{13}\text{C}^{16}\text{O}^{18}\text{O}^{17}\text{O}$ $\text{H}_2^{13}\text{C}^{16}\text{O}^{17}\text{O}^{18}\text{O}$	$^{13}\text{C}^{18}\text{O}^{17}\text{O}$ $^{13}\text{C}^{18}\text{O}^{16}\text{O}$ $^{13}\text{C}^{17}\text{O}^{18}\text{O}$ $^{13}\text{C}^{17}\text{O}^{16}\text{O}$ $^{13}\text{C}^{16}\text{O}^{18}\text{O}$ $^{13}\text{C}^{16}\text{O}^{17}\text{O}$	48 47 48 46 47 46	0.1691819 0.1659230 0.1698016 0.1636285 0.1671893 0.1642757
$^{12}\text{C}^{18}\text{O}^{17}\text{O}^{17}\text{O}$	64	2.84145E-10	$\text{H}_2^{12}\text{C}^{18}\text{O}^{17}\text{O}^{17}\text{O}$ $\text{H}_2^{12}\text{C}^{17}\text{O}^{18}\text{O}^{17}\text{O}$ $\text{H}_2^{12}\text{C}^{17}\text{O}^{17}\text{O}^{18}\text{O}$	$^{12}\text{C}^{18}\text{O}^{17}\text{O}$ $^{12}\text{C}^{17}\text{O}^{18}\text{O}$ $^{12}\text{C}^{17}\text{O}^{17}\text{O}$	47 47 46	0.3344749 0.3356125 0.3299126
$^{13}\text{C}^{17}\text{O}^{17}\text{O}^{17}\text{O}$	64	6.04936E-13	$\text{H}_2^{13}\text{C}^{17}\text{O}^{17}\text{O}^{17}\text{O}$	$^{13}\text{C}^{17}\text{O}^{17}\text{O}$	47	1

Table 3-1. (Continued)

Isotopologue of CO_3^{2-} Reactant	Mass [‡]	Abundance [§] of CO_3^{2-} Isotopologues	Isotopologue of H_2CO_3 Intermediate [£]	Isotopologue of CO_2 Product	Mass [‡]	Fraction [¥]
$^{13}\text{C}^{18}\text{O}^{18}\text{O}^{16}\text{O}$	65	4.43626E-08	$\text{H}_2^{13}\text{C}^{18}\text{O}^{18}\text{O}^{16}\text{O}$	$^{13}\text{C}^{18}\text{O}^{18}\text{O}$	49	0.3407615
			$\text{H}_2^{13}\text{C}^{18}\text{O}^{16}\text{O}^{18}\text{O}$	$^{13}\text{C}^{18}\text{O}^{16}\text{O}$	47	0.3283773
			$\text{H}_2^{13}\text{C}^{16}\text{O}^{18}\text{O}^{18}\text{O}$	$^{13}\text{C}^{16}\text{O}^{18}\text{O}$	47	0.3308612
$^{12}\text{C}^{18}\text{O}^{18}\text{O}^{17}\text{O}$	65	1.49978E-09	$\text{H}_2^{12}\text{C}^{18}\text{O}^{18}\text{O}^{17}\text{O}$	$^{12}\text{C}^{18}\text{O}^{18}\text{O}$	48	0.3367737
			$\text{H}_2^{12}\text{C}^{18}\text{O}^{17}\text{O}^{18}\text{O}$	$^{12}\text{C}^{18}\text{O}^{17}\text{O}$	47	0.3310555
			$\text{H}_2^{12}\text{C}^{17}\text{O}^{18}\text{O}^{18}\text{O}$	$^{12}\text{C}^{17}\text{O}^{18}\text{O}$	47	0.3321708
$^{13}\text{C}^{18}\text{O}^{17}\text{O}^{17}\text{O}$	65	3.19299E-12	$\text{H}_2^{13}\text{C}^{18}\text{O}^{17}\text{O}^{17}\text{O}$	$^{13}\text{C}^{18}\text{O}^{17}\text{O}$	48	0.3344739
			$\text{H}_2^{13}\text{C}^{17}\text{O}^{18}\text{O}^{17}\text{O}$	$^{13}\text{C}^{17}\text{O}^{18}\text{O}$	48	0.3356870
			$\text{H}_2^{13}\text{C}^{17}\text{O}^{17}\text{O}^{18}\text{O}$	$^{13}\text{C}^{17}\text{O}^{17}\text{O}$	47	0.3298391
$^{12}\text{C}^{18}\text{O}^{18}\text{O}^{18}\text{O}$	66	7.91619E-09	$\text{H}_2^{12}\text{C}^{18}\text{O}^{18}\text{O}^{18}\text{O}$	$^{12}\text{C}^{18}\text{O}^{18}\text{O}$	48	1
$^{13}\text{C}^{18}\text{O}^{18}\text{O}^{17}\text{O}$	66	1.68533E-11	$\text{H}_2^{13}\text{C}^{18}\text{O}^{18}\text{O}^{17}\text{O}$	$^{13}\text{C}^{18}\text{O}^{18}\text{O}$	49	0.3368476
			$\text{H}_2^{13}\text{C}^{18}\text{O}^{17}\text{O}^{18}\text{O}$	$^{13}\text{C}^{18}\text{O}^{17}\text{O}$	48	0.3309813
			$\text{H}_2^{13}\text{C}^{17}\text{O}^{18}\text{O}^{18}\text{O}$	$^{13}\text{C}^{17}\text{O}^{18}\text{O}$	48	0.3321711
$^{13}\text{C}^{18}\text{O}^{18}\text{O}^{18}\text{O}$	67	8.89558E-11	$\text{H}_2^{13}\text{C}^{18}\text{O}^{18}\text{O}^{18}\text{O}$	$^{13}\text{C}^{18}\text{O}^{18}\text{O}$	49	1

[‡] Nominal cardinal mass in amu.

[§] Stochastic abundances, i.e., the abundances when all the isotopes are stochastically distributed within the reactant carbonate, with a bulk isotopic composition of $\delta^{13}\text{C}_{\text{VPDB}}=0\text{\textperthousand}$ and $\delta^{18}\text{O}_{\text{VSMOW}}=0\text{\textperthousand}$.

[£] Oxygen atoms in H_2CO_3 intermediate are expressed in the order of atom 2, 3, 4 in Fig. 3-1, and the underlined atoms (atom 4) are the ones to be abstracted during phosphoric acid digestion.

[¥] Predicted respective fractions of different product CO_2 isotopologues from the reactant CO_3^{2-} isotopologues at 25°C, based on our H_2CO_3 model.

We calculate the proportions of CO_2 isotopologues produced by dissociation of each H_2CO_3 isotopologue based on a formulation that is exemplified as follows for the case of $\text{H}_2^{12}\text{C}^{18}\text{O}^{16}\text{O}_2$. This isotopologue of carbonic acid can dissociate to form two isotopologues of CO_2 , $^{12}\text{C}^{18}\text{O}^{16}\text{O}$ and $^{12}\text{C}^{16}\text{O}_2$. The relative abundance of each of these products is calculated through the functions:

$$n_{^{12}C^{16}O^{16}O-H_2^{12}C^{18}O^{16}O^{16}O} = \frac{R_{^{12}C^{16}O^{16}O-H_2^{12}C^{18}O^{16}O^{16}O}}{R_{^{12}C^{16}O^{16}O-H_2^{12}C^{18}O^{16}O^{16}O} + R_{^{12}C^{18}O^{16}O-H_2^{12}C^{18}O^{16}O^{16}O} + R_{^{12}C^{16}O^{18}O-H_2^{12}C^{18}O^{16}O^{16}O}} \times n_{H_2^{12}C^{18}O^{16}O^{16}O}$$

$$n_{^{12}C^{18}O^{16}O-H_2^{12}C^{18}O^{16}O^{16}O} = \frac{R_{^{12}C^{18}O^{16}O-H_2^{12}C^{18}O^{16}O^{16}O}}{R_{^{12}C^{16}O^{16}O-H_2^{12}C^{18}O^{16}O^{16}O} + R_{^{12}C^{18}O^{16}O-H_2^{12}C^{18}O^{16}O^{16}O} + R_{^{12}C^{16}O^{18}O-H_2^{12}C^{18}O^{16}O^{16}O}},$$

where $n_{^{12}C^{16}O^{16}O-H_2^{12}C^{18}O^{16}O^{16}O}$ and $n_{^{12}C^{18}O^{16}O-H_2^{12}C^{18}O^{16}O^{16}O}$ denote the total numbers of molecules of $^{12}C^{16}O^{16}O$ and $^{12}C^{18}O^{16}O$ produced from dissociation of $H_2^{12}C^{18}O^{16}O_2$; $n_{H_2^{12}C^{18}O^{16}O^{16}O}$ is the number of molecules of reactant $H_2^{12}C^{18}O^{16}O_2$ (which we take to equal the abundance of $X^{12}C^{18}O^{16}O_2$ in the carbonate undergoing phosphoric acid digestion; i.e., we ignore, for the time being, any isotopic discrimination associated with step 1 of the overall reaction, as defined above); and $R_{^{12}C^{16}O^{16}O-H_2^{12}C^{18}O^{16}O^{16}O}$, $R_{^{12}C^{18}O^{16}O-H_2^{12}C^{18}O^{16}O^{16}O}$ and $R_{^{12}C^{16}O^{18}O-H_2^{12}C^{18}O^{16}O^{16}O}$ denote the dissociation rates of the three isotopomers of $H_2^{12}C^{18}O^{16}O^{16}O$ (Fig. 3-1e, 3-1f, 3-1g). These R values are calculated based on statistical thermodynamic principles, as described in section 2.1 and exemplified below:

$$R_{^{12}C^{16}O^{16}O-H_2^{12}C^{18}O^{16}O^{16}O} = |v_L^\dagger|_{H_2^{12}C^{16}O^{16}\underline{O^{18}O}} \times \frac{Q^{\dagger}_{H_2^{12}C^{16}O^{16}O^{18}O}}{Q_{H_2^{12}C^{16}O^{16}O^{18}O}} \times [H_2^{12}C^{16}O^{16}O^{18}O];$$

$$R_{^{12}C^{18}O^{16}O-H_2^{12}C^{18}O^{16}O^{16}O} = |v_L^\dagger|_{H_2^{12}C^{18}O^{16}\underline{O^{16}O}} \times \frac{Q^{\dagger}_{H_2^{12}C^{18}O^{16}O^{16}O}}{Q_{H_2^{12}C^{18}O^{16}O^{16}O}} \times [H_2^{12}C^{18}O^{16}O^{16}O];$$

$$R_{^{12}C^{16}O^{18}O-H_2^{12}C^{18}O^{16}O^{16}O} = |v_L^\dagger|_{H_2^{12}C^{16}O^{18}\underline{O^{16}O}} \times \frac{Q^{\dagger}_{H_2^{12}C^{16}O^{18}O^{16}O}}{Q_{H_2^{12}C^{16}O^{18}O^{16}O}} \times [H_2^{12}C^{16}O^{18}O^{16}O],$$

where the underscores in the subscripts denote the structural site of the O whose bond with C is broken during dissociation (e.g., $H_2^{12}C^{16}O^{16}O\underline{O^{18}O}$ refers to the situation illustrated in Figure 1e, $H_2^{12}C^{18}O^{16}O\underline{O^{16}O}$ refers to Figure 1f, and $H_2^{12}C^{16}O^{18}O\underline{O^{16}O}$ refers to

Fig. 3-1g); and $[H_2^{12}C^{16}O^{16}O^{18}O]$, $[H_2^{12}C^{18}O^{16}O^{16}O]$, $[H_2^{12}C^{16}O^{18}O^{16}O]$ are the abundances of the different isotopomers of $H_2^{12}C^{18}O^{16}O_2$. Because the lifetime of carbonic acid is relatively long under anhydrous conditions (Loerting et al., 2000), we assume the concentrations of these various carbonic acid isotopomers are in equilibrium (presumably through the exchanges of protons):

$$\frac{[H_2^{12}C^{16}O^{16}O^{18}O]}{Q_{H_2^{12}C^{16}O^{16}O^{18}O}} = \frac{[H_2^{12}C^{18}O^{16}O^{16}O]}{Q_{H_2^{12}C^{18}O^{16}O^{16}O}} = \frac{[H_2^{12}C^{16}O^{18}O^{16}O]}{Q_{H_2^{12}C^{16}O^{18}O^{16}O}}$$

therefore,

$$R_{^{12}C^{16}O^{16}O-H_2^{12}C^{18}O^{16}O^{16}O} : R_{^{12}C^{18}O^{16}O-H_2^{12}C^{18}O^{16}O^{16}O} : R_{^{12}C^{16}O^{18}O-H_2^{12}C^{18}O^{16}O^{16}O}$$

$$= (|\nu_L^\dagger| \times Q^{\dagger})_{H_2^{12}C^{16}O^{16}O^{18}O} : (|\nu_L^\dagger| \times Q^{\dagger})_{H_2^{12}C^{18}O^{16}O^{16}O} : (|\nu_L^\dagger| \times Q^{\dagger})_{H_2^{12}C^{16}O^{18}O^{16}O}$$

The relations given above for the case of $H_2^{12}C^{18}O^{16}O_2$ are applied to all the isotopologues of H_2CO_3 that are capable of producing more than one CO_2 isotopologue (for H_2CO_3 isotopologues capable of producing only one CO_2 isotopologue, n_i values for that CO_2 isotopologue produced from that H_2CO_3 isotopologue equal n_j of that H_2CO_3 isotopologue, e.g., for isotopologue $H_2^{12}C^{16}O_3$, $n_{^{12}C^{16}O^{16}O-H_2^{12}C^{16}O^{16}O^{16}O} = n_{H_2^{12}C^{16}O^{16}O^{16}O}$). The summation of all n_i values for the various isotopologues of CO_2 produced from all isotopologues of H_2CO_3 allow us to calculate the net isotopic fractionations associated with acid digestion (Table 3-1).

2.3.3 Exploration of cation effects during phosphoric acid digestion through cluster models

The cation compositions of carbonate minerals apparently exert a second-order, but measurable influence on the oxygen isotope fractionation associated with phosphoric acid digestion (e.g., Gilg et al., 2003). The H_2CO_3 -dissociation model we described above cannot account for such effects because it considers isotopic fractionation only after separation of carbonate ion units from the metals to which they were bonded in the crystal lattice. Thus, while our approach has the advantage of allowing for a relatively rigorous treatment of part of the acid digestion process, it is an over-simplification that will not permit full understanding of differences in fractionations between various types of carbonate minerals. We have tried to develop an understanding of these second-order effects by constructing a cluster model that describes the dissociation of H_2CO_3 attached to XCO_3 clusters, which simulates the situation where H_2CO_3 is influenced by bonds on the surface of adjacent, un-reacted carbonate. Similar ab initio cluster models have been used previously to investigate local properties and reactions of carbonate surfaces, such as hydration (Mao and Siders, 1997) and adsorption (Ruuska et al., 1999). In this study, we limit our model to small clusters comprising only two XCO_3 units, i.e., $(\text{XCO}_3)_2 \cdot \text{H}_2\text{CO}_3$, where $\text{X} = \text{Mg}^{2+}, \text{Ca}^{2+}, \text{Mn}^{2+}, \text{Fe}^{2+}, \text{Zn}^{2+}, \text{Sr}^{2+}, \text{Pb}^{2+}, \text{Ba}^{2+}$.

Following the same method outlined in previous sections, we obtain the structures of the transition states for these clusters (Fig. 3-2) and derive the isotope fractionations during phosphoric acid digestion of different carbonate minerals. Note, we will confine our discussion on this cluster model to section 4.4. In other parts of the text, “model” refers to the H_2CO_3 –only model described in section 2.2.1, unless stated otherwise.

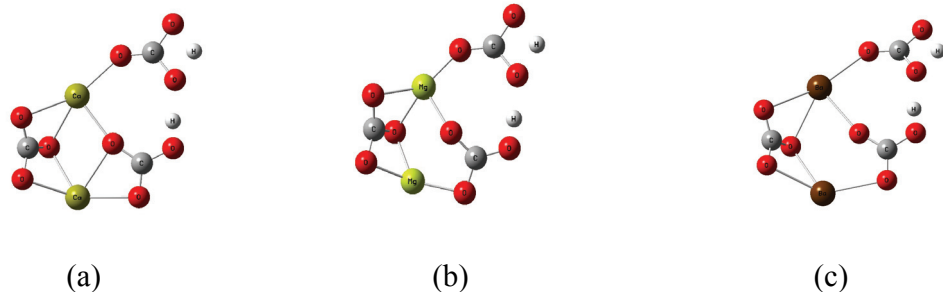


Figure 3-2: Representative transition state structures during phosphoric acid digestion of carbonate minerals, as in our ‘cluster models’ that attempt to describe interactions between disassociating H_2CO_3 and adjacent mineral surfaces. Individual structures are: **(a)** $(\text{CaCO}_3)_2 \cdot \text{H}_2\text{CO}_3$; **(b)** $(\text{MgCO}_3)_2 \cdot \text{H}_2\text{CO}_3$; and **(c)** $(\text{BaCO}_3)_2 \cdot \text{H}_2\text{CO}_3$. Letters identify the chemical identity of each atom.

2.3 Computational methods

Molecular geometries were optimized and bond frequencies were calculated for the transition state isotopologues using the Jaguar program (Ringnalda et al., 2005), on a workstation cluster with 79 Dell PowerEdge-2650 server nodes (Xeno, 2.2-2.4GHz, 512K) in the Materials and Process Simulation Center at Caltech. The singlet state electron wave functions of the molecular configurations were built using a density functional theory with hybrid functionals, B3LYP, and extended basis sets 6–31G* (for the H_2CO_3 model) and LACV3P (for the cluster model). These were selected based on their previous success in similar ab initio models (Foresman and Frisch, 1993; Scott and Radom, 1996; Ringnalda et al., 2005).

Ab initio calculations tend to overestimate vibration frequencies, mostly because they neglect the effects of anharmonicity (Scott and Radom, 1996). Therefore, a scaling factor based on the comparison between the calculated bond vibration frequencies and experimentally measured frequencies usually need to be applied to harmonic frequencies derived from ab initio models. No experimentally-measured frequencies of the transition

state are available for comparison with our ab initio model. Therefore, we have used a universal frequency scaling factor of 0.9614, previously shown to be appropriate for B3LYP/6-31G* calculations (Scott and Radom, 1996). To test the effectiveness of this assumed frequency scaling factor, we computed the vibration frequencies for the carbonic acid molecule using the B3LYP/6-31G* method, applied the 0.9614 scaling factor, and compared the scaled bond-vibration frequencies to the previously published results (Tossell, 2006) from more sophisticated, higher level calculations (CCSD/6-311+G(2d,p) level) and anharmonicity corrections (B3LYP/CBSB7 level). Results from these two independent models are generally consistent with each other (Fig. 3-3), suggesting that our scaling of the B3LYP/6-31G* model adequately accounts for systematic errors due to anharmonicity and related effects. No frequency scaling was employed for the cluster model calculations, due to the absence of a universal scaling factor for the LACV3P basis set. However, we show below that any influence of the scaling factor is likely to be negligible for the general conclusions we reach based on our cluster model.

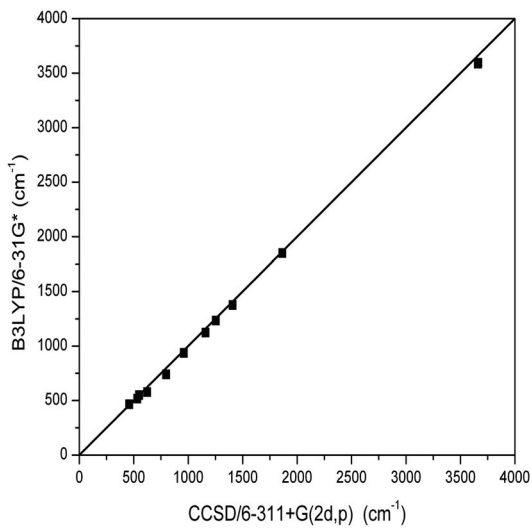


Figure 3-3: Comparison of vibration frequencies of gas-phase carbonic acid (H_2CO_3) obtained in this study using B3LYP/6-31G* ab initio models with a scaling factor of 0.9614 vs. those obtained through more sophisticated higher level calculations and anharmonicity corrections (CCSD/6-311+G(2d,p)) with B3LYP/CBSB7 based anharmonic calculations and corrections; Tossell, 2006). The solid line indicates a 1:1 correlation.

3. EXPERIMENTAL METHODS

Starting materials for the experiments consisted of three different calcite materials: NBS19 carbonate standard distributed from IAEA (1 aliquot); MZ carbonate preheated at 1100°C from Ghosh et al. 2006 (1 aliquot); and Sigma-carb purchased from Sigma-Aldrich Co. (2 aliquots). The materials were loaded into Pt capsules, which were then sealed by welding and inserted into CaF₂ cell assemblies. The experiments were conducted in a piston-cylinder apparatus at 1550 or 1650°C and either 2 or 3 GPa for 24 hours. Temperature was monitored using type C thermocouples, uncorrected for the effect of pressure on emf. The temperature and pressure conditions were chosen to be close to or above the melting point of CaCO₃ (Suito et al., 2001) to ensure complete stochastic distributions of isotopes (which might not occur over laboratory timescales due to solid-state recrystallization alone; Ghosh et al., 2006). Experimental charges were quenched rapidly by turning off the power to the furnace, resulting in cooling to below 200°C in less than 20 seconds and to room temperature within 1 minute. Carbonate crystals were recovered by carefully stripping off the Pt capsule. The phase of each sample was verified using X-ray diffraction, and the aliquots were then reacted with anhydrous phosphoric acid ($\rho=1.91\text{g/cm}^3$) at 25°C for 18-24 hrs. The Δ_{47} values of released CO₂ were analyzed on a gas source mass spectrometer configured to simultaneously measure masses 44 to 49. A detailed description of the mass spectrometer configuration and analysis procedures is given by Ghosh et al (2006).

4. RESULTS AND DISCUSSION

4.1 Experimentally determined acid-digestion fractionation of Δ_{47}

We assume that heating CaCO_3 to temperatures and pressures above its melting point should drive its ^{13}C and ^{18}O toward a stochastic distribution. Thus, we anticipate that the Δ_{47} value of the CO_2 extracted from CaCO_3 that has been quenched from melt should equal 0 (the stochastic value) plus any fractionation associated with phosphoric acid digestion. There is no simple way for us prove that the stochastic distribution in carbonate is preserved during rapid quenching from a melt, but this seems like a reasonable inference given previous evidence that isotopic redistribution in crystalline calcite is inefficient at laboratory timescales, even at high temperature (Ghosh et al., 2006). X-ray diffraction analyses confirmed that CaCO_3 samples quenched from heating experiments are all of the calcite structure. The Δ_{47} values of CO_2 gases derived from these CaCO_3 samples average $0.232 \pm 0.015\text{\textperthousand}$ (1σ), and show no systematic difference between the experiments at $1550^\circ\text{C}/2\text{Gpa}$ and at $1650^\circ\text{C}/3\text{Gpa}$, nor any correlation with the Δ_{47} values of the CO_2 extracted from these samples before recrystallization (Table 2; note such a correlation was observed by Ghosh et al., 2006, in the products of solid-state recrystallization experiments, leading them to conclude that such treatment led to only partial approach to the stochastic distribution). These results support our inference that our heating experiments succeeded at driving these samples to a stochastic distribution, and thus imply that the ‘clumped isotope’ fractionation of $^{13}\text{C}-^{18}\text{O}$ bonds during phosphoric acid digestion of calcite corresponds to an increase in Δ_{47} of $0.23\text{\textperthousand}$ at 25°C .

Table 3-2 Fractionation of multiply-substituted isotopologues, Δ_{47}^* (see text for the definition), during phosphoric acid digestion of CaCO_3 at 25°C determined through phosphoric acid digestion of high temperature and pressure equilibrated CaCO_3 (calcite) samples.

Sample	Before re-crystallization			Re-crystallization experiments			After re-crystallization			
	Δ_{47} (‰)	$\delta^{13}\text{C}$ VPDB (‰)	$\delta^{18}\text{O}$ VSMOW (‰)	T (°C)	P (GPa)	t (hrs)	Δ_{47} (‰)	$1\sigma^{\ddagger}$	$\delta^{13}\text{C}$ VPDB (‰)	$\delta^{18}\text{O}$ VSMOW (‰)
Re-crystallized MZ	0.267	-13.66	34.61	1550	2	24	0.234	0.025(3)	-17.03	34.11
NBS19 standard	0.334	2.01	39.28	1550	2	24	0.210	0.012(2)	-4.82	38.64
Sigma carbonate	0.468	-42.28	20.55	1550	2	24	0.243	0.015(3)	-33.96	20.44
				1650	3	24	0.239	0.009(2)	-25.82	20.78

[‡] 1σ denotes the external standard deviation. Numbers in the bracket indicate the numbers of independent replicate extraction and isotopic analyses of the carbonate samples after re-crystallization.

4.2 Model results for the oxygen-isotope and clumped-isotope fractionations associated with carbonic acid dissociation

Table 3-3 summarizes the vibration frequencies we calculate for the various isotopologues of H_2CO_3 . The negative frequencies, ω_1 , correspond to the decomposition frequencies ν_L^{\dagger} in section 3.1. Following procedures outlined in section 3, these frequencies are used in our transition-state-based predictions of the proportions of different CO_2 isotopologues that are produced by dissociation of the H_2CO_3 intermediate, and the temperature dependence of those proportions. Unless stated otherwise, all of our calculations assume that reactant carbonate has a $\delta^{13}\text{C}_{\text{VPDB}}$ value of 0‰, a $\delta^{18}\text{O}_{\text{VSMOW}}$ value of 0‰ and a stochastic distribution of multiply-substituted isotopologues (Table 1), and that the H_2CO_3 intermediate is identical in isotopic composition to reactant carbonate.

Table 3-3 Scaled vibration frequencies (unit: cm^{-1}) for different transition state (TS) isotopologues during phosphoric acid digestion of carbonate minerals (H_2CO_3 model, DFT-B3LYP/6-31G* with a frequency scaling factor of 0.9614). The underlined atoms denote the ones to be abstracted during acid digestion.

Isotopologue	ω_1	ω_2	ω_3	ω_4	ω_5	ω_6	ω_7	ω_8	ω_9	ω_{10}	ω_{11}	ω_{12}
$\text{H}_2^{12}\text{C}^{16}\text{O}^{16}\text{O}^{16}\text{O}$	-1650.22	381.74	489.85	588.65	720.73	760.00	927.16	1246.50	1267.18	1903.52	2102.57	3573.50
$\text{H}_2^{13}\text{C}^{16}\text{O}^{16}\text{O}^{16}\text{O}$	-1643.59	380.77	488.29	577.55	710.57	754.21	920.93	1234.69	1266.94	1881.48	2069.33	3573.50
$\text{H}_2^{12}\text{C}^{17}\text{O}^{16}\text{O}^{16}\text{O}$	-1649.47	381.07	489.52	587.30	716.91	750.19	925.95	1230.07	1266.52	1901.17	2101.66	3573.50
$\text{H}_2^{12}\text{C}^{16}\text{O}^{17}\text{O}^{16}\text{O}$	-1650.10	378.19	488.88	587.13	719.09	755.13	926.78	1237.11	1266.92	1896.67	2094.47	3573.50
$\text{H}_2^{12}\text{C}^{16}\text{O}^{16}\text{O}^{17}\text{O}$	-1649.38	377.05	487.91	587.36	713.34	757.87	924.34	1246.34	1265.39	1902.99	2102.51	3567.31
$\text{H}_2^{12}\text{C}^{18}\text{O}^{16}\text{O}^{16}\text{O}$	-1648.80	380.42	489.21	586.08	713.11	741.52	924.84	1215.38	1265.98	1899.15	2100.89	3573.50
$\text{H}_2^{12}\text{C}^{16}\text{O}^{18}\text{O}^{16}\text{O}$	-1649.99	374.93	488.00	585.78	717.47	750.72	926.43	1228.35	1266.80	1890.27	2087.85	3573.50
$\text{H}_2^{12}\text{C}^{16}\text{O}^{16}\text{O}^{18}\text{O}$	-1648.64	372.65	486.21	586.06	706.41	756.43	921.86	1246.19	1263.81	1902.53	2102.45	3561.83
$\text{H}_2^{13}\text{C}^{17}\text{O}^{16}\text{O}^{16}\text{O}$	-1642.83	380.13	488.01	576.12	707.41	744.04	919.75	1217.63	1266.31	1878.83	2068.74	3573.50
$\text{H}_2^{13}\text{C}^{16}\text{O}^{17}\text{O}^{16}\text{O}$	-1643.46	377.27	487.23	576.01	708.42	750.10	920.55	1225.28	1266.72	1872.20	2063.05	3573.50
$\text{H}_2^{13}\text{C}^{16}\text{O}^{16}\text{O}^{17}\text{O}$	-1642.75	376.08	486.35	576.41	704.07	751.04	918.05	1234.52	1265.14	1881.01	2069.22	3567.30
$\text{H}_2^{12}\text{C}^{17}\text{O}^{17}\text{O}^{16}\text{O}$	-1649.35	377.52	488.56	585.76	715.41	745.12	925.59	1220.74	1266.33	1894.08	2093.59	3573.50
$\text{H}_2^{12}\text{C}^{17}\text{O}^{16}\text{O}^{17}\text{O}$	-1648.63	376.41	487.58	585.96	709.09	748.37	923.15	1229.93	1264.71	1900.64	2101.59	3567.31
$\text{H}_2^{12}\text{C}^{16}\text{O}^{17}\text{O}^{17}\text{O}$	-1649.26	373.46	486.96	585.84	711.98	752.68	923.96	1236.95	1265.12	1896.15	2094.39	3567.31
$\text{H}_2^{12}\text{C}^{18}\text{O}^{16}\text{O}^{16}\text{O}$	-1642.14	379.51	487.73	574.82	704.33	734.92	918.66	1202.37	1265.78	1876.56	2068.24	3573.50
$\text{H}_2^{13}\text{C}^{16}\text{O}^{18}\text{O}^{16}\text{O}$	-1643.34	374.05	486.27	574.66	706.31	746.40	920.21	1216.51	1266.59	1863.66	2058.04	3573.50
$\text{H}_2^{12}\text{C}^{16}\text{O}^{16}\text{O}^{18}\text{O}$	-1642.00	371.68	484.64	575.27	697.76	748.85	915.50	1234.38	1263.55	1880.60	2069.11	3561.83
$\text{H}_2^{12}\text{C}^{18}\text{O}^{17}\text{O}^{16}\text{O}$	-1648.68	376.86	488.26	584.53	711.79	736.22	924.50	1206.14	1265.81	1891.85	2092.85	3573.50
$\text{H}_2^{12}\text{C}^{18}\text{O}^{16}\text{O}^{17}\text{O}$	-1647.96	375.78	487.27	584.69	704.84	740.04	922.07	1215.25	1264.17	1898.62	2100.82	3567.30
$\text{H}_2^{12}\text{C}^{17}\text{O}^{18}\text{O}^{16}\text{O}$	-1649.24	374.25	487.71	584.41	713.89	740.56	925.26	1212.10	1266.21	1887.46	2087.00	3573.50
$\text{H}_2^{12}\text{C}^{17}\text{O}^{16}\text{O}^{18}\text{O}$	-1647.89	372.02	485.88	584.61	701.79	747.20	920.69	1229.81	1263.12	1900.18	2101.54	3561.83
$\text{H}_2^{12}\text{C}^{16}\text{O}^{18}\text{O}^{17}\text{O}$	-1649.15	370.15	486.11	584.50	710.69	747.92	923.62	1228.19	1265.00	1889.76	2087.76	3567.31
$\text{H}_2^{12}\text{C}^{16}\text{O}^{17}\text{O}^{18}\text{O}$	-1648.51	369.01	485.28	584.55	705.19	751.07	921.48	1236.82	1263.53	1895.70	2094.33	3561.83
$\text{H}_2^{13}\text{C}^{17}\text{O}^{17}\text{O}^{16}\text{O}$	-1642.70	376.62	486.96	574.56	705.29	739.84	919.39	1208.33	1266.13	1869.28	2062.50	3573.50
$\text{H}_2^{13}\text{C}^{17}\text{O}^{16}\text{O}^{17}\text{O}$	-1641.99	375.46	486.07	574.94	700.60	741.04	916.89	1217.48	1264.51	1878.36	2068.62	3567.30
$\text{H}_2^{13}\text{C}^{16}\text{O}^{17}\text{O}^{17}\text{O}$	-1642.62	372.53	485.31	574.88	702.27	746.55	917.68	1225.12	1264.92	1871.74	2062.91	3567.30

Table 3-3 (Continued)

Isotopologue	Φ₁	Φ₂	Φ₃	Φ₄	Φ₅	Φ₆	Φ₇	Φ₈	Φ₉	Φ₁₀	Φ₁₁	Φ₁₂
H ₂ ¹² C ¹⁷ O ¹⁷ O ¹⁷ O <u>Q</u>	-1648.51	372.80	486.65	584.43	707.89	742.97	922.80	1220.60	1264.52	1893.56	2093.51	3567.30
H ₂ ¹² C ¹⁸ O ¹⁸ O ¹⁶ O <u>Q</u>	-1648.57	373.59	487.42	583.16	710.40	731.48	924.19	1197.60	1265.70	1885.04	2086.30	3573.50
H ₂ ¹² C ¹⁸ O ¹⁶ O ¹⁸ O <u>Q</u>	-1647.21	371.41	485.56	583.28	697.20	739.13	919.62	1215.14	1262.56	1898.16	2100.76	3561.82
H ₂ ¹² C ¹⁶ O ¹⁸ O ¹⁸ O <u>Q</u>	-1648.40	365.67	484.44	583.22	704.07	746.11	921.15	1228.05	1263.40	1889.31	2087.69	3561.83
H ₂ ¹³ C ¹⁸ O ¹⁷ O ¹⁶ O <u>Q</u>	-1642.01	375.99	486.70	573.25	702.27	730.63	918.33	1193.18	1265.62	1866.79	2062.04	3573.50
H ₂ ¹³ C ¹⁸ O ¹⁶ O ¹⁷ O <u>Q</u>	-1641.30	374.86	485.79	573.61	697.17	732.16	915.83	1202.23	1263.98	1876.09	2068.12	3567.30
H ₂ ¹³ C ¹⁷ O ¹⁸ O ¹⁶ O <u>Q</u>	-1642.58	373.39	486.01	573.20	703.17	736.12	919.08	1199.68	1266.01	1860.50	2057.53	3573.50
H ₂ ¹³ C ¹⁷ O ¹⁶ O ¹⁸ O <u>Q</u>	-1641.23	371.07	484.35	573.76	693.95	739.07	914.36	1217.36	1262.91	1877.95	2068.52	3561.82
H ₂ ¹³ C ¹⁶ O ¹⁸ O ¹⁷ O <u>Q</u>	-1642.50	369.27	484.37	573.53	700.54	742.45	917.34	1216.33	1264.79	1863.21	2057.90	3567.30
H ₂ ¹³ C ¹⁶ O ¹⁷ O ¹⁸ O <u>Q</u>	-1641.87	368.09	483.62	573.74	696.18	744.09	915.14	1224.97	1263.33	1871.34	2062.80	3561.82
H ₂ ¹² C ¹⁸ O ¹⁷ O ¹⁷ O <u>Q</u>	-1647.84	372.17	486.35	583.15	703.81	734.43	921.73	1206.01	1264.00	1891.33	2092.77	3567.30
H ₂ ¹² C ¹⁷ O ¹⁸ O ¹⁷ O <u>Q</u>	-1648.40	369.49	485.81	583.08	706.73	738.01	922.48	1211.96	1264.41	1886.95	2086.92	3567.30
H ₂ ¹² C ¹⁷ O ¹⁷ O ¹⁸ O <u>Q</u>	-1647.76	368.38	484.96	583.09	700.72	741.63	920.33	1220.48	1262.93	1893.11	2093.45	3561.82
H ₂ ¹³ C ¹⁸ O ¹⁷ O ¹⁷ O <u>Q</u>	-1641.85	371.91	485.04	573.39	698.92	736.38	916.54	1208.18	1264.33	1868.83	2062.36	3567.30
H ₂ ¹² C ¹⁸ O ¹⁸ O ¹⁶ O <u>Q</u>	-1641.90	372.76	485.76	571.88	700.13	726.89	918.04	1184.64	1265.50	1857.79	2057.10	3573.50
H ₂ ¹³ C ¹⁸ O ¹⁶ O ¹⁸ O <u>Q</u>	-1640.55	370.49	484.08	572.38	690.16	730.46	913.32	1202.12	1262.38	1875.68	2068.02	3561.82
H ₂ ¹³ C ¹⁶ O ¹⁸ O ¹⁸ O <u>Q</u>	-1641.75	364.78	482.70	572.40	694.69	739.72	914.81	1216.18	1263.20	1862.82	2057.77	3561.82
H ₂ ¹² C ¹⁸ O ¹⁸ O ¹⁷ O <u>Q</u>	-1647.73	368.85	485.53	581.79	702.81	729.25	921.42	1197.47	1263.89	1884.52	2086.21	3567.30
H ₂ ¹² C ¹⁸ O ¹⁷ O ¹⁸ O <u>Q</u>	-1647.09	367.76	484.66	581.75	696.27	733.38	919.28	1205.90	1262.40	1890.88	2092.70	3561.82
H ₂ ¹² C ¹⁷ O ¹⁸ O ¹⁸ O <u>Q</u>	-1647.65	365.03	484.14	581.75	699.73	736.48	920.02	1211.83	1262.81	1886.50	2086.84	3561.82
H ₂ ¹³ C ¹⁸ O ¹⁷ O ¹⁷ O <u>Q</u>	-1641.17	371.29	484.78	572.05	695.63	727.32	915.50	1193.04	1263.82	1866.33	2061.90	3567.30
H ₂ ¹³ C ¹⁷ O ¹⁸ O ¹⁷ O <u>Q</u>	-1641.74	368.63	484.12	572.03	697.26	732.17	916.23	1199.52	1264.21	1860.05	2057.39	3567.30
H ₂ ¹³ C ¹⁷ O ¹⁷ O ¹⁸ O <u>Q</u>	-1641.10	367.48	483.35	572.22	692.51	734.13	914.02	1208.05	1262.73	1868.42	2062.24	3561.82
H ₂ ¹² C ¹⁸ O ¹⁸ O ¹⁸ O <u>Q</u>	-1646.98	364.40	483.85	580.40	695.42	728.04	918.98	1197.36	1262.30	1884.07	2086.13	3561.82
H ₂ ¹³ C ¹⁸ O ¹⁸ O ¹⁷ O <u>Q</u>	-1641.05	368.01	483.87	570.68	694.07	722.97	915.21	1184.49	1263.70	1857.34	2056.96	3567.30
H ₂ ¹³ C ¹⁸ O ¹⁷ O ¹⁸ O <u>Q</u>	-1640.42	366.88	483.09	570.83	688.88	725.32	913.00	1192.92	1262.22	1865.93	2061.78	3561.82
H ₂ ¹³ C ¹⁷ O ¹⁸ O ¹⁸ O <u>Q</u>	-1640.99	364.17	482.44	570.86	691.14	729.60	913.71	1199.39	1262.62	1859.66	2057.26	3561.82
H ₂ ¹³ C ¹⁸ O ¹⁸ O ¹⁸ O <u>Q</u>	-1640.31	363.56	482.19	569.46	687.64	720.61	912.71	1184.37	1262.10	1856.95	2056.82	3561.82

We define the fractionations of oxygen isotope ($1000\ln\alpha^*$) and multiply substituted species ($\Delta_{47}^*, \Delta_{48}^*, \Delta_{49}^*$) during acid digestion as the differences between $\delta^{18}\text{O}$, Δ_{47} , Δ_{48} , Δ_{49} in the product CO_2 and $\delta^{18}\text{O}$, Δ_{63} , Δ_{64} , Δ_{65} in the reactant carbonates, respectively:

$$1000\ln\alpha^* = 1000\ln\frac{\delta^{18}\text{O}_{\text{CO}_2}/1000+1}{\delta^{18}\text{O}_{\text{XCO}_3}/1000+1}, \Delta_{47}^* = \Delta_{47} - \Delta_{63}, \Delta_{48}^* = \Delta_{48} - \Delta_{64}, \Delta_{49}^* = \Delta_{49} - \Delta_{65}$$

where Δ_{48} , Δ_{49} , Δ_{63} , Δ_{64} and Δ_{65} are defined, similar to Δ_{47} , following the same principle as in Eiler and Schauble (2004):

$$\begin{aligned} \Delta_{48} &= \left(\frac{R_{actual}^{48}}{R_{stochastic}^{48}} - 1 \right) \times 1000 = \left(\frac{\frac{[{}^{12}\text{C}{}^{18}\text{O}{}^{18}\text{O}]}{[{}^{12}\text{C}{}^{16}\text{O}{}^{16}\text{O}]} + \frac{[{}^{13}\text{C}{}^{18}\text{O}{}^{17}\text{O}]}{[{}^{12}\text{C}{}^{18}\text{O}{}^{18}\text{O}]}_s}{\frac{[{}^{12}\text{C}{}^{18}\text{O}{}^{18}\text{O}]}{[{}^{12}\text{C}{}^{16}\text{O}{}^{16}\text{O}]}_s + \frac{[{}^{13}\text{C}{}^{18}\text{O}{}^{17}\text{O}]}{[{}^{12}\text{C}{}^{16}\text{O}{}^{16}\text{O}]}_s} - 1 \right) \times 1000 \\ \Delta_{49} &= \left(\frac{R_{actual}^{49}}{R_{stochastic}^{49}} - 1 \right) \times 1000 = \left(\frac{\frac{[{}^{13}\text{C}{}^{18}\text{O}{}^{18}\text{O}]}{[{}^{12}\text{C}{}^{16}\text{O}{}^{16}\text{O}]}_s}{\frac{[{}^{12}\text{C}{}^{16}\text{O}{}^{16}\text{O}]}{[{}^{12}\text{C}{}^{16}\text{O}{}^{16}\text{O}]}_s} - 1 \right) \times 1000 \\ \Delta_{63} &= \left(\frac{R_{actual}^{63}}{R_{stochastic}^{63}} - 1 \right) \times 1000 = \left(\frac{\frac{[{}^{13}\text{C}{}^{18}\text{O}{}^{16}\text{O}{}^{16}\text{O}]}{[{}^{12}\text{C}{}^{16}\text{O}{}^{16}\text{O}{}^{16}\text{O}]} + \frac{[{}^{12}\text{C}{}^{18}\text{O}{}^{17}\text{O}{}^{16}\text{O}]}{[{}^{12}\text{C}{}^{16}\text{O}{}^{16}\text{O}{}^{16}\text{O}]} + \frac{[{}^{13}\text{C}{}^{17}\text{O}{}^{17}\text{O}{}^{16}\text{O}]}{[{}^{12}\text{C}{}^{16}\text{O}{}^{16}\text{O}{}^{16}\text{O}]} + \frac{[{}^{12}\text{C}{}^{17}\text{O}{}^{17}\text{O}{}^{17}\text{O}]}{[{}^{12}\text{C}{}^{16}\text{O}{}^{16}\text{O}{}^{16}\text{O}]}_s}{\frac{[{}^{12}\text{C}{}^{16}\text{O}{}^{16}\text{O}{}^{16}\text{O}]}{[{}^{13}\text{C}{}^{18}\text{O}{}^{16}\text{O}{}^{16}\text{O}]}_s + \frac{[{}^{12}\text{C}{}^{18}\text{O}{}^{17}\text{O}{}^{16}\text{O}]}{[{}^{13}\text{C}{}^{18}\text{O}{}^{17}\text{O}{}^{16}\text{O}]}_s + \frac{[{}^{13}\text{C}{}^{17}\text{O}{}^{17}\text{O}{}^{16}\text{O}]}{[{}^{12}\text{C}{}^{17}\text{O}{}^{17}\text{O}{}^{17}\text{O}]}_s + \frac{[{}^{12}\text{C}{}^{17}\text{O}{}^{17}\text{O}{}^{17}\text{O}]}{[{}^{12}\text{C}{}^{17}\text{O}{}^{17}\text{O}{}^{17}\text{O}]}_s} - 1 \right) \times 1000 \\ \Delta_{64} &= \left(\frac{R_{actual}^{64}}{R_{stochastic}^{64}} - 1 \right) \times 1000 = \left(\frac{\frac{[{}^{12}\text{C}{}^{18}\text{O}{}^{18}\text{O}{}^{16}\text{O}]}{[{}^{12}\text{C}{}^{16}\text{O}{}^{16}\text{O}{}^{16}\text{O}]} + \frac{[{}^{13}\text{C}{}^{18}\text{O}{}^{17}\text{O}{}^{16}\text{O}]}{[{}^{12}\text{C}{}^{16}\text{O}{}^{16}\text{O}{}^{16}\text{O}]} + \frac{[{}^{12}\text{C}{}^{18}\text{O}{}^{18}\text{O}{}^{17}\text{O}]}{[{}^{12}\text{C}{}^{16}\text{O}{}^{16}\text{O}{}^{16}\text{O}]} + \frac{[{}^{13}\text{C}{}^{17}\text{O}{}^{17}\text{O}{}^{17}\text{O}]}{[{}^{12}\text{C}{}^{16}\text{O}{}^{16}\text{O}{}^{16}\text{O}]}_s}{\frac{[{}^{12}\text{C}{}^{18}\text{O}{}^{18}\text{O}{}^{16}\text{O}]}{[{}^{13}\text{C}{}^{18}\text{O}{}^{17}\text{O}{}^{16}\text{O}]}_s + \frac{[{}^{13}\text{C}{}^{18}\text{O}{}^{17}\text{O}{}^{16}\text{O}]}{[{}^{12}\text{C}{}^{18}\text{O}{}^{17}\text{O}{}^{16}\text{O}]}_s + \frac{[{}^{12}\text{C}{}^{18}\text{O}{}^{18}\text{O}{}^{17}\text{O}]}{[{}^{12}\text{C}{}^{17}\text{O}{}^{17}\text{O}{}^{17}\text{O}]}_s + \frac{[{}^{13}\text{C}{}^{17}\text{O}{}^{17}\text{O}{}^{17}\text{O}]}{[{}^{12}\text{C}{}^{17}\text{O}{}^{17}\text{O}{}^{17}\text{O}]}_s} - 1 \right) \times 1000 \\ \Delta_{65} &= \left(\frac{R_{actual}^{65}}{R_{stochastic}^{65}} - 1 \right) \times 1000 = \left(\frac{\frac{[{}^{12}\text{C}{}^{18}\text{O}{}^{18}\text{O}{}^{17}\text{O}]}{[{}^{12}\text{C}{}^{16}\text{O}{}^{16}\text{O}{}^{16}\text{O}]} + \frac{[{}^{13}\text{C}{}^{18}\text{O}{}^{18}\text{O}{}^{16}\text{O}]}{[{}^{12}\text{C}{}^{16}\text{O}{}^{16}\text{O}{}^{16}\text{O}]} + \frac{[{}^{13}\text{C}{}^{18}\text{O}{}^{17}\text{O}{}^{17}\text{O}]}{[{}^{12}\text{C}{}^{16}\text{O}{}^{16}\text{O}{}^{16}\text{O}]}_s}{\frac{[{}^{12}\text{C}{}^{18}\text{O}{}^{18}\text{O}{}^{17}\text{O}]}{[{}^{12}\text{C}{}^{18}\text{O}{}^{18}\text{O}{}^{17}\text{O}]}_s + \frac{[{}^{13}\text{C}{}^{18}\text{O}{}^{18}\text{O}{}^{16}\text{O}]}{[{}^{13}\text{C}{}^{18}\text{O}{}^{18}\text{O}{}^{16}\text{O}]}_s + \frac{[{}^{13}\text{C}{}^{18}\text{O}{}^{17}\text{O}{}^{17}\text{O}]}{[{}^{12}\text{C}{}^{18}\text{O}{}^{17}\text{O}{}^{17}\text{O}]}_s} - 1 \right) \times 1000, \end{aligned}$$

where ‘s’ in the subscript denotes the abundance of an isotopologue when all the isotopes are stochastically distributed.

Fig. 3-4 and Table 3-4 present the oxygen isotope fractionations that accompany phosphoric acid digestion over a range of relevant temperatures, as predicted by our transition-state theory model. The predicted oxygen isotope fractionation and its temperature dependence are broadly similar to those determined for different carbonate minerals in previous laboratory studies. At 25°C, our model predicted oxygen isotope fractionation of 10.72‰, is in the middle of the range of observed fractionations among different carbonate minerals (from 10.06‰ for MnCO₃ to 11.92‰ for MgCO₃), and is very close to the experimental determined fractionation for calcite (10.20‰). The temperature sensitivity of our predicted oxygen isotope fractionation during phosphoric acid digestion (-0.055‰/°C at 25°C) is also only slightly above the range of temperature sensitivities experimentally determined for different carbonate minerals (MnCO₃ appears to possess the highest temperature sensitivity of oxygen isotope aid digestion fractionation, -0.052‰/°C at 25°C).

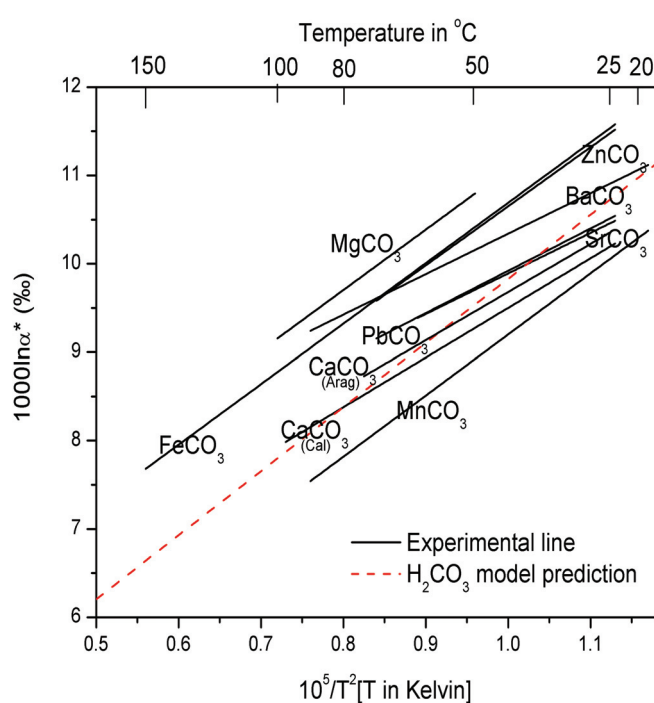


Figure 3-4: Oxygen isotope fractionations ($1000 \ln \alpha^*$, where α^* is the $^{18}\text{O}/^{16}\text{O}$ ratio of product CO₂ divided by that for reactant carbonate) plotted vs. $10^5 T^{-2}$ in K (the upper horizontal edge indicates T in °C, for reference). The dashed line is the predicted temperature dependent fractionation based on our model of H₂CO₃ dissociation. Labeled solid lines are measured experimental values for various metal carbonates (Table 4). The structurally simple transition-state structure model we propose captures the first-order magnitude and temperature dependence of observed fractionations, and mostly closely approaches the best-determined value for calcite

Table 3-4 Comparison of model predicted and experimentally observed phosphoric acid digestion fractionations.

Carbonate Minerals	$\delta^{18}\text{O}_{\text{SMOW}}^*$ (‰, $X\text{CO}_3$)	Temperature range (°C)	1000ln α * (‰, 25°C [§])	Δ_{47}^* (‰, 25°C [¥])	1000ln α * (‰ [§])	1000ln α * Reference
Calcite	Dolomite(CaMg(CO ₃) ₂)	11.53	25	11.03	0.214	N/A
	Magnesite(MgCO ₃)	18.23	50-100	11.92	0.198	0.213
	Simthsonite(ZnCO ₃)	26.01	25-72	11.49	0.205	0.187
	Siderite(FeCO ₃)	4.22	25-150	11.54	0.204	0.155
	Rhodochrosite(MnCO ₃)	18.15	20-90	10.06	0.234	0.123
Aragonite	Calcite(CaCO ₃)	6.43	25-95	10.20	0.231	0.232
	Aragonite(CaCO ₃)	10.57	25-75	10.36	0.229	0.232
	Strontianite(SrCO ₃)	14.57	25-62	10.46	0.225	0.238
	Cerussite(PbCO ₃)	15.97	25-72	10.52	0.224	0.190
	Witherite(BaCO ₃)	6.20	20-90	10.91	0.216	0.249
H_2CO_3 Model [£]	1000ln α *	0	10.72		2.58+7.25×10 ⁵ /T ²	<i>This work</i>
	Δ_{47}^*		0.220		0.0186+0.179×10 ⁵ /T ²	<i>This work</i>
	Δ_{48}^*		0.137		-0.0787+0.192×10 ⁵ /T ²	<i>This work</i>
	Δ_{49}^*		0.593		-0.0386+0.561×10 ⁵ /T ²	<i>This work</i>

[†] Oxygen isotope compositions of the reactant carbonate minerals.[‡] Equations for experimentally determined temperature dependence from Gilg et al., 2003, where T is in the unit of Kelvin. Isotope fractionations during phosphoric acid fractionation at 25°C are estimated from these equations.[¥] Predicted Δ_{47}^* for different carbonate minerals at 25°C, based on the inverse correlation between 1000ln α * and Δ_{47}^* (first column) or the absolute Δ_{47}^* value (second column) predicted by our cluster model. See section 4.4.3 for details.[£] Calculations here assumes $\delta^{13}\text{C}_{\text{VPDB}}=0\text{‰}$, $\delta^{18}\text{O}_{\text{SMOW}}=0\text{‰}$ and stochastic distribution of multiply-substituted isotopologues for the reactant carbonate.

Our transition-state-theory model of phosphoric acid digestion predicts that CO₂ produced by dissociation of an H₂CO₃ intermediate has abundances of ¹³C-¹⁸O bonds, as reflected by the Δ_{47}^* value, +0.220‰ higher than the Δ_{63} value of reactant carbonate at 25°C, with a temperature sensitivity of -0.0010‰/°C over the temperature range of 25°C to 80°C (Fig. 3-5). The predicted fractionation at 25°C is indistinguishable from this study's experimentally determined value of 0.232‰ for calcite (Table 3-2), and the

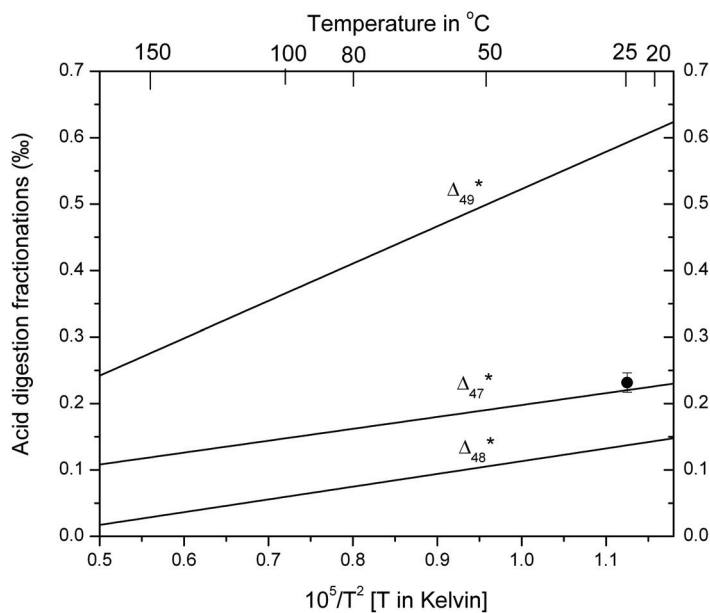


Figure 3-5: Fractionations of multiply-substituted species (Δ_{47}^* , Δ_{48}^* , Δ_{49}^*) during phosphoric acid digestion predicted by our H₂CO₃ dissociation model, plotted as a function of 10^5T^{-2} , in K. The solid circle is the average value of Δ_{47}^* experimentally determined during phosphoric acid digestion of calcite at 25°C (Table 3-2; this study). The bar is 1 standard deviation (1σ) of multiple replicate extractions of this calcite (the standard error of the average is approximately the size of the symbol).

temperature dependence is close to the experimentally measured value of ca. -0.0016‰/°C (Ghosh et al, 2006). There are no experimental data documenting

fractionations of $^{12}\text{C}^{18}\text{O}_2$ and $^{13}\text{C}^{18}\text{O}_2$ isotopologues during acid digestion of carbonates, but for future reference we note here that our transition state theory model predicts Δ_{48}^* to be 0.137‰ at 25°C with a temperature dependence of -0.0011‰/°C, and Δ_{49}^* to be 0.593‰ at 25°C with a temperature dependence of -0.0033‰/°C (Fig. 3-5).

The most obvious weakness of our transition state theory model is the need to choose a frequency scaling factor (which presumably reflects the effects of anharmonicity; see section 2.3, above). We tested the potential effects of this assumption by repeating our calculations with no scaling factors. In this case, the predicted acid digestion fractionations at 25°C are 11.32‰ for $\delta^{18}\text{O}^*$, 0.235‰ for Δ_{47}^* , 0.156‰ for Δ_{48}^* , and 0.642‰ for Δ_{49}^* . These results are sufficiently similar to the results of our preferred model that we do not regard the frequency scaling factors as plausible sources of large systematic error.

Our transition state theory model also predicts the mass dependency of the oxygen isotope fractionation that accompanies phosphoric acid digestion. This is relevant for analyses of the bulk isotopic compositions of reactant carbonates because one must assume the mass dependence of the acid digestion fractionation in order to ion-correct the measured mass spectrum of product CO₂. Generally speaking, measurements of the carbon and oxygen isotope compositions of CO₂ on a gas source isotope ratio mass spectrometer examine CO₂ isotopologue ions having nominal molecular masses of 44, 45 and 46 amu. Because the instruments commonly used for this purpose cannot mass resolve $^{13}\text{C}^{16}\text{O}_2$ from $^{12}\text{C}^{17}\text{O}^{16}\text{O}$, one must make some assumption to correct for the contribution of $^{12}\text{C}^{17}\text{O}^{16}\text{O}$ to the mass 45 amu ion beam. This is generally accomplished

by assuming a relationship between ^{17}O and ^{18}O abundance of the form: $\frac{^{17}R_A}{^{17}R_B} = \left(\frac{^{18}R_A}{^{18}R_B} \right)^\lambda$

(Assonov and Brenninkmeijer, 2003; Miller et al., 2007), where the value λ must be assumed or determined by independent experiments (such as fluorination of reactant carbonate and product CO_2 followed by isotopic analyses of the resulting O_2 gases). To the best of our knowledge, there are no experimental determinations of λ associated with phosphoric acid digestion of carbonate minerals; a value 0.528 has been suggested (Assonov and Brenninkmeijer, 2003; Miller et al., 2007). This value of λ characterizes the isotopic variations of natural waters (Li and Meijer, 1998; Barkan and Luz, 2005), and presumably is inherited by carbonate minerals that form in isotopic equilibrium with natural waters, although there is no reason to suppose it also is characteristic of the acid digestion reaction process by which carbonates are measured. Our transition state theory of phosphoric acid digestion predicts that the value of λ associated with its isotopic fractionations is 0.5281. Thus, our model agrees with and provides an independent theoretical justification for the suggested value of 0.528 for CO_2 extracted from carbonate samples (Miller et al., 2007) and standards (e.g., PDB and NBS-19; Assonov and Brenninkmeijer, 2003).

4.3 Dependence of acid digestion fractionations on the isotopic compositions of reactant carbonate minerals?

A striking peculiarity of Kim and O’Neil’s (1997) experimental determinations of oxygen isotope fractionations associated with phosphoric acid digestion is the apparent variations of the fractionation factors even within the same type of carbonate minerals at the same digestion temperature (25°C). Apparent fractionation factors at 25°C were

observed to vary by up to 0.5‰ for calcite (CaCO_3), 0.6‰ for witherite (BaCO_3), and 2.5‰ for octavite (CdCO_3). We are not aware of any detailed explanation that has been put forward for the observed variations. Kim and O’Neil (1997) suggested these effects might be related to differences in the preparation conditions of those carbonates.

We performed a statistical analysis of the experimental data presented in Kim and O’Neil (1997), and observed statistically significant correlations between the oxygen isotope acid digestion fractionations and the oxygen isotope compositions of the reactant carbonates, with proportionalities of: 0.03‰ change in fractionation per permil in reactant ^{18}O for calcite; 0.036‰ per permil for octavite; and 0.06‰ per permil for witherite (Fig. 3-6). Interestingly, we find these observed correlations might help explain discrepancies between independent determinations of acid digestion fractionation factors. For example, the oxygen isotope acid digestion fractionation for octavite determined by Sharma and Clayton (1965) (11.9‰ at 25°C), falls on the trend of fractionation vs. reactant $\delta^{18}\text{O}$ determined for octavite by Kim and O’Neil (1997) (Fig. 3-6). The relatively small acid digestion fractionation determined for calcite by Sharma and Clayton (1965) might also be consistent with such a trend (Fig. 3-6). On the other hand, the discrepancy between these two studies in the acid digestion fractionation for witherite can not be explained in this way. The possibility that acid digestion fractionations depend on reactant $\delta^{18}\text{O}$ is generally neglected in studies of carbonate stable isotope composition, despite the fact that the existence of such an effect could lead to significant systematic errors for some materials.

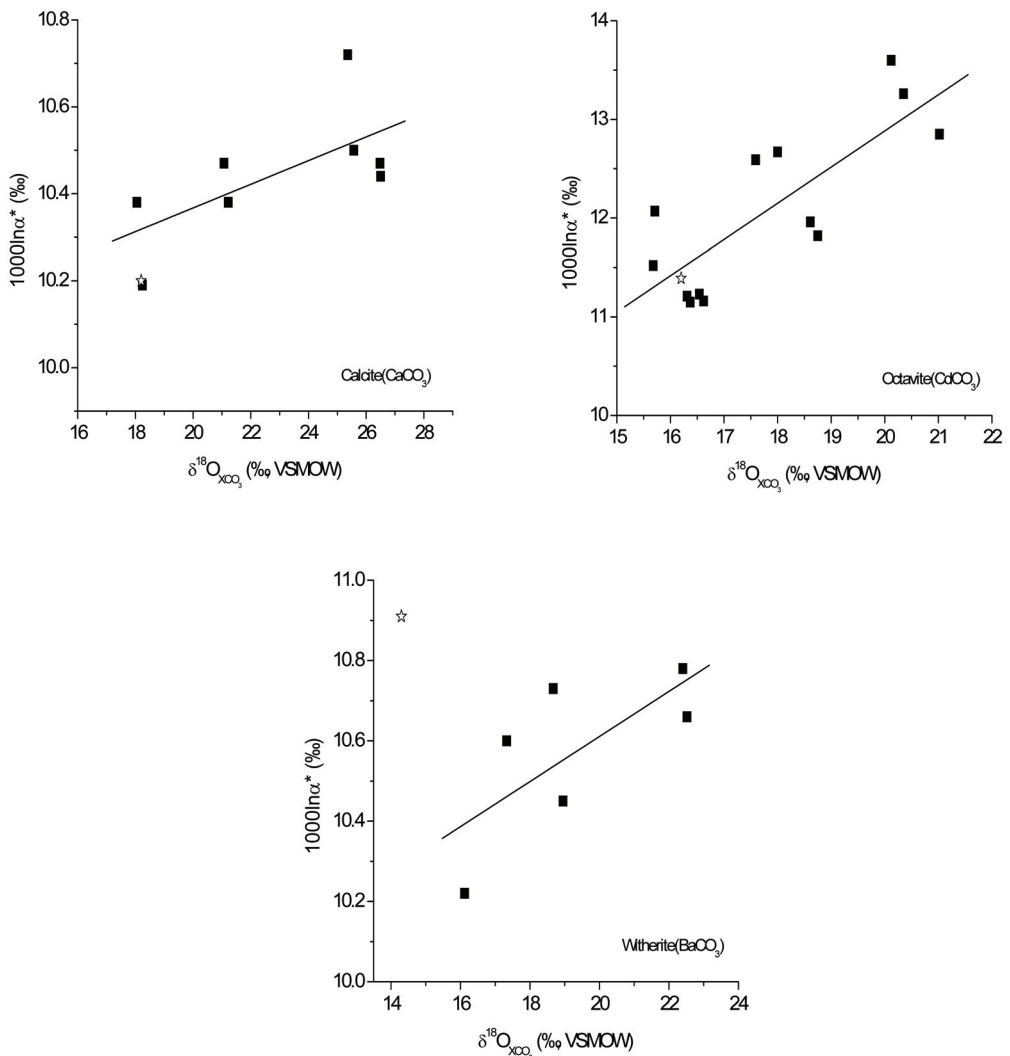


Figure 3-6: Empirically observed correlations between the oxygen isotope fractionations associated with phosphoric acid digestion and the oxygen isotopic composition of reactant carbonates. Experimental data are from Kim and O'Neil (1997) and the solid lines are the least square regressions to the experimental data:

$$\text{Caclite, } 1000\ln\alpha^* = (9.82209 \pm 0.29103) + (0.02725 \pm 0.01262) \times \delta^{18}\text{O}_{\text{XCO}_3}, R = 0.66124;$$

$$\text{Octavite, } 1000\ln\alpha^* = (5.54713 \pm 1.50518) + (0.36680 \pm 0.08406) \times \delta^{18}\text{O}_{\text{XCO}_3}, R = 0.79615;$$

$$\text{Witherite, } 1000\ln\alpha^* = (9.48846 \pm 0.54236) + (0.05612 \pm 0.02784) \times \delta^{18}\text{O}_{\text{XCO}_3}, R = 0.70985,$$

where R is the respective correlation coefficient.

Also shown for comparison (star symbols) are the data from Sharma and Clayton (1965). Neither our H_2CO_3 dissociation model nor our more complex 'cluster' models predict a correlation between these two variables.

Table 3-5 Dependences of phosphoric acid digestion fractionations on the isotopic compositions and the distributions of multiply-substituted isotopologues in reactant carbonates at 25°C.

	$\delta^{13}\text{C}_{\text{VPDB}}(\text{\textperthousand})$	0	10	0	0	10	0	0	10	0
	$\delta^{18}\text{O}_{\text{VSMOW}}(\text{\textperthousand})$	0	0	10	0	0	10	0	0	10
	Equil. T [‡] (K)	Random	Random	Random	500	500	500	300	300	300
CO_3^{2-} in	$\Delta_{63}^{\ddagger} (\text{\textperthousand})$	0	0	0	0.101	0.101	0.101	0.382	0.382	0.382
Reactant	$\Delta_{64}^{\ddagger} (\text{\textperthousand})$	0	0	0	0.042	0.042	0.042	0.155	0.155	0.155
Carbonate	$\Delta_{65}^{\ddagger} (\text{\textperthousand})$	0	0	0	0.248	0.248	0.248	0.937	0.937	0.937
<hr/>										
	$\delta^{18}\text{O}_{\text{VSMOW}}(\text{\textperthousand})$	10.776	10.776	20.884	10.776	10.776	20.884	10.774	10.774	20.882
Model	$\Delta_{47} (\text{\textperthousand})$	0.220	0.220	0.220	0.324	0.324	0.324	0.615	0.615	0.615
Prediction on	$\Delta_{48} (\text{\textperthousand})$	0.137	0.137	0.137	0.180	0.180	0.180	0.297	0.297	0.297
Product CO ₂	$\Delta_{49} (\text{\textperthousand})$	0.593	0.593	0.592	0.847	0.847	0.847	1.555	1.555	1.555
<hr/>										
	$1000 \ln \alpha^*$	10.719	10.719	10.719	10.718	10.718	10.718	10.717	10.717	10.717
Acid	$\Delta_{47}^* (\text{\textperthousand})$	0.220	0.220	0.220	0.223	0.223	0.223	0.233	0.233	0.233
Digestion	$\Delta_{48}^* (\text{\textperthousand})$	0.137	0.137	0.137	0.138	0.138	0.138	0.142	0.142	0.142
Fractionation	$\Delta_{49}^* (\text{\textperthousand})$	0.593	0.593	0.593	0.660	0.660	0.660	0.618	0.618	0.618

[‡] Hypothetical equilibration temperature for the distributions of multiply-substituted isotopologues inside reactant carbonates. Δ_{63} , Δ_{64} , and Δ_{65} (see text for definitions) are estimated based on calculations for an isolated CO_3^{2-} group in the gas phase (see Appendix for details).

We examined this issue by recalculating our transition state theory model for a range of bulk isotopic compositions and initial multiply-substituted isotopologue proportions (i.e., values of Δ_{63} , Δ_{64} , etc.) in the reactant carbonate (assumed identical to H_2CO_3 intermediate) at a constant assumed acid digestion temperature of 25°C (Table 3-5). We observe no dependence of the oxygen isotope acid digestion fractionation ($1000\ln\alpha^*$) on the $\delta^{18}\text{O}$ value of the reactant carbonate, and thus our model does not provide an explanation of such trends in the experimental data of Kim and O’Neil (1997). Given the general success of our model in describing the magnitude and temperature dependence of $1000\ln\alpha^*$ (Fig. 3-4), this discrepancy likely indicates that the trends observed by Kim and O’Neil (Fig. 3-6) are not an intrinsic feature of the kinetic isotope effect that accompanies phosphoric acid digestion of carbonate. Such trends might reflect systematic errors in the fluorination measurements that were used to determine the bulk $\delta^{18}\text{O}$ of reactant carbonates (e.g., as might result from an unrecognized analytical blank or contaminant), or, as suggested by Kim and O’Neil (1997), some cryptic artifact particular to the synthesis of the carbonate standards they studied.

The transition-state-theory models summarized in Table 3-5 show an unexpected dependence of the fractionations of multiply-substituted isotopologues (i.e., values of Δ_{47}^* , Δ_{48}^* and Δ_{49}^*) on proportions of multiply substituted isotopologues of reactant carbonates (i.e., values of Δ_{63} , Δ_{64} , and Δ_{65}). Most importantly, Δ_{47}^* , the fractionation that directly influences the results of carbonate clumped isotope thermometry, is predicted to increase by ~0.035‰ for every 1‰ increase in the Δ_{63} value of reactant carbonate. The proportions of multiply substituted isotopologues inside reactant carbonate are calculated based on the equilibrium constants of isotope exchange reactions

between different carbonate ion isotopologues, following the similar algorithm as presented in Wang et al. (2004) (see Appendix for details). This non-ideality in the clumped isotope fractionations (i.e., a dependence of fractionation factor on reactant isotopic composition) is real, but arises from a peculiarity in the way the Δ_i values are defined. The Δ_i^* values for any particular isotopologue is independent of reactant composition. That is, $\Delta_{^{13}\text{C}^{18}\text{O}^{16}\text{O}}^*$ of product CO_2 differs from $\Delta_{^{13}\text{C}^{18}\text{O}^{16}\text{O}^{16}\text{O}}^*$ of reactant carbonate by an amount that varies with temperature but is independent of the $\Delta_{^{13}\text{C}^{18}\text{O}^{16}\text{O}^{16}\text{O}}^*$ of reactant carbonate. However, for the fractionation of total mass 47 isotopologues,

$$\begin{aligned}\Delta_{47}^* &= \Delta_{47} - \Delta_{63} \\ &\approx \left(f_{^{13}\text{C}^{18}\text{O}^{16}\text{O}} \times \Delta_{^{13}\text{C}^{18}\text{O}^{16}\text{O}} + f_{^{12}\text{C}^{18}\text{O}^{17}\text{O}} \times \Delta_{^{12}\text{C}^{18}\text{O}^{17}\text{O}} + f_{^{13}\text{C}^{17}\text{O}^{17}\text{O}} \times \Delta_{^{13}\text{C}^{17}\text{O}^{17}\text{O}} \right) - \\ &\quad \left(f_{^{13}\text{C}^{18}\text{O}^{16}\text{O}^{16}\text{O}} \times \Delta_{^{13}\text{C}^{18}\text{O}^{16}\text{O}^{16}\text{O}} + f_{^{12}\text{C}^{18}\text{O}^{17}\text{O}^{16}\text{O}} \times \Delta_{^{12}\text{C}^{18}\text{O}^{17}\text{O}^{16}\text{O}} + f_{^{13}\text{C}^{17}\text{O}^{17}\text{O}^{16}\text{O}} \times \Delta_{^{13}\text{C}^{17}\text{O}^{17}\text{O}^{16}\text{O}} + f_{^{12}\text{C}^{17}\text{O}^{17}\text{O}^{17}\text{O}} \times \Delta_{^{12}\text{C}^{17}\text{O}^{17}\text{O}^{17}\text{O}} \right)\end{aligned},$$

where $f_{^{13}\text{C}^{18}\text{O}^{16}\text{O}}$, $f_{^{12}\text{C}^{18}\text{O}^{17}\text{O}}$, $f_{^{13}\text{C}^{17}\text{O}^{17}\text{O}}$ are the relative abundance fractions of isotopologues $^{13}\text{C}^{18}\text{O}^{16}\text{O}$, $^{12}\text{C}^{18}\text{O}^{17}\text{O}$ and $^{13}\text{C}^{17}\text{O}^{17}\text{O}$ in all the mass 47 isotopologues of product CO_2 , $f_{^{13}\text{C}^{18}\text{O}^{16}\text{O}^{16}\text{O}}$, $f_{^{12}\text{C}^{18}\text{O}^{17}\text{O}^{16}\text{O}}$, $f_{^{13}\text{C}^{17}\text{O}^{17}\text{O}^{16}\text{O}}$, $f_{^{12}\text{C}^{17}\text{O}^{17}\text{O}^{17}\text{O}}$ are the relative abundance fractions of isotopologues $^{13}\text{C}^{18}\text{O}^{16}\text{O}^{16}\text{O}$, $^{12}\text{C}^{18}\text{O}^{17}\text{O}^{16}\text{O}$, $^{13}\text{C}^{17}\text{O}^{17}\text{O}^{16}\text{O}$ and $^{12}\text{C}^{17}\text{O}^{17}\text{O}^{17}\text{O}$ in all the mass 63 isotopologues of reactant carbonate CO_3^{2-} .

We define

$$\Delta_{^{13}\text{C}^{18}\text{O}^{16}\text{O}}^* = \Delta_{^{13}\text{C}^{18}\text{O}^{16}\text{O}} - \Delta_{^{13}\text{C}^{18}\text{O}^{16}\text{O}^{16}\text{O}}; \Delta_{^{12}\text{C}^{18}\text{O}^{17}\text{O}}^* = \Delta_{^{12}\text{C}^{18}\text{O}^{17}\text{O}} - \Delta_{^{12}\text{C}^{18}\text{O}^{17}\text{O}^{16}\text{O}}; \Delta_{^{13}\text{C}^{17}\text{O}^{17}\text{O}}^* = \Delta_{^{13}\text{C}^{17}\text{O}^{17}\text{O}} - \Delta_{^{13}\text{C}^{17}\text{O}^{17}\text{O}^{16}\text{O}}$$

as the fractionations of specific isotopologue during phosphoric acid digestion. Substituting these definitions in the equation above, we obtain

$$\begin{aligned}\Delta_{47}^* \approx & \left(f_{^{13}\text{C}^{18}\text{O}^{16}\text{O}} \times \Delta_{^{13}\text{C}^{18}\text{O}^{16}\text{O}}^* + f_{^{12}\text{C}^{18}\text{O}^{17}\text{O}} \times \Delta_{^{12}\text{C}^{18}\text{O}^{17}\text{O}}^* + f_{^{13}\text{C}^{17}\text{O}^{17}\text{O}} \times \Delta_{^{13}\text{C}^{17}\text{O}^{17}\text{O}}^* \right) \\ & + \left(f_{^{13}\text{C}^{18}\text{O}^{16}\text{O}} - f_{^{13}\text{C}^{18}\text{O}^{16}\text{O}^{16}\text{O}} \right) \times \Delta_{^{13}\text{C}^{18}\text{O}^{16}\text{O}^{16}\text{O}}^* + \left(f_{^{12}\text{C}^{18}\text{O}^{17}\text{O}} - f_{^{12}\text{C}^{18}\text{O}^{17}\text{O}^{16}\text{O}} \right) \times \Delta_{^{12}\text{C}^{18}\text{O}^{17}\text{O}^{16}\text{O}}^* + \left(f_{^{13}\text{C}^{17}\text{O}^{17}\text{O}} - f_{^{13}\text{C}^{17}\text{O}^{17}\text{O}^{16}\text{O}} \right) \times \Delta_{^{13}\text{C}^{17}\text{O}^{17}\text{O}^{16}\text{O}}^* \\ & - f_{^{12}\text{C}^{17}\text{O}^{17}\text{O}^{17}\text{O}} \times \Delta_{^{12}\text{C}^{17}\text{O}^{17}\text{O}^{17}\text{O}}^*\end{aligned}$$

In carbonates of natural isotopic compositions,

$$\left(f_{^{13}\text{C}^{18}\text{O}^{16}\text{O}} - f_{^{13}\text{C}^{18}\text{O}^{16}\text{O}^{16}\text{O}} \right) \approx -\left(f_{^{12}\text{C}^{18}\text{O}^{17}\text{O}} - f_{^{12}\text{C}^{18}\text{O}^{17}\text{O}^{16}\text{O}} \right) \gg -\left(f_{^{13}\text{C}^{17}\text{O}^{17}\text{O}} - f_{^{13}\text{C}^{17}\text{O}^{17}\text{O}^{16}\text{O}} \right) \gg f_{^{12}\text{C}^{17}\text{O}^{17}\text{O}^{17}\text{O}}$$

and $\Delta_{^{13}\text{C}^{18}\text{O}^{16}\text{O}^{16}\text{O}}^* \gg \Delta_{^{12}\text{C}^{18}\text{O}^{17}\text{O}^{16}\text{O}}^*$ (e.g., for calcite $\Delta_{^{13}\text{C}^{18}\text{O}^{16}\text{O}^{16}\text{O}}^* = 0.406\text{\textperthousand}$ and

$\Delta_{^{12}\text{C}^{18}\text{O}^{17}\text{O}^{16}\text{O}}^* = 0.071\text{\textperthousand}$ at 300K; Schauble et al. 2006), the above equation can therefore be

further approximated as

$$\begin{aligned}\Delta_{47}^* \approx & \left(f_{^{13}\text{C}^{18}\text{O}^{16}\text{O}} \times \Delta_{^{13}\text{C}^{18}\text{O}^{16}\text{O}}^* + f_{^{12}\text{C}^{18}\text{O}^{17}\text{O}} \times \Delta_{^{12}\text{C}^{18}\text{O}^{17}\text{O}}^* + f_{^{13}\text{C}^{17}\text{O}^{17}\text{O}} \times \Delta_{^{13}\text{C}^{17}\text{O}^{17}\text{O}}^* \right) + \left(f_{^{13}\text{C}^{18}\text{O}^{16}\text{O}} - f_{^{13}\text{C}^{18}\text{O}^{16}\text{O}^{16}\text{O}} \right) \times \Delta_{^{13}\text{C}^{18}\text{O}^{16}\text{O}^{16}\text{O}}^* \\ \approx & \text{Constant} + \left(f_{^{13}\text{C}^{18}\text{O}^{16}\text{O}} - f_{^{13}\text{C}^{18}\text{O}^{16}\text{O}^{16}\text{O}} \right) \times \Delta_{63}^*\end{aligned}$$

As mentioned above, the Δ_i^* values are independent of Δ_i of the reactant carbonate and are a function of only acid digestion temperature, and thus can be regarded as constant at given temperature. At 25°C, $\Delta_{^{13}\text{C}^{18}\text{O}^{16}\text{O}}^* = 0.225\text{\textperthousand}$, $\Delta_{^{12}\text{C}^{18}\text{O}^{17}\text{O}}^* = 0.070\text{\textperthousand}$ and $\Delta_{^{13}\text{C}^{17}\text{O}^{17}\text{O}}^* = 0.277\text{\textperthousand}$, respectively.

For carbonates with $\delta^{13}\text{C}=0\text{\textperthousand}$ and $\delta^{18}\text{O}=0\text{\textperthousand}$, as assumed in our model, $f_{^{13}\text{C}^{18}\text{O}^{16}\text{O}^{16}\text{O}} = 0.9671$ and $f_{^{13}\text{C}^{18}\text{O}^{16}\text{O}} = 0.9366$. Therefore, we expect the dependence of Δ_{47}^* on Δ_{63} of the reactant carbonate to have a slope of ~ 0.0305 , based on the above analyses. This agrees well with our quantitative H_2CO_3 model prediction, $\sim 0.035\text{\textperthousand}$ increase in Δ_{47}^* for every 1‰ increase in Δ_{63} . The small discrepancy is believed to arise from the approximations adopted in the derivation of the above equations. Note that this slope for the dependence of Δ_{47}^* on Δ_{63} varies little for carbonates of different bulk isotopic compositions, since both $f_{^{13}\text{C}^{18}\text{O}^{16}\text{O}}$ and $f_{^{13}\text{C}^{18}\text{O}^{16}\text{O}^{16}\text{O}}$ are insensitive to the changes in the bulk

isotopic compositions. The slope increases by only ~0.002 for 50‰ increase in $\delta^{13}\text{C}$, and decrease by ~0.0005 for 50‰ increase in $\delta^{18}\text{O}$.

The available experimental data do not directly test our predicted dependence of Δ_{47}^* on Δ_{63} of reactant carbonate (and it would be difficult to make such a direct test without independently knowing the temperature dependence of Δ_{63}). However, the predicted effect does offer a partial explanation why the experimentally determined relationship between the Δ_{47} of CO_2 produced by acid digestion of calcite and calcite growth temperature (Ghosh et al., 2006) is more sensitive to temperature than the theoretically predicted temperature dependence for Δ_{63} (including contributions from both $\Delta_{^{13}\text{C}^{18}\text{O}^{16}\text{O}^{16}\text{O}}$ and $\Delta_{^{12}\text{C}^{18}\text{O}^{17}\text{O}^{16}\text{O}}$) in carbonates (Schauble et al., 2006). For example, over the temperature range of 0–50°C, Schauble et al. (2006) predicts Δ_{63} in thermodynamically equilibrated calcite solids decreases by 0.00279‰ for every degree increase of its growth temperature; Assuming calcite has the same dependence of Δ_{47}^* on Δ_{63} as predicted by our above H_2CO_3 model, we predict the Δ_{47} of CO_2 produced by acid digestion of calcite will have a temperature sensitivity of -0.00289‰/°C, which is closer to the -0.00453‰/°C determined experimentally by Ghosh et al. (2006).

4.4 Cation effects on acid digestion fractionations

The transition-state model we present in preceding sections simultaneously explains a variety of features of the kinetic isotope effects associated with phosphoric acid digestion of carbonates, including the magnitude and temperature dependence of $1000\ln\alpha^*$ and Δ_{47}^* fractionations. Given that all of these predictions are strictly independent of the experimental data to which they are compared, we contend that our

model closely captures the most important mechanistic details of this reaction. However, phosphoric acid digestion of carbonates is also known to exhibit a dependence of $1000\ln\alpha^*$ on the cation chemistry (and possibly crystal structure) of reactant carbonate (Table 3-4; Fig. 3-4). At 25°C, the observed oxygen isotope fractionations among different carbonate minerals vary from 10.06‰ (MnCO_3) to 11.92‰ (MgCO_3), and the temperature sensitivity of oxygen isotope fractionations during phosphoric acid digestion vary from -0.027‰/°C (BaCO_3) to -0.041‰/°C (MnCO_3) over the temperature range of 25°C to 80°C (Table 3-4; Fig. 3-4). Nothing in our model of H_2CO_3 dissociation can explain such observations. In this section, we use a cluster model of the reacting carbonate surface (Section 2.2.3 and Fig. 3-2) to explore the possible causes of these effects.

4.4.1 Cluster model results on the oxygen isotope fractionation among different carbonate minerals

Table 3-6 and Fig. 3-7 present the predictions of our cluster model on the variations of oxygen isotope fractionation among different carbonate minerals, and the comparisons between these cluster model predictions and the results determined from previous experimental studies. Our cluster model of the carbonate surface, in which the H_2CO_3 intermediate interacts with adjacent metal-carbonate groups, succeeds in capturing the experimentally-observed dependence of $1000\ln\alpha^*$ on cation composition, but fails to exhibit the excellent agreement with the absolute values and absolute temperature dependences of $1000\ln\alpha^*$ (and Δ_{47}^*) characteristic of our simpler H_2CO_3 dissociation

Table 3-6 Variations of acid digestion isotope fractionations and their temperature dependencies among different carbonate minerals, predicted from our cluster model. The cation radius and mass are shown for comparison.

Carbonate minerals	MgCO ₃	ZnCO ₃	FeCO ₃	MnCO ₃	CaCO ₃	SrCO ₃	PbCO ₃	BaCO ₃	⁴⁰ MgCO ₃	⁴⁰ BaCO ₃	
Cation radius [‡] r, (Å)	0.65	0.70	0.79	0.80	-1.02(cal) -1.26(arag)	1.35	1.41	1.55	0.65	1.55	
Cation mass (amu)	24	65	56	55	40	88	207	137	40	40	
1000lnα [*]	3.4844	3.3885	3.6518	3.3369	3.0630	2.8842	1.7706	3.0994	3.5143	3.0923	
25°C	Δ ₄₇ [*] Δ ₄₈ [*] Δ ₄₉ [*]	0.0651 -0.0494 0.0877	0.0572 -0.0311 0.0810	0.0474 -0.0581 0.0427	0.0375 -0.0538 0.0264	0.0708 -0.0460 0.1028	0.0725 -0.0439 0.1083	0.0581 -0.0386 0.0836	0.0761 -0.0367 0.1227	0.0648 -0.0501 0.0864	0.0762 -0.0366 0.1230
1000lnα [*]	3.1975	3.0878	3.2966	3.0043	2.8263	2.6674	1.6603	2.8628	3.2209	2.8575	
50°C	Δ ₄₇ [*] Δ ₄₈ [*] Δ ₄₉ [*]	0.0577 -0.0390 0.0824	0.0508 -0.0233 0.0762	0.0422 -0.0450 0.0446	0.0337 -0.0414 0.0304	0.0625 -0.0367 0.0944	0.0639 -0.0352 0.0988	0.0514 -0.0309 0.0771	0.0669 -0.0295 0.1105	0.0574 -0.0394 0.0815	0.0669 -0.0294 0.1108
1000lnα [*]	2.9007	2.7821	2.9404	2.6726	2.5792	2.4400	1.5416	2.6150	2.9185	2.6110	
80°C	Δ ₄₇ [*] Δ ₄₈ [*] Δ ₄₉ [*]	0.0499 -0.0297 0.0751	0.0440 -0.0166 0.0694	0.0367 -0.0337 0.0439	0.0295 -0.0308 0.0319	0.0538 -0.0285 0.0843	0.0549 -0.0274 0.0876	0.0443 -0.0239 0.0691	0.0573 -0.0230 0.0970	0.0497 -0.0300 0.0744	0.0574 -0.0229 0.0971

[‡] Cation radii from Golyshev et al. (1981). For CaCO₃, the Ca cation radii are different in its two polymorphs, calcite and aragonite, and are 1.02 Å and 1.26 Å respectively.

model (above). In particular, our cluster model predicts values of $1000\ln\alpha^*$ at 25°C from 1.771‰ (PbCO_3) to 3.652‰ (FeCO_3) for the eight different carbonate minerals studied. Except for PbCO_3 , these predicted oxygen isotope fractionations are approximately one-third the experimentally observed values — a large discrepancy. Nevertheless, the predicted differences in oxygen isotope fractionation between different minerals generally reproduce those observed in previous experimental studies (Fig 3-7a). The oxygen isotope fractionation predicted by our cluster model for PbCO_3 is an exception, falling far below the trend defined by other carbonate minerals. This might be related to the spin-orbit effects and the basis set superposition error in ab initio calculations of Pb-containing complexes with effective core potential basis sets (Ramirez et al., 2006). We evaluate the temperature sensitivity of oxygen isotope acid digestion fractionation

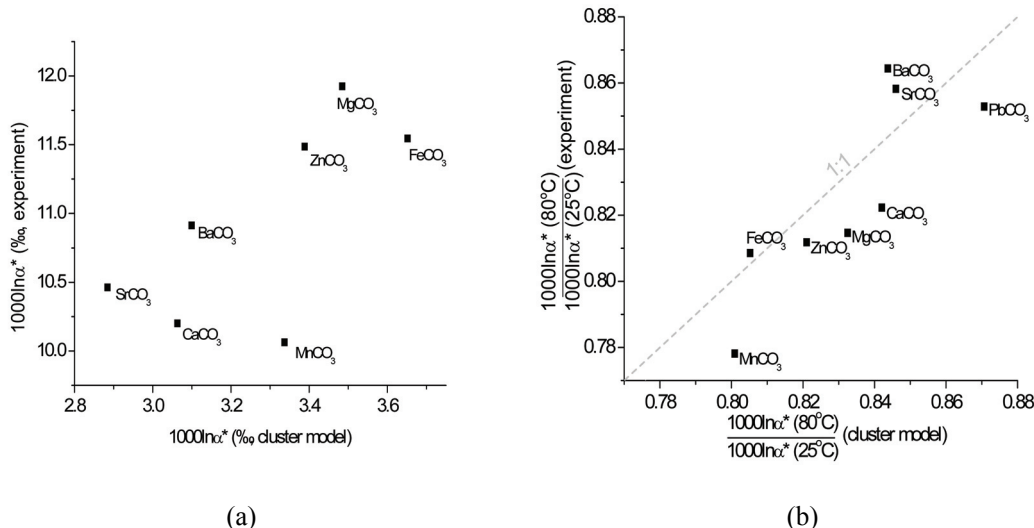


Figure 3-7: Comparison of the isotope fractionations associated with phosphoric acid digestion predicted by our ‘cluster models’ with experimentally observed fractionations for various metal carbonates. Panel (a) depicts the oxygen isotope fractionation at 25°C ; (b) depicts the temperature sensitivity of the oxygen isotope fractionation, as measured by the ratio of oxygen isotope fractionations at 80°C and 25°C . Experimental data were based on equations in Table 3-4. The dashed line in Figure (b) indicates a 1:1 correlation.

predicted by our cluster model as the ratio of predicted oxygen isotope fractionation between 80°C and 25°C, and compare them with the experimental observations (Fig. 3-7b). The model prediction and experimental data fall close to 1:1 correlation, indicating our cluster model also correctly predicts the variations of the temperature sensitivity of oxygen isotope acid digestion fractionation among different carbonate minerals (including PbCO₃; Fig 3-7b).

We conclude that our cluster model captures the essence of cation effects during phosphoric acid digestion (i.e., they result from interactions between the dissociating H₂CO₃ intermediate and metals and carbonate ions on the surface of the reactant carbonate), but is quantitatively inaccurate because it fails to describe the structural relationship between H₂CO₃ and the crystal surface. This deficiency is likely due to the small size and simple geometry of the clusters we have modeled. It should be possible to refine this model so that it simultaneously describes the absolute values and temperature dependencies of the acid digestion fractionations and their dependence on reactant composition and structure, although we suspect this would require a sophisticated treatment of the extended structures of surfaces that is beyond the scope of this study. Nevertheless, the fact our cluster model reproduces the observed size and temperature sensitivity differences in oxygen isotope fractionations among several carbonate minerals, combined with the substantial success of our simpler model in describing the systematics of phosphoric acid fractionations generally suggests that the conceptual framework we have followed is broadly correct.

4.4.2 Controls on the variations of acid digestion isotope fractionations among different carbonate minerals

Previous attempts (e.g., Bottcher 1996 and Gilg et al., 2003) to understand the variations of acid digestion fractionation among different carbonate minerals examined empirical correlations between the intercept in a plot of $1000\ln\alpha^*$ vs. $1/T^2$ and the radius or mass of the cation in the reactant carbonate (following the suggestion of Sharma and Sharma; 1969b). These efforts failed to reveal any simple correlation shared by all minerals. (Note that, O’Neil (1986) made an alternate suggestion that $1000\ln\alpha^*$ values for phosphoric acid digestion reactions might also be controlled by reaction rate; Kim and O’Nei, 1997) However, it is not clear what physiochemical meaning should be attached to the intercept in a plot of acid digestion fractionation vs. $1/T^2$. We focus on the differences of $1000\ln\alpha^*$ among different carbonate minerals at a given temperature (e.g., 25°C) and its temperature dependencies separately, which we think are more likely to reflect differences in kinetic isotope effects associated with phosphoric acid digestion.

We compare values of $1000\ln\alpha^*$ at 25°C and the temperature dependencies of $1000\ln\alpha^*$ (from both model prediction and experimental determination) for different carbonate minerals against their respective cation radius (Fig. 3-8). The theoretically predicted values of $1000\ln\alpha^*$ at 25°C positively correlate with the reciprocal of cation radius (Fig. 3-8a). The theoretically predicted, as opposed to experimentally determined, $1000\ln\alpha^*$ at 25°C show better correlations in this comparison, because significant uncertainties are associated with experimental determinations of $1000\ln\alpha^*$ (more specifically, associated with the determination of total oxygen isotopic compositions of reactant carbonates through the fluorination methods; Kim et. al., 2007). In contrast, both

theoretically predicted and the experimentally determined temperature dependencies of $1000\ln\alpha^*$ exhibit positive correlations with the reciprocal of cation radius (Fig 3-8c, 3-8d).

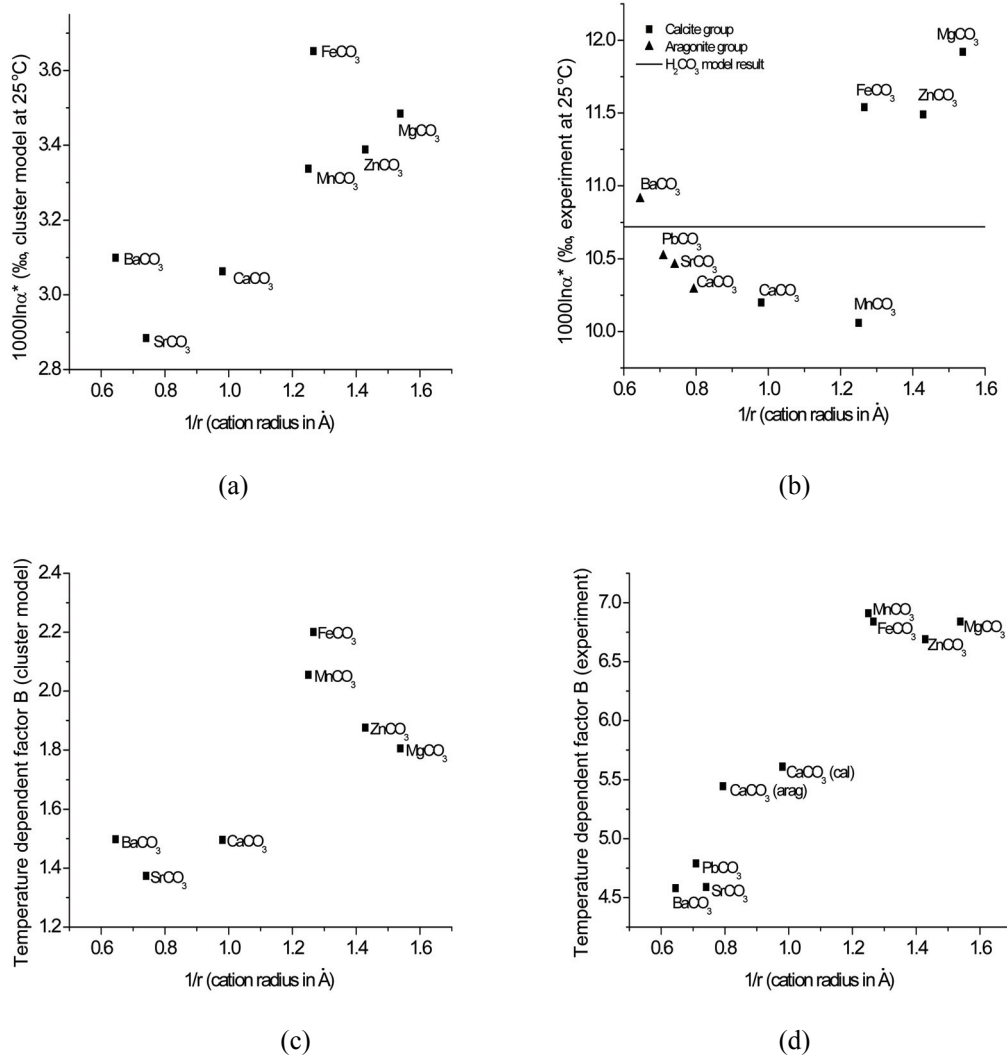


Figure 3-8: Correlations between fractionations of oxygen isotopes associated with acid digestion and the ionic radius of the cation in the reactant carbonate. Panel **(a)** depicts the predicted fractionations of our ‘cluster model’ for phosphoric acid digestion at 25°C ; **(b)** experimentally determined acid digestion fractionation at 25°C ; **(c)** shows ‘cluster model’ predicted temperature dependence factor B for oxygen isotope acid digestion fractionation (as expressed in the form of $1000\ln\alpha^*=A+B\times 10^5/T^2$; Table 3-4); **(d)** experimentally determined temperature dependence factor B for oxygen isotope acid digestion fractionation, against cation radius. These observed correlations indicate cation radius is the

predominant factor controlling the variations of acid digestion fractionations among different carbonate minerals. Data on the cation radii are from Golyshev et al. (1981).

The experimental determinations of the temperature dependencies of the oxygen isotope acid fractionation have much smaller uncertainties (since the uncertainties associated with fluorination methods cancel out in the determination of temperature dependence), and therefore show better correlation in the above comparison. The existence of these correlations suggests that cation radius is the most important mineral-specific factor controlling acid digestion fractionations.

To examine the possible effects of cation mass on the acid digestion fractionation, we adopt a similar strategy to that employed by Schauble et al. (2006) in their discussion of equilibrium carbon and oxygen isotope fractionations among different carbonate minerals, and create two hypothetical isotopic carbonates, $^{40}\text{MgCO}_3$ and $^{40}\text{BaCO}_3$. In these cluster models, all the optimization and calculation were performed as outlined above for their isotopically normal equivalents, except the atomic masses of Mg and Ba were both assigned as 40 amu instead of their normal masses (24.3 amu and 137.3 amu, respectively). If cation mass controls the acid digestion fractionation, we would expect the model predicted fractionation for these two hypothetical carbonates to closely resemble the predicted fractionation for CaCO_3 , which has a cation mass of 40.1 amu. Instead, we observe negligible differences in predicted acid digestion fractionations between these hypothetical carbonates and their isotopically normal equivalents (within 0.03‰ for MgCO_3 and 0.01‰ for BaCO_3 ; Table 3-6). Thus, the cation effect on acid digestion fractionation reflects cation size, not mass.

Besides cation radius and mass, crystal structure has been invoked by previous studies as another potential factor that might place important controls on the acid

digestion fractionation (Gilg et al., 2003). The CaCO₃ polymorphs calcite and aragonite are ideal for testing this proposition, since the two share the same cation composition but differ in their crystal structures. Sharma and Clayton (1965) first determined the oxygen isotope acid digestion fractionation for calcite and aragonite at 25°C, and observed only a 0.09‰ difference between the two (10.20‰ for calcite vs. 10.29‰ for aragonite). Recently, Kim et al. (2007) re-determined the acid digestion fractionation for calcite and aragonite between 25°C and 75°C with much higher experimental precision, and indicated instead a significantly bigger difference, 0.32‰ at 25°C ($10.25\% \pm 0.07$ for calcite vs. $10.57\% \pm 0.10$ for aragonite; 1se). However, our re-examination of the data from Kim et al. (2007) suggests a possible systematic bias during their determination of total oxygen isotopic composition of reactant aragonite — an inverse correlation appears to exist between the total oxygen isotopic composition of reactant aragonite and the total oxygen yield from decarbonation and fluorination steps ($\delta^{18}O_{\text{aragonite}} = -0.1362 \times \text{Yield}\% + 38.642$). Kim et al. (2007) didn't discuss this correlation, and averaged the data as the best estimation of total oxygen isotopic composition of their reactant aragonite. But, in view of existence of this correlation, we suggest that a more accurate estimate of the total oxygen isotopic composition of the reactant aragonite is the total oxygen isotopic composition at 100% oxygen yield. Following the observed correlation, this approach yields a total oxygen isotopic composition for the reactant aragonite 0.19‰ higher than what was originally reported in Kim et al. (2007) (25.02‰ vs. 24.83‰). This leads to an oxygen isotopic acid digestion fractionation for aragonite of $10.38\% \pm 0.10$ (1se) at 25°C based on data in Kim et al. (2007), consistent with the value of 10.29‰ determined by Sharma and Clayton (1965). Consequently, the acid

digestion fractionation difference between calcite and aragonite is 0.13‰, also much consistent with the 0.09‰ difference determined in Sharma and Clayton (1965). Based on the above analyses, we conclude the acid digestion fractionation difference between calcite and aragonite is very small, around 0.1‰. This suggests that the crystal structure, like cation mass, exerts only very weak control on the acid digestion fractionation. The fact that our cluster model, which did not consider the effects of crystal structure, managed to semi-quantitatively reproduce the general trend of variations of acid digestion fractionations among different carbonate minerals (Fig. 3-7) also supports this argument.

4.4.3 Cluster model results on the fractionation of ^{13}C - ^{18}O doubly substituted isotopologues during phosphoric acid digestion

Our cluster model predicts that the Δ_{47}^* values associated with phosphoric acid digestion at 25°C range from 0.0375‰ (MnCO_3) to 0.0761‰ (BaCO_3) among the eight carbonates mineral studied (Table 3-6). As for oxygen isotope acid digestion fractionations, our cluster model appears to underestimate the absolute values of Δ_{47}^* fractionations associated with phosphoric acid digestion. Most of the predicted values of Δ_{47}^* are approximately 1/3 to 1/4 of experimental observed Δ_{47}^* for calcite (0.23‰, section 4.1).

We observe that values of Δ_{47}^* predicted by our cluster model correlate negatively with their respective predicted $1000\ln\alpha^*$ fractionations during phosphoric acid digestion (Fig. 3-9). If this correlation is general to all carbonate minerals, one could predict the

Δ_{47}^* during acid digestion of any carbonate mineral, XCO_3 (where X is a cation), at temperature T:

$$\Delta_{47}^*(XCO_3, T) = \frac{1000 \ln \alpha^*(H_2CO_3, T)}{1000 \ln \alpha^*(XCO_3, T)} \times \Delta_{47}^*(H_2CO_3, T) \quad , \quad (5)$$

where $1000 \ln \alpha^*(XCO_3, T)$ is the experimentally determined oxygen isotope acid fractionation at temperature T, and $1000 \ln \alpha^*(H_2CO_3, T)$ and $\Delta_{47}^*(H_2CO_3, T)$ are the predicted oxygen isotope and Δ_{47}^* acid digestion fractionation at temperature T from our transition-state-theory H_2CO_3 dissociation model. Note that the choice of above functionality is mostly for simplicity and somewhat arbitrary; the relationship present in Fig. 3-9 is apparently more complex.

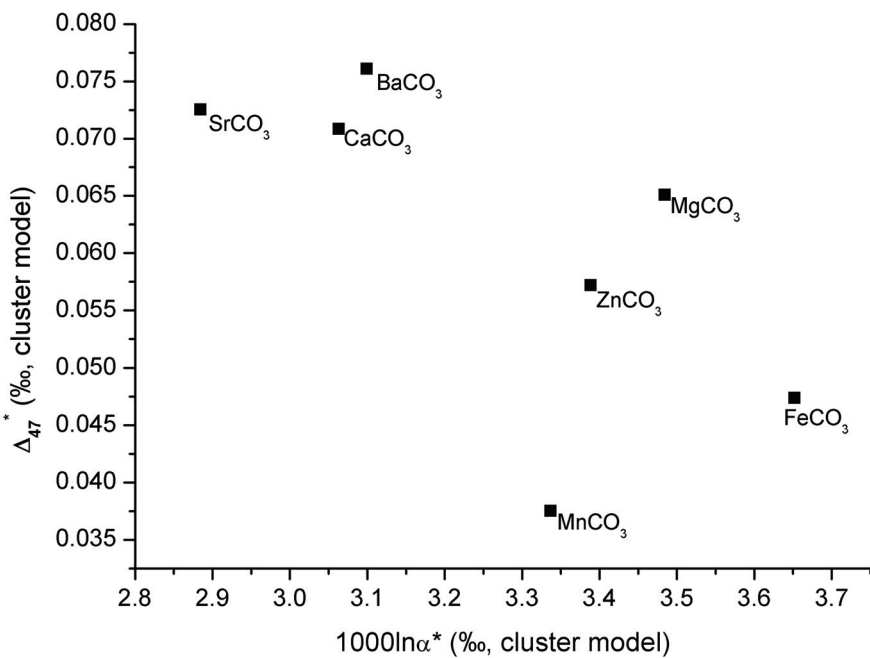


Figure 3-9: Inverse correlation between the oxygen isotope fractionation and Δ_{47}^* fractionation during phosphoric acid digestion of different carbonate minerals, predicted from our cluster model.

At 25°C, this gives $\Delta_{47}^* = \frac{10.72}{1000 \ln \alpha^*(XCO_3, 25^\circ C)} \times 0.220$. This relationship predicts that

the acid digestion fractionation, Δ_{47}^* , for different carbonates ranges from 0.198‰ (MgCO₃) to 0.234‰ (MnCO₃) at 25°C (Table 3-4). More specifically, it predicts that the acid digestion fractionation, Δ_{47}^* , for calcite is 0.231‰ at 25°C — in excellent agreement with our experimentally determined value of 0.232±0.015‰.

The method outlined above of estimating Δ_{47}^* for different carbonate minerals requires experimental data on their oxygen isotope acid digestion fractionation (i.e., $1000 \ln \alpha^*(XCO_3, T)$ in the above equation), and is thus influenced by the significant uncertainties associated with the experimental determinations of $1000 \ln \alpha^*$. To circumvent this issue, we consider an alternative way to estimate Δ_{47}^* , that is based on the cluster model predicted Δ_{47}^* for different carbonate minerals and the experimentally determined Δ_{47}^* for calcite. Given the success of our cluster model in capturing the general trend of variations of oxygen isotope acid digestion fractionation among different carbonate minerals (Fig. 3-7, section 4.3), we assume the cluster model predicted Δ_{47}^* also represent the actual trend of Δ_{47}^* variation among different carbonate minerals despite the apparent underestimation. We therefore predict the actual Δ_{47}^* expected for different carbonate minerals:

$$\Delta_{47}^*(XCO_3, T) = \frac{\Delta_{47}^*(XCO_3, T)_{\text{cluster}}}{\Delta_{47}^*(CaCO_3, T)_{\text{cluster}}} \times \Delta_{47}^*(CaCO_3, T)_{\text{experimental}} , \quad (6)$$

where $\Delta_{47}^*(XCO_3, T)_{\text{cluster}}$ and $\Delta_{47}^*(CaCO_3, T)_{\text{cluster}}$ are our cluster model predicted Δ_{47}^* for XCO₃ and CaCO₃, respectively, at temperature T; and $\Delta_{47}^*(CaCO_3, T)_{\text{experimental}}$ is the experimentally determined Δ_{47} acid fractionation for CaCO₃ (here, calcite; section 4.1) at temperature T. At 25°C, this relationship predicts that the acid digestion fractionation,

Δ_{47}^* , for different carbonates ranges from 0.12‰ (MnCO_3) to 0.25 ‰ (BaCO_3) among the eight different carbonate minerals studied.

For most of the carbonate minerals, the differences in Δ_{47}^* predicted from the above two methods are relatively small, within 0.03‰ (Table 3-4). FeCO_3 and MnCO_3 are the two exceptions, where the predicted Δ_{47}^* from the first method are bigger than those from the second method by 0.05‰ and 0.11‰, respectively. Studies are underway to experimentally determine the Δ_{47}^* for MnCO_3 at 25°C, and thus to distinguish the more accurate of the above two estimation methods. For the moment, we will adopt the Δ_{47}^* estimated from the first method in the following discussion.

We combine previous theoretical estimations on the temperature dependence of ^{13}C - ^{18}O and ^{18}O - ^{17}O clumping in various carbonate minerals (Schauble et al., 2006) with our predicted acid digestion fractionations, Δ_{47}^* , to predict the temperature calibration lines for the clumped isotope thermometer in various carbonates (i.e., Δ_{47} of CO_2 derived from the phosphoric acid digestion vs. temperature; Fig. 3-10). Note that, ^{18}O - ^{17}O clumping was reported only for calcite in Schauble et al. (2006). At our request, E. A. Schauble (personal communication) adapted the lattice dynamics models originally published in Schauble et al. (2006) to estimate ^{17}O - ^{18}O clumping effects for aragonite, dolomite, magnesite and witherite, and found little variation (less than 0.008‰ at 25°C) among different carbonate minerals. On this basis, we have used in our estimation the same ^{18}O - ^{17}O clumping as in calcite for all carbonate minerals. The combination of these two theoretical approaches suggests that the Δ_{47} value of CO_2 extracted at a given temperature from carbonates minerals grown at a given temperature can vary by as much as 0.05‰,

decreasing in the order: CaCO_3 (aragonite) > CaCO_3 (calcite) > BaCO_3 (witherite) > CaMgCO_3 (dolomite) ~ MgCO_3 (magnesite).

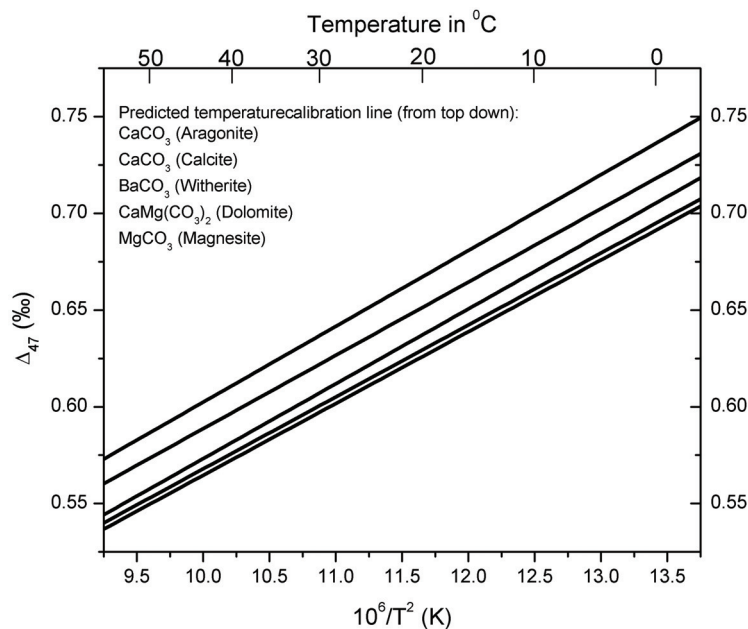


Figure 3-10: Predicted temperature calibration lines for different carbonate clumped isotope thermometers, by combining predicted equilibrium ^{13}C - ^{18}O and ^{18}O - ^{17}O clumping effects inside the carbonate minerals (Schauble et al., 2006) and predicted Δ_{47}^* kinetic fractionations during phosphoric acid digestion of carbonate minerals (this study; see text for details). Phosphoric acid digestions of carbonate minerals are assumed to be at 25°C. CaCO_3 (aragonite), $\Delta_{47}=0.2104+0.0392\times 10^6/T^2$; CaCO_3 (calcite), $\Delta_{47}=0.2097+0.0379\times 10^6/T^2$; BaCO_3 (witherite), $\Delta_{47}=0.1862+0.0387\times 10^6/T^2$; $\text{CaMg}(\text{CO}_3)_2$ (dolomite), $\Delta_{47}=0.1959+0.0372\times 10^6/T^2$; MgCO_3 (magnesite), $\Delta_{47}=0.1936+0.0371\times 10^6/T^2$.

The temperature calibration line predicted in this way for calcite and aragonite closely approach the available experimental calibrations (Ghosh et al., 2006, 2007; Came et al., 2007; Fig. 3-11). However, the slope of our theoretical calibration line is significantly shallower than that of the experimental calibration line, with a temperature sensitivity of $-0.00289\text{‰}/^\circ\text{C}$ over the temperature range 0-50°C, as compared to the -

0.00453‰/°C sensitivity determined experimentally. This discrepancy, as discussed in section 4.3, is suspected to result from the uncertainties in both experimental and theoretical estimations, and should be resolved by more detailed and accurate studies in the future.

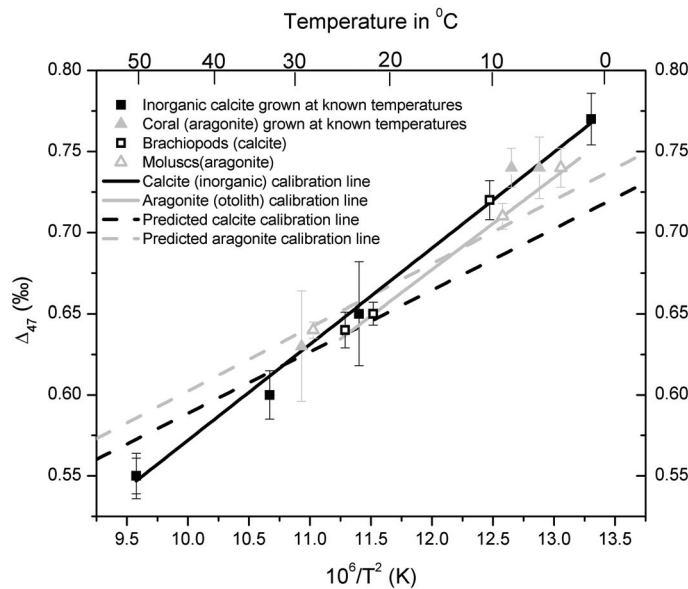


Figure 3-11: Comparison between predicted temperature calibration lines for CaCO_3 (calcite and aragonite) clumped isotope thermometer (this study) and the experimental temperature calibration data (Ghosh et al., 2006; Ghosh et al., 2007; Came et al., 2007). Phosphoric acid digestions of carbonate minerals are performed at 25°C.

Finally, for future reference, our predicted calibration line for calcite, dolomite, and magnesite can be represented over the temperature range 260-1500K by

$$\Delta_{47} = -\frac{3.33040 \times 10^9}{T^4} + \frac{2.32415 \times 10^7}{T^3} - \frac{2.91282 \times 10^3}{T^2} - \frac{5.54042}{T} + 0.23252 \quad \text{Calcite}$$

$$\Delta_{47} = -\frac{3.43068 \times 10^9}{T^4} + \frac{2.35766 \times 10^7}{T^3} - \frac{8.06003 \times 10^2}{T^2} - \frac{6.90300}{T} + 0.22893 \quad \text{Aragonite}$$

$$\Delta_{47} = -\frac{3.31647 \times 10^9}{T^4} + \frac{2.29414 \times 10^7}{T^3} - \frac{2.38375 \times 10^3}{T^2} - \frac{5.71692}{T} + 0.21502 \quad \text{Dolomite}$$

$$\Delta_{47} = -\frac{3.31658 \times 10^9}{T^4} + \frac{2.19871 \times 10^7}{T^3} - \frac{2.83346 \times 10^3}{T^2} - \frac{8.39513}{T} + 0.19897 \quad \text{Magnesite}$$

where T is the temperature in Kelvin.

5. SUMMARY

We present the first quantitative theoretical models of the isotope fractionations during phosphoric acid digestion of carbonate minerals by using classical transition state theory and ab initio calculations to predict the relative rates of reaction of all the isotopologues of reactant carbonate species. These models assume that the critical reaction intermediate is H_2CO_3 , and thus that isotope fractionations during acid digestion are controlled by kinetic isotope effects during dissociation of H_2CO_3 . The simplest form of this model (which considers only H_2CO_3 dissociation as a fractionating step) predicts the isotope fractionations between product CO_2 and reactant carbonate to be:

$$1000\ln\alpha^* = 2.58 + 7.25 \times 10^5 / T^2,$$

$$\Delta_{47}^* = 0.0242 + 0.189 \times 10^5 / T^2,$$

$$\Delta_{48}^* = -0.0825 + 0.213 \times 10^5 / T^2,$$

$$\Delta_{49}^* = -0.0308 + 0.602 \times 10^5 / T^2,$$

where T is the temperature of acid digestion and in the unit of Kelvin. Both the magnitudes ($10.72\text{\textperthousand}$, $0.220\text{\textperthousand}$, $0.137\text{\textperthousand}$, $0.592\text{\textperthousand}$ for $1000\ln\alpha^*$, Δ_{47}^* , Δ_{48}^* , Δ_{49}^* respectively, at 25°C) and the temperature-dependences of the these predicted isotope fractionations agree well with available experimental data on oxygen isotope

fractionations and our newly determined Δ_{47} fractionation of $0.232 \pm 0.015\text{\textperthousand}$ for calcite during phosphoric acid digestion.

A subset of our models attempt to take into account also the influence of cation composition by permitting the H_2CO_3 reaction intermediate to interact with an adjacent metal carbonate group. These ‘cluster models’ underestimate the magnitude of isotope fractionations associated with phosphoric acid digestion by a factor of ~ 3 , presumably because we have incorrectly described the structure of nearest-neighbor interactions between H_2CO_3 reaction intermediate and the reacting mineral surface. Nevertheless, our cluster models reproduce the general trend of variations (in both size and temperature sensitivity) of oxygen isotope acid digestion fractionation among different carbonate minerals, which suggests the general concept framework we followed in our models is broadly correct.

ACKNOWLEDGEMENTS

We would like to thank Edwin Schauble for checking into the $^{18}\text{O}-^{17}\text{O}$ clumped isotope effects in carbonate minerals other than calcite.

REFERENCE

- Assonov S. S. and Brenninkmeijer C. A. M. (2003). On the ^{17}O correction for CO_2 mass spectrometric isotopic analysis. *Rapid Commun. Mass Spectrom.* **17**: 1007-1016.
 Barkan E. and Luz B. (2005). High precision measurements of $^{17}\text{O}/^{16}\text{O}$ and $^{18}\text{O}/^{16}\text{O}$ ratios in H_2O . *Rapid Commun. Mass Spectrom.* **19**: 3737-3742.

- Bottcher M. (1996). $^{18}\text{O}/^{16}\text{O}$ and $^{13}\text{C}/^{12}\text{C}$ fractionation during the reaction of carbonates with phosphoric acid: Effects of cationic substitution and reaction temperature. *Isot. Environ. Health Stud.* **32**: 299-305.
- Came R. E., Eiler J. M., Veizer J., Azmy K., Brand U. and Weidman C. R. (2007). Coupling of surface temperatures and atmospheric CO_2 concentrations during the Palaeozoic era. *Nature*. **449**: 198-201.
- Coplen T. B., Kendall C. and Hopple J. (1983). Comparison of stable isotope reference samples. *Nature*. **302**: 236-8.
- Das Sharma S., Patil D. J. and Gopalan K. (2002). Temperature dependence of oxygen isotope fractionation of CO_2 from magnesite-phosphoric acid reaction. *Geochim. Cosmochim. Acta* **66**: 589-593.
- Eiler J. M. and Schauble E. (2004). $^{18}\text{O}^{13}\text{C}^{16}\text{O}$ in Earth's atmosphere. *Geochim. Cosmochim. Acta* **68**: 4767-4777.
- Eyring H. (1935a). Activated complex in chemical reactions. *J. Chem. Phys.* **3**: 107-15.
- Eyring H. (1935b). The activated complex and the absolute rate of chemical reactions. *Chem. Rev.* **17**: 65-77.
- Felipe M. A., Xiao Y. and Kubicki J. D. (2001). Molecular orbital modeling and transition state theory in geochemistry. *Rev. Mineral. Geochem.* **42**: 485-531.
- Foresman J. B. and Frisch A. (1993). Exploring chemistry with electronic structure methods. Gaussian, Inc.
- Ghosh P., Adkins J., Affek H. P., Balta B., Guo W., Schauble E. A., Schrag D. and Eiler J. M. (2006). $^{13}\text{C}-^{18}\text{O}$ bonds in carbonate minerals: A new kind of paleothermometer. *Geochim. Cosmochim. Acta* **70**: 1439-1456.
- Ghosh P., Eiler J., Campana S. E. and Feeney R. F. (2007). Calibration of the carbonate 'clumped isotope' paleothermometer for otoliths. *Geochim. Cosmochim. Acta* **71**: 2736-2744.
- Gilg H. A., Struck U., Vennemann T. and Boni M. (2003). Phosphoric acid fractionation factors for smithsonite and cerussite between 25 and 72°C. *Geochim. Cosmochim. Acta* **67**: 4049-4055.
- Kim S.-T., Mucci A. and Taylor B. E. (2007). Phosphoric acid fractionation factors for calcite and aragonite between 25 and 75°C: Revisited. *Chem. Geol.* **246**: 135-146.

- Kim S.-T. and O'Neil J. R. (1997). Equilibrium and nonequilibrium oxygen isotope effects in synthetic carbonates. *Geochim. Cosmochim. Acta* **61**: 3461-3475.
- Land L. S. (1980). The isotopic and trace element geochemistry of dolomite: the state of the art. In *SEPM Special Publications*. **28**. 87-110.
- Li W. J. and Meijer H. A. J. (1998). The use of electrolysis for accurate $d^{17}\text{O}$ and $d^{18}\text{O}$ isotope measurements in water. *Isotopes Environ. Health Stud.* **34**: 349-369.
- Loerting T., Tautermann C., Kroemer R. T., Kohl I., Hallbrucker A., Mayer E. and Liedl K. R. (2000). On the surprising kinetic stability of carbonic acid (H_2CO_3). *Angew. Chem. Int. Ed.* **39**: 892-894.
- Mao Y. and Siders P. D. (1997). Molecular Hartree-Fock model of calcium carbonate. *Journal of Molecular Structure-Theochem* **419**: 173-184.
- McCrea J. M. (1950). The isotopic chemistry of carbonates and a paleo-temperature scale. *Journal of Chemical Physics* **18**: 849-57.
- Melander L. and Saunders J. W. H. (1987). Reaction rates of isotopic molecules. John Wiley & Sons, Inc.
- Miller M. F., Röckmann T. and P. W. I. (2007). A general algorithm for the ^{17}O abundance correction to $^{13}\text{C}/^{12}\text{C}$ determinations from CO_2 isotopologue measurements, including CO_2 characterised by 'mass-independent' oxygen isotope distributions. *Geochim. Cosmochim. Acta* **71**: 3145-3161.
- O'Neil J. R. (1986). Theoretical and experimental aspects of isotopic fractionation. In *Stable isotopes in high temperature geological processes*. Rev. Mineral. **16**. 1-40.
- Ramirez J.-Z., Vargas R., Garza J. and Hay B. P. (2006). Performance of the effective core potentials of Ca, Hg, and Pb in complexes with ligands containing N and O donor atoms. *J. Chem. Theory Comput.* **2**: 1510-1519.
- Ringnalda M. N., Langlois J.-M., Greeley B. H., Russo T. V., Muller R. P., Marten B., Won Y., Donnelly R. E., Pollard J., W. Thomas, Miller G. H., Goddard W. A. I. and Friesner R. A. (2005). Jaguar, version 6.5. Schrodinger, LLC, New York, NY.
- Rollion-Bard C., Mangin D. and Champenois M. (2007). Development and application of oxygen and carbon isotopic measurements of biogenic carbonates by ion microprobe. *Geostand. Geoanal. Res.* **31**: 39-50.

- Rosenbaum J. and Sheppard S. M. F. (1986). An isotopic study of siderites, dolomites and ankerites at high temperatures. *Geochim. Cosmochim. Acta* **50**: 1147-50.
- Ruuska H., Hirva P. and Pakkanen T. A. (1999). Cluster models for calcite surfaces: ab initio quantum chemical studies. *J. Phys. Chem. B.* **103**: 6734-6740.
- Schauble E. A., Ghosh P. and Eiler J. M. (2006). Preferential formation of ^{13}C - ^{18}O bonds in carbonate minerals, estimated using first-principles lattice dynamics. *Geochim. Cosmochim. Acta* **70**: 2510-2529.
- Scott A. P. and Radom L. (1996). Harmonic vibrational frequencies: an evaluation of Hartree-Fock, Moeller-Plesset, Quadratic Configuration Interaction, Density Functional Theory, and semiempirical scale factors. *J. Phys. Chem.* **100**: 16502-16513.
- Sharma S. K. and Sharma T. (1969a). Oxygen isotope fractionation factor between carbon dioxide and carbonate ion. *Int. J. Mass Spectrom. Ion Phys.* **2**: 367-71.
- Sharma S. K. and Sharma T. (1969b). Intramolecular kinetic isotope effect in the acid decomposition of carbonates. *Int. J. Mass Spectrom. Ion Phys.* **2**: 485-93.
- Sharma T. and Clayton R. N. (1965). Measurement of $^{18}\text{O}/^{16}\text{O}$ ratios of total oxygen of carbonates. *Geochim. Cosmochim. Acta* **29**: 1347-1354.
- Sharp Z. D. and Cerling T. E. (1996). A laser GC-IRMS technique for in situ stable isotope analyses of carbonates and phosphates. *Geochim. Cosmochim. Acta* **60**: 2909-2916.
- Suito K., Namba J., Horikawa T., Taniguchi Y., Sakurai N., Kobayashi M., Onodera A., Shimomura O. and Kikegawa T. (2001). Phase relations of CaCO_3 at high pressure and high temperature. *Am. Mineral.* **86**: 997-1002.
- Swart P. K., Burns S. J. and Leder J. J. (1991). Fractionation of the stable isotopes of oxygen and carbon in carbon dioxide during the reaction of calcite with phosphoric acid as a function of temperature and technique. *Chem. Geol.* **86**: 89-96.
- Tossell J. A. (2006). H_2CO_3 and its oligomers: Structures, stabilities, vibrational and NMR spectra, and acidities. *Inorg. Chem.* **45**: 5961-5970.
- Urey H. C. (1947). Thermodynamic properties of isotopic substances. *J. Chem. Soc.*: 562-581.

Wang Z., Schauble E. A. and Eiler J. M. (2004). Equilibrium thermodynamics of multiply substituted isotopologues of molecular gases. *Geochim. Cosmochim. Acta* **68**: 4779-4797.

APPENDIX

Estimation on the distributions of multiply-substituted isotopologues inside reactant carbonate mineral at hypothetical equilibration temperatures and bulk isotopic compositions

We calculate the distributions of multiply-substituted isotopologues (and all other isotopologues) inside reactant carbonate mineral at hypothetical equilibration temperatures, following the similar methodology and algorithm as presented by Wang et al. (2004) in their theoretical estimations of abundances of multiply-substituted isotopologues of molecular gases. CO_3^{2-} has a total of 20 isotopologues. To determine the abundances of all isotopologues, we select the abundances of non-substituted ($^{12}\text{C}^{16}\text{O}^{16}\text{O}^{16}\text{O}^{2-}$) and singly-substituted isotopologues ($^{13}\text{C}^{16}\text{O}^{16}\text{O}^{16}\text{O}^{2-}$, $^{12}\text{C}^{18}\text{O}^{16}\text{O}^{16}\text{O}^{2-}$ and $^{12}\text{C}^{17}\text{O}^{16}\text{O}^{16}\text{O}^{2-}$) as the fundamental unknowns, and express the abundances of the other 16 multiply-substituted isotopologues as functions of these fundamental unknowns and the equilibrium constants of the related isotope exchange reactions:

$$[^{13}\text{C}^{18}\text{O}^{16}\text{O}^{16}\text{O}^{2-}] = \frac{[^{13}\text{C}^{16}\text{O}^{16}\text{O}^{16}\text{O}^{2-}] \times [^{12}\text{C}^{18}\text{O}^{16}\text{O}^{16}\text{O}^{2-}]}{[^{12}\text{C}^{16}\text{O}^{16}\text{O}^{16}\text{O}^{2-}]} \times K_{3866} \quad (\text{a1})$$

$$[^{13}\text{C}^{17}\text{O}^{16}\text{O}^{16}\text{O}^{2-}] = \frac{[^{13}\text{C}^{16}\text{O}^{16}\text{O}^{16}\text{O}^{2-}] \times [^{12}\text{C}^{17}\text{O}^{16}\text{O}^{16}\text{O}^{2-}]}{[^{12}\text{C}^{16}\text{O}^{16}\text{O}^{16}\text{O}^{2-}]} \times K_{3766} \quad (\text{a2})$$

$$[^{12}\text{C}^{17}\text{O}^{16}\text{O}^{16}\text{O}^{2-}] = \frac{[^{12}\text{C}^{17}\text{O}^{16}\text{O}^{16}\text{O}^{2-}]}{[^{12}\text{C}^{16}\text{O}^{16}\text{O}^{16}\text{O}^{2-}]}^2 \times K_{2776} \quad (\text{a3})$$

$$[{}^{12}\text{C}^{17}\text{O}^{18}\text{O}^{16}\text{O}^{2-}] = \frac{[{}^{12}\text{C}^{17}\text{O}^{16}\text{O}^{16}\text{O}^{2-}] \times [{}^{12}\text{C}^{18}\text{O}^{16}\text{O}^{16}\text{O}^{2-}]}{[{}^{12}\text{C}^{16}\text{O}^{16}\text{O}^{16}\text{O}^{2-}]} \times K_{2786} \quad (\text{a4})$$

$$[{}^{13}\text{C}^{17}\text{O}^{17}\text{O}^{16}\text{O}^{2-}] = \frac{[{}^{13}\text{C}^{16}\text{O}^{16}\text{O}^{16}\text{O}^{2-}] \times [{}^{12}\text{C}^{17}\text{O}^{16}\text{O}^{16}\text{O}^{2-}]}{[{}^{12}\text{C}^{16}\text{O}^{16}\text{O}^{16}\text{O}^{2-}]}^2 \times K_{3766} \quad (\text{a5})$$

$$[{}^{12}\text{C}^{17}\text{O}^{17}\text{O}^{17}\text{O}^{2-}] = \frac{[{}^{12}\text{C}^{17}\text{O}^{16}\text{O}^{16}\text{O}^{2-}]}{[{}^{12}\text{C}^{16}\text{O}^{16}\text{O}^{16}\text{O}^{2-}]}^3 \times K_{2777} \quad (\text{a6})$$

$$[{}^{12}\text{C}^{18}\text{O}^{18}\text{O}^{16}\text{O}^{2-}] = \frac{[{}^{12}\text{C}^{18}\text{O}^{16}\text{O}^{16}\text{O}^{2-}]}{[{}^{12}\text{C}^{16}\text{O}^{16}\text{O}^{16}\text{O}^{2-}]}^2 \times K_{2886} \quad (\text{a7})$$

$$[{}^{13}\text{C}^{17}\text{O}^{18}\text{O}^{16}\text{O}^{2-}] = \frac{[{}^{13}\text{C}^{16}\text{O}^{16}\text{O}^{16}\text{O}^{2-}] \times [{}^{12}\text{C}^{17}\text{O}^{16}\text{O}^{16}\text{O}^{2-}] \times [{}^{12}\text{C}^{18}\text{O}^{16}\text{O}^{16}\text{O}^{2-}]}{[{}^{12}\text{C}^{16}\text{O}^{16}\text{O}^{16}\text{O}^{2-}]} \times K_{3786} \quad (\text{a8})$$

$$[{}^{12}\text{C}^{17}\text{O}^{17}\text{O}^{18}\text{O}^{2-}] = \frac{[{}^{12}\text{C}^{17}\text{O}^{16}\text{O}^{16}\text{O}^{2-}]}{[{}^{12}\text{C}^{16}\text{O}^{16}\text{O}^{16}\text{O}^{2-}]}^2 \times [{}^{12}\text{C}^{18}\text{O}^{16}\text{O}^{16}\text{O}^{2-}] \times K_{2778} \quad (\text{a9})$$

$$[{}^{13}\text{C}^{17}\text{O}^{17}\text{O}^{17}\text{O}^{2-}] = \frac{[{}^{13}\text{C}^{16}\text{O}^{16}\text{O}^{16}\text{O}^{2-}] \times [{}^{12}\text{C}^{17}\text{O}^{16}\text{O}^{16}\text{O}^{2-}]}{[{}^{12}\text{C}^{16}\text{O}^{16}\text{O}^{16}\text{O}^{2-}]}^3 \times K_{3777} \quad (\text{a10})$$

$$[{}^{13}\text{C}^{18}\text{O}^{18}\text{O}^{16}\text{O}^{2-}] = \frac{[{}^{13}\text{C}^{16}\text{O}^{16}\text{O}^{16}\text{O}^{2-}] \times [{}^{12}\text{C}^{18}\text{O}^{16}\text{O}^{16}\text{O}^{2-}]}{[{}^{12}\text{C}^{16}\text{O}^{16}\text{O}^{16}\text{O}^{2-}]}^2 \times K_{3886} \quad (\text{a11})$$

$$[{}^{12}\text{C}^{17}\text{O}^{18}\text{O}^{18}\text{O}^{2-}] = \frac{[{}^{12}\text{C}^{17}\text{O}^{16}\text{O}^{16}\text{O}^{2-}]}{[{}^{12}\text{C}^{16}\text{O}^{16}\text{O}^{16}\text{O}^{2-}]}^2 \times [{}^{12}\text{C}^{18}\text{O}^{16}\text{O}^{16}\text{O}^{2-}] \times K_{2788} \quad (\text{a12})$$

$$[{}^{13}\text{C}^{17}\text{O}^{18}\text{O}^{18}\text{O}^{2-}] = \frac{[{}^{13}\text{C}^{16}\text{O}^{16}\text{O}^{16}\text{O}^{2-}] \times [{}^{12}\text{C}^{17}\text{O}^{16}\text{O}^{16}\text{O}^{2-}] \times [{}^{12}\text{C}^{18}\text{O}^{16}\text{O}^{16}\text{O}^{2-}]}{[{}^{12}\text{C}^{16}\text{O}^{16}\text{O}^{16}\text{O}^{2-}]}^3 \times K_{3788} \quad (\text{a13})$$

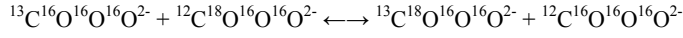
$$[{}^{12}\text{C}^{18}\text{O}^{18}\text{O}^{18}\text{O}^{2-}] = \frac{[{}^{12}\text{C}^{18}\text{O}^{16}\text{O}^{16}\text{O}^{2-}]}{[{}^{12}\text{C}^{16}\text{O}^{16}\text{O}^{16}\text{O}^{2-}]}^3 \times K_{2888} \quad (\text{a14})$$

$$[{}^{13}\text{C}^{17}\text{O}^{18}\text{O}^{18}\text{O}^{2-}] = \frac{[{}^{13}\text{C}^{16}\text{O}^{16}\text{O}^{16}\text{O}^{2-}] \times [{}^{12}\text{C}^{17}\text{O}^{16}\text{O}^{16}\text{O}^{2-}] \times [{}^{12}\text{C}^{18}\text{O}^{16}\text{O}^{16}\text{O}^{2-}]}{[{}^{12}\text{C}^{16}\text{O}^{16}\text{O}^{16}\text{O}^{2-}]}^3 \times K_{3788} \quad (\text{a15})$$

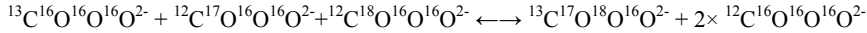
$$[{}^{13}\text{C}^{18}\text{O}^{18}\text{O}^{18}\text{O}^{2-}] = \frac{[{}^{13}\text{C}^{16}\text{O}^{16}\text{O}^{16}\text{O}^{2-}] \times [{}^{12}\text{C}^{18}\text{O}^{16}\text{O}^{16}\text{O}^{2-}]}{[{}^{12}\text{C}^{16}\text{O}^{16}\text{O}^{16}\text{O}^{2-}]}^3 \times K_{3888} \quad (\text{a16})$$

,

where K denote the equilibrium constants for the related isotope exchange reactions at the specified equilibration temperature, e.g.,



$$K_{3866} = \frac{Q_{^{13}\text{C}^{18}\text{O}^{16}\text{O}^{2-}} \times Q_{^{12}\text{C}^{16}\text{O}^{16}\text{O}^{2-}}}{Q_{^{13}\text{C}^{16}\text{O}^{16}\text{O}^{2-}} \times Q_{^{12}\text{C}^{18}\text{O}^{16}\text{O}^{2-}}}$$



$$K_{3786} = \frac{Q_{^{13}\text{C}^{17}\text{O}^{18}\text{O}^{16}\text{O}^{2-}} \times (Q_{^{12}\text{C}^{16}\text{O}^{16}\text{O}^{2-}})^2}{Q_{^{13}\text{C}^{16}\text{O}^{16}\text{O}^{2-}} \times Q_{^{12}\text{C}^{17}\text{O}^{16}\text{O}^{2-}} \times Q_{^{12}\text{C}^{18}\text{O}^{16}\text{O}^{2-}}}$$

Q here refer to the partition functions of different CO_3^{2-} isotopologues, and can be evaluated with their respective scaled vibration frequencies through principles of statistical thermodynamics (Urey 1947).

However, a full-scale calculation of these 16 equilibrium constants for multiply-substituted isotopologues in carbonate lattices, as Schauble et al. (2006) did for K_{3866} and K_{2876} , demands significant computation power and is out of the scope of this study. Instead we calculate the corresponding equilibrium constants for an isolated CO_3^{2-} ion in the gas phase, and use them to approximate the equilibrium constants in carbonate lattice. The distribution of multiply-substituted isotopologues inside the two are remarkably similar (e.g., at equilibration temperature of 300K, $K_{3866}= 1.0004034$ in isolated CO_3^{2-} , this study; vs. $K_{3866}=1.0004066$ in calcite lattice, Schauble et al. 2006), and therefore this approximation will not introduce any significant systematic errors on our model results. The geometry optimization and frequency calculation for the isolated CO_3^{2-} ion are performed at DFT-B3LYP/6-31G* level, and the frequencies are scaled with the universal scaling factor of 0.9614 as discussed in section 2.3 (Table 3-A1).

Table 3-A1 Scaled vibration frequencies (unit: cm^{-1}) for different CO_3^{2-} isotopologues (isolated CO_3^{2-} in the gas phase, DFT-B3LYP/6-31G* with a frequency scaling factor of 0.9614).

Isotopologue	w ₁	w ₂	w ₃	w ₄	w ₅	w ₆
¹² C ¹⁶ O ¹⁶ O	638.23	638.23	837.82	975.97	1396.24	1396.24
¹² C ¹⁷ O ¹⁶ O	631.11	633.21	836.17	966.25	1389.37	1396.21

Table 3-A1 (Continued)

Isotopologue	ϖ_1	ϖ_2	ϖ_3	ϖ_4	ϖ_5	ϖ_6
$^{12}\text{C}^{18}\text{O}^{16}\text{O}^{16}\text{O}$	624.53	628.54	834.70	957.47	1383.83	1395.88
$^{12}\text{C}^{17}\text{O}^{17}\text{O}^{16}\text{O}$	625.24	627.02	834.52	956.49	1385.68	1392.85
$^{12}\text{C}^{17}\text{O}^{18}\text{O}^{16}\text{O}$	618.74	622.36	833.05	947.66	1380.84	1391.67
$^{12}\text{C}^{18}\text{O}^{18}\text{O}^{16}\text{O}$	612.66	617.32	831.58	938.83	1376.69	1389.69
$^{12}\text{C}^{17}\text{O}^{17}\text{O}^{17}\text{O}$	620.13	620.13	832.86	946.71	1385.66	1385.66
$^{12}\text{C}^{17}\text{O}^{17}\text{O}^{18}\text{O}$	612.81	616.30	831.39	937.86	1380.24	1384.94
$^{12}\text{C}^{17}\text{O}^{18}\text{O}^{18}\text{O}$	607.32	610.76	829.91	928.96	1376.98	1381.94
$^{12}\text{C}^{18}\text{O}^{18}\text{O}^{18}\text{O}$	603.55	603.55	828.44	920.03	1376.28	1376.28
$^{13}\text{C}^{16}\text{O}^{16}\text{O}^{16}\text{O}$	636.73	636.73	811.56	975.97	1355.65	1355.65
$^{13}\text{C}^{17}\text{O}^{16}\text{O}^{16}\text{O}$	629.55	631.86	809.86	966.22	1348.54	1355.62
$^{13}\text{C}^{18}\text{O}^{16}\text{O}^{16}\text{O}$	622.91	627.33	808.34	957.36	1342.81	1355.30
$^{13}\text{C}^{17}\text{O}^{17}\text{O}^{16}\text{O}$	623.72	625.72	808.15	956.46	1344.69	1352.15
$^{13}\text{C}^{17}\text{O}^{18}\text{O}^{16}\text{O}$	617.19	621.16	806.63	947.59	1339.67	1350.95
$^{13}\text{C}^{18}\text{O}^{18}\text{O}^{16}\text{O}$	611.13	616.17	805.11	938.73	1335.35	1348.93
$^{13}\text{C}^{17}\text{O}^{17}\text{O}^{17}\text{O}$	618.75	618.75	806.44	946.71	1344.67	1344.67
$^{13}\text{C}^{17}\text{O}^{17}\text{O}^{18}\text{O}$	611.38	615.06	804.92	937.84	1339.01	1343.97
$^{13}\text{C}^{17}\text{O}^{18}\text{O}^{18}\text{O}$	605.94	609.54	803.40	928.94	1335.62	1340.86
$^{13}\text{C}^{18}\text{O}^{18}\text{O}^{18}\text{O}$	602.28	602.28	801.87	920.03	1334.94	1334.94

We combine the above equations with the constraints from the bulk isotopic composition of the CO_3^{2-} ion,

$$[^{13}\text{C}^{16}\text{O}^{16}\text{O}^{16}\text{O}^{2-}] + [^{13}\text{C}^{17}\text{O}^{16}\text{O}^{16}\text{O}^{2-}] + [^{13}\text{C}^{18}\text{O}^{16}\text{O}^{16}\text{O}^{2-}] + [^{13}\text{C}^{17}\text{O}^{17}\text{O}^{16}\text{O}^{2-}] + [^{13}\text{C}^{17}\text{O}^{18}\text{O}^{16}\text{O}^{2-}] + [^{13}\text{C}^{18}\text{O}^{16}\text{O}^{16}\text{O}^{2-}] \\ + [^{13}\text{C}^{17}\text{O}^{17}\text{O}^{17}\text{O}^{2-}] + [^{13}\text{C}^{17}\text{O}^{17}\text{O}^{18}\text{O}^{2-}] + [^{13}\text{C}^{17}\text{O}^{18}\text{O}^{18}\text{O}^{2-}] + [^{13}\text{C}^{18}\text{O}^{18}\text{O}^{18}\text{O}^{2-}] = [^{13}\text{C}] \quad (\text{a17})$$

$$[^{12}\text{C}^{18}\text{O}^{16}\text{O}^{16}\text{O}^{2-}] + [^{12}\text{C}^{17}\text{O}^{18}\text{O}^{16}\text{O}^{2-}] + [^{12}\text{C}^{17}\text{O}^{17}\text{O}^{18}\text{O}^{2-}] + [^{13}\text{C}^{18}\text{O}^{16}\text{O}^{16}\text{O}^{2-}] + [^{13}\text{C}^{17}\text{O}^{18}\text{O}^{16}\text{O}^{2-}] + [^{13}\text{C}^{17}\text{O}^{17}\text{O}^{18}\text{O}^{2-}] \\ + 2 \times [^{12}\text{C}^{18}\text{O}^{18}\text{O}^{16}\text{O}^{2-}] + 2 \times [^{12}\text{C}^{17}\text{O}^{18}\text{O}^{18}\text{O}^{2-}] + 2 \times [^{13}\text{C}^{18}\text{O}^{18}\text{O}^{16}\text{O}^{2-}] + 2 \times [^{13}\text{C}^{17}\text{O}^{18}\text{O}^{18}\text{O}^{2-}] + 3 \times [^{12}\text{C}^{18}\text{O}^{18}\text{O}^{18}\text{O}^{2-}] \\ + 3 \times [^{13}\text{C}^{18}\text{O}^{18}\text{O}^{18}\text{O}^{2-}] = 3 \times [^{18}\text{O}] \quad (\text{a18})$$

$$3 \times [^{12}\text{C}^{16}\text{O}^{16}\text{O}^{16}\text{O}^{2-}] + 2 \times [^{12}\text{C}^{17}\text{O}^{16}\text{O}^{16}\text{O}^{2-}] + 2 \times [^{12}\text{C}^{18}\text{O}^{16}\text{O}^{16}\text{O}^{2-}] + [^{12}\text{C}^{17}\text{O}^{17}\text{O}^{16}\text{O}^{2-}] + [^{12}\text{C}^{17}\text{O}^{18}\text{O}^{16}\text{O}^{2-}] + [^{12}\text{C}^{18}\text{O}^{18}\text{O}^{16}\text{O}^{2-}] \\ + 3 \times [^{13}\text{C}^{16}\text{O}^{16}\text{O}^{16}\text{O}^{2-}] + 2 \times [^{13}\text{C}^{17}\text{O}^{16}\text{O}^{16}\text{O}^{2-}] + 2 \times [^{13}\text{C}^{18}\text{O}^{16}\text{O}^{16}\text{O}^{2-}] + [^{13}\text{C}^{17}\text{O}^{17}\text{O}^{16}\text{O}^{2-}] + [^{13}\text{C}^{17}\text{O}^{18}\text{O}^{16}\text{O}^{2-}] \\ + [^{13}\text{C}^{18}\text{O}^{18}\text{O}^{16}\text{O}^{2-}] = 3 \times [^{16}\text{O}] \quad (\text{a19})$$

$$\begin{aligned}
& [^{12}\text{C}^{16}\text{O}^{16}\text{O}^{16}\text{O}^{2-}] + [^{12}\text{C}^{17}\text{O}^{16}\text{O}^{16}\text{O}^{2-}] + [^{12}\text{C}^{18}\text{O}^{16}\text{O}^{16}\text{O}^{2-}] + [^{12}\text{C}^{17}\text{O}^{17}\text{O}^{16}\text{O}^{2-}] + [^{12}\text{C}^{17}\text{O}^{18}\text{O}^{16}\text{O}^{2-}] + [^{12}\text{C}^{18}\text{O}^{18}\text{O}^{16}\text{O}^{2-}] \\
& + [^{12}\text{C}^{17}\text{O}^{17}\text{O}^{17}\text{O}^{2-}] + [^{12}\text{C}^{17}\text{O}^{17}\text{O}^{18}\text{O}^{2-}] + [^{12}\text{C}^{17}\text{O}^{18}\text{O}^{18}\text{O}^{2-}] + [^{12}\text{C}^{18}\text{O}^{18}\text{O}^{18}\text{O}^{2-}] + [^{13}\text{C}^{16}\text{O}^{16}\text{O}^{16}\text{O}^{2-}] + [^{13}\text{C}^{17}\text{O}^{16}\text{O}^{16}\text{O}^{2-}] \\
& + [^{13}\text{C}^{18}\text{O}^{16}\text{O}^{16}\text{O}^{2-}] + [^{13}\text{C}^{17}\text{O}^{17}\text{O}^{16}\text{O}^{2-}] + [^{13}\text{C}^{17}\text{O}^{18}\text{O}^{16}\text{O}^{2-}] + [^{13}\text{C}^{18}\text{O}^{18}\text{O}^{16}\text{O}^{2-}] + [^{13}\text{C}^{17}\text{O}^{17}\text{O}^{17}\text{O}^{2-}] + [^{13}\text{C}^{17}\text{O}^{17}\text{O}^{18}\text{O}^{2-}] \\
& + [^{13}\text{C}^{17}\text{O}^{18}\text{O}^{18}\text{O}^{2-}] + [^{13}\text{C}^{18}\text{O}^{18}\text{O}^{18}\text{O}^{2-}] = 1 \tag{a20}
\end{aligned}$$

where $[^{13}\text{C}]$, $[^{18}\text{O}]$, $[^{16}\text{O}]$ refer to the bulk ^{13}C , ^{18}O and ^{16}O abundances in the CO_3^{2-} respectively and can be calculated from its given bulk isotopic composition. By simultaneously solving these 20 equations (using fsolve function in MATLAB program, version 7.04), we obtain the abundances of all 20 isotopologues at specified bulk isotopic composition and equilibration temperature (Table 3-A2).

Table 3-A2 Estimated abundances of all CO_3^{2-} isotopologues at different equilibration temperatures and with different bulk isotopic compositions.

Isotopologue of CO_3^{2-} Reactant	Mass [‡] $\delta^{18}\text{O}_{\text{VSMOW}} (\text{\textperthousand})$	Abundances					
		Equil. T (K)			Equil. T (K)		
		500	500	500	300	300	300
$^{12}\text{C}^{16}\text{O}^{16}\text{O}^{16}\text{O}$	60	0.981845501	0.981736407	0.981780829	0.981845495	0.981736401	0.981780823
$^{13}\text{C}^{16}\text{O}^{16}\text{O}^{16}\text{O}$	61	0.011033192	0.011142286	0.011032465	0.011033186	0.011142280	0.011032460
$^{12}\text{C}^{17}\text{O}^{16}\text{O}^{16}\text{O}$	61	0.001119007	0.001118883	0.001124698	0.001119001	0.001118877	0.001124692
$^{12}\text{C}^{18}\text{O}^{16}\text{O}^{16}\text{O}$	62	0.005906388	0.005905731	0.005965059	0.005906382	0.005905726	0.005965053
$^{13}\text{C}^{17}\text{O}^{16}\text{O}^{16}\text{O}$	62	1.257521E-05	1.269955E-05	1.263916E-05	1.257710E-05	1.270146E-05	1.264106E-05
$^{12}\text{C}^{17}\text{O}^{17}\text{O}^{16}\text{O}$	62	6.637827E-05	6.703460E-05	6.703764E-05	6.639792E-05	6.705445E-05	6.705748E-05
$^{13}\text{C}^{18}\text{O}^{16}\text{O}^{16}\text{O}$	63	4.487818E-06	4.487320E-06	4.555747E-06	4.488118E-06	4.487619E-06	4.556051E-06
$^{12}\text{C}^{18}\text{O}^{17}\text{O}^{16}\text{O}$	63	4.251179E-07	4.250706E-07	4.294809E-07	4.251298E-07	4.250826E-07	4.294930E-07
$^{13}\text{C}^{17}\text{O}^{17}\text{O}^{16}\text{O}$	63	1.184398E-05	1.184267E-05	1.208125E-05	1.184530E-05	1.184399E-05	1.208260E-05
$^{12}\text{C}^{17}\text{O}^{17}\text{O}^{17}\text{O}$	63	5.043864E-08	5.093736E-08	5.120209E-08	5.0464478E-08	5.096376E-08	5.122862E-08
$^{12}\text{C}^{18}\text{O}^{18}\text{O}^{16}\text{O}$	64	4.777666E-09	4.824907E-09	4.826700E-09	4.779286E-09	4.826542E-09	4.828336E-09
$^{13}\text{C}^{18}\text{O}^{17}\text{O}^{16}\text{O}$	64	1.331213E-07	1.344375E-07	1.357881E-07	1.332149E-07	1.345321E-07	1.358836E-07
$^{12}\text{C}^{18}\text{O}^{17}\text{O}^{17}\text{O}$	64	5.383609E-11	5.383010E-11	5.466880E-11	5.384187E-11	5.383588E-11	5.467467E-11
$^{13}\text{C}^{17}\text{O}^{17}\text{O}^{17}\text{O}$	64	8.525078E-10	8.524131E-10	8.698698E-10	8.5266778E-10	8.5255730E-10	8.700330E-10
$^{13}\text{C}^{18}\text{O}^{18}\text{O}^{16}\text{O}$	65	4.499842E-09	4.499342E-09	4.613632E-09	4.501037E-09	4.500536E-09	4.614857E-09
$^{12}\text{C}^{18}\text{O}^{18}\text{O}^{17}\text{O}$	65	7.917198E-09	7.916318E-09	8.156559E-09	7.919962E-09	7.919082E-09	8.159407E-09
$^{13}\text{C}^{18}\text{O}^{17}\text{O}^{17}\text{O}$	65	6.050678E-13	6.110505E-13	6.144267E-13	6.054144E-13	6.114005E-13	6.14778E-13
$^{12}\text{C}^{18}\text{O}^{18}\text{O}^{18}\text{O}$	66	9.581874E-12	9.676617E-12	9.777016E-12	9.589474E-12	9.684291E-12	9.784770E-12
$^{13}\text{C}^{18}\text{O}^{18}\text{O}^{17}\text{O}$	66	5.057908E-11	5.107919E-11	5.185810E-11	5.063019E-11	5.113081E-11	5.191051E-11
$^{13}\text{C}^{18}\text{O}^{18}\text{O}^{18}\text{O}$	67	8.899522E-11	8.987519E-11	9.168583E-11	8.910502E-11	8.998607E-11	9.179895E-11

Chapter 4**ISOTOPIC FRACTIONATIONS ASSOCIATED WITH DEGASSING
OF CO₂ FROM AQUEOUS SOLUTIONS AND IMPLICATIONS FOR
CARBONATE CLUMPED ISOTOPE THERMOMETRY**

Weifu Guo ¹, Mathieu Daëron ^{1,2}, Paul Niles ³, William A. Goddard ⁴, John M. Eiler ¹

- a. Division of Geological and Planetary Sciences, California Institute of Technology,
Pasadena, CA, 91125, USA
- b. Laboratoire des Sciences du Climat et de l'Environnement, CNRS - CEA - Univ.
Versailles St-Quentin, Paris, France
- c. NASA Johnson Space Center, Houston, TX, USA
- d. Materials and Process Simulation Center, California Institute of Technology,
Pasadena, CA, 91125, USA

ABSTRACT

Degassing of CO₂ from aqueous solutions occurs through bicarbonate dehydration ($\text{H}^+ + \text{HCO}_3^- (\text{aq}) \rightarrow \text{H}_2\text{CO}_3 \rightarrow \text{CO}_2 + \text{H}_2\text{O}$) and bicarbonate dehydroxylation ($\text{HCO}_3^- (\text{aq}) \rightarrow \text{CO}_2 + \text{OH}^-$). Kinetic isotope fractionations occur during this process, influencing the isotopic compositions not only of the degassed CO₂, but also of the carbonate minerals that precipitate from partially degassed solutions. We present here models of isotopic fractionations associated with HCO₃⁻ dehydration and dehydroxylation in aqueous solution, calculated using techniques from ab initio transition state theory, and tests of these models based on measurements of synthetic cryogenic carbonates and natural modern speleothems and laboratory synthesized speleothem-like carbonates, all of which grow from solutions that actively degas CO₂.

Our model predicts the kinetic isotopic fractionations associated with bicarbonate dehydration and dehydroxylation for ¹³C/¹²C, ¹⁸O/¹⁶O ratios, as well as abundance anomalies (i.e., relative to a stochastic distribution) of ¹³C-¹⁸O and ¹⁸O-¹⁷O multiply-substituted species; these fractionations are, respectively, -29.7‰, -9.0‰, -0.05‰, -0.0002‰ and -0.004‰ for HCO₃⁻ dehydration; and -22.5‰, -16.7‰, 0.10‰ and -0.06‰ for HCO₃⁻ dehydroxylation, both at 25°C. These fractionations increase the δ¹³C and δ¹⁸O but decrease the relative proportion of ¹³C-¹⁸O bonds in the residual HCO₃⁻, and thus potentially in the carbonate minerals that precipitate from that HCO₃⁻. We combine the estimated isotope fractionations that accompany CO₂ degassing with models of isotopic fractionations accompanying carbonate precipitation to predict that at 25°C the ¹³C/¹²C ratio of carbonate increases by 1.1-3.2‰ and its Δ₄₇ value decrease by 0.017-0.026‰ for every 1‰ kinetic enrichment in its ¹⁸O/¹⁶O, with the exact values depending

on the pathway for CO₂ degassing (i.e., HCO₃⁻ dehydration vs. HCO₃⁻ dehydroxylation) and on the amount of carbonate formation accompanying the degassing. If one does not account for the kinetically controlled reductions of Δ₄₇ values of carbonate minerals that grow from partially degassed solutions, one would overestimate the carbonate growth temperature (i.e., using carbonate clumped isotope thermometry) by 3~6°C for every 1‰ kinetic enrichment in carbonate ¹⁸O/¹⁶O. These predictions compare favorably with the experimental constraints from our lab synthesized cryogenic carbonates and with the available isotopic data of both natural modern speleothems and speleothem-like carbonates synthesized in the laboratory, though some discrepancies between model and data are observed. These discrepancies could arise from the kinetic isotope fractionations associated with rapid precipitation of the carbonate minerals, or might reflect errors in our models.

CO₂ produced from HCO₃⁻ dehydration and HCO₃⁻ dehydroxylation reactions are predicted to be depleted in ¹³C-¹⁸O clumped isotope anomalies relative to CO₂ in thermodynamic equilibrium, by ~0.40‰ for HCO₃⁻ dehydration and by ~0.12‰ for HCO₃⁻ dehydroxylation at 25°C. This effect might explain why CO₂ produced by respiration appears to be depleted in ¹³C-¹⁸O bonds relative to thermodynamic equilibrium (Affek et al., 2007).

1. INTRODUCTION

Isotopic compositions of carbon dioxide and carbonate minerals are among the most important proxies in geochemistry research, with applications to the global carbon cycle and paleoclimate reconstruction (among many others). However, the isotopic

compositions of these materials can be interpreted only in light of a detailed understanding of the various equilibrium and kinetic isotopic fractionation processes that have influenced them; this is particularly true of ancient materials preserved in the geological record. While our understanding of the equilibrium isotope fractionation processes involving CO₂ and carbonates are relatively well understood, the understanding of kinetic isotope fractionations is rather limited and semi-quantitative. In this study, we focus on the kinetic isotope fractionations associated with degassing of CO₂ from aqueous solutions.

Degassing of CO₂ from aqueous solutions proceeds through bicarbonate dehydration ($\text{H}^+ + \text{HCO}_3^- \text{(aq)} \rightarrow \text{H}_2\text{CO}_3 \rightarrow \text{CO}_2 + \text{H}_2\text{O}$) and bicarbonate dehydroxylation ($\text{HCO}_3^- \text{(aq)} \rightarrow \text{CO}_2 + \text{OH}^-$). These reactions occur in all aqueous solutions that contain dissolved inorganic carbon, and are involved in a number of important geologic processes, including cryogenic carbonate formation (Clark and Lauriol, 1992), speleothem deposition (Fairchild et al., 2007), air-sea CO₂ exchange (Siegenthaler and Munnich, 1981), and CO₂ degassing from hydrothermal fluids (Gaillardet and Galy, 2008). It has been documented that, significant kinetic isotope fractionations occur during this process (Marlier and O'Leary, 1984; Paneth and O'Leary, 1985; Clark and Lauriol, 1992; O'Leary et al., 1992; Zeebe and Wolf-Gladrow, 2001). These kinetic isotope fractionations influence the isotopic compositions of both the degassed CO₂ and carbonate minerals that might grow from degassing solutions, and often lead to deviations of the isotopic composition of carbonate minerals from their expected equilibrium values. Such kinetic isotopic fractionations complicate the interpretation of isotopic signals in potential

paleoclimate records such as speleothems (Fairchild et al., 2006) and cryogenic carbonates (Lacelle, 2007).

To-date a complete quantitative understanding of the kinetic isotope fractionations that accompany CO₂ degassing from aqueous solutions has not been presented. To the best of our knowledge, Marlier and O'Leary (1984) and Paneth and O'Leary (1985) are the only two studies that attempted to systematically characterize these isotope fractionations. They experimentally determined the carbon isotope fractionations between evolved CO₂ and residual dissolved inorganic carbon ('DIC') to be -21.8‰ and -19.8‰, respectively, for HCO₃⁻ dehydration and dehydroxylation at 24°C (according to O'Leary et al., 1992 and Zebee and Wolf-Gladrow, 2001). For comparison, kinetic fractionations between evolved CO₂ and residual DIC of -31.2‰ for carbon isotope and -5.5‰ for oxygen isotopes have been inferred for HCO₃⁻ dehydration based on experiments in which solutions that were saturated in Ca(HCO₃)₂ were quickly frozen to synthesize cryogenic carbonates (Clark and Lauriol, 1992). These fractionations presumably apply at 0 °C (though the exact temperature of carbonate growth is not well defined in these experiments).

Recent evidence suggests that speleothem growth might be accompanied by a kinetic isotopic fractionation that influences the proportions of ¹³C-¹⁸O bonds in carbonates (the basis of carbonate "clumped isotope" thermometer(Ghosh et al., 2006; Schauble et al., 2006). Two recent studies, one of a modern speleothem from Soreq cave in Israel (Affek et al., 2008), the other of modern speleothems from caves in France, Austria and Patagonia and of speleothem-like carbonates synthesized in the laboratory (Daeron et al., 2008), have found that the relative proportions of ¹³C-¹⁸O bonds in

carbonates are lower than those expected for equilibrium at their respective carbonate growth temperatures. These non-equilibrium effects would, if unaccounted for, lead to overestimations of carbonate formation temperature of 4–22°C if the carbonate clumped isotope thermometer were applied to these materials (Table 4-1). The presence of this kinetic isotope fractionation of ^{13}C - ^{18}O bonds during speleothem deposition complicates the application of carbonate clumped isotope thermometry to speleothem samples, adding a new reason why we require a quantitative understanding of isotope fractionations that accompany CO_2 degassing from aqueous solutions.

In this study we apply transition state theory (Eyring, 1935a; Eyring, 1935b) to predict the isotopic fractionations (including fractionations of multiply-substituted isotopologues) associated with HCO_3^- dehydration and dehydroxylation reactions in aqueous solution. We then integrate the results of this model with a model of the isotopic fractionations associated with carbonate precipitation to quantitatively predict the combined effects of kinetic and equilibrium isotopic fractionations on the isotopic composition (including distribution of multiply-substituted isotopologues) of carbonate minerals that grow from a partially degassed solution. Finally, we compare the predictions of these models with isotopic measurements of cryogenic carbonates grown from freezing, degassing solutions, natural modern speleothems, and synthetic carbonates grown in a fashion resembling speleothems formation. Some of these data are newly reported in this study and others are taken from recent studies (Affek et al., 2008; Daeron et al., 2008). We observe a loose agreement between our model predictions and all of these experimental and natural data sets. On this basis, we propose a quantitative framework for understanding the isotopic compositions of speleothem carbonates,

Table 4-1 Isotopic compositions of natural modern speleothem and lab synthesized “speleothem” (IVS series). Data are reproduced from Daeron et al., 2008 and Affek et al. 2008 (sample 12-1-57).

Sample No.	Cave site	Type	T_{cave} (°C)	$\delta^{18}\text{O}_{\text{water}}$ (‰)	Expected equil. Values			Observed Values		
					$\delta^{18}\text{O}_{\text{cc}}$ (‰)	Δ_{47} (‰)	$\delta^{13}\text{C}_{\text{cc}}$ (‰)	$\delta^{18}\text{O}_{\text{cc}}$ (‰)	$\delta^{13}\text{C}_{\text{cc}}$ (‰)	σ (‰)
Vil-plq8	Villars, France	Stalag-mite	11.3±0.1	-6.26±0.08	25.24	0.712	-11.33	25.85	0.684 (5)	0.023
Vil-10B	Villars, France	Stalag-mite	12.3±0.2	-6.2±0.08	25.07	0.706	-10.07	25.38	0.688 (3)	0.006
Vil-Gal	Villars, France	Pebble	11.5±0.1	-6.42±0.06	25.03	0.711	-10.94	25.70	0.671 (8)	0.012
Vil-1A	Villars, France	Stalag-mite	11.3±0.1	-6.3±0.1	25.20	0.712	-10.91	26.00	0.643 (4)	0.011
Fau-stm6	La Faurie, France	Stalag-mite	12.9±0.1	-6.10±0.02	25.04	0.703	-9.76	26.27	0.673 (5)	0.015
K-RZ6	Katerloch, Austria	Glass plate	5.7±0.3	-8.6±0.2	24.13	0.741	-11.36	24.69	0.688 (1)	0.010
K-Top3	Katerloch, Austria	Stalag-mite	3.7±0.3	-8.8±0.2	24.40	0.752	-8.16	25.24	0.692 (1)	0.009
Bar-A	Le Baron, Patagonia	Soda straw	9.2	-5.98±0.05	26.01	0.722	0.39	28.52	0.621 (3)	0.026
Cas-B	Cassis, Patagonia	Cave coral	7.3	-5.6±0.05	26.85	0.733	14.89	31.76	0.635 (2)	0.003

Table 4-1 (Continued)

Sample No.	Cave site	Type	T_{cave} (°C)	$\delta^{18}\text{O}_{\text{water}}$ (‰)	Expected equil. Values		Observed. Values		
					$\delta^{18}\text{O}_{\text{cc}}$ (‰)	Δ_{47} (‰)	$\delta^{13}\text{C}_{\text{cc}}$ (‰)	$\delta^{18}\text{O}_{\text{cc}}$ (‰)	$\delta^{13}\text{C}_{\text{cc}}$ (‰)
Mor-A	La Moraine, Patagonia	Soda straw	9.1	-6.12±0.05	25.89	0.723	7.62	30.71	0.621 (2)
IVS-1	Paris Lab, France	Synth. Calcite	13.1±0.4	-6.89±0.05	24.18	0.741	-28.54	25.52	0.623 (3)
IVS-2	Paris Lab, France	Synth. Calcite.	13.1±0.4	-6.89±0.05	24.18	0.752	-28.13	25.55	0.640 (3)
IVS-3	Paris Lab, France	Synth. Calcite.	13.1±0.4	-6.89±0.05	24.18	0.722	-24.53	26.42	0.610 (3)
12-1-57	Soreq, Israel	Stalagmite	18-19	-5.32±0.76	24.60	0.676	-9.53	25.55	0.642 (6)

* T_{Apparent} denote the apparent formation temperatures estimated for cryogenic carbonates, based on their observed Δ_{47} (if the cryogenic carbonates were formed in isotopic equilibrium).

& Number in the bracket indicate the number of replicate isotope analyses for that carbonate sample

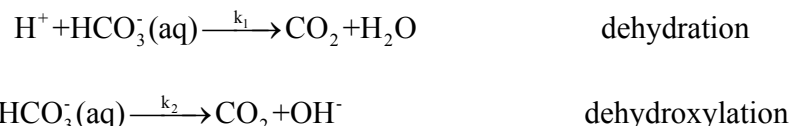
including carbon isotope, oxygen isotope and multiply-substituted isotopologues. This scheme may provide a useful basis for quantitative paleotemperature reconstructions from speleothem records. We also use this set of models to predict the isotopic composition of CO₂ degassed from aqueous solution, and discuss the implications of this prediction for understanding the abundances of ¹³C-¹⁸O doubly-substituted isotopologues in atmospheric CO₂.

To the best of our knowledge, this study constitutes the first systematic theoretical study of kinetic isotope fractionations of multiply-substituted isotopologues arising from irreversible chemical reactions in natural systems. Although we focus on the study of dissolved inorganic carbonate (due to its relevance to carbonate clumped isotope thermometry), the principles and methods we employ could be applied to other chemical systems, including nitrates and sulfates.

2. THEORETICAL AND COMPUTATIONAL METHODS

2.1 Kinetics of HCO_3^- dehydration and dehydroxylation reactions

Degassing of CO₂ from aqueous solutions may proceed through two different reaction pathways—HCO₃⁻ dehydration and HCO₃⁻ dehydroxylation (Eigen et al. 1961):



where k_1 and k_2 are the rate constants for the respective reactions and vary with the temperature and salinity of the aqueous solutions in which the reactions take place (Schulz et al., 2006 and reference therein):

$$k_1 = \frac{e^{1,246.98 - \frac{6.19 \times 10^4}{T} - 183.0 \ln(T)}}{K_1^*}$$

$$k_2 = \frac{499,002.24 \times e^{4.2986 \times 10^{-4} S^2 + 5.75499 \times 10^{-5} S - \frac{90,166.83}{RT}}}{K_1^*},$$

where T is the temperature in Kelvin, S is the salinity in practical salinity unit (UNESCO, 1985), R is the universal gas constant, and K_1^* is the first dissociation constant of carbonic acid, which can be evaluated as (Roy et al., 1993):

$$\ln(K_1^*) = 2.83655 - \frac{2307.1266}{T} - 1.5529413 \times \ln(T) + (-0.20760841 - \frac{4.0484}{T}) \times S^{0.5} + 0.0846834 \times S - 0.00654208 \times S^{1.5}.$$

The relative importance of the HCO_3^- dehydration and dehydroxylation reactions during CO_2 degassing processes varies with the pH of the aqueous solution, with HCO_3^- dehydration dominating at low pH and HCO_3^- dehydroxylation dominating at high pH (Fig. 4-1a):

$$f_{\text{dehydration}} = \frac{k_1 \times [\text{HCO}_3^-] \times [\text{H}^+]}{k_1 \times [\text{HCO}_3^-] \times [\text{H}^+] + k_2 \times [\text{HCO}_3^-]}$$

$$f_{\text{dehydroxylation}} = \frac{k_2 \times [\text{HCO}_3^-]}{k_1 \times [\text{HCO}_3^-] \times [\text{H}^+] + k_2 \times [\text{HCO}_3^-]}.$$

$f_{\text{dehydration}}$ and $f_{\text{dehydroxylation}}$ here denote the relative fractional contribution of HCO_3^- dehydration and dehydroxylation reactions to the degassing of CO_2 respectively; $[\text{HCO}_3^-]$ and $[\text{H}^+]$ are the concentrations of dissolved HCO_3^- and H^+ in the aqueous solution. Besides pH, the relative rates of HCO_3^- dehydration and dehydroxylation also depend weakly on the solution temperature and salinity, with HCO_3^- dehydration reactions contributing more to the degassing of CO_2 at lower temperature and lower salinity (Fig. 4-1b and 4-1c).

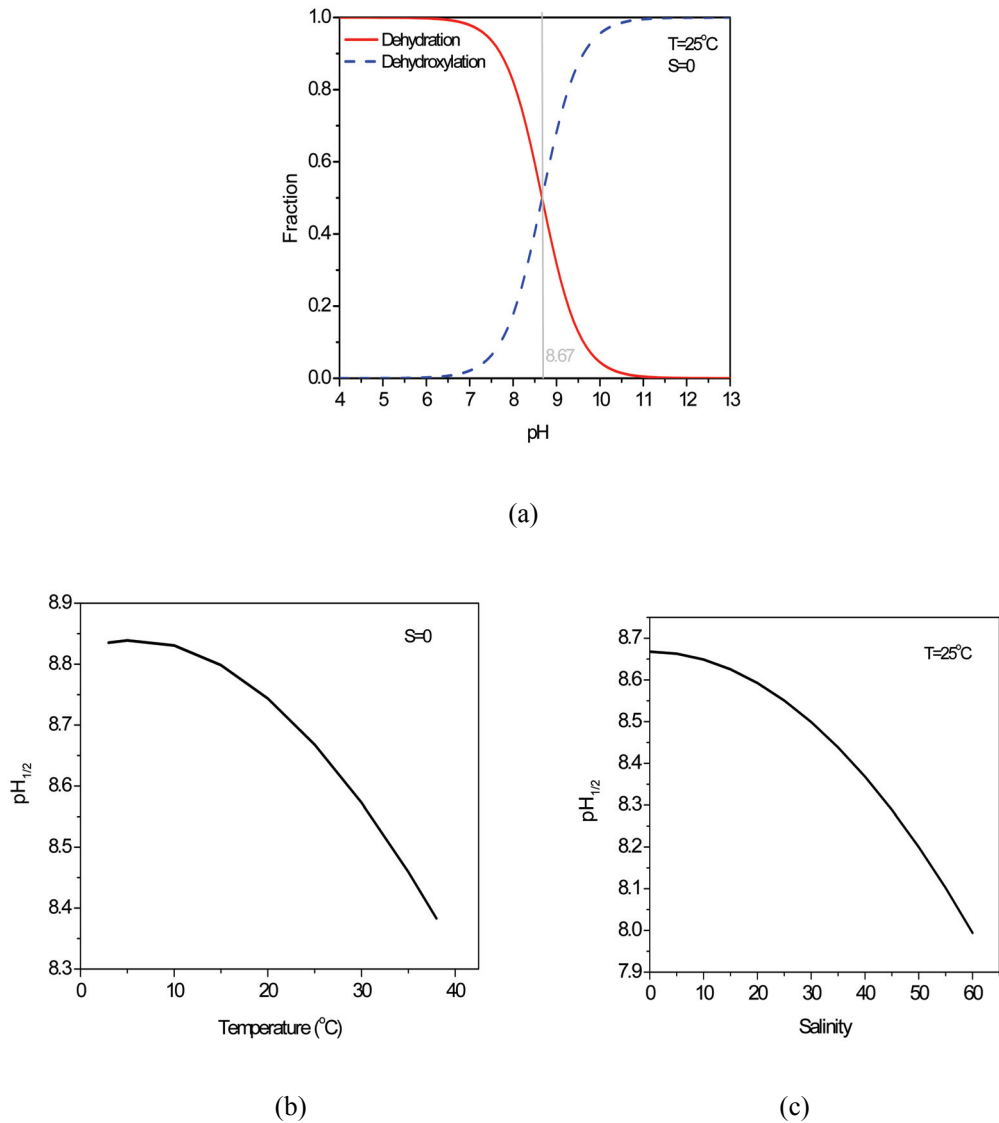


Figure 4-1: Dependence of relative importance of bicarbonate dehydration and dehydroxylation on the solution (a) pH, (b) temperature and (c) salinity. (a) relative contributions of dehydration and dehydroxylation reactions during degassing of CO₂ aqueous solutions (pure water) of different pH at 25°C; (b) Variation of pH_{1/2} with solution temperature in pure water; (c) Variation of pH_{1/2} with solution salinity at 25°C. pH_{1/2} here denotes the pH value at which HCO₃⁻ dehydration and HCO₃⁻ dehydroxylation each contribute 50% of CO₂ degassing. Reaction kinetic data are from Schulz et al. (2006).

At conditions typical for speleothem deposition (solutions with pH<8, T<30°C and S~0), HCO₃⁻ dehydration is the dominant pathway for degassing of CO₂. For example, HCO₃⁻ dehydration contributes 97.9% of CO₂ degassing at pH=7, T=25°C and S=0. However, in typical seawater (i.e., pH=8.2, T=25°C, S=35), both HCO₃⁻ dehydration and dehydroxylation contribute significantly, 63.4% and 36.6% respectively, to the degassing of CO₂ from aqueous solution, e.g. during air-sea CO₂ exchange.

2.2 Transition state theory and the reaction mechanisms of HCO₃⁻ dehydration and HCO₃⁻ dehydroxylation

2.2.1 Transition state theory

Transition state theory is long established as a tool for studies of chemical kinetics (Eyring, 1935a; Eyring, 1935b) and has been applied to irreversible reactions in geosciences problems (see Lasaga, 1998 and Felipe et al., 2001 for recent reviews). Based on classical transition state theory, the kinetic isotope effect associated with an irreversible chemical reaction, α , defined as the ratio of the reaction rate constants (k values) for different reactant isotopologues or isotopomers, can be expressed as (Melander and Saunders, 1987):

$$\alpha = \frac{k_{(1)}}{k_{(2)}} = \frac{|\nu_L^\dagger|_{(1)} K_{(1)}}{|\nu_L^\dagger|_{(2)} K_{(2)}}, \quad (1)$$

where subscripts (1) and (2) denote different isotopic variants of the reactants and transition states; ν_L^\dagger is the ‘decomposition frequency’ (defined as the reciprocal of the average life time) of transition state M^\dagger ; K is the equilibrium constant between reactants

(A, B) and transition state M^\dagger , and can be evaluated using statistical thermodynamics (Urey, 1947):

$$K = \frac{Q^\dagger}{Q_A \times Q_B} = \frac{s_A \times s_B}{s^\dagger} \frac{\prod_i^{3N^\dagger - 7} (u_i^\dagger \times \frac{1}{e^{\frac{1}{2}u_i^\dagger}} \times \frac{1}{1 - e^{-u_i^\dagger}})}{\prod_{j_A}^{3N_A - 6} (u_{j_A} \times \frac{1}{e^{\frac{1}{2}u_{j_A}}} \times \frac{1}{1 - e^{-u_{j_A}}}) \times \prod_{j_B}^{3N_B - 6} (u_{j_B} \times \frac{1}{e^{\frac{1}{2}u_{j_B}}} \times \frac{1}{1 - e^{-u_{j_B}}})} \quad (2)$$

$$u_i^\dagger = \frac{hc\varpi_i^\dagger}{kT}, u_{j_A} = \frac{hc\varpi_{j_A}}{kT}, u_{j_B} = \frac{hc\varpi_{j_B}}{kT}, \quad (3)$$

where Q^\dagger, Q_A, Q_B are the reduced partition functions of transition state M^\dagger and reactants A and B, respectively; $\varpi_i^\dagger, \varpi_{j_A}, \varpi_{j_B}$ are the vibration frequencies, in wave numbers, for the transition state M^\dagger and reactants A and B, respectively (one such term is required for each mode of vibration of each species); s^\dagger, s_A, s_B are the symmetry numbers for transition state M^\dagger and reactants A and B, respectively; N^\dagger, N_A, N_B are the numbers of atoms within transition state M^\dagger and reactants A and B, respectively; h is Plank's constant; c is the velocity of light; k is the Boltzmann constant; and T is the reaction temperature in Kelvin.

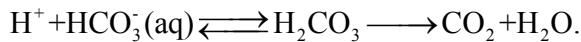
A more detailed description of transition state theory can be found in our recent study (Guo et al., 2008b), where we have applied it to investigate the kinetic isotope fractionations associated with phosphoric acid digestion of carbonate minerals.

2.2.2 Reaction mechanisms of HCO_3^- dehydration

HCO_3^- dehydration in aqueous solution is commonly thought to proceed through intermediate H_2CO_3 (Kern, 1960), i.e.,



where k_{11} and k_{12} refer to the rate constants for the respective reaction steps; $k_{11}[\text{H}^+]$ is up to seven orders of magnitude greater than k_{12} (Kern, 1960; Johnson, 1982). Therefore, the second step of the above reaction, the decomposition of carbonic acid, is the rate limiting step during HCO_3^- dehydration, and thus the one controlling the kinetic isotope fractionations associated with HCO_3^- dehydration in aqueous solution. Since the first step of the reaction (and its reverse) proceeds so fast (Kern, 1960; Johnson, 1982), we assume H_2CO_3 is always in isotopic equilibrium with HCO_3^- , i.e.,



Thus, any kinetic isotope effects that arise from decomposition of H_2CO_3 will be quantitatively transferred to HCO_3^- (i.e., H_2CO_3 and HCO_3^- will maintain a constant isotopic offset equal to their equilibrium partitioning). Therefore, we focus on the kinetic isotope fractionations associated with decomposition of H_2CO_3 in aqueous solution.

Previous theoretical studies, using also transition state theory, suggest that H_2CO_3 decomposition in aqueous solution involves a transition state structure that is significantly influenced by interactions with adjacent water molecules (Nguyen et al., 1997; Loerting et al., 2000; Tautermann et al., 2002). The participation of water molecules in the reaction stabilizes the transition state structure, lowers the activation energy required for the reaction, and thus facilitates the decomposition of H_2CO_3 in aqueous solution. In particular, Nguyen et al. (1997) examined the possible transition state structures for hydration of CO_2 in aqueous solution (the reverse reaction of H_2CO_3 decomposition) with different numbers of participating water molecules, and suggested that it involves formation of a bridge-complex consisting one CO_2 and three H_2O

molecules. In turn, this suggests H_2CO_3 decomposition in aqueous solution may proceed with the aid of two water molecules. In this study, we adopt this conclusion from Nguyen et al. (1997), and use the corresponding structures of reactant and transition state as our initial guesses for further geometry optimizations (Fig. 4-2a).

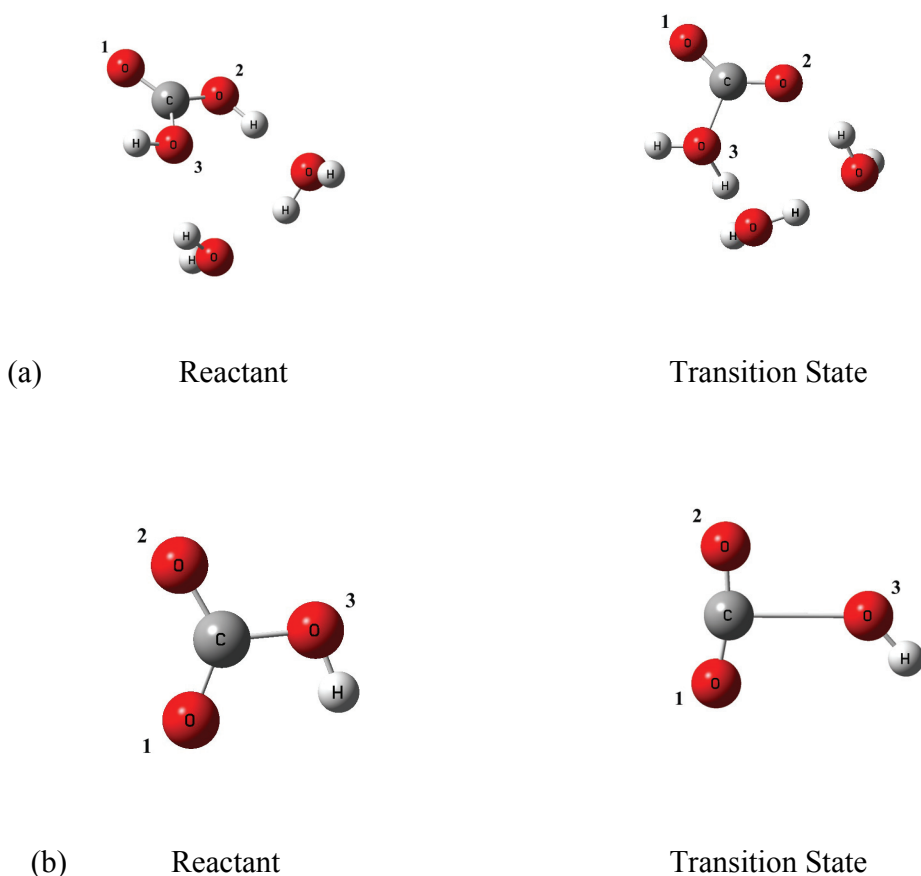


Figure 4-2: Optimized reactant and transition state structures for HCO_3^- dehydration and HCO_3^- dehydroxylation reactions in aqueous solution. (a) HCO_3^- dehydration with the aid of two water molecules; (b) HCO_3^- dehydroxylation, both optimized with DFT-B3LYP/ cc-pvtz(-f) method and with a continuum solvation model.

2.2.3 Reaction mechanisms of HCO_3^- dehydroxylation

The reaction mechanism of HCO_3^- dehydroxylation in aqueous solution has received much less attention than that for HCO_3^- dehydration. Previous theoretical studies have

focused on determining the kinetics of its reverse reaction, CO₂ hydroxylation, and tried to simulate and explain the energy barrier for this reaction in aqueous solution (Peng and Merz, 1992; Peng and Merz, 1993; Davidson et al., 1994; Nemukhin et al., 2002; Iida et al., 2007; Leung et al., 2007). In this study, we assume HCO₃⁻ dehydroxylation in aqueous solution proceeds with the similar transition state structure as determined for CO₂ hydroxylation (Leung et al., 2007), i.e., adopted those transition state structures as the initial guess in our calculation (Fig. 4-2b).

2.3 A model of isotopic fractionations associated with carbonate precipitation induced from CO₂ degassing

A solution containing Ca²⁺ and dissolved inorganic carbon that undergoes degassing of CO₂ will increase in pH, driving precipitation of calcium carbonate. In this section, we outline a model to account for these isotopic effects in carbonate minerals induced by CO₂ degassing. Later sections present theoretical calculations of isotopic fractionations associated with individual steps in this overall process; integration of these steps into the model we present here will lead to quantitative predictions of the isotopic compositions of carbonates produced by degassing of CO₂ from aqueous solutions. Similar isotope models have been proposed previously, but considered only carbon isotope and (in a few cases) oxygen isotope fractionations (Clark and Lauriol, 1992; Mickler et al., 2004; Zak et al., 2004; Mickler et al., 2006; Muehlinghaus et al., 2007; Romanov et al., 2008) . We extend these models to consider fractionations of all isotopologues (¹³C/¹²C, ¹⁸O/¹⁶O, and multiply-substituted isotopologues); our model also makes several assumptions that differ from those adopted by previous studies, as detailed below.

The model on which we primarily focus assumes that kinetic isotope effects occur by HCO_3^- dehydration and dehydroxylation reactions, and that carbonate then precipitates in equilibrium with the fractionated pool of residual HCO_3^- . In section 4.3, we examine alternate models in which this relatively simple process is modified by other fractionations, such as isotopic exchange between HCO_3^- and water, and/or kinetic isotope fractionations between precipitated carbonate and HCO_3^- (section 4.3).

2.3.1 Rayleigh distillation effects

Our model describes kinetic isotope fractionations associated with HCO_3^- dehydration and dehydroxylation in aqueous solution that lead to changes in the isotopic composition of residual HCO_3^- , and thus in the compositions of carbonate minerals that precipitation from that pool of HCO_3^- . If the pool of residual dissolved HCO_3^- does not undergo isotopic re-equilibration with water, its isotopic composition will evolve as a result of dehydration and dehydroxylation, following a Rayleigh distillation relationship:

$$R_{\text{HCO}_3^-}(t) = R_{\text{HCO}_3^-}(0) \times F^{\alpha-1}, \quad (4)$$

where $R(0)$ and $R(t)$ are the abundance ratios between any isotopically-substituted isotopologue (including multiply-substituted isotopologues) and the isotopically-non-substituted isotopologue — generally the most abundant isotopologue for the species we consider — (i.e., $R = [\text{rare_isotopologue}] / [\text{most_abundant_isotopologue}]$) at time zero and

at time t , respectively; $F = \frac{[\text{HCO}_3^-]_t}{[\text{HCO}_3^-]_0}$ denotes the fraction of HCO_3^- remaining in the

aqueous solution at time t ; $\alpha = \frac{R_{\text{leaving}}}{R_{\text{residual}}}$ is the isotope fractionation factor between the

consumed HCO_3^- pool and the residual HCO_3^- pool (a different value will apply for each

isotopologue). Note that, the consumed HCO_3^- pool consists not only HCO_3^- that degas to form CO_2 (i.e., through HCO_3^- dehydration and HCO_3^- dehydroxylation), but also those incorporated into the carbonate minerals (if the degassing is accompanied by carbonate precipitation). Accordingly, α here should be the weighted average of the respective isotope fractionation factors associated with each sub-pool of consumed HCO_3^- . We discuss the choice of α under different scenarios in detail section 2.3.2.

If a carbonate mineral precipitates in isotopic equilibrium with the remaining HCO_3^- , its isotopic composition can be expressed as:

$$R_{\text{carbonate}}(t) = \alpha_{\text{carb}-\text{HCO}_3}^{\text{equil}} \times R_{\text{HCO}_3}(t), \quad (5)$$

where $\alpha_{\text{carb}-\text{HCO}_3}^{\text{equil}}$ is an equilibrium isotope fractionation factor between the precipitated carbonate mineral and dissolved HCO_3^- , and is evaluated with data from previous calibration studies, e.g., for carbon isotope (Deines, 1974) and oxygen isotopes (Kim and O'Neil, 1997; Beck et al., 2005).

Substituting the Rayleigh distillation relationship (equation 4) into the above equation, we obtain

$$\begin{aligned} R_{\text{carbonate}}(t) &= \alpha_{\text{carb}-\text{HCO}_3}^{\text{equil}} \times R_{\text{HCO}_3}(0) \times F^{\alpha-1} \\ &= R_{\text{carb}}^{\text{equil}}(0) \times F^{\alpha-1}. \end{aligned} \quad (6)$$

$R_{\text{carb}}^{\text{equil}}(0) = R_{\text{HCO}_3}(0) \times \alpha_{\text{carb}-\text{HCO}_3}^{\text{equil}}$ is the expected isotope composition in the carbonate mineral if it formed in isotopic equilibrium with the initial HCO_3^- pool (at time zero). Therefore, the kinetic isotope fractionations for carbon isotope and oxygen isotope (i.e., for ^{13}C singly-substituted isotopologue and ^{18}O singly-substituted isotopologue) in the carbonate minerals can be expressed as:

$$\frac{R_{carb}(t)}{R_{carb}^{equil}(0)} = F^{\alpha-1}, \quad (7)$$

where α , as defined above, is the isotope fractionation factor for the corresponding isotopologue between the consumed HCO_3^- pool and residual HCO_3^- pool.

Note, the equation 7 applies not only ^{13}C singly-substituted isotopologue and ^{18}O singly-substituted isotopologues, but all the isotopologues of HCO_3^- . Thus, for $^{13}\text{C}-^{18}\text{O}$ bearing doubly-substituted isotopologue in the carbonate mineral which are most relevant to carbonate clumped isotope thermometry, we have

$$\frac{R_{carb}^t(^{13}\text{C}^{18}\text{O}^{16}\text{O}_2)}{R_{carb}^{0, equil}(^{13}\text{C}^{18}\text{O}^{16}\text{O}_2)} = F^{\alpha_{^{13}\text{C}^{18}\text{O}^{16}\text{O}_2}-1}. \quad (8)$$

We combine equation 8 with the similar relationships for ^{13}C singly-substituted isotopologue and ^{18}O singly-substituted isotopologue, i.e.,

$$\frac{R_{carb}^t(^{13}\text{C}^{16}\text{O}_3)}{R_{carb}^{0, equil}(^{13}\text{C}^{16}\text{O}_3)} = F^{\alpha_{^{13}\text{C}^{16}\text{O}_3}-1} \quad (9)$$

$$\frac{R_{carb}^t(^{12}\text{C}^{18}\text{O}^{16}\text{O}_2)}{R_{carb}^{0, equil}(^{12}\text{C}^{18}\text{O}^{16}\text{O}_2)} = F^{\alpha_{^{12}\text{C}^{18}\text{O}^{16}\text{O}_2}-1} \quad (10)$$

and obtain

$$\frac{\frac{R_{carb}^t(^{13}\text{C}^{18}\text{O}^{16}\text{O}_2)}{R_{carb}^t(^{13}\text{C}^{16}\text{O}_3) \times R_{carb}^t(^{12}\text{C}^{18}\text{O}^{16}\text{O}_2)}}{\frac{R_{carb}^{0, equil}(^{13}\text{C}^{18}\text{O}^{16}\text{O}_2)}{R_{carb}^{0, equil}(^{13}\text{C}^{16}\text{O}_3) \times R_{carb}^{0, equil}(^{12}\text{C}^{18}\text{O}^{16}\text{O}_2)}} = \frac{\frac{\Delta_{^{13}\text{C}^{18}\text{O}^{16}\text{O}_2}^{carb}(t)}{1000} + 1}{\frac{\Delta_{^{13}\text{C}^{18}\text{O}^{16}\text{O}_2}^{carb}(0)}{1000} + 1} = \frac{F^{\alpha_{^{13}\text{C}^{18}\text{O}^{16}\text{O}_2}-1}}{F^{\alpha_{^{13}\text{C}^{16}\text{O}_3}-1} \times F^{\alpha_{^{12}\text{C}^{18}\text{O}^{16}\text{O}_2}-1}}, \quad (11)$$

where $\Delta_{^{13}\text{C}^{18}\text{O}^{16}\text{O}_2}^{carb}$ is the abundance anomaly of the $^{13}\text{C}-^{18}\text{O}$ bearing doubly-substituted isotopologue in the carbonate mineral, the basis of carbonate clumped isotope thermometry, and is expressed as $\Delta_{^{13}\text{C}^{18}\text{O}^{16}\text{O}_2}^{carb} = \left(\frac{R_{carb}(^{13}\text{C}^{18}\text{O}^{16}\text{O}_2)}{R_{carb}(^{13}\text{C}^{16}\text{O}_3) \times R_{carb}(^{12}\text{C}^{18}\text{O}^{16}\text{O}_2)} - 1 \right) \times 1000$; $\alpha_{^{13}\text{C}^{18}\text{O}^{16}\text{O}_2}$, $\alpha_{^{13}\text{C}^{16}\text{O}_3}$ and $\alpha_{^{12}\text{C}^{18}\text{O}^{16}\text{O}_2}$ are the isotope fractionation factors for isotopologues

$\text{H}^{13}\text{C}^{18}\text{O}^{16}\text{O}_2^-$, $\text{H}^{13}\text{C}^{16}\text{O}_3^-$ and $\text{H}^{12}\text{C}^{18}\text{O}^{16}\text{O}_2^-$ respectively, between the consumed HCO_3^- pool and the residual HCO_3^- pool.

Since $\Delta_{^{13}\text{C}^{18}\text{O}^{16}\text{O}_2}^{\text{carb}}(t) \ll 1$, and $\Delta_{^{13}\text{C}^{18}\text{O}^{16}\text{O}_2}^{\text{carb}}(0) \ll 1$, the effect of kinetic fractionations associated with CO_2 degassing on the abundances of $^{13}\text{C}-^{18}\text{O}$ bonds in carbonate that precipitates from the residual HCO_3^- pool equals,

$$\frac{\Delta_{^{13}\text{C}^{18}\text{O}^{16}\text{O}_2}^{\text{carb}}(t) - \Delta_{^{13}\text{C}^{18}\text{O}^{16}\text{O}_2}^{\text{carb}}(0)}{\Delta_{^{13}\text{C}^{18}\text{O}^{16}\text{O}_2}^{\text{carb}}(0) + 1} \approx \frac{\frac{1000}{\Delta_{^{13}\text{C}^{18}\text{O}^{16}\text{O}_2}^{\text{carb}}(0) + 1} + 1}{1000} = \frac{F^{\alpha_{^{13}\text{C}^{18}\text{O}^{16}\text{O}_2}^{-1}}}{F^{\alpha_{^{13}\text{C}^{16}\text{O}_3}^{-1}} \times F^{\alpha_{^{12}\text{C}^{18}\text{O}^{16}\text{O}_2}^{-1}}} \quad (12)$$

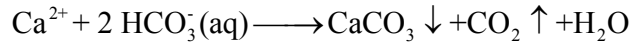
The method outlined above can also be applied to calculate the kinetic isotope fractionations of clumped isotope anomalies of other multiply-substituted isotopologues, e.g.,

$$\Delta_{^{12}\text{C}^{18}\text{O}^{17}\text{O}^{16}\text{O}}^{\text{carb}}(t) - \Delta_{^{12}\text{C}^{18}\text{O}^{17}\text{O}^{16}\text{O}}^{\text{carb}}(0) \approx \frac{F^{\alpha_{^{12}\text{C}^{18}\text{O}^{17}\text{O}^{16}\text{O}}^{-1}}}{F^{\alpha_{^{12}\text{C}^{18}\text{O}^{16}\text{O}_3}^{-1}} \times F^{\alpha_{^{12}\text{C}^{17}\text{O}^{16}\text{O}_2}^{-1}}} \quad (13)$$

$$\Delta_{^{12}\text{C}^{18}\text{O}^{18}\text{O}^{16}\text{O}}^{\text{carb}}(t) - \Delta_{^{12}\text{C}^{18}\text{O}^{18}\text{O}^{16}\text{O}}^{\text{carb}}(0) \approx \frac{F^{\alpha_{^{12}\text{C}^{18}\text{O}^{18}\text{O}^{16}\text{O}}^{-1}}}{F^{\alpha_{^{12}\text{C}^{18}\text{O}^{16}\text{O}_3}^{-1}} \times F^{\alpha_{^{12}\text{C}^{18}\text{O}^{16}\text{O}_2}^{-1}}} \quad (14)$$

2.3.2 Changes in the Rayleigh distillation model arising from significant amounts of carbonate precipitation

Previous studies have inferred that in natural environments in which carbonate precipitation is driven by CO_2 degassing from aqueous solutions (e.g., cave deposits) one mol of carbonate precipitates for every mol of CO_2 degassed from the solution (Fairchild et al., 2007):



If this is the case, the isotope fractionation factor, α , that describes the change in isotopic composition of the residual HCO_3^- pool in the above equations should reflect the combined effects of isotope fractionation factors resulting from both CO_2 degassing and the carbonate formation:

$$\alpha = \frac{R_{leaving}}{R_{initial}} = \frac{\alpha_{\text{degassing}} + \alpha_{\text{carb-HCO}_3^-}^{\text{equil}}}{2}, \quad (15)$$

where $\alpha_{\text{degassing}}$ and $\alpha_{\text{carb-HCO}_3^-}^{\text{equil}}$ are the isotopic fractionation factors associated with CO_2 degassing, and the equilibrium isotope fractionation factor between carbonate and HCO_3^- respectively, as defined above.

In order to apply the model scheme outlined above to isotope fractionations of multiply substituted isotopologues we must estimate the relevant equilibrium fractionation factors between carbonate minerals and dissolved HCO_3^- (i.e., $\alpha_{\text{carb-HCO}_3^-}^{\text{equil}}$ in equation 15), which have not been previously studied. We have approached this problem using statistical thermodynamics theory. This theory is applicable to all of the multiply substituted isotopologues of carbonate minerals and DIC species, but we present only the details relevant to isotopologues containing ^{13}C - ^{18}O bonds, which are most relevant to carbonate clumped isotope thermometry.

The equilibrium isotope fractionations between two phases (e.g., between carbonate and water) arise from differences among the related isotopologues in the two phases in the vibrational energies of intramolecular bonds. These fractionations can be expressed as functions of the reduced partition functions of the phases of interest (Urey, 1947), e.g.,

$$\alpha_{\text{carb-HCO}_3^-}^{\text{equil}}(^{13}\text{C}^{16}\text{O}_3) = \frac{Q_{\text{Ca}^{13}\text{C}^{16}\text{O}_3}}{Q_{\text{Ca}^{12}\text{C}^{16}\text{O}_3}} \left/ \frac{Q_{\text{H}^{13}\text{C}^{16}\text{O}_3^-}}{Q_{\text{H}^{12}\text{C}^{16}\text{O}_3^-}} \right. \quad (16)$$

$$\alpha_{carb-HCO_3}^{equil}(^{12}C^{18}O^{16}O_2) = \frac{Q_{Ca^{12}C^{18}O^{16}O_2}}{Q_{Ca^{12}C^{16}O_3}} \Bigg/ \frac{Q_{H^{12}C^{18}O^{16}O_2^-}}{Q_{H^{12}C^{16}O_3^-}} \quad (17)$$

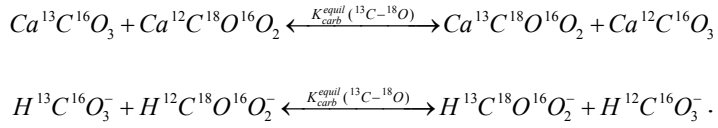
$$\alpha_{carb-HCO_3}^{equil}(^{13}C^{18}O^{16}O_2) = \frac{Q_{Ca^{13}C^{18}O^{16}O_2}}{Q_{Ca^{12}C^{16}O_3}} \Bigg/ \frac{Q_{H^{13}C^{18}O^{16}O_2^-}}{Q_{H^{12}C^{16}O_3^-}}, \quad (18)$$

where $\alpha_{carb-HCO_3}^{equil}(^{13}C^{16}O_3)$, $\alpha_{carb-HCO_3}^{equil}(^{12}C^{18}O^{16}O_2)$ and $\alpha_{carb-HCO_3}^{equil}(^{13}C^{18}O^{16}O_2)$ denote the equilibrium isotope fractionation factors of ^{13}C singly-substituted isotopologue (i.e. carbon isotope), ^{18}O singly-substituted isotopologue (i.e., oxygen isotope) and $^{13}\text{C}-^{18}\text{O}$ doubly-substituted isotopologue of the carbonate ion between calcium carbonate mineral and dissolved HCO_3^- ; Q are the reduced partition functions for the respective isotopologues indicated in the subscript of each Q .

Rearranging equation 16-18, we obtain

$$\begin{aligned} \frac{\alpha_{carb-HCO_3}^{equil}(^{13}C^{18}O^{16}O_2)}{\alpha_{carb-HCO_3}^{equil}(^{13}C^{16}O_3) \times \alpha_{carb-HCO_3}^{equil}(^{12}C^{18}O^{16}O_2)} &= \frac{\frac{Q_{Ca^{13}C^{18}O^{16}O_2} \times Q_{Ca^{12}C^{16}O_3}}{Q_{Ca^{13}C^{16}O_3} \times Q_{Ca^{12}C^{18}O^{16}O_2}}}{\frac{Q_{H^{13}C^{18}O^{16}O_2^-} \times Q_{H^{12}C^{16}O_3^-}}{Q_{H^{13}C^{16}O_3^-} \times Q_{H^{12}C^{18}O^{16}O_2^-}}} \\ &= \frac{K_{carb}^{equil}(^{13}\text{C}-^{18}\text{O})}{K_{HCO_3^-}^{equil}(^{13}\text{C}-^{18}\text{O})}, \end{aligned} \quad (19)$$

where $K_{carb}^{equil}(^{13}\text{C}-^{18}\text{O}) = \frac{Q_{Ca^{13}C^{18}O^{16}O_2} \times Q_{Ca^{12}C^{16}O_3}}{Q_{Ca^{13}C^{16}O_3} \times Q_{Ca^{12}C^{18}O^{16}O_2}}$ and $K_{HCO_3^-}^{equil}(^{13}\text{C}-^{18}\text{O}) = \frac{Q_{H^{13}C^{18}O^{16}O_2^-} \times Q_{H^{12}C^{16}O_3^-}}{Q_{H^{13}C^{16}O_3^-} \times Q_{H^{12}C^{18}O^{16}O_2^-}}$ are the equilibrium constants for the $^{13}\text{C}-^{18}\text{O}$ isotope ‘clumping’ reactions in the carbonate mineral and the dissolved HCO_3^- respectively:



Both $K_{carb}^{equil}(^{13}\text{C}-^{18}\text{O})$ and $K_{HCO_3^-}^{equil}(^{13}\text{C}-^{18}\text{O})$ have been theoretically estimated in

previous studies, using first principle lattice dynamics (Schauble et al., 2006) and quantum mechanics (Guo et al., 2008a) respectively. Based on these theoretical estimations, at any given temperature $K_{carb}^{equil}(^{13}C - ^{18}O)$ and $K_{HCO_3^-}^{equil}(^{13}C - ^{18}O)$ are very nearly identical to each other, e.g., $K_{carb}^{equil}(^{13}C - ^{18}O) = 1.000410$ (Schauble et al. 2006) vs. $K_{HCO_3^-}^{equil}(^{13}C - ^{18}O) = 1.000427$ (Guo et al. 2008a) at 25°C. The difference between the two is within the uncertainties of theoretical estimations (e.g. $1-3 \times 10^{-5}$, Schauble et al., 2006). We therefore assume in this study $\frac{K_{carb}^{equil}(^{13}C - ^{18}O)}{K_{HCO_3^-}^{equil}(^{13}C - ^{18}O)} = 1$, and estimate equilibrium isotope fractionation factor of $^{13}C - ^{18}O$ doubly-substituted isotopologue of the carbonate ion between calcium carbonate mineral and dissolved HCO_3^- :

$$\alpha_{carb-HCO_3^-}^{equil}(^{13}C^{18}O^{16}O_2) = \alpha_{carb-HCO_3^-}^{equil}(^{13}C^{16}O_3) \times \alpha_{carb-HCO_3^-}^{equil}(^{12}C^{18}O^{16}O_2). \quad (20)$$

The same method outlined above can also be applied to calculate the equilibrium isotope fractionation factor of other multiply-substituted isotopologues between calcium carbonate mineral and dissolved HCO_3^- , e.g.,

$$\alpha_{carb-HCO_3^-}^{equil}(^{12}C^{18}O^{17}O^{16}O) = \alpha_{carb-HCO_3^-}^{equil}(^{12}C^{18}O^{16}O_2) \times \alpha_{carb-HCO_3^-}^{equil}(^{12}C^{17}O^{16}O_2) \quad (21)$$

$$\alpha_{carb-HCO_3^-}^{equil}(^{12}C^{18}O^{18}O^{16}O) = \alpha_{carb-HCO_3^-}^{equil}(^{12}C^{18}O^{16}O_2) \times \alpha_{carb-HCO_3^-}^{equil}(^{12}C^{18}O^{16}O_2), \quad (22)$$

where $\alpha_{carb-HCO_3^-}^{equil}(^{12}C^{17}O^{16}O_2)$ is the equilibrium isotope fractionation factor of ^{17}O singly-substituted isotopologues of the carbonate ion between calcium carbonate mineral and dissolved HCO_3^- , and is estimated assuming a mass dependence exponent $\lambda = 0.528$ between $\alpha_{carb-HCO_3^-}^{equil}(^{12}C^{17}O^{16}O_2)$ and $\alpha_{carb-HCO_3^-}^{equil}(^{12}C^{18}O^{16}O_2)$ (Barkan and Luz, 2005), i.e.,

$$\alpha_{carb-HCO_3^-}^{equil}(^{12}C^{17}O^{16}O_2) = \left\{ \alpha_{carb-HCO_3^-}^{equil}(^{12}C^{18}O^{16}O_2) \right\}^{0.528} \quad (23)$$

It is noted that, the above 1:1 proportionality between CO₂ degassing and carbonate formation holds true only if there are no independent limitations on the rate of carbonate precipitation from the solution. If some kinetic barrier to carbonate precipitation causes it to proceed slower than the rate of CO₂ degassing, of the solution will become supersaturated. Cave waters are generally supersaturated with respect to calcium carbonate (saturation index for calcite up to 0.5-0.6 or more; Fairchild et al., 2007), perhaps suggesting that in cave waters CO₂ degassing outstrips carbonate precipitation (i.e, the proportionality between CO₂ degassing and carbonate formation is bigger than 1:1). This disparity between CO₂ degassing and carbonate precipitation will affect the isotopic compositions of dissolved HCO₃⁻ and thus the isotopic compositions of the speleothems deposited from this supersaturated solution.

The exact disparity between CO₂ degassing and carbonate precipitation may vary among different cave waters, and might be difficult to evaluate or reconstruct. To account for this disparity, we also model another extreme case, in which CO₂ degassing is the only isotope fractionation process influencing the isotopic composition of HCO₃⁻ in aqueous solution (i.e., no carbonate precipitation occurs). In this case (CO₂ degassing is associated with negligible carbonate growth), the proportionality between CO₂ degassing and carbonate formation equals infinity, and the fractionation factor between the consumed HCO₃⁻ pool and the residual HCO₃⁻ pool will be:

$$\alpha = \frac{R_{leaving}}{R_{initial}} = \alpha_{degassing} = f_{dehydration} \times \alpha_{dehydration} + f_{dehydroxylation} \times \alpha_{dehydroxylation}, \quad (24)$$

where $\alpha_{dehydration}$ and $\alpha_{dehydroxylation}$ are the kinetic isotope fractionation factors associated with HCO₃⁻ dehydration and HCO₃⁻ dehydroxylation reaction in aqueous solution

respectively; $f_{\text{dehydration}}$ and $f_{\text{dehydroxylation}}$ are relative contributions of dehydration and dehydroxylation reactions to the degassing of CO₂, as discussed in section 2.1.

2.4 Computational methods

Molecular geometries of reactants and transition states were optimized and bond frequencies were calculated for different isotopologues using the Jaguar program (Version 7.0, release 207; Ringnalda et al., 2007) on a workstation cluster with 79 Dell PowerEdge-2650 server nodes (Xeno, 2.2-2.4GHz, 512K) in the Materials and Process Simulation Center at Caltech. The singlet state electron wave functions of the molecular configurations were built using a density functional theory with hybrid functionals, B3LYP, and extended basis sets cc-pvtz(-f). We also perform an alternate set of these transition state theory calculations for HCO₃⁻ dehydroxylation reaction using the LMP2/cc-pvtz(-f) method (Ringnalda et al., 2007). We simulated the aqueous environment in which modeled reactions take place using a self consistent reaction field method, using the Poisson-Boltzmann solver imbedded in the Jaguar program (Ringnalda et al., 2007). The dielectric constant for water was assumed to be 80.37.

A universal frequency scaling factor of 0.9614 was employed on the calculated vibration frequencies for both reactants and transition states to correct for the general overestimation of vibration frequencies by ab initio calculations (Scott and Radom, 1996). We discuss the effects of scaling factor on our model results in section 4.2.

3. EXPERIMENTAL METHODS

3.1 Synthesis of cryogenic carbonates

We synthesized six separate samples of cryogenic carbonates at Johnson Space Center (Houston) by rapidly freezing saturated $\text{Ca}(\text{HCO}_3)_2$ solutions. The typical preparation procedure is described as below, and details unique to each sample are listed in Table 4-2.

0.6 grams of $\text{Ca}(\text{OH})_2$ powder were first added into 1500ml of de-ionized water. Then, pure CO_2 gas (99.96%, Air Liquide) was bubbled through this $\text{Ca}(\text{OH})_2$ solution at room temperature for 1-2hr. After complete dissolution of $\text{Ca}(\text{OH})_2$, the solution (now saturated regarding $\text{Ca}(\text{HCO}_3)_2$) was sealed in a glass jar and its headspace was flushed with the pure CO_2 gas. The solution was either stored at room temperature ($\sim 20^\circ\text{C}$) or equilibrated at temperatures of 1-7°C for hours to days before being frozen (Table 4-2). Note that samples 0412-07 and 0418-07 were prepared from two aliquots of the same bulk solution, as were samples 0611A-07 and 0611B-07.

At the beginning of each freezing experiment, the solution was transferred from the glass jar into a large, flat tupperware container. We then measured the solution pH using an Accumet 925 pH/Ion Meter and collected an aliquot of solution for later determination of the $\delta^{13}\text{C}$ of DIC and the $\delta^{18}\text{O}$ of the water. Then, the tupperware container was sealed and placed in a freezer held at a constant temperature of approximately $-15^\circ\text{C} \pm 4^\circ\text{C}$. The chilled solutions froze thoroughly, during which we inferred that dissolved CO_2 degassed from the solution, increasing the pH of the solution and driving carbonate precipitation. The whole solution typically froze completely within 3 hours. At the end of each experiment, we thawed the frozen solution either at room temperature or at 1-3°C (in a refrigerator), and then filtered the carbonate precipitates from the solution. The collected carbonates were dried at 50°C in a drying oven or freeze-

dried before isotopic analyses. The yields of carbonate solids varied among different experiments, and were estimated to average around 10% of calcium in the solution.

Table 4-2 Preparation conditions of cryogenic carbonates synthesized in this study.

Sample No.		0412-07	0418-07	0504A-07	0611A-07	0611B-07	0920A-07
Solution equilibration	T (°C)	~20	~20	7.6	6	3.1	1-3
	Time (hrs)	2-3	Days	Days	Days	Days	~48
pH		5.7	5.7	5.5	5.5	5.5	5.5
$\delta^{13}\text{C}_{\text{DIC}}$ (‰)		-31.2	-31.2	-31	-32.8	-32.6	-27.3
# $\delta^{13}\text{C}_{\text{HCO}_3}$ (‰)		-21.9	-21.9	-21	-21.8	-22.7	-17.3
$\delta^{18}\text{O}_{\text{water}}$ (‰)		-2.5	-2.5	-2.5	-2.4	-2.2	-1.3
T Freeze (°C)		-15	-15	-15	-15	-15	-15
T Defreeze (°C)		~20	~20	~20	~20	~20	1-3
Drying method		Oven	Oven	Oven	Oven	Oven	Freeze dryer

$\delta^{13}\text{C}_{\text{HCO}_3}$ are estimated based on measured carbon isotopic composition of the total DIC, assuming the carbon isotope equilibrium among different DIC species (see section 4.3 for details). All $\delta^{13}\text{C}$ and $\delta^{18}\text{O}$ are reported vs. VPDB and VSMOW, respectively.

3.2 Mass spectrometric analysis

The $\delta^{18}\text{O}$ of the water and $\delta^{13}\text{C}$ of DIC in the cryogenic carbonate experiments were determined at Johnson Space Center, by analysis of solution aliquots on a Finnigan MAT-253 gas source mass spectrometer that is equipped with a Gas Bench II apparatus and operating in continuous flow mode. For $\delta^{18}\text{O}$ measurements of the water samples, the CO₂–H₂O equilibration method was employed (Epstein and Mayeda, 1953; Horita et al., 1989). 0.7 ml of solution was equilibrated with helium gas—mixed with 0.3% CO₂—overnight, at constant temperature 30°C. The equilibrated gas was then analyzed by flowing it into the MAT-253 mass spectrometer using the Gas Bench II apparatus and a

helium carrier gas. The $\delta^{13}\text{C}$ of the DIC was determined in a similar manner (Spotl, 2005). Three drops of 100% phosphoric acid was added to a sealed glass exetainer. After flushing the exetainer with pure helium gas, a 0.1 ml portion of the sample solution was then added into the exetainer. The gas evolved from this mixture was then analyzed using the Gas Bench II and MAT-253 mass spectrometer. Sample solutions were analyzed for $\delta^{18}\text{O}$ alongside in-house water standards which have been calibrated through repeat analyses of SMOW, SLAP, and GISP standards. The oxygen isotopic compositions of all of the waters was obtained through plotting the data on a scale normalized to the values of SMOW (0‰ VSMOW) and SLAP (-55.5‰ VSMOW). The $\delta^{13}\text{C}$ analyses of the unknowns were also normalized in a similar manner using NBS-19 and NBS-18. The precision (1σ) of the water $\delta^{18}\text{O}$ and DIC $\delta^{13}\text{C}$ analyses, on the basis of replicate analyses of the laboratory standards, was estimated at $\pm 0.1\text{‰}$ and $\pm 0.1\text{‰}$, respectively.

Isotopic analyses of carbonate minerals — $\delta^{13}\text{C}$, $\delta^{18}\text{O}$ and Δ_{47} value — were performed by reacting the carbonate anhydrous phosphoric acid ($\rho=1.92\text{g/cm}^3$) at 25°C for 18-24 hours and then analyzing the released CO₂ at Caltech on a Finnigan MAT-253 gas source spectrometer that was configured to simultaneously measure masses 44 through 49 AMU, inclusive. Δ_{47} is a measure of the relative proportion of ¹³C-¹⁸O bonds inside carbonate lattice, defined as the deviation of actual mass 47 abundance in the CO₂ derived from phosphoric acid digestion of carbonate minerals relative to its expected

mass 47 abundance if all the isotopes were randomly distributed, $\Delta_{47} = \left(\frac{R_{actual}^{47}}{R_{stochastic}^{47}} - 1 \right) \times 1000$

(Eiler and Schauble, 2004; Ghosh et al., 2006). A more detailed description of the mass spectrometer configuration and analysis procedure is given by Ghosh et al (2006). The

external precision of our isotope analyses averages around 0.04‰, 0.01‰, 0.015‰ (1 standard deviation) for $\delta^{13}\text{C}$, $\delta^{18}\text{O}$ and Δ_{47} , respectively, based on replicate measurements of carbonate standards and sample materials. Values of $\delta^{13}\text{C}$ and $\delta^{18}\text{O}$ were standardized by comparison with CO_2 generated by phosphoric acid digestion of NBS-19 and are reported vs. VPDB and VSMOW, respectively.

4. RESULTS AND DISCUSSION

4.1 Model results for the kinetic isotope fractionations associated with HCO_3^- dehydration and HCO_3^- dehydroxylation reactions

The calculated vibration frequencies (scaled with a universal scaling factor of 0.9614, section 2.4) for all the isotopologues (and isotopomers) of reactants and transition states during HCO_3^- dehydration and dehydroxylation reactions in aqueous solutions are presented in Appendix (Tables 4-A1 to 4-A4).

Of all the studied species, experimentally determined vibration frequencies exist only for dissolved HCO_3^- (all the other species are either transition state structures or unstable in aqueous solutions). Fig. 4-3 presents the comparison between our model predicted vibration frequencies for dissolved HCO_3^- and the most recent experimentally determined frequencies (Rudolph et al., 2006). For most modes of vibration, our model calculation underestimates the frequencies by about 100cm^{-1} relative to the experimentally observed frequencies. The largest discrepancy was observed for the highest mode of vibration (assigned as vCO-H vibration mode), with the model predicted frequency $\sim 1085\text{cm}^{-1}$ higher than the experimentally determined frequency. Similar discrepancies seem to be typical for the ab initio estimations of vibration frequencies for

dissolved HCO_3^- , and have been also reported in several previous theoretical studies (Davidson et al., 1994; Rudolph et al., 2006). They are suspected to arise from the insufficiency of the continuum solvation model to describe the aqueous environment, the inability of the theoretical model (e.g., DFT method and LMP2 method) to fully characterize the hydrogen bonds in aqueous solutions, and the experimental uncertainties associated with determination of vibration frequencies for dissolved ions in aqueous solutions (Rudolph et al., 2006).

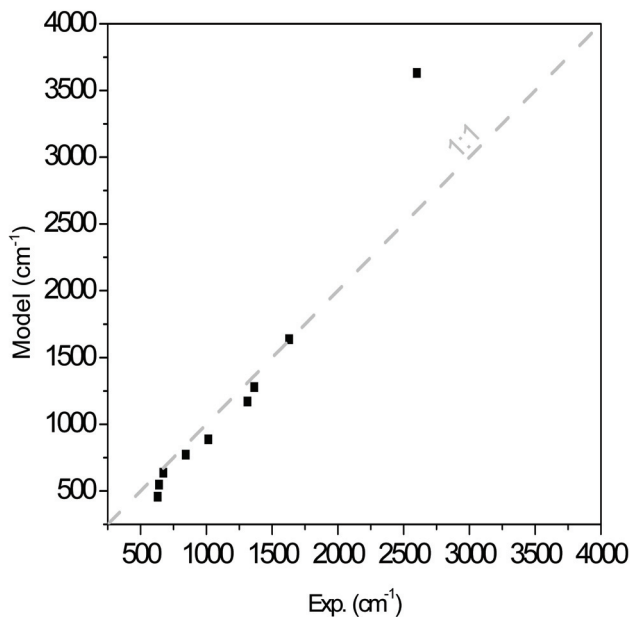


Figure 4-3: Comparison of our calculated vibration frequencies for dissolved HCO_3^- (DFT-B3LYP/cc-pvtz(-f) with a continuum solvation model, scaled with a universal frequency scaling factor 0.9614; this study) with the experimentally determined vibration frequencies (Rudolph et al., 2006).

A full-scale theoretical investigation (e.g., by improving the theoretical method) to resolve these discrepancies between model predicted frequencies and experimentally observed frequencies are beyond the scope of this study. However, there are several reasons why we think it unlikely that these discrepancies will lead to first-order errors in

calculated isotopic fractionations: 1) when calculating isotope fractionations that arise from statistical thermodynamic effects, the ratios of vibration frequencies among different isotopologues tend to be more important than the absolute values of the frequencies (Urey, 1947); 2) the “vCO-H” vibration mode of dissolved HCO_3^- , the vibration mode showing the largest frequency discrepancy between model prediction and experimental observation, is not among the primary vibration modes involved in the HCO_3^- dehydroxylation reaction, and thus is not expected to introduce any substantial systematic errors in our model predictions on the kinetic isotope fractionation factors; and 3) previous theoretical studies on CO_2 hydroxylation (the reverse reaction of HCO_3^- dehydroxylation) employed similar theoretical methods with similar discrepancies in predicted bicarbonate vibrational frequencies of dissolved bicarbonate ion yet yielded kinetic data agreeing reasonably with experimental values (Davidson et al., 1994; Nemukhin et al., 2002).

We proceed by using our estimated frequencies to theoretically evaluate the magnitude of expected kinetic isotope effects associated with HCO_3^- dehydration and dehydroxylation reactions and compare these calculated fractionations to the experimentally determined kinetic isotope fractionation factors associated with CO_2 degassing from aqueous solutions.

Following the procedures outlined in section 2.2.1, we calculate the kinetic isotope fractionation factors for all isotopologues (and isotopomers) associated with HCO_3^- dehydration and dehydroxylation reactions (see Tables 4-A5 and 4-A6 in Appendix). For the sake of simplicity, we present below the model results only for some representative

isotopologues (Table 4-3 and Fig. 4-4, 4-5), which are defined as (i.e., equation 1 in section 2.2.1):

$$\alpha_{H^{13}C^{16}O_3^-} = \frac{k_{H^{13}C^{16}O_3^-}}{k_{H^{12}C^{16}O_3^-}}$$

i.e., the fractionation of $H^{13}C^{16}O_3^-$ isotopologue

$$\alpha_{H^{12}C^{18}O^{16}O_2^-} = \frac{k_{H^{12}C^{18}O^{16}O_2^-}}{k_{H^{12}C^{16}O_3^-}}$$

i.e., the fractionation of $H^{12}C^{18}O^{16}O_2^-$ isotopologue

$$\alpha_{H^{12}C^{17}O^{16}O_2^-} = \frac{k_{H^{12}C^{17}O^{16}O_2^-}}{k_{H^{12}C^{16}O_3^-}}$$

i.e., the fractionation of $H^{12}C^{17}O^{16}O_2^-$ isotopologue

$$\alpha_{H^{13}C^{18}O^{16}O_2^-} = \frac{k_{H^{13}C^{18}O^{16}O_2^-}}{k_{H^{13}C^{16}O_3^-}}$$

i.e., the fractionation of $H^{13}C^{18}O^{16}O_2^-$ isotopologue

$$\alpha_{H^{12}C^{18}O^{17}O^{16}O^-} = \frac{k_{H^{12}C^{18}O^{17}O^{16}O^-}}{k_{H^{12}C^{16}O_3^-}}$$

i.e., the fractionation of $H^{12}C^{18}O^{17}O^{16}O^-$ isotopologue.

Follow the definitions of clumped isotope anomalies that are used in carbonate clumped isotope thermometry (e.g., $\Delta_{47} = \left(\frac{^{47}R_{actual}}{^{47}R_{stochastic}} - 1 \right) \times 1000$, Eiler and Schauble, 2004), we further define:

$$A^{13-18} = \left(\frac{\left(\alpha_{H^{13}C^{18}O^{16}O_2^-} \right)_{actual}}{\left(\alpha_{H^{13}C^{18}O^{16}O_2^-} \right)_{stochastic}} - 1 \right) \times 1000 = \left(\frac{\alpha_{H^{13}C^{18}O^{16}O_2^-}}{\alpha_{H^{13}C^{16}O_3^-} \times \alpha_{H^{12}C^{18}O^{16}O_2^-}} - 1 \right) \times 1000 = \left(\frac{k_{H^{13}C^{18}O^{16}O_2^-}}{k_{H^{13}C^{16}O_3^-} \times k_{H^{12}C^{18}O^{16}O_2^-}} - 1 \right) \times 1000$$

$$A^{18-17} = \left(\frac{\left(\alpha_{^{12}C^{18}O^{17}O^{16}O} \right)_{actual}}{\left(\alpha_{^{12}C^{18}O^{17}O^{16}O} \right)_{stochastic}} - 1 \right) \times 1000 = \left(\frac{\alpha_{^{12}C^{18}O^{17}O^{16}O}}{\alpha_{^{12}C^{18}O^{16}O_2} \times \alpha_{^{12}C^{17}O^{16}O_2}} - 1 \right) \times 1000 = \left(\frac{k_{^{12}C^{18}O^{17}O^{16}O}}{k_{^{12}C^{18}O^{16}O_2} \times k_{^{12}C^{17}O^{16}O_2}} - 1 \right) \times 1000$$

A^{13-18} and A^{18-17} here have a physical meaning similar to the Δ_{47} value, and indicate the clumped isotope anomaly (i.e., departure from the stochastic distribution) associated with the kinetic reaction. That is, we calculate the difference between the composition of the

reacted pool and the composition it would have if it conformed to the ‘the rule of geometric mean’ (Bigeleisen, 1955).

Over the temperature range of 0-100°C, our calculated isotope fractionation factors associated with HCO_3^- dehydration in aqueous solution can be represented by (through polynomial fitting of fractionation factors computed at a number of different temperatures; Tables 4-A5 and 4-A6)

$$1000 \ln(\alpha_{\text{H}^{13}\text{C}^{16}\text{O}_3^-}) = -\frac{0.1998 \times 10^6}{T^2} - \frac{7.964 \times 10^3}{T} - 0.707 \quad (25\text{a})$$

$$1000 \ln(\alpha_{\text{H}^{12}\text{C}^{18}\text{O}^{16}\text{O}_2^-}) = -\frac{0.0168 \times 10^6}{T^2} - \frac{2.49 \times 10^3}{T} - 0.4863 \quad (25\text{b})$$

$$1000 \ln(\alpha_{\text{H}^{12}\text{C}^{17}\text{O}^{16}\text{O}_2^-}) = -\frac{0.007 \times 10^6}{T^2} - \frac{1.3305 \times 10^3}{T} - 0.2244 \quad (25\text{c})$$

$$1000 \ln(\alpha_{\text{H}^{13}\text{C}^{18}\text{O}^{16}\text{O}_2^-}) = -\frac{0.2234 \times 10^6}{T^2} - \frac{10.425 \times 10^3}{T} - 1.2688 \quad (25\text{d})$$

$$1000 \ln(\alpha_{\text{H}^{12}\text{C}^{18}\text{O}^{17}\text{O}^{16}\text{O}^-}) = -\frac{0.0257 \times 10^6}{T^2} - \frac{3.8096 \times 10^3}{T} - 0.7267 \quad (25\text{e})$$

$$\Delta^{13-18} = -\frac{0.0068 \times 10^6}{T^2} + \frac{0.0289 \times 10^3}{T} - 0.0755 \quad (25\text{f})$$

$$\Delta^{18-17} = -\frac{0.0018 \times 10^6}{T^2} + \frac{0.0109 \times 10^3}{T} - 0.016 \quad (25\text{g})$$

Similarly, over the temperature range of 0-100°C, our calculated isotope fractionation factors associated with HCO_3^- dehydroxylation in aqueous solution can be represented by:

$$1000 \ln(\alpha_{\text{H}^{13}\text{C}^{16}\text{O}_3^-}) = -\frac{0.7622 \times 10^6}{T^2} - \frac{4.0314 \times 10^3}{T} - 0.3008 \quad (26\text{a})$$

Table 4-3 Predicted kinetic isotope fractionations associated with HCO_3^- dehydration and HCO_3^- dehydroxylation reactions at 25°C. See text for the definitions of the fractionation factors.

Method ^a	Frequency Scaling Factor ^x	$1000\ln \alpha_{H^{13}\text{C}^{16}\text{O}_3}$			$1000\ln \alpha_{H^{12}\text{C}^{18}\text{O}^{16}\text{O}_2}$			A^{13-18}			$\text{CO}_2 - \text{HCO}_3^-$			
		O1*	O2*	O3*	Aver	O1*	O2*	O3*	Aver	$1000\ln \alpha^{13}$	$1000\ln \alpha^{18}$	A^{13-18}		
B3LYP cc-pvtz(-f)	0.9614	-29.7	-4.7	-9.3	-13.1	-9.0	-0.06	0.24	-0.35	-0.05	-29.7	-7.0	0.09	
HCO_3^- dehydration	B3LYP cc-pvtz(-f)	N/A	-30.9	-5.0	-9.8	-13.5	-9.4	-0.06	0.26	-0.37	-0.06	-30.9	-7.3	0.10
B3LYP cc-pvtz(-f)	1.0318	-32.0	-5.2	-10.1	-13.7	-9.7	-0.07	0.27	-0.38	-0.06	-32.0	-7.6	0.10	
B3LYP cc-pvtz(-f)	0.9614	-22.5	12.7	12.5	-75.2	-16.7	0.39	0.35	-0.45	0.10	-22.4	12.6	0.37	
HCO_3^- dehydroxylation	B3LYP cc-pvtz(-f)	N/A	-23.7	13.0	12.8	-78.7	-17.6	0.40	0.36	-0.47	0.10	-23.7	12.9	0.38
B3LYP cc-pvtz(-f)	1.0318	-24.7	13.4	13.1	-81.6	-18.4	0.41	0.37	-0.28	0.10	-24.8	13.2	0.40	
LMP2 ^b cc-pvtz(-f)	0.9614	-24.8	11.8	11.4	-69.4	-15.4	0.27	0.33	-0.27	0.11	-24.8	11.6	0.30	

^x Fractionation factors predicted with different calculation methods and frequency scaling factors are shown to compare with predictions from our standard model method (bolded), and thus to evaluate their influence on our model predictions (see text for details).

^{*} Different isotopomers of the same isotologue differs in their predicted isotope fractionation factors, depending on the positions of isotopic substitution. O1, O2 and O3 here denote isotopomers with ^{18}O substitution at oxygen positions 1, 2 and 3, respectively (as labeled in Fig. 4-2).

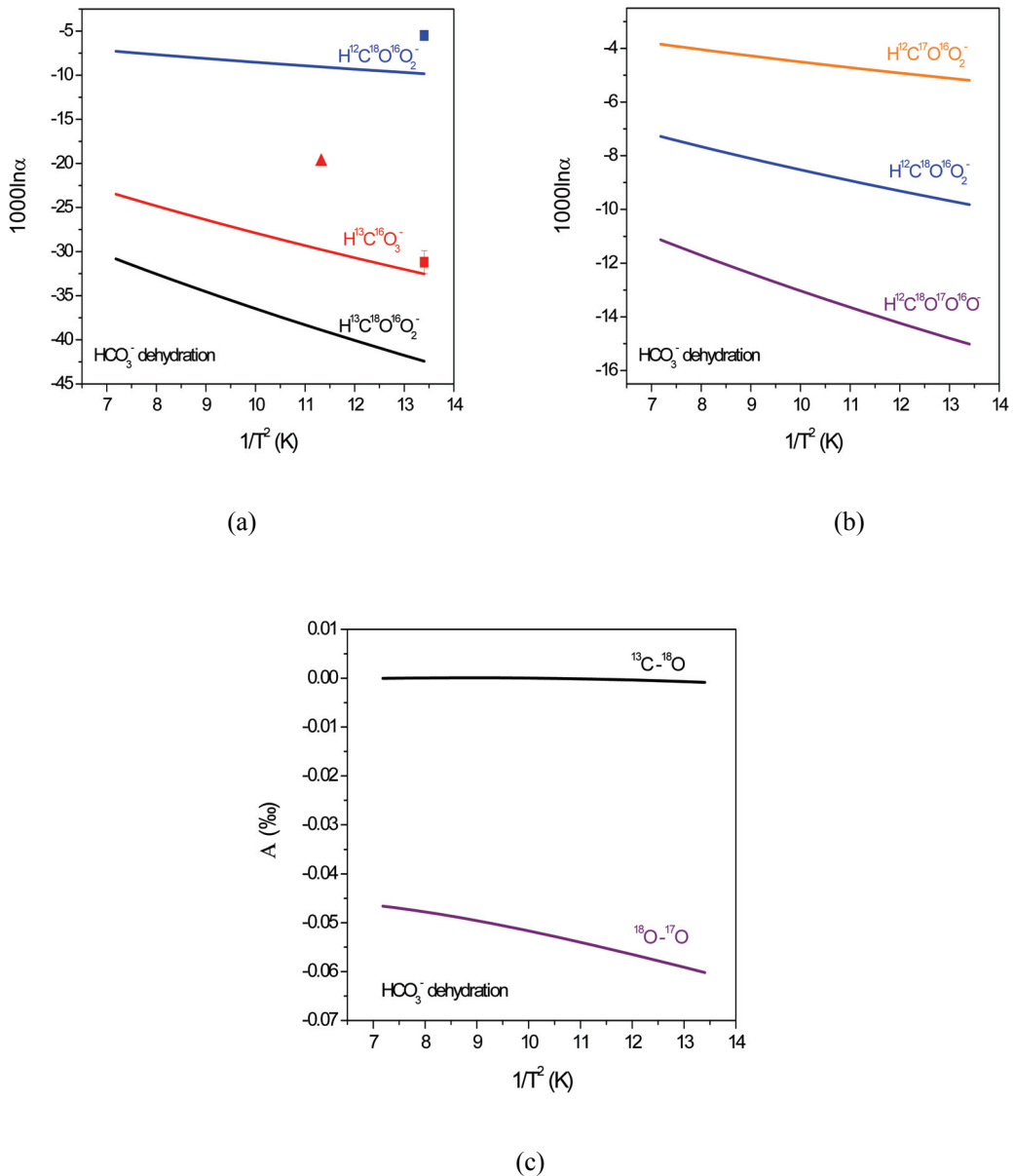


Figure 4-4: Model predicted kinetic isotope fractionation factors associated with HCO_3^- dehydration reaction (0-100°C): (a) fractionation of $\text{H}^{13}\text{C}^{16}\text{O}_3^-$, $\text{H}^{12}\text{C}^{18}\text{O}^{16}\text{O}_2^-$ and $\text{H}^{13}\text{C}^{18}\text{O}^{16}\text{O}_2^-$ isotopologues; (b) fractionation of $\text{H}^{12}\text{C}^{18}\text{O}^{16}\text{O}_2^-$, $\text{H}^{12}\text{C}^{17}\text{O}^{16}\text{O}_2^-$, and $\text{H}^{12}\text{C}^{18}\text{O}^{17}\text{O}^{16}\text{O}^-$ isotopologues; (c) fractionation of $^{13}\text{C}-^{18}\text{O}$ and $^{18}\text{O}-^{17}\text{O}$ clumped isotopic anomalies. See section 4.1 for the definitions of the plotted fractionation factors. Also shown for comparison are the available experimental estimations on these kinetic isotope fractionations from previous studies (triangle, O'Leary et al. 1992; squares, Clark and Laruriol, 1992).

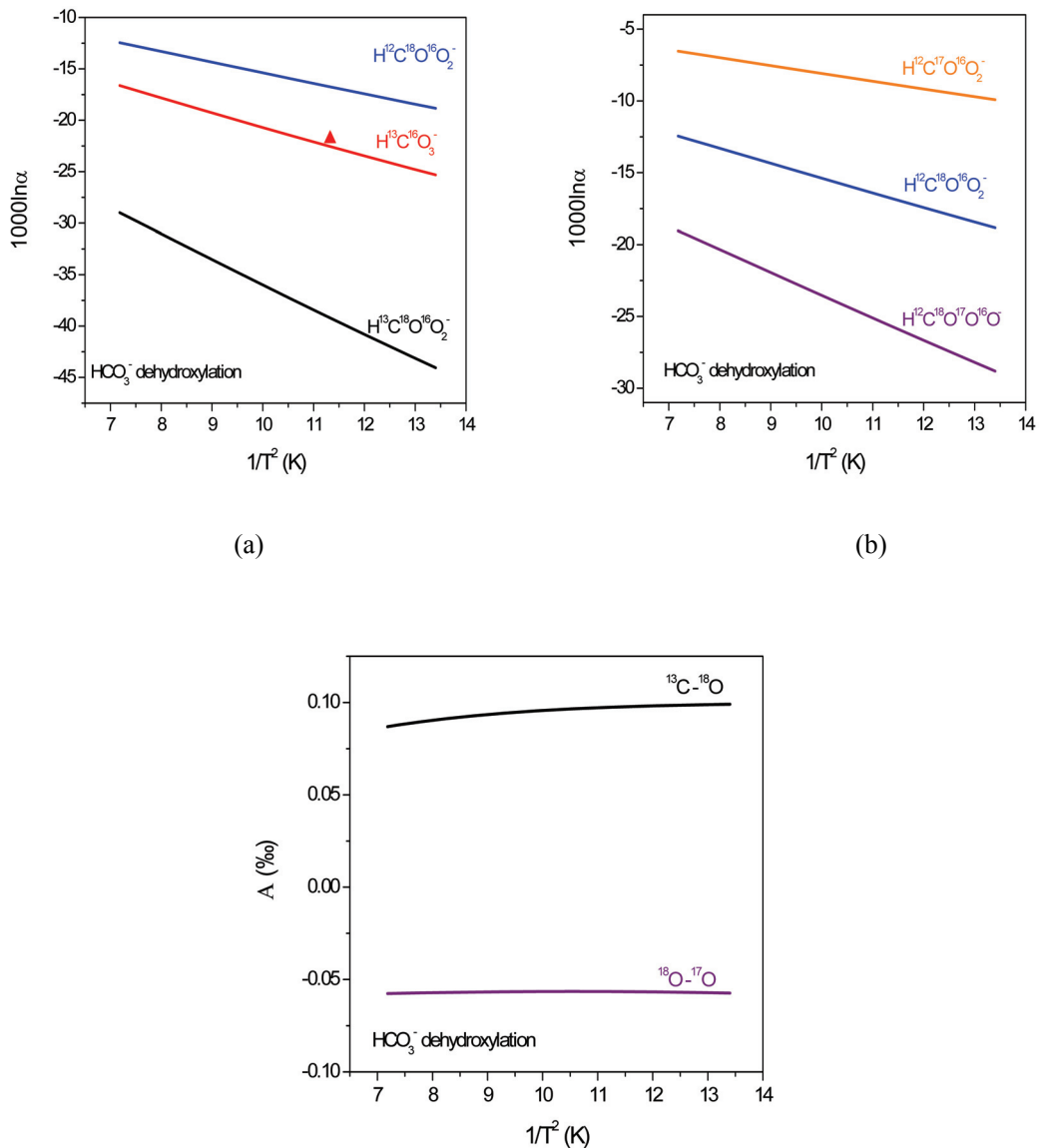


Figure 4-5: Model predicted kinetic isotope fractionation factors associated with HCO_3^- dehydroxylation reaction (0-100°C): (a) fractionation of $\text{H}^{13}\text{C}^{16}\text{O}_3^-$, $\text{H}^{12}\text{C}^{18}\text{O}^{16}\text{O}_2^-$ and $\text{H}^{13}\text{C}^{18}\text{O}^{16}\text{O}_2^-$ isotopologues; (b) fractionation of $\text{H}^{12}\text{C}^{18}\text{O}^{16}\text{O}_2^-$, $\text{H}^{12}\text{C}^{17}\text{O}^{16}\text{O}_2^-$, and $\text{H}^{12}\text{C}^{18}\text{O}^{17}\text{O}^{16}\text{O}^-$ isotopologues; (c) fractionation of $^{13}\text{C}-^{18}\text{O}$ and $^{18}\text{O}-^{17}\text{O}$ clumped isotopic anomalies. See section 4.1 for the definitions of the plotted fractionation factors. Also shown for comparison are the available experimental estimations on these kinetic isotope fractionations from previous study (triangle, O'Leary et al. 1992).

$$1000 \ln(\alpha_{H^{12}C^{18}O^{16}O_2^-}) = -\frac{0.8666 \times 10^6}{T^2} - \frac{1.0297 \times 10^3}{T} - 3.4607 \quad (26b)$$

$$1000 \ln(\alpha_{H^{12}C^{17}O^{16}O_2^-}) = -\frac{0.4504 \times 10^6}{T^2} - \frac{0.6007 \times 10^3}{T} - 1.6845 \quad (26c)$$

$$1000 \ln(\alpha_{H^{13}C^{18}O^{16}O_2^-}) = -\frac{1.6445 \times 10^6}{T^2} - \frac{4.9746 \times 10^3}{T} - 3.822 \quad (26d)$$

$$1000 \ln(\alpha_{H^{12}C^{18}O^{17}O^{16}O^-}) = -\frac{1.3211 \times 10^6}{T^2} - \frac{1.6039 \times 10^3}{T} - 5.2443 \quad (26e)$$

$$A^{13-18} = -\frac{0.0117 \times 10^6}{T^2} + \frac{0.0865 \times 10^3}{T} - 0.0605 \quad (26f)$$

$$A^{18-17} = -\frac{0.0041 \times 10^6}{T^2} + \frac{0.0265 \times 10^3}{T} - 0.0991, \quad (26g)$$

where T is the temperature in the unit of Kelvin.

At 25°C, our model predicted carbon isotope and oxygen isotope fractionations (i.e., fractionations of ^{13}C singly-substituted isotopologue $\alpha_{H^{13}C^{16}O_2^-}$ and ^{18}O singly-substituted isotopologue $\alpha_{H^{12}C^{18}O^{16}O_2^-}$) are $-29.7\text{\textperthousand}$ and $-9.0\text{\textperthousand}$ respectively for HCO_3^- dehydration, and $-22.5\text{\textperthousand}$ and $-16.7\text{\textperthousand}$ respectively for HCO_3^- dehydroxylation. These predictions agree reasonably well with the available experimental data on the carbon isotope and oxygen fractionation associate with HCO_3^- dehydration and dehydroxylation at 24°C and 0°C (O’Leary et al., 1992 and Clark et al., 1992, Fig. 4-4, 4-5). We also predict the oxygen isotope fractionations associate with HCO_3^- dehydration and HCO_3^- dehydroxylation in aqueous solution follow the mass dependence exponent $\lambda = 0.5279$ and $\lambda = 0.5261$, respectively, where $\alpha_{H^{12}C^{17}O^{16}O_2^-} = (\alpha_{H^{12}C^{17}O^{16}O_2^-})^\lambda$. As for kinetic fractionations for $^{13}\text{C}-^{18}\text{O}$, $^{18}\text{O}-^{17}\text{O}$ clumped isotopic species ($\alpha_{H^{13}C^{18}O^{16}O_2^-}$ and $\alpha_{H^{12}C^{18}O^{17}O^{16}O^-}$), our model predict $-38.8\text{\textperthousand}$, $-13.8\text{\textperthousand}$ respectively for HCO_3^- dehydration, and $-39.0\text{\textperthousand}$, $-25.5\text{\textperthousand}$ respectively for HCO_3^- dehydroxylation.

dehydroxylation at 25°C. In comparison, the kinetic fractionations for ^{13}C - ^{18}O , ^{18}O - ^{17}O clumped isotopic anomaly (A^{13-18} and A^{18-17}), are predicted to be 0.05‰, -0.0002‰, respectively for HCO_3^- dehydration, and 0.10‰, -0.06‰, respectively for HCO_3^- dehydroxylation at 25°C. (A^{13-18} and A^{18-17}). Unfortunately, we cannot directly compare these predictions with experimental data.

Note that different isotopomers of the same isotopologue differ significantly in their predicted isotope fractionation factors, depending on the positions of isotopic substitution. For example, at 25°C, our modeled transition state structures (Fig. 4-2) predict that the oxygen isotope fractionations associated with HCO_3^- dehydration and dehydroxylation are -4.7‰, -9.3‰, -13.1‰ and 12.7‰, -75.2‰, 12.5‰ respectively for ^{18}O substitution at positions 1, 2 and 3, (as labeled in Fig. 4-2); Similarly, the fractionation of ^{13}C - ^{18}O ‘clumped isotope’ anomaly associated with HCO_3^- dehydration and dehydroxylation are -0.06‰, 0.24‰, -0.35‰ and 0.39‰, -0.45‰, 0.35‰ respectively for ^{18}O substitution at positions 1, 2 and 3, (Table 3, Fig. 4-6). These position-specific isotope fractionation effects arise from the different bonding environments for different oxygen atoms inside HCO_3^- and their different involvements in the dehydration and dehydroxylation reactions. The isotope fractionation factors presented in the above equations (17a-g and 18a-g) are the average of the fractionation factors of all the isotopomers of the relevant isotopologue (Tables 4-A5 and 4-A6).

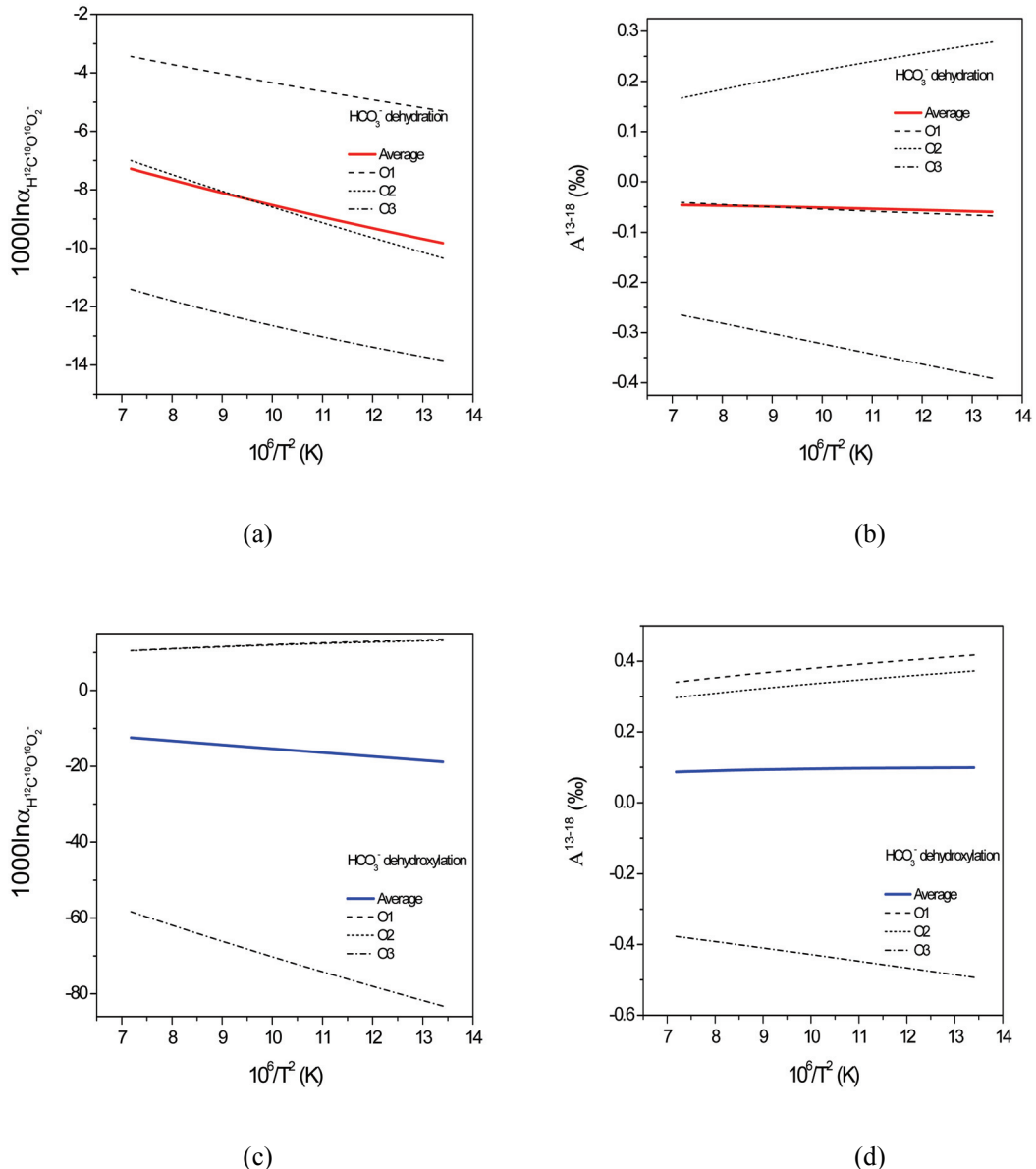


Figure 4-6: Position specificity of kinetic isotope fractionations of (a) oxygen isotope and (b) $^{13}\text{C}-^{18}\text{O}$ clumped isotopologues associated with HCO_3^- dehydration; of (c) oxygen isotope and (d) $^{13}\text{C}-^{18}\text{O}$ clumped isotopologues associated with HCO_3^- dehydroxylation. O1, O2 and O3 here denote isotopomers with ^{18}O substitution at oxygen position 1, 2 and 3 respectively (as labeled in Figure 2).

Our model also makes predictions about the isotopic compositions of the CO₂ produced by dehydration or dehydroxylation of DIC (Table 4-3 and Fig. 4-7, 4-8); this should correspond to the isotopic composition of CO₂ degassed from super-saturated solutions unless some other isotopically fractionating process modifies its composition: for HCO₃⁻ dehydration

$$1000 \ln \alpha^{13} (\text{CO}_2\text{-HCO}_3^-) = 1000 \ln (\alpha_{H^{13}\text{C}^{16}\text{O}_3^-}) = -\frac{0.1998 \times 10^6}{T^2} - \frac{7.964 \times 10^3}{T} - 0.707 \quad (28\text{a})$$

$$1000 \ln \alpha^{18} (\text{CO}_2\text{-HCO}_3^-) = -\frac{0.1282 \times 10^6}{T^2} - \frac{1.8414 \times 10^3}{T} + 0.6373 \quad (28\text{b})$$

$$1000 \ln \alpha^{17} (\text{CO}_2\text{-HCO}_3^-) = -\frac{0.0663 \times 10^6}{T^2} - \frac{0.989 \times 10^3}{T} + 0.3555 \quad (28\text{c})$$

$$1000 \ln \alpha^{13-18} (\text{CO}_2\text{-HCO}_3^-) = -\frac{0.3282 \times 10^6}{T^2} - \frac{9.7602 \times 10^3}{T} - 0.1264 \quad (28\text{d})$$

$$1000 \ln \alpha^{18-17} (\text{CO}_2\text{-HCO}_3^-) = -\frac{0.1901 \times 10^6}{T^2} - \frac{2.8317 \times 10^3}{T} + 0.9788 \quad (28\text{e})$$

$$1000 \ln A^{13-18} (\text{CO}_2\text{-HCO}_3^-) = -\frac{0.0003 \times 10^6}{T^2} + \frac{0.0452 \times 10^3}{T} - 0.0567 \quad (28\text{f})$$

$$1000 \ln A^{18-17} (\text{CO}_2\text{-HCO}_3^-) = -\frac{0.0045 \times 10^6}{T^2} - \frac{0.0012 \times 10^3}{T} - 0.014, \quad (28\text{g})$$

for HCO₃⁻ dehydroxylation

$$1000 \ln \alpha^{13} (\text{CO}_2\text{-HCO}_3^-) = 1000 \ln (\alpha_{H^{13}\text{C}^{16}\text{O}_3^-}) = -\frac{0.7622 \times 10^6}{T^2} - \frac{4.0314 \times 10^3}{T} - 0.3008 \quad (29\text{a})$$

$$1000 \ln \alpha^{18} (\text{CO}_2\text{-HCO}_3^-) = -\frac{0.5705 \times 10^6}{T^2} + \frac{6.5416 \times 10^3}{T} - 2.9418 \quad (29\text{b})$$

$$1000 \ln \alpha^{17} (\text{CO}_2\text{-HCO}_3^-) = -\frac{0.2968 \times 10^6}{T^2} + \frac{3.4066 \times 10^3}{T} - 1.4776 \quad (29\text{c})$$

$$1000 \ln \alpha^{13-18} (\text{CO}_2\text{-HCO}_3^-) = -\frac{1.3428 \times 10^6}{T^2} + \frac{2.6262 \times 10^3}{T} - 3.1905 \quad (29\text{d})$$

$$1000 \ln \alpha^{18-17} (\text{CO}_2\text{-HCO}_3^-) = -\frac{0.8587 \times 10^6}{T^2} + \frac{9.9606 \times 10^3}{T} - 4.4739 \quad (29e)$$

$$A^{13-18} (\text{CO}_2\text{-HCO}_3^-) = -\frac{0.0061 \times 10^6}{T^2} + \frac{0.116 \times 10^3}{T} + 0.0521 \quad (29f)$$

$$A^{18-17} (\text{CO}_2\text{-HCO}_3^-) = -\frac{0.0087 \times 10^6}{T^2} + \frac{0.0124 \times 10^3}{T} - 0.0545, \quad (29g)$$

where $\alpha^{13} (\text{CO}_2\text{-HCO}_3^-)$, $\alpha^{18} (\text{CO}_2\text{-HCO}_3^-)$, $\alpha^{17} (\text{CO}_2\text{-HCO}_3^-)$, $\alpha^{13-18} (\text{CO}_2\text{-HCO}_3^-)$, $\alpha^{18-17} (\text{CO}_2\text{-HCO}_3^-)$, $A^{13-18} (\text{CO}_2\text{-HCO}_3^-)$ and $A^{18-17} (\text{CO}_2\text{-HCO}_3^-)$ refer to the kinetic fractionation factor for ^{13}C singly substituted isotopologue (i.e., carbon isotope), ^{18}O singly substituted isotopologue (i.e., oxygen isotope), ^{17}O singly substituted isotopologue, ^{13}C - ^{18}O clumped isotopologue, ^{18}O - ^{17}O clumped isotopologue, ^{13}C - ^{18}O clumped isotope anomaly and ^{18}O - ^{17}O clumped isotope anomaly between product CO_2 and reactant HCO_3^- , respectively, and are defined as above for $\alpha_{H^{13}\text{C}^{16}\text{O}_3^-}$, $\alpha_{H^{12}\text{C}^{18}\text{O}^{16}\text{O}_2^-}$, $\alpha_{H^{12}\text{C}^{17}\text{O}^{16}\text{O}_2^-}$, $\alpha_{H^{13}\text{C}^{18}\text{O}^{16}\text{O}_2^-}$, $\alpha_{H^{12}\text{C}^{18}\text{O}^{17}\text{O}^{16}\text{O}^-}$, A^{13-18} and A^{18-17} . However, instead of averaging the fractionation factors of all the relevant isotopomers of each isotopologue (e.g., as we do for $\alpha_{H^{12}\text{C}^{18}\text{O}^{16}\text{O}_2^-}$ and $\alpha_{H^{13}\text{C}^{18}\text{O}^{16}\text{O}_2^-}$; see above), $\alpha^{18} (\text{CO}_2\text{-HCO}_3^-)$ and $\alpha^{13-18} (\text{CO}_2\text{-HCO}_3^-)$ are calculated by averaging only the kinetic isotope fractionation factors from the isotopomers that are capable of producing ^{18}O -substituted and ^{13}C - ^{18}O doubly substituted CO_2 (i.e., isotopomers with ^{18}O substitution at oxygen atom position 1 or 2; Fig. 4-2). At 25°C, the kinetic oxygen isotope and ^{13}C - ^{18}O clumped isotope anomaly fractionations between product CO_2 and reactant HCO_3^- are predicted to be $-7.0\text{\textperthousand}$, $0.09\text{\textperthousand}$ and $+12.6\text{\textperthousand}$, $0.37\text{\textperthousand}$, for HCO_3^- dehydration and dehydroxylation reaction, respectively.

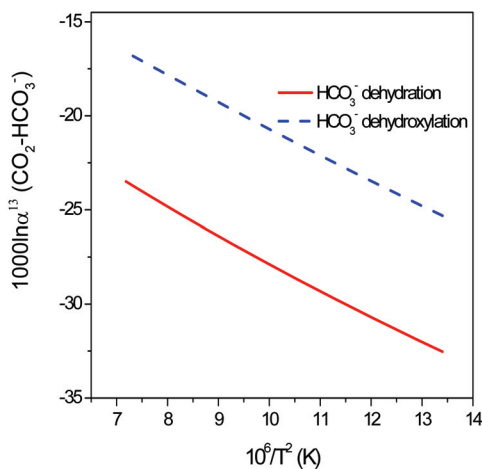


Fig. 7(a)

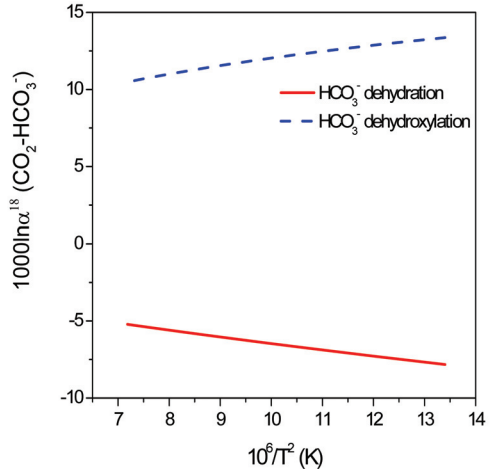


Fig. 7(b)

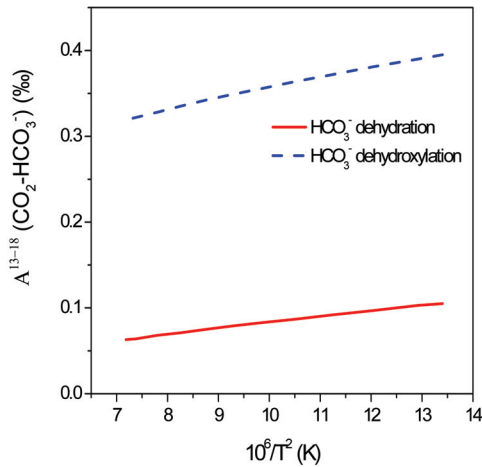


Fig. 7(c)

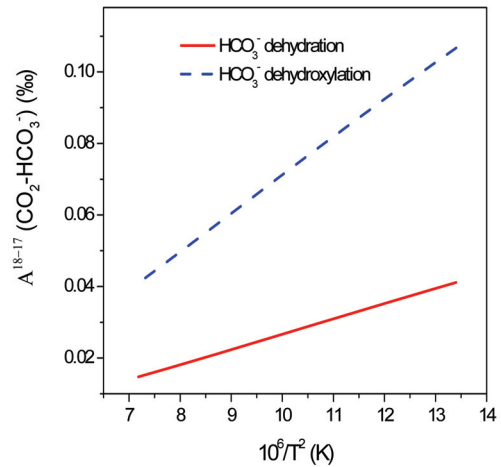


Fig. 7(d)

Figure 4-7: Model predicted fractionations of (a) carbon isotope; (b) oxygen isotope; (c) ¹³C-¹⁸O clumped isotopic anomaly and (d) ¹⁸C-¹⁷O clumped isotopic anomaly between degassed CO₂ and reactant HCO₃⁻ during HCO₃⁻ dehydration and HCO₃⁻ dehydroxylation.

We investigated the influence of our choice of frequency scaling factor (i.e., the proportionality between modeled vibrational frequencies and those measured for aqueous HCO₃⁻) on our model results, by using 1) no scaling factor and 2) a scaling factor of

1.0318 (determined by the comparison between our model predicted and the experimentally determined vibration frequencies for dissolved HCO_3^- , excluding the vCO-H vibration mode). In both cases, our model predicted kinetic isotope fractionations are sufficiently close to our model results that were calculated using the preferred scaling factor of 0.9614 (e.g., differ by less than 2.5‰, 2.0‰ and 0.01‰, respectively for carbon isotope, oxygen isotope and ^{13}C - ^{18}O clumped isotope fractionations at 25°C; Table 4-3). We conclude that uncertainties regarding the frequency scaling factor contribute to the absolute accuracy of our models, but are not a first-order systematic error; i.e., the general features of our modeled fractionations are insensitive to this constant.

Similarly, our calculation of isotopic fractionations for HCO_3^- dehydration reaction made with the transition-state structure based on the LMP2 method (with the same frequency scaling factor of 0.9614) also predicts kinetic isotope fractionations close to our standard model results based on the B3LYP method (e.g., -24.8‰, -15.4‰ and 0.11‰ for carbon isotope, oxygen isotope and ^{13}C - ^{18}O clumped isotope fractionations respectively at 25°C; LMP2 method; Table 4-3). Therefore our choice of the B3LYP calculation method does not seem to have dictated the general characteristics of our model result.

4.2 Predicted influence of kinetic isotope fractionations on carbonate minerals grown from degassing aqueous solutions

Our models of the kinetic isotope fractionation factors associated with HCO_3^- dehydration and dehydroxylation reaction make predictions regarding the evolution of abundances of different HCO_3^- isotopologues in aqueous solution that is undergoing CO_2

degassing. In order to relate these model predictions to the expected isotopic compositions of carbonates, we must consider isotopic fractionations between DIC and solid carbonates and the relative rates of CO₂ degassing and carbonate growth (following the procedures outlined in section 2.3). Fig. 4-8 illustrates predicted carbon isotope, oxygen isotope, $\Delta_{^{13}\text{C}^{18}\text{O}^{16}\text{O}_2}$ and $\Delta_{^{12}\text{C}^{18}\text{O}^{17}\text{O}^{16}\text{O}}$ compositions in carbonate minerals that grow as CO₂ degassing progresses (where the extent of degassing is expressed as the fraction of dissolved HCO₃⁻ remaining in aqueous solution).

Four different scenarios are considered (as discussed in section 2.3.2):

1) HCO₃⁻ dehydration is the only isotope fractionation process that influences the isotopic composition of HCO₃⁻ in aqueous solution; 2) HCO₃⁻ dehydroxylation is the only isotope fractionation process that influences the isotopic composition of HCO₃⁻ in aqueous solution. These two cases would describe a system in which a negligible amount of carbonate grows despite extensive degassing; 3) The HCO₃⁻ dehydration reaction is coupled with carbonate precipitation, at a molar ratio of 1:1; and 4) the HCO₃⁻ dehydroxylation reaction is coupled with carbonate precipitation, at a molar ratio of 1:1. In all cases, we assume that solid carbonate grows in equilibrium with co-existing DIC.

The predicted kinetic fractionations of various isotopologues are correlated with each other (Table 4-4); i.e., the kinetic mechanism we consider has a distinctive isotopic ‘fingerprint’, distinct from that for equilibrium fractionations and possibly other processes, that might be used to identify carbonates grown from degassing aqueous solutions. For example, at 25°C,

1) If CO₂ degassing reactions (i.e., HCO₃⁻ dehydration and HCO₃⁻ dehydroxylation) are the only isotope fractionation processes that influence the isotopic composition of

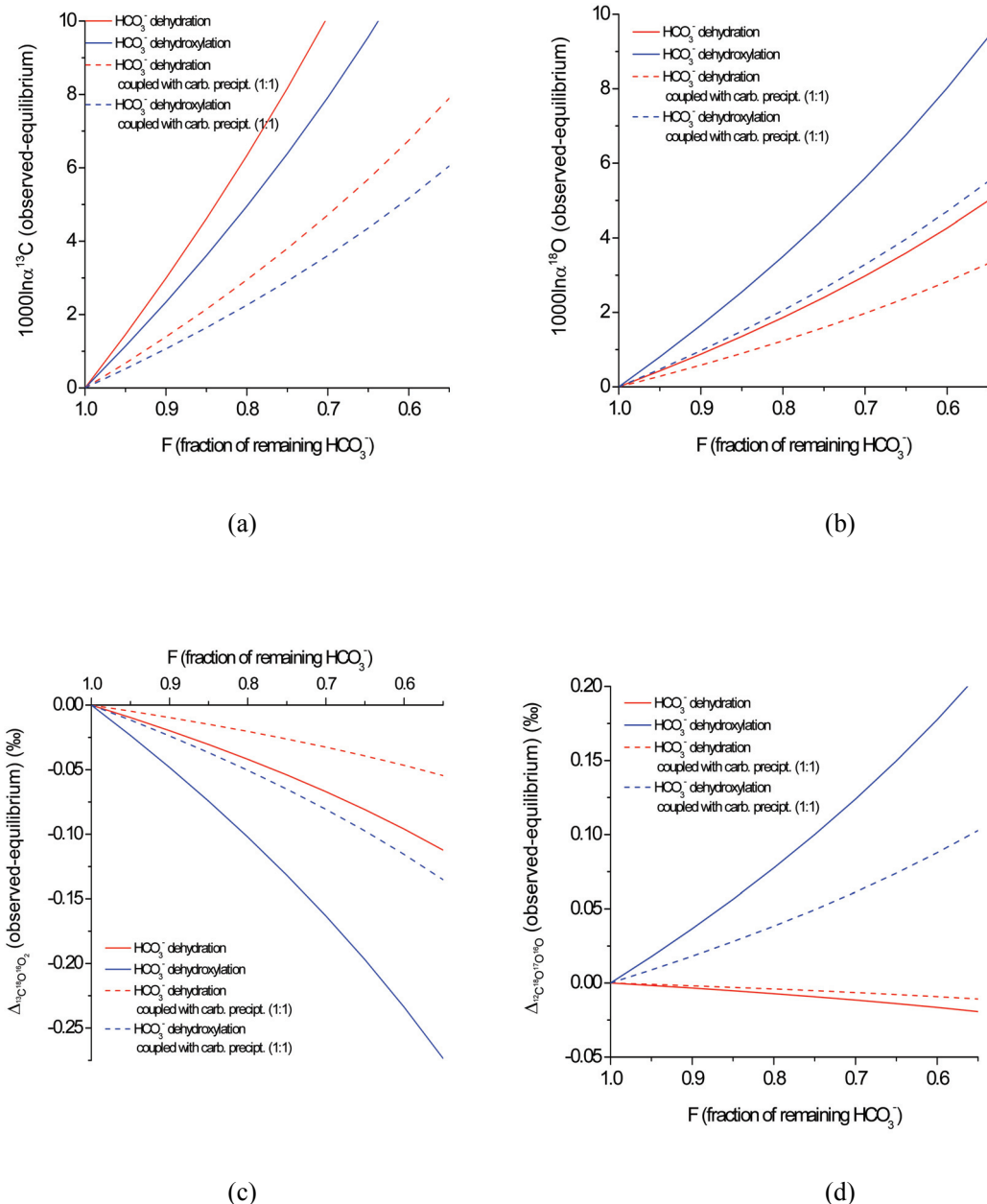


Figure 4-8: The kinetic fractionations of (a) carbon isotope, (b) oxygen isotope, (c) $\Delta_{\text{C}}^{12}\text{C}^{18}\text{O}^{16}\text{O}_2$ and (d) $\Delta_{\text{C}}^{13}\text{C}^{18}\text{O}^{16}\text{O}_2$ in the carbonate mineral as a function of the fraction of remaining HCO_3^- (F), predicted by our model. Four different cases are considered, as labeled in the legend (see text for details).

Table 4-4 The co-variations of carbon isotope, $\Delta_{^{13}\text{C}^{18}\text{O}^{16}\text{O}_2}$, $\Delta_{^{12}\text{C}^{18}\text{O}^{17}\text{O}^{16}\text{O}}$ and Δ_{63} fractionations in carbonate mineral, relative to 1‰ kinetic increase in its $^{18}\text{O}/^{16}\text{O}$, predicted from our model.

		Temperature (°C)			CO ₂ degassing Only			CO ₂ degassing coupled with carbonate formation (molar ratio 1:1)		
		$^{13}\text{C}/^{12}\text{C}$	$\Delta_{^{13}\text{C}^{18}\text{O}^{16}\text{O}_2}$	$\Delta_{^{12}\text{C}^{18}\text{O}^{17}\text{O}^{16}\text{O}}$	Δ_{63}	$^{13}\text{C}/^{12}\text{C}$	$\Delta_{^{13}\text{C}^{18}\text{O}^{17}\text{O}^{16}\text{O}_2}$	$\Delta_{^{12}\text{C}^{18}\text{O}^{17}\text{O}^{16}\text{O}}$	Δ_{63}	
		0	3.276	-0.0261	-0.0048	-0.0247	2.378	-0.0199	-0.0040	-0.0189
		5	3.271	-0.0256	-0.0047	-0.0242	2.376	-0.0194	-0.0040	-0.0184
		10	3.267	-0.0250	-0.0046	-0.0237	2.370	-0.0190	-0.0039	-0.0180
HCO_3^- dehydration	15	3.263	-0.0245	-0.0045	-0.0232	2.359	-0.0185	-0.0038	-0.0175	
	20	3.259	-0.0239	-0.0045	-0.0226	2.345	-0.0180	-0.0038	-0.0171	
	25	3.255	-0.0234	-0.0044	-0.0222	2.328	-0.0175	-0.0037	-0.0166	
	30	3.251	-0.0229	-0.0043	-0.0217	2.308	-0.0170	-0.0036	-0.0152	
	0	1.416	-0.0314	0.0226	-0.0280	1.117	-0.0268	0.0194	-0.0239	
	5	1.416	-0.0309	0.0225	-0.0275	1.116	-0.0264	0.0193	-0.0235	
	10	1.416	-0.0304	0.0224	-0.0271	1.113	-0.0260	0.0191	-0.0231	
HCO_3^- dehydroxylation	15	1.416	-0.0300	0.0223	-0.0267	1.109	-0.0255	0.0190	-0.0227	
	20	1.415	-0.0296	0.0222	-0.0263	1.104	-0.0250	0.0188	-0.0222	
	25	1.414	-0.0292	0.0221	-0.0259	1.098	-0.0245	0.0186	-0.0218	
	30	1.414	-0.0288	0.0220	-0.0255	1.090	-0.0241	0.0184	-0.0214	

HCO_3^- in aqueous solution, we predict for HCO_3^- dehydration that every 1‰ kinetic increase in carbonate $^{18}\text{O}/^{16}\text{O}$ will be accompanied by an increase in carbonate $^{13}\text{C}/^{12}\text{C}$ of 3.26‰, a decrease in $\Delta_{^{13}\text{C}^{18}\text{O}^{16}\text{O}_2}$ of 0.0222‰, and a $\Delta_{^{12}\text{C}^{18}\text{O}^{17}\text{O}^{16}\text{O}}$ decrease of 0.004‰. Similarly, for every 1‰ increase in carbonate d18O produced by HCO_3^- dehydroxylation, carbonate $^{13}\text{C}/^{12}\text{C}$ will increase by 1.41‰, $\Delta_{^{13}\text{C}^{18}\text{O}^{16}\text{O}_2}$ will decrease by 0.0292‰, and $\Delta_{^{12}\text{C}^{18}\text{O}^{17}\text{O}^{16}\text{O}}$ will increase by 0.0221‰.

2) If the progress of CO_2 degassing reactions are coupled to carbonate growth at a molar ratio of 1:1 (i.e., for every one CO_2 molecule degassed from the solution, one formula unit of carbonate precipitates), then our model predicts for HCO_3^- dehydration that for every 1‰ kinetic increase in carbonate $^{18}\text{O}/^{16}\text{O}$, carbonate $^{13}\text{C}/^{12}\text{C}$ will increase by 2.34‰, $\Delta_{^{13}\text{C}^{18}\text{O}^{16}\text{O}_2}$ will decrease by 0.0175‰, $\Delta_{^{12}\text{C}^{18}\text{O}^{17}\text{O}^{16}\text{O}}$ will decrease by 0.004‰ and $\Delta_{^{12}\text{C}^{18}\text{O}^{18}\text{O}^{16}\text{O}}$ will decrease by 0.006‰. And for HCO_3^- will increase by 2.38‰, $\Delta_{^{13}\text{C}^{18}\text{O}^{16}\text{O}_2}$ will decrease by 0.0165‰, $\Delta_{^{12}\text{C}^{18}\text{O}^{17}\text{O}^{16}\text{O}}$ will increase by 2.38‰, $\Delta_{^{13}\text{C}^{18}\text{O}^{16}\text{O}_2}$ will decrease by 0.0165‰, $\Delta_{^{12}\text{C}^{18}\text{O}^{17}\text{O}^{16}\text{O}}$ will decrease by 0.003‰ and $\Delta_{^{12}\text{C}^{18}\text{O}^{18}\text{O}^{16}\text{O}}$ will decrease by 0.006‰. And for HCO_3^- dehydroxylation, for every 1‰ kinetic increase in carbonate $^{18}\text{O}/^{16}\text{O}$, carbonate $^{13}\text{C}/^{12}\text{C}$ will increase by 1.10‰, $\Delta_{^{13}\text{C}^{18}\text{O}^{16}\text{O}_2}$ will decrease by 0.0245‰, $\Delta_{^{12}\text{C}^{18}\text{O}^{17}\text{O}^{16}\text{O}}$ will increase by 0.0186‰ and $\Delta_{^{12}\text{C}^{18}\text{O}^{18}\text{O}^{16}\text{O}}$ will increase by 0.0352‰.

These co-variations of different kinetic isotope fractionations vary little with temperature (Table 4-4).

The predicted effects of kinetic isotope fractionations on clumped isotope anomalies in precipitated carbonate minerals are relatively large, despite the fact that fractionations of multiply substituted isotopologues of the HCO_3^- are relatively modest. For example,

we predict that the HCO_3^- dehydration reaction will lead to a 0.0234‰ decrease in $\Delta_{^{13}\text{C}^{18}\text{O}^{16}\text{O}_2}$ in the carbonate mineral for every 1‰ kinetic enrichment in its $^{18}\text{O}/^{16}\text{O}$, even though the increase in $\Delta_{^{13}\text{C}^{18}\text{O}^{16}\text{O}_2}$ directly caused by kinetic fractionations of $^{13}\text{C}-^{18}\text{O}$ substituted isotopologues is only 0.005‰ for every 1‰ kinetic enrichment in its $^{18}\text{O}/^{16}\text{O}$ (Table 4-3, section 4.1). This somewhat counter-intuitive amplification of the change in $\Delta^{13}\text{C}^{18}\text{O}^{16}\text{O}_2$ arises from the fact that $\Delta_{^{13}\text{C}^{18}\text{O}^{16}\text{O}_2}$ (and all other clumped isotope anomalies), is not a conservative compositional parameter (Eiler and Schauble, 2004); in this respect, it is unlike $\delta^{13}\text{C}$ and $\delta^{18}\text{O}$ values. That is, in any system undergoing irreversible fractionations such as those we model, carbon and oxygen isotope changes must conform to the mass balance relations:

$$n_{\text{initial}} \times R_{\text{initial}}^{13} = n_{\text{consumed}} \times R_{\text{consumed}}^{13} + n_{\text{residual}} \times R_{\text{residual}}^{13}$$

$$n_{\text{initial}} \times R_{\text{initial}}^{18} = n_{\text{consumed}} \times R_{\text{consumed}}^{18} + n_{\text{residual}} \times R_{\text{residual}}^{18},$$

where n_{initial} , n_{consumed} and n_{residual} represent the moles of HCO_3^- in the initial, consumed and residual pools respectively. But for clumped isotope anomalies like $\Delta_{^{13}\text{C}^{18}\text{O}^{16}\text{O}_2}$ this does not hold true:

$$n_{\text{initial}} \times \Delta_{^{13}\text{C}^{18}\text{O}^{16}\text{O}_2}^{\text{initial}} \neq n_{\text{consumed}} \times \Delta_{^{13}\text{C}^{18}\text{O}^{16}\text{O}_2}^{\text{consumed}} + n_{\text{residual}} \times \Delta_{^{13}\text{C}^{18}\text{O}^{16}\text{O}_2}^{\text{residual}}.$$

This characteristic of clumped isotope anomalies was first demonstrated by Eiler and Schauble (2004) for the case of mixing two pools of CO_2 . If the two end members differ significantly in $\delta^{18}\text{O}$ and/or $\delta^{13}\text{C}$, their mixture may take on a Δ_{47} value that differs from the weighted average of the Δ_{47} values of the end members. This ‘nonlinearity’ of mixing ultimately reflects the fact that the abundances of multiply-substituted isotopologues expected for a stochastic distribution (the ‘0’ point on the Δ_i scale) is a non-

linear function of bulk isotopic composition. Similarly, mixing of two pools of HCO_3^- with the *same* $\Delta_{^{13}\text{C}^{18}\text{O}^{16}\text{O}_2}$ but with different bulk isotopic compositions (i.e., $^{13}\text{C}/^{12}\text{C}$, $^{18}\text{O}/^{16}\text{O}$) will produce a mixed pool having a $\Delta_{^{13}\text{C}^{18}\text{O}^{16}\text{O}_2}$ different from that of the end members. The same principle also applies to separation, the reverse of mixing; i.e., if one separates a portion of a HCO_3^- pool that differs in bulk isotopic composition from its initial pool but is identical to that pool in $\Delta_{^{13}\text{C}^{18}\text{O}^{16}\text{O}_2}$, the $\Delta_{^{13}\text{C}^{18}\text{O}^{16}\text{O}_2}$ value of the residual HCO_3^- pool can change. The exact amount of this $\Delta_{^{13}\text{C}^{18}\text{O}^{16}\text{O}_2}$ change depends on the difference in bulk isotopic composition between the separated pool and the initial pool; in case the case we consider in our CO_2 degassing models, this difference corresponds to the carbon and oxygen isotope fractionations between the consumed HCO_3^- pool and residual HCO_3^- pool (i.e., α in equation 4).

We combine our model predicted kinetic fractionations for $\Delta_{^{13}\text{C}^{18}\text{O}^{16}\text{O}_2}$ and $\Delta_{^{12}\text{C}^{18}\text{O}^{17}\text{O}^{16}\text{O}}$ to estimate the kinetic fractionation for Δ_{63} (the abundance anomaly of mass 63 of carbonate ion, defined as $\Delta_{63} = \frac{[63]_{actual}}{[63]_{stochastic}} / \frac{[60]_{actual}}{[60]_{stochastic}}$; Guo et al., 2008b) in the carbonate mineral:

$$\Delta_{63} \approx f_{^{13}\text{C}^{18}\text{O}^{16}\text{O}_2} \times \Delta_{^{13}\text{C}^{18}\text{O}^{16}\text{O}_2} + f_{^{12}\text{C}^{18}\text{O}^{17}\text{O}^{16}\text{O}} \times \Delta_{^{12}\text{C}^{18}\text{O}^{17}\text{O}^{16}\text{O}},$$

where $f_{^{13}\text{C}^{18}\text{O}^{16}\text{O}_2}$ and $f_{^{12}\text{C}^{18}\text{O}^{17}\text{O}^{16}\text{O}}$ are the relative abundance fractions of isotopologues $^{13}\text{C}^{18}\text{O}^{16}\text{O}_2^{2-}$ and $^{12}\text{C}^{18}\text{O}^{17}\text{O}^{16}\text{O}^{2-}$ in all the mass 63 isotopologues of CO_3^{2-} in the carbonate mineral (Table 4). For typical isotopic compositions of terrestrial carbonates (e.g., $\delta^{13}\text{C}_{\text{VPDB}} = -5\text{\textperthousand}$ and $\delta^{18}\text{O}_{\text{VSMOW}} = 30\text{\textperthousand}$), $f_{^{13}\text{C}^{18}\text{O}^{16}\text{O}_2} \approx 93.5\%$ and $f_{^{12}\text{C}^{18}\text{O}^{17}\text{O}^{16}\text{O}} \approx 6.5\%$. We predict, at 25°C, for every 1‰ kinetic increase in carbonate $^{18}\text{O}/^{16}\text{O}$, carbonate Δ_{63} decreases by 0.0222‰ and 0.0259‰ respectively for HCO_3^- dehydration and

dehydroxylation when these CO₂ degassing reactions are the only processes influencing the isotopic composition of the dissolved HCO₃⁻. If the HCO₃⁻ dehydration and dehydroxylation reactions are coupled with carbonate precipitation, the predicted Δ₆₃ decreases are 0.0166‰ and 0.0218‰ respectively for every 1‰ kinetic increase in carbonate ¹⁸O/¹⁶O (Table 4-4; assuming 1 mole of carbonate precipitates for every mole of CO₂ evolved). The Δ₄₇ value in the CO₂ derived from acid digestion of carbonate minerals (the basis of carbonate clumped isotope thermometry) is proportional to the Δ₆₃ in that carbonate mineral (Guo et al., 2008b). Therefore, we will expect that the effects of kinetic fractionations on the Δ₄₇ in the CO₂ derived from acid digestion of carbonate minerals will equal the calculated changes in Δ₆₃ for those carbonates (Fig. 4-9).

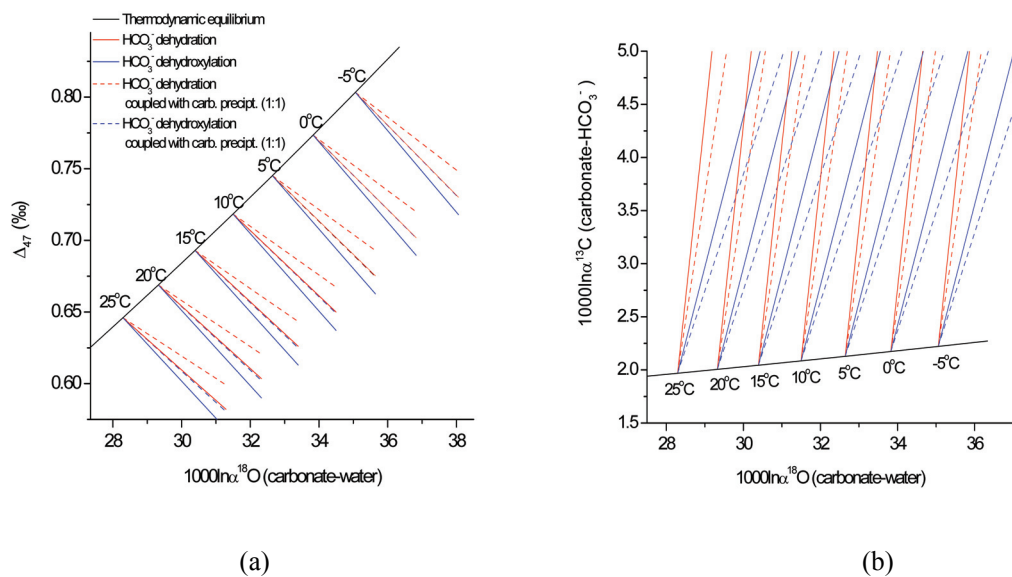


Figure 4-9: Correlations between kinetic carbon isotope, oxygen isotope and Δ₄₇ clumped isotope fractionations expected in the carbonate mineral, based on our predictions of the kinetic isotope fractionation associated with HCO₃⁻ dehydration and dehydroxylation reactions and our carbonate precipitation model: (a) correlations between kinetic Δ₄₇ clumped isotope and oxygen isotope fractionations; (b) correlations between kinetic carbon isotope and oxygen isotope fractionations. Four different scenarios are considered, as labeled in the legend (see text for details).

4.3 Isotopic compositions of cryogenic carbonates

All of the synthetic cryogenic carbonates examined in this study are enriched in $\delta^{13}\text{C}$ and in $\delta^{18}\text{O}$ relative to the expected compositions for calcite in equilibrium with their parent waters (except 0611B-07). These carbonates are also all lower in Δ_{47} than expected values if they grew at equilibrium at 0°C (Table 4-5). The magnitudes of departures from expected, equilibrium isotopic compositions vary among the different samples, from 1.1‰ to 6.4‰ for $\delta^{13}\text{C}$, from 0.4‰ to 2.0‰ for $\delta^{18}\text{O}$, and from 0.043‰ to 0.086‰ for Δ_{47} . The size of the departure from isotopic equilibrium does not exhibit any obvious correlations with the sample preparation conditions (Tables 4-2 and 4-5).

Table 4-5 Isotopic compositions of cryogenic carbonates synthesized in this study.

	Sample No.	0412-07	0418-07	0504A-07	0611A-07	0611B-07	0920A-07
Expected equil. values	$\delta^{13}\text{C}_{\text{cc}} (\text{\textperthousand})$	-19.8	-19.8	-18.9	-19.7	-20.6	-15.2
	$\delta^{18}\text{O}_{\text{cc}} (\text{\textperthousand})$	31.8	31.8	31.8	31.9	32.1	33.1
	$\Delta_{47} (\text{\textperthousand})$	0.773	0.773	0.773	0.773	0.773	0.773
Observed values	$\delta^{13}\text{C}_{\text{cc}} (\text{\textperthousand})$	-13.42	-15.83	-17.73	-15.1	-15.12	-12.91
	$\delta^{18}\text{O}_{\text{cc}} (\text{\textperthousand})$	33.71	32.19	32.84	33.38	31.43	34.66
	$^{\&}\Delta_{47} (\text{\textperthousand})$	0.692(4)	0.730(3)	0.715(2)	0.724(3)	0.687(3)	0.716(4)
1σ (‰)	(‰)	0.014	0.002	0.006	0.003	0.007	0.014
	$^{\ast}\text{T}_{\text{Apparent}}$ (°C)	15.2	7.8	10.6	8.9	16.1	16.5

* $\text{T}_{\text{Apparent}}$ denote the apparent formation temperatures estimated for cryogenic carbonates, based on their observed Δ_{47} (if the cryogenic carbonates were formed in isotopic equilibrium).

& Number in the bracket indicates the number of replicate isotope analyses for that carbonate sample.

The expected equilibrium isotope compositions of the cryogenic carbonates were estimated based on the $\delta^{13}\text{C}$ of the dissolved HCO_3^- , $\delta^{18}\text{O}$ of the solution water and the known equilibrium isotope fractionation factors between carbonate and dissolved HCO_3^- and water (carbon isotope, Deines et al., 1974; oxygen isotope, Kim and O'Neil, 1997, Beck et al., 2005; Δ_{47} , Ghosh et al., 2006). Note that, only $\delta^{13}\text{C}$ of the total dissolved inorganic carbon (DIC) were determined in the cryogenic experiments. To derive the initial $\delta^{13}\text{C}$ of the dissolved HCO_3^- , we first determine the speciation of the dissolved inorganic carbon in the solution based on the determined solution pH and known dissociation constants of carbonic acid (Roy et al., 1993), and then combine this speciation information with the experimentally determined $\delta^{13}\text{C}$ of the total DIC and with the known equilibrium carbon isotope fractionation among different DIC species (Zhang et al., 1995).

Both the solution pH and $\delta^{13}\text{C}$ of the total DIC used in the above computation were determined at the starting of the freezing experiments (i.e., at either room temperature or 3–7°C; section 3.1), and do not necessarily represent the actual $\delta^{13}\text{C}$ of the DIC at the beginning of CO_2 degassing (i.e., at 0°C, the temperature of cryogenic carbonate formation). Although the temperature change itself is not expected to significantly affect $\delta^{13}\text{C}$ of the total DIC or solution pH, the possibility of further dissolution of headspace CO_2 in the container during the cooling might change both $\delta^{13}\text{C}_{\text{DIC}}$ and solution pH. Similarly, the $\delta^{18}\text{O}$ values of water used in the above estimation of expected equilibrium carbonate isotopic composition were also determined at the starting of freezing experiments and were assumed to remain unchanged as the solution froze. However, previous studies on cryogenic carbonates indicate the $\delta^{18}\text{O}$ of water

might decrease significantly during ice formation due to the preferential incorporation of ^{18}O into water ice (Zak et al., 2004). The errors introduced by these effects on our estimation of expected equilibrium isotopic composition for carbonates are difficult to quantify, but might partially explain the depletion (as opposed to enrichment) of the oxygen isotopic compositions of sample 0611B-07 relative to its expected equilibrium oxygen isotope value (i.e., because we failed to consider the effect of ice formation on the $\delta^{18}\text{O}$ of water and thus overestimated the expected equilibrium oxygen isotopic composition of the carbonate). Future cryogenic experiments should be performed under more controlled settings and conditions (e.g., like settings in Killawee et al., 1999), so that the $\delta^{13}\text{C}$ of the total DIC and solution pH can be determined at 0°C and the $\delta^{18}\text{O}$ of water can be monitored as the solution freezes.

Our observed enrichments of $\delta^{13}\text{C}$ and $\delta^{18}\text{O}$ and depletion of Δ_{47} in cryogenic carbonates, relative to their expected equilibrium values at 0°C, are consistent with previous carbon and oxygen isotope studies of cryogenic carbonates (Clark and Lauriol, 1992), and with our model predictions on the isotopic compositions of carbonates that form from the degassing solution (section 4.2). Note that, both cryogenic carbonates synthesized in this study and natural speleothems form from the same physiochemical mechanism, i.e., degassing of CO₂ from aqueous solution. Therefore our observed deviations of their isotopic compositions from expected equilibrium values are very similar to those observed for speleothem carbonates (carbon and oxygen isotope, Mickler et al., 2004 and 2006; clumped isotope, Affek et al., 2008, Daeron et al., 2008). In particular, the depletions of Δ_{47} in our cryogenic carbonates, if unaccounted for, will lead to apparent overestimation of their formation temperatures by 8–16°C as determined by

carbonate clumped isotope thermometer (Table 4-5). This compares with the 8-22°C overestimation of carbonate formation temperature when applying carbonate clumped isotope thermometer to natural speleothem and speleothem-like carbonates synthesized in the laboratory (Table 4-1; Affek et al., 2008 and Daeron et al., 2008).

4.4 Comparison between model predictions and isotopic compositions of natural and synthetic carbonates

We compare our model predicted co-variations of kinetic fractionations in carbonate $^{13}\text{C}/^{12}\text{C}$, $^{18}\text{O}/^{16}\text{O}$ and Δ_{47} with the available experimental data on cryogenic carbonates (this study) and on speleothem carbonates (both natural modern speleothems and carbonates grown in the laboratory under conditions resembling natural speleothem growth; Affek et al., 2008; Daeron et al., 2008). Fig. 4-10 and 4-11 plot the deviations of isotopic compositions of these carbonates from their expected equilibrium isotopic compositions. Note that we are unable to determine the expected equilibrium carbon isotopic composition of any of the speleothem samples because we do not know the $\delta^{13}\text{C}_{\text{HCO}_3^-}$ values of the solutions from which they grew. Therefore, for these samples we assume the lowest $\delta^{13}\text{C}$ and $\delta^{18}\text{O}$ value in a speleothem is the equilibrium value (Fig. 4-11b).

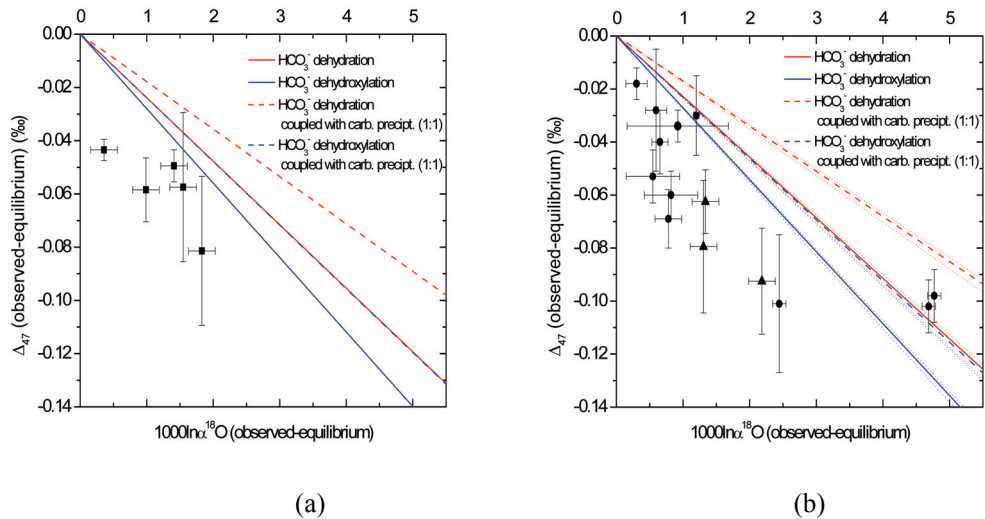


Figure 4-10: Comparison of our model predicted correlation between kinetic Δ_{47} clumped isotope fractionation and kinetic oxygen isotope fractionation, with the observed isotopic compositions of (a) cryogenic carbonates (formed at $\sim 0^\circ\text{C}$, this study), and (b) natural modern speleothems (circles) and speleothem-like carbonates synthesized in the laboratory (triangles) (Affek et al. 2008; Daeron et al., 2008). Dotted lines in (b) indicate the variations of predicted correlations over the range of observed cave temperatures (3.7 - 12.9°C); Plotted error bars represent 2 standard error (2σ).

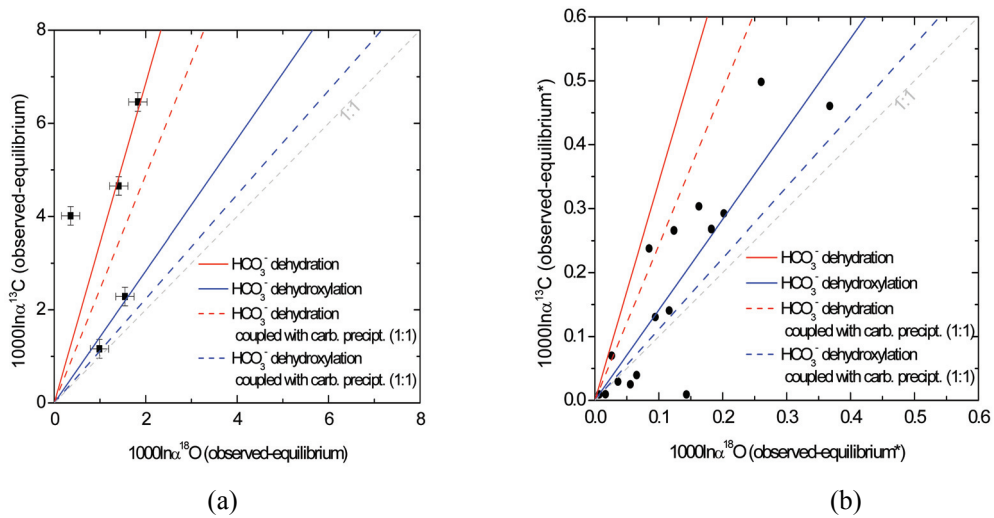


Figure 4-11: Comparison of our model predicted correlation between kinetic carbon isotope fractionation and kinetic oxygen isotope fractionation, with the observed isotopic compositions of (a) cryogenic carbonates (formed at $\sim 0^\circ\text{C}$, this study), and (b) the observed isotopic variations among different pieces of speleothem Vil-Gal (Daeron et al., 2008); see text for details. Plotted error bars represent 2 standard error (2σ).

If HCO_3^- dehydration and HCO_3^- dehydroxylation reactions, with or without carbonate accompanying carbonate precipitation, are the only isotopically fractionating processes (as we assumed in our standard model), we would expect the measured isotopic compositions of natural and synthetic carbonate minerals considered by this study to lie within the area confined by our model predictions for the four scenarios outlined above (section 4.2; Fig. 4-9). Based on the known or estimated pH's of the solutions from which these carbonates grew (pH<8 for natural and lab synthesized speleothem, Daeron et al., 2008; pH=5.5~5.7 for synthesized cryogenic carbonate, Table 4-2), HCO_3^- dehydration should be the dominant pathway for CO_2 degassing during both cryogenic carbonate growth and speleothem deposition (section 2.1). Therefore, the observed isotopic compositions of the carbonate minerals are expected to lie closer to the area confined by the model predictions for the two scenarios where HCO_3^- dehydration reactions are the dominant fractionating step, i.e., the two red lines (HCO_3^- dehydration only and HCO_3^- dehydration coupled with carbonate formation, respectively) in Fig. 4-10 and Fig. 4-11.

The correlations between kinetic fractionations of Δ_{47} and oxygen isotopes observed for all cryogenic carbonates and most of the speleothems define a trend parallel to our model predictions, and lie below the model predictions for all four scenarios (Fig. 4-10). The observed correlations between carbon isotope and oxygen isotopes defined by most the cryogenic carbonates and most of the speleothems lie within our range of model predictions for the four scenarios, but differ noticeably from the HCO_3^- dehydration dominated scenarios, which we expected would best describe the data (Fig. 4-11).

The discrepancies between our model predictions and experimental data could arise from kinetic isotope fractionations between the carbonate mineral and dissolved

HCO_3^- during carbonate growth (i.e., because we assumed that carbonates grow in equilibrium with co-existing DIC). Most speleothems form from supersaturated solutions and can grow quickly (Fairchild et al., 2007). The same could be true for growth cryogenic carbonates because rapid degassing during freezing could result in high supersaturation in the solution, driving rapid growth (though these experiments are not sufficiently well controlled to tell definitively if this is the case). It is known that rapid precipitation of carbonate from solution leads to kinetic isotope fractionations between DIC and precipitating carbonate. These effects generally lead to depletions of both $\delta^{13}\text{C}$ and $\delta^{18}\text{O}$ in the carbonate minerals relative to their values expected from equilibrium with dissolved HCO_3^- (e.g., $\sim 2.3\text{\textperthousand}$ depletion in $\delta^{13}\text{C}$ at 25°C , Turner, 1982; and $\sim 0.5\text{\textperthousand}$ depletion in $\delta^{18}\text{O}$ at 25°C , Kim et al., 2006). There are so far no systematic studies on the kinetic fractionations of clumped isotope anomalies associated with fast precipitation of carbonate minerals. However, in our preliminary experiments where we precipitated aragonite by pumping and mixing concentrated seawater and sodium carbonate solution together, we observed the depletion of Δ_{47} and $\delta^{18}\text{O}$ in the aragonite precipitates as the pumping rate (and thus precipitation rate) increases (Fig. 4-12; Eiler et al., 2008 and Gabitov et al., 2006). These observations suggest that rapid precipitation of carbonate minerals leads to depletion in carbon isotope, oxygen isotopes and Δ_{47} values of carbonates relative to equilibrium with co-existing DIC. The directions of these kinetic depletions are consistent with the discrepancies observed between the predictions of our CO_2 degassing models and the experimental data.

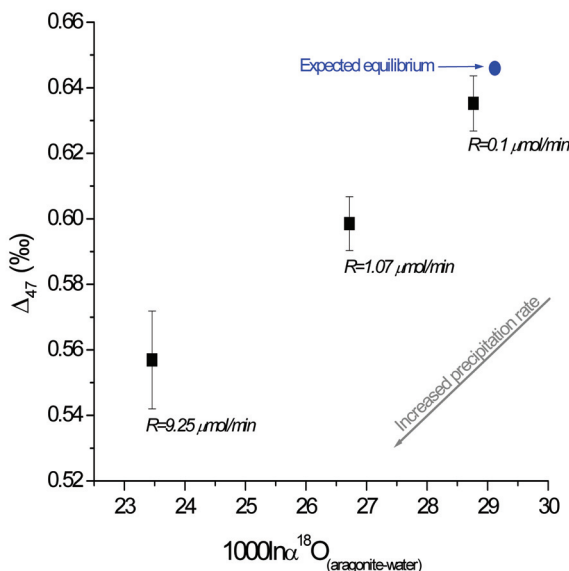


Figure 4-12: Depletion of Δ_{47} and $^{18}\text{O}/^{16}\text{O}$ in aragonite during its fast precipitation (samples from Gabitov et al. 2006). R is the rate at which concentrated seawater and Na_2CO_3 solution were pumped and mixed together, expressed as μmol of pumped CO_3^{2-} per minute. Circle represents the expected isotopic composition of the aragonite if it formed in isotopic equilibrium with the solution at experimental temperature (25°C).

Even if the non-equilibrium fractionations that occur during growth of some carbonates are well described by the CO_2 degassing model we present, it is not obvious what controls the extent of that dis-equilibrium for a given sample; i.e., even if samples are displaced from equilibrium along composition space vectors parallel to our model trends in Fig. 4-9 and 4-10, we still must establish how far they are displaced along such a trend. This question is particularly important for the interpretation of the stable isotope compositions of speleothems. The following paragraphs review some of the factors that likely control the extent of isotopic disequilibrium shown up in speleothem samples.

- 1) The proportion of HCO_3^- degassed and precipitated from the solution (relative to the initial HCO_3^- present in the solution), ‘1-F’ (where F is the fraction of HCO_3^-

remaining in the aqueous solution; see equation 2), must control the extent of isotopic disequilibrium and sets an upper-limit of isotopic disequilibrium that can be exhibited in the speleothem carbonates.

2) The pathway of CO₂ degassing — dehydration vs. dehydroxylation — and the ratio between the progress of degassing reactions and carbonate precipitation (i.e., the four different scenarios we discussed above) influence the kinetic isotope fractionation factors (α values in equation 2) and thus also affect the upper-limit of isotopic disequilibrium that could be exhibited in the speleothem carbonates. Even with the same fractions of HCO₃⁻ removed from the solution (i.e., the same F values, above), different reaction pathways cause different extents of kinetic disequilibrium in the residual HCO₃⁻ and thus in any carbonate minerals that grow from that residual DIC (Fig. 4-7).

3) The kinetic isotope fractionation processes described by our model must compete with isotope re-equilibration reactions — including isotope re-equilibration among the DIC species and between the dissolved HCO₃ and water. These re-equilibration reactions will tend to reduce or completely remove the effects of kinetic isotope fractionation, by an amount that is proportional to the relative rates of CO₂ degassing reactions vs. re-equilibration reactions. Carbon isotope isotopic compositions of dissolved inorganic carbonate species re-equilibrate with one another quickly (e.g., 17.5s at 25°C, for a solution with a salinity of 35 and at pH 8.2; Zeebe et al., 1999). In contrast, re-equilibration of their oxygen isotope compositions through exchange with water requires that C-O bonds break and re-form and is much slower (e.g., half-times for oxygen isotope exchange between HCO₃⁻ and H₂O is ~1.4 hrs at 25°C, Beck et al., 2004). There are so far no data available on the time required for the re-equilibration of the Δ_{47}

clumped isotope anomaly in the DIC system. However, these values reflect isotopic ordering among C-O bonds, so we suspect it should be of the same order of magnitude as the time for oxygen isotope re-equilibration.

Isotope re-equilibration processes should most strongly influence the isotopic compositions of speleothem carbonates that form under a relatively thick layer of water (e.g., pool carbonates and some flowstones) because in such cases the rate of CO₂ degassing is limited by diffusion (Buhmann and Dreybrodt, 1985). Therefore, we expect that carbonate growth from sufficiently thick water layers will be accompanied by isotope re-equilibrations reactions that out-compete kinetic isotope fractionation processes (i.e., CO₂ degassing). And, slower CO₂ degassing from thick water layers will also lead to lower degrees of supersaturation in the solution, lower carbonate precipitation rates, and thus diminished opportunity for any additional kinetic isotopic fractionations associated with fast precipitation of carbonate minerals. As a result, we expect those carbonate mineral formed under a sufficient thick water body/film will show oxygen isotope and clumped isotope compositions (i.e., Δ_{47} values) that are in equilibrium with the isotopic compositions of the cave water and cave temperatures. Evidence supporting this hypothesis can be found in studies of carbon isotope compositions of DIC in cave water (Bar-Matthews et al., 1996) and of the oxygen isotopic compositions of carbonates synthesized in the lab through CO₂ degassing (Wiedner et al., 2008).

It will be helpful for paleo-climate reconstructions to find speleothem samples that exhibit equilibrium isotope compositions, including clumped isotope compositions, so that we can circumvent the complications resulted from kinetic isotope fractionation processes. Based on the evidence presented above, we propose that pool carbonates are

promising candidates.

4.5 Implications for the isotopic studies in other natural systems

Besides cryogenic carbonates and speleothems, the model we present can also be applied to other systems in which the degassing of CO₂ from aqueous solution is an important process.

4.5.1 Other natural carbonate formations induced by the degassing of CO₂

Soil carbonates, evaporative carbonate (e.g., caliches), tufas and travertine deposits are carbonate formations that are often influenced by CO₂ degassing from aqueous solutions. Despite the importance of their isotopic compositions as proxies for paleoclimate and paleoelevation reconstruction, our quantitative understanding of the mechanisms by which these types of carbonates form remains limited (Andrews, 2006; Quade et al., 2007). One often observes that co-genetic suites of these classes of carbonates exhibit co-variations of δ¹³O and δ¹⁸O that resemble those observed in some speleothem carbonates (Cerling and Quade, 1993; Knauth et al., 2003; Andrews, 2006). This co-incidence is consistent with the notion that kinetic isotope effects associated with CO₂ degassing contribute to isotopic diversity in diverse carbonate types. However, it is important to note that these other carbonate types grown in complex, dynamic systems and almost certainly also exhibit isotopic diversity due to evaporation of water (perhaps combined with degassing; i.e., in the case of tufas; Andrew, 2006), the combined effects from evaporation and microbial activity (i.e., in caliches; Knauth, 2003), or the combined effects from precipitation and carbon cycling by plants (i.e., in soil carbonates, Cerling

and Quade, 1993). A detailed discussion of isotope fractionations accompanying formation of these diverse and complex carbonate types is beyond the scope of this study. However, if the kinetic isotope fractionations associated with CO₂ degassing are among the causes of δ¹³O and δ¹⁸O variations observed in these carbonates, we would expect an accompanying depletion of their Δ₄₇ relative to the expected equilibrium values, i.e., an overestimation of their formation temperature as determined by carbonate clumped isotope thermometry. A recent clumped isotope study of soil carbonates from Tibet yielded apparent temperatures greater than plausible growth temperatures, consistent with our expectation (M. Daeron, personal communications). Though this does not constitute proof of a role of CO₂ degassing in soil carbonates, we conclude that the kinetic isotope fractionations associated with CO₂ degassing should be considered in future stable isotope studies (including clumped isotope studies) of carbonates formed in environments that might contain aqueous solutions that are super-saturated in CO₂.

4.5.2 Air-sea CO₂ exchange and isotopic composition of respiration CO₂

Our model of kinetic isotope effects associated with degassing of aqueous solutions predicts that the isotope composition of the outgassed CO₂ differs significantly from that of the dissolved HCO₃⁻ and from the expected values if the CO₂ was in isotopic equilibrium with the solution water. Particularly, the ¹³C-¹⁸O clumped isotope anomalies in the degassed CO₂ are predicted to be ~0.09‰ and ~0.37‰ (for CO₂ produced by HCO₃⁻ dehydration or HCO₃⁻ dehydroxylation, respectively) higher than that of the dissolved HCO₃⁻ at 25°C, and therefore are ~0.40‰ and ~0.12‰ lower than their expected equilibrium values (assuming equilibrium ¹³C-¹⁸O clumped isotope anomaly in

dissolved HCO_3^- and in gaseous CO_2 are 0.43‰ [Guo et al., 2008a] and 0.92‰ [Wang et al., 2004] respectively at 25°C). These isotope effects, if fully expressed, could greatly influence the isotopic budget of atmospheric CO_2 , by way of both the air-sea exchange flux and the respiration flux (if the respiration CO_2 first dissolves in aqueous solutions, i.e., forms dissolved HCO_3^- , before its emissions into atmosphere).

A recent study of the clumped isotope composition of atmospheric CO_2 (Affek et al., 2007) found that, Δ_{47} values of most air samples differ significantly from (mostly lower than) that expected from based on thermodynamic equilibrium and exhibit considerable seasonal and diurnal variations (as much as 0.25‰ and 0.14‰ respectively; Affek et al., 2007). Both depletion in Δ_{47} relative to thermodynamic equilibrium and the seasonal and diurnal variations have been largely attributed to the terrestrial respiration flux, which is estimated to have Δ_{47} values of $0.77 \pm 0.28\text{‰}$ (Affek et al., 2007). Similarly, study of Δ_{47} in human breath revealed a similar Δ_{47} value, $0.76 \pm 0.03\text{‰}$ (Affek and Eiler, 2006). Both of these estimations of Δ_{47} in respiration CO_2 lie close to our predicted Δ_{47} values for CO_2 degassed from HCO_3^- dehydration and dehydroxylation (0.52‰ and 0.80‰, respectively, at 25°C; see above), suggesting kinetic isotope fractionations associated with HCO_3^- dehydration and HCO_3^- dehydroxylation reactions as a possible explanation for the depletion of $^{13}\text{C}-^{18}\text{O}$ bonds (relative to thermodynamic equilibrium) in respiration CO_2 .

It is however noted that, air samples collected from Cape Grim, Tasmania and Barrow, Alaska (considered to likely reflect hemispheric background air and to be affected by air-sea exchange) have Δ_{47} values close to those expected for thermodynamic equilibrium at ambient temperatures (Affek et al., 2007). This result is consistent with

previous studies of the carbon isotope budget of air-sea CO₂ exchange (Siegenthaler and Munnich, 1981; Inoue and Sugimura, 1985), which show that the carbon isotope fractionation during air-sea CO₂ exchange is dominated by diffusion (-1.8 to -2.3‰ for atmosphere-to-ocean transfer, and -9.7 to -10.2‰ for ocean-to-atmosphere transfer) rather than a kinetic isotope effect associated with dehydration or dehydroxylation. The relative unimportance of dehydration and dehydroxylation reactions (and their reverse) presumably reflects the slow kinetics of hydration/dehydration and hydroxylation/dehydroxylation reactions compared to the rapid renewal of CO₂ in the surface layer through turbulence. For example, at 20°C, the CO₂ lifetime for hydration is ~50s (Kern, 1960) and is 25 times longer than for the typical time constant for surface CO₂ renewal through turbulence (Siegenthaler and Munnich, 1981). Accordingly, the kinetic isotope fractionations associated with these reactions will be diminished by a factor by 25 during air-sea CO₂ exchange (Siegenthaler and Munnich, 1981). If our model predicted kinetic fractionations associated with HCO₃⁻ dehydration and dehydroxylation reactions are diminished by this factor, the total expected impact on the isotopic composition of CO₂ exchanged with the ocean is ~1‰, ~0.4‰ and ~0.02‰ for δ¹³O, δ¹⁸O and Δ₄₇ respectively. It would be challenging to detect such small effects in natural samples; in any event, it is consistent with findings from previous isotope studies (Siegenthaler and Munnich, 1981; Inoue and Sugimura, 1985; Affek et al., 2007).

5. SUMMARY

Based on ab initio models of molecular structures and transition state theory models of irreversible reactions, we calculate the isotope fractionations (including $^{13}\text{C}/^{12}\text{C}$, $^{18}\text{O}/^{16}\text{O}$, and multiply-substituted isotopologues) associated with degassing of CO_2 aqueous solutions, considering both CO_2 produced by HCO_3^- dehydration and HCO_3^- dehydroxylation. When coupled with a model for the isotope fractionations associated with carbonate precipitation, we predict that the isotope fractionations during CO_2 degassing from aqueous solutions increase the $\delta^{13}\text{O}$, $\delta^{18}\text{O}$ and deplete the distribution of $^{13}\text{C}-^{18}\text{O}$ clumped isotopologues of the residual DIC species and in carbonate minerals that precipitate from the DIC pool. For example, our model predicts that at 25°C $\delta^{13}\text{C}$ and Δ_{47} in carbonate will increase by 1.1-3.3‰ and decrease by 0.017-0.026‰ respectively, for every 1‰ kinetic enrichment in its $\delta^{18}\text{O}$, depending on the exact pathway for CO_2 degassing and carbonate formation. The reduction in Δ_{47} in the carbonate minerals accompanying these kinetic fractionations mostly arise from the non-linear relationship between bulk isotope composition (i.e., $\delta^{18}\text{O}$ and $\delta^{13}\text{C}$) and abundances of clumped isotopic species, combined with a large difference in $\delta^{18}\text{O}$ and $\delta^{13}\text{C}$ between the consumed and residual HCO_3^- pools. These predictions approximately agree with the isotopic compositions (including carbon isotope, oxygen isotope and Δ_{47} clumped isotope) of cryogenic carbonates observed in this study and modern natural speleothem and lab synthesized speleothem-like carbonate samples from previous studies. This agreement suggests that kinetic isotope fractionations associated with CO_2 degassing are among the primary causes for the disequilibrium isotopic compositions observed in cryogenic carbonates and speleothem samples. The discrepancies between Δ_{47} values observed in

carbonate minerals and our model predictions might result from the additional kinetic isotope fractionations associated with the fast precipitation of carbonate mineral from supersaturated solutions.

The extents of isotopic disequilibrium found in natural carbonates are controlled not only by the kinetic isotope fractionations described by our model, but also by isotope re-equilibration reactions that tend to remove the isotopic disequilibrium effects. We propose that speleothem samples formed under water films/bodies of sufficient thickness (e.g., pool carbonates, flowstones, etc) are most likely to exhibit equilibrium oxygen isotope and Δ_{47} compositions due to the suppression of CO₂ degassing processes relative to isotope re-equilibration reactions. Such materials should be targeted in future applied studies of the clumped isotope geochemistry of cave deposits.

This study constitutes the first systematic theoretical and experimental study of kinetic isotope fractionations associated with HCO₃⁻ dehydration and dehydroxylation reactions (especially for multiply-substituted isotopologues). The method and principles employed in this study can be applied to studies of other chemical reactions, e.g., CO₂ hydration and hydroxylation reactions, which are also important in natural systems (e.g., in biogenic carbonates, plant photosynthesis and respiration, air-sea exchange, etc.).

ACKNOWLEDGEMENTS

We would like to thank Rinat Gabitov for providing the synthesized aragonite samples for analyses, Haigt Affek and Anna Meckler for helpful discussions.

REFERENCES

- Affek H. P., Bar-Matthews M., Ayalon A., Matthews A. and Eiler J. M. (2008). Glacial/interglacial temperature variations in Soreq cave speleothems as recorded by 'clumped isotope' thermometry. *Geochim. Cosmochim. Acta* **in press**.
- Affek H. P. and Eiler J. M. (2006). Abundance of mass 47 CO₂ in urban air, car exhaust, and human breath. *Geochim. Cosmochim. Acta*. **70**: 1-12.
- Affek H. P., Xu X. and Eiler J. M. (2007). Seasonal and diurnal variations of ¹³C¹⁸O¹⁶O in air: Initial observations from Pasadena, CA. *Geochim. Cosmochim. Acta*. **71**: 5033-5043.
- Andrews J. E. (2006). Palaeoclimatic records from stable isotopes in riverine tufas: synthesis and review. *Earth Sci. Rev.* **75**: 85-104.
- Bar-Matthews M., Ayalon A., Matthews A., Sass E. and Halicz L. (1996). Carbon and oxygen isotope study of the active water-carbonate system in a karstic Mediterranean cave: Implications for paleoclimate research in semiarid regions. *Geochim. Cosmochim. Acta*. **60**: 337-347.
- Barkan E. and Luz B. (2005). High precision measurements of ¹⁷O/¹⁶O and ¹⁸O/¹⁶O ratios in H₂O. *Rapid Commun. Mass Spectrom.* **19**: 3737-3742.
- Beck W. C., Grossman E. L. and Morse J. W. (2005). Experimental studies of oxygen isotope fractionation in the carbonic acid system at 15°, 25°, and 40°C. *Geochim. Cosmochim. Acta*. **69**: 3493-3503.
- Bigeleisen J. (1955). Statistical mechanics of isotopic systems with small quantum corrections .1. General considerations and the rule of the geometric mean. *J. Phys. Chem.* **23**: 2264-2267.
- Buhmann D. and Dreybrodt W. (1985). The kinetics of calcite dissolution and precipitation in geologically relevant situations of karst areas. 1. Open system. *Chem. Geol.* **48**: 189-211.
- Cerling T. E. and Quade J. (1993). Stable carbon and oxygen isotopes in soil carbonates. In *Climate Change in Continental Isotopic Records*. American Geophysical Union Geophysical Monograph. 217-231.

- Clark I. D. and Lauriol B. (1992). Kinetic enrichment of stable isotopes in cryogenic calcites. *Chem. Geol.* **102**: 217-28.
- Daeron M., Guo W., Genty D. and Eiler J. M. (2008). ^{13}C - ^{18}O clumped isotope compositions of modern speleothems. **in prep**
- Davidson M. M., Hillier I. H., Hall R. J. and Burton N. A. (1994). Modeling the reaction $\text{OH}^- + \text{CO}_2 > \text{HCO}_3^-$ in the gas phase and in aqueous solution: a combined density functional continuum approach. *Mol. Phys.* **83**: 327-333.
- Deines P., Langmuir D. and Harmon, R.S. (1974). Stable carbon isotope ratios and the existence of a gas phase in the evolution of carbonate ground waters. *Geochim. Cosmochim. Acta* **38**: 1147-1164.
- Eiler J. M. and Schauble E. (2004). ^{18}O - ^{13}C - ^{16}O in Earth's atmosphere. *Geochim. Cosmochim. Acta* **68**: 4767-4777.
- Eiler J., Affek H., Daeron M., Ferry J., Guo W., Huntington K., Thiagarajan N. and Tripati A. (2008). Carbonate 'clumped isotope' thermometry: a status report, *Geochim. Cosmochim. Acta* **72**: A239-A239.
- Epstein S. and Mayeda T. (1953) Variation of O^{18} content of waters from natural sources. *Geochim. Cosmochim. Acta* **4**: 213-224.
- Eyring H. (1935a). Activated complex in chemical reactions. *J. Chem. Phys.* **3**: 107-15.
- Eyring H. (1935b). The activated complex and the absolute rate of chemical reactions. *Chem. Rev.* **17**: 65-77.
- Fairchild I. J., Frisia S., Borsato A. and Tooth A. F. (2007). Speleothems. In *Geochemical Sediments and Landscapes*, Blackwells, Oxford.
- Fairchild I. J., Smith C. L., Baker A., Fuller L., Spoel C., Mattey D. and McDermott F. (2006). Modification and preservation of environmental signals in speleothems. *Earth Sci. Rev.* **75**: 105-153.
- Gabitov, R. I., Cohen, A. L., Gaetani, G. A., Holcomb, M. and Watson, E. B. (2006). Growth rate dependence of Mg, Sr, and U incorporation into aragonite: experimental constraints on the origin of vital effects. *Eos Trans. AGU*, 87(52), Fall Meet. Suppl., Abstract B13B-1076.
- Gaillardet J. and Galy A. (2008). Himalaya-Carbon Sink or Source? *Science*. **320**: 1727-1728.

- Ghosh P., Adkins J., Affek H., Balta B., Guo W., Schauble E. A., Schrag D. and Eiler J. M. (2006). ^{13}C - ^{18}O bonds in carbonate minerals: A new kind of paleothermometer. *Geochim. Cosmochim. Acta* **70**: 1439-1456.
- Guo W., Daeron M., Niles P. B., Genty D., Kim S.-T., Vonhof H. B., Affek H. P., Blamart D., Wainer K. and Eiler J. M. (2008a). ^{13}C - ^{18}O bonds in dissolved inorganic carbon: implications for carbonate clumped Isotope thermometry. *Geochim. Cosmochim. Acta* **72**: A336-A336.
- Guo W., Mosenfelder J. L., Goddard W. A. and Eiler J. M. (2008b). Isotopic fractionations associated with phosphoric acid digestion of carbonate minerals. *Geochim. Cosmochim. Acta* **in review**.
- Horita J., Ueda A., Mizukami K., and Takatori I. (1989) Automatic δD and $\delta^{18}\text{O}$ analyses of multi-water samples using H_2 -water and CO_2 -water equilibration methods with a common equilibration set-up. *Appl. Rad. Isot.* **40**: 801-805.
- Iida K., Yokogawa D., Sato H. and Sakaki S. (2007). The barrier origin on the reaction of $\text{CO}_2 + \text{OH}^-$ in aqueous solution. *Chem. Phys. Lett.* **443**: 264-268.
- Inoue H. and Sugimura Y. (1985). Carbon isotopic fractionation during the CO_2 exchange process between air and sea-water under equilibrium and kinetic conditions. *Geochim. Cosmochim. Acta* **49**: 2453-2460.
- Johnson K. S. (1982). Carbon dioxide hydration and dehydration kinetics in seawater. *Limno. Oceano.* **27**: 849-855.
- Kern D. M. H. (1960). The hydration of carbon dioxide. *J. Chem. Educ.* **37**: 14-23.
- Kim S.-T. and O'Neil J. R. (1997). Equilibrium and nonequilibrium oxygen isotope effects in synthetic carbonates. *Geochim. Cosmochim. Acta* **61**: 3461-3475.
- Knauth L. P., Brilli M. and Klonowski S. (2003). Isotope geochemistry of caliche developed on basalt. *Geochim. Cosmochim. Acta* **67**: 185-195.
- Lacelle D. (2007). Environmental setting, (micro)morphologies and stable C–O isotope composition of cold climate carbonate precipitates—a review and evaluation of their potential as paleoclimatic proxies. *Quat. Sci. Rev.* **26**: 1670-1689.
- Leung K., Nielsen I. M. B. and Kurtz I. (2007). Ab initio molecular dynamics study of carbon dioxide and bicarbonate hydration and the nucleophilic attack of hydroxide on CO_2 . *J. Phys. Chem. B.* **111**: 4453-4459.

- Loerting T., Tautermann C., Kroemer R. T., Kohl I., Hallbrucker A., Mayer E. and Liedl K. R. (2000). On the surprising kinetic stability of carbonic acid (H_2CO_3). *Angew. Chem. Int. Ed.* **39**: 892-894.
- Marlier J. F. and O'Leary M. H. (1984). Carbon kinetic isotope effects on the hydration of carbon dioxide and the dehydration of bicarbonate ion. *J. Am. Chem. Soc.* **106**: 5054-5057.
- Mickler P. J., Banner J. L., Stern L., Asmerom Y., Edwards R. L. and Ito E. (2004). Stable isotope variations in modern tropical speleothems: Evaluating equilibrium vs. kinetic isotope effects. *Geochim. Cosmochim. Acta* **68**: 4381-4393.
- Mickler P. J., Stern L. A. and Banner J. L. (2006). Large kinetic isotope effects in modern speleothems. *Geol. Soc. Amer. Bull.* **118**: 65-81.
- Muehlinghaus C., Scholz D. and Mangini A. (2007). Modelling stalagmite growth and $\delta^{13}\text{C}$ as a function of drip interval and temperature. *Geochim. Cosmochim. Acta* **71**: 2780-2790.
- Nemukhin A. V., Topol I. A., Grigorenko B. L. and Burt S. K. (2002). On the origin of potential barrier for the reaction $\text{OH}^- + \text{CO}_2 \rightarrow \text{HCO}_3^-$ in water: Studies by using continuum and cluster solvation methods. *J. Phys. Chem. B* **106**: 1734-1740.
- Nguyen M. T., Raspoet G., Vanquickenborne L. G. and Van Duijnen P. T. (1997). How many water molecules are actively involved in the neutral hydration of carbon dioxide? *J. Phys. Chem. A* **101**: 7379-7388.
- O'Leary M. H., Madhavan S. and Paneth P. (1992). Physical and chemical basis of carbon isotope fractionation in plants. *Plant, Cell and Environment*. **15**: 1099-104.
- Paneth P. and O'Leary M. H. (1985). Mechanism of the spontaneous dehydration of bicarbonate ion. *J. Amer. Chem. Soc.* **107**: 7381-7384.
- Peng Z. and Merz K. M. (1992). The gas-phase and solution-phase free energy surfaces for carbon dioxide reaction with hydroxide ($\text{CO}_2 + \text{OH}^- \rightarrow \text{HCO}_3^-$). *J. Amer. Chem. Soc.* **114**: 2733-2734.
- Peng Z. and Merz K. M., Jr. (1993). Theoretical investigation of the $\text{CO}_2 + \text{OH}^- \rightarrow \text{HCO}_3^-$ reaction in the gas and aqueous phases. *J. Am. Chem. Soc.* **115**: 9640-7.
- Quade J., Garzione C. and Eiler J. M. (2007). Paleoelevation reconstruction using pedogenic carbonates. *Rev. Miner. Geochem.* **66**: 53-87.

- Ringnalda M. N., Langlois J.-M., Greeley B. H., Russo T. V., Muller R. P., Marten B., Won Y., Donnelly R. E., Pollard J., W. Thomas, Miller G. H., Goddard W. A. I. and Friesner R. A. (2007). Jaguar, version 7.0, release 207, Schrodinger, LLC, New York, NY.
- Romanov D., Kaufmann G. and Dreybrodt W. (2008). $\delta^{13}\text{C}$ profiles along growth layers of stalagmites: Comparing theoretical and experimental results. *Geochim. Cosmochim. Acta.* **72:** 438-448.
- Roy R. N., Roy L. N., Vogel K. M., Porter-Moore C., Pearson T., Good C. E., Millero F. J. and Campbell D. M. (1993). The dissociation constants of carbonic acid in seawater at salinities 5 to 45 and temperatures 0 to 45°C. *Mar. Chem.* **44:** 249-67.
- Rudolph W. W., Fischer D. and Irmer G. (2006). Vibrational spectroscopic studies and density functional theory calculations of speciation in the CO₂-water system. *Appl. Spectrosc.* **60:** 130-144.
- Schauble E. A., Ghosh P. and Eiler J. M. (2006). Preferential formation of ¹³C-¹⁸O bonds in carbonate minerals, estimated using first-principles lattice dynamics. *Geochim. Cosmochim. Acta.* **70:** 2510-2529.
- Scott A. P. and Radom L. (1996). Harmonic vibrational frequencies: an evaluation of Hartree-Fock, Moeller-Plesset, Quadratic Configuration Interaction, Density Functional Theory, and semiempirical scale factors. *J. Phys. Chem.* **100:** 16502-16513.
- Siegenthaler U. and Munnich K. O. (1981). ¹³C/¹²C fractionation during CO₂ transfer from air to sea. In *Carbon Cycle Modelling*. Scope **16**. 249-258.
- Spotl C. (2005) A robust and fast method of sampling and analysis of $\delta^{13}\text{C}$ of dissolved inorganic carbon in ground waters. *Isot. Environ. Health Stud.* **41:** 217-221.
- Tautermann C. S., Voegele A. F., Loerting T., Kohl I., Hallbrucker A., Mayer E. and Liedl K. R. (2002). Towards the experimental decomposition rate of carbonic acid (H₂CO₃) in aqueous solution. *Chem.--Eur. J.* **8:** 66-73.
- UNESCO (1985). The International System of Units (SI) in Oceanography. *UNESCO Tech. Pap. Mar. Sci., no. 45.*: pp124.
- Urey H. C. (1947). Thermodynamic properties of isotopic substances. *J. Chem. Soc.:* 562-581.

- Urey H. C. (1947). The thermodynamic properties of isotopic substances. *J. Chem. Soc.*: 562-581.
- Wiedner E., Scholz D., Mangini A., Polag D., Mühlinghaus C. and Segl M. (2008). Investigation of the stable isotope fractionation in speleothems with laboratory experiments. *Quat. Intl. in press*.
- Zak K., Urban J., Cilek V. and Hercman H. (2004). Cryogenic cave calcite from several Central European caves: age, carbon and oxygen isotopes and a genetic model. *Chem. Geol.* **206**: 119-136.
- Zeebe R. E. and Wolf-Gladrow D. A. (2001). CO₂ in seawater: Equilibrium, kinetics, isotope. Elsevier.
- Zhang J., Quay P. D. and Wilbur D. O. (1995). Carbon isotope fractionation during gas-water exchange and dissolution of CO₂. *Geochim. Cosmochim. Acta* **59**: 107-14.

APPENDIX

Table 4-A1 Scaled vibration frequencies (unit: cm⁻¹) for all 54 isotopologues of our modeled reactant during HCO₃⁻ dehydration reaction in aqueous solution (Fig. 4-2a; DFT-B3LYP/cc-pvTZ(-f) with a frequency scaling factor of 0.9614; see sections 2.2 and 2.4 for details). The frequency set contains 30 modes of vibration frequencies for each isotopologue. Due to space limitation, they are presented as here two sub-tables (a) ω_1 to ω_{15} ; (b) ω_{16} to ω_{30} .

Sub-table (a)

Isotopologue ^a	ω_1	ω_2	ω_3	ω_4	ω_5	ω_6	ω_7	ω_8	ω_9	ω_{10}	ω_{11}	ω_{12}	ω_{13}	ω_{14}	ω_{15}
H ₂ ¹² C ¹⁶ O ¹⁶ O ¹⁶ O	13.80	51.77	82.34	98.66	158.25	188.72	236.08	253.89	325.06	346.39	375.97	533.56	550.78	607.12	658.46
H ₂ ¹³ C ¹⁶ O ¹⁶ O ¹⁶ O	13.84	51.77	82.20	98.54	158.25	188.71	235.92	253.63	325.04	346.35	375.97	533.23	549.18	605.44	658.08
H ₂ ¹² C ¹⁸ O ¹⁶ O ¹⁶ O	12.20	51.51	82.14	98.55	158.23	188.68	235.64	253.08	325.04	346.32	375.94	531.99	544.83	597.11	657.36
H ₂ ¹² C ¹⁶ O ¹⁸ O ¹⁶ O	15.71	51.58	81.64	97.12	158.25	188.71	235.72	253.76	324.69	346.08	375.85	530.79	542.93	599.19	657.36
H ₂ ¹² C ¹⁶ O ¹⁶ O ¹⁸ O	14.34	51.14	82.10	96.72	158.24	188.64	235.12	253.02	324.91	346.32	375.56	531.74	544.72	599.15	655.53
H ₂ ¹³ C ¹⁸ O ¹⁶ O ¹⁶ O	12.28	51.51	82.01	98.42	158.23	188.66	235.47	252.86	325.01	346.27	375.93	531.38	543.61	595.34	657.03
H ₂ ¹³ C ¹⁶ O ¹⁸ O ¹⁶ O	15.72	51.57	81.51	97.01	158.25	188.69	235.55	253.51	324.67	346.03	375.84	530.24	541.53	597.80	657.07
H ₂ ¹³ C ¹⁶ O ¹⁶ O ¹⁸ O	14.36	51.13	81.97	96.61	158.24	188.63	234.95	252.80	324.88	346.27	375.56	531.15	543.50	597.41	655.18
H ₂ ¹² C ¹⁷ O ¹⁶ O ¹⁶ O	13.01	51.64	82.24	98.60	158.24	188.70	235.86	253.47	325.05	346.36	375.95	532.90	547.62	601.82	657.84
H ₂ ¹² C ¹⁶ O ¹⁷ O ¹⁶ O	14.85	51.68	81.99	97.85	158.25	188.71	235.90	253.82	324.87	346.23	375.91	532.17	546.60	603.13	657.86
H ₂ ¹² C ¹⁶ O ¹⁶ O ¹⁷ O	14.08	51.45	82.22	97.66	158.25	188.68	235.60	253.43	324.98	346.35	375.76	532.75	547.56	603.03	656.82
H ₂ ¹² C ¹⁷ O ¹⁸ O ¹⁸ O	15.57	50.84	81.35	95.14	158.23	188.61	234.55	252.58	324.53	345.97	375.42	525.31	536.62	585.24	654.52
H ₂ ¹² C ¹⁸ O ¹⁷ O ¹⁸ O	14.03	50.79	81.58	95.82	158.22	188.59	234.48	252.30	324.69	346.09	375.46	525.90	537.84	583.96	654.51
H ₂ ¹² C ¹⁸ O ¹⁸ O ¹⁷ O	14.74	51.01	81.35	96.03	158.23	188.63	234.78	252.59	324.59	345.97	375.59	525.46	536.81	584.32	655.31
H ₂ ¹² C ¹⁶ O ¹⁸ O ¹⁸ O	16.15	50.98	81.44	95.19	158.24	188.63	234.78	252.93	324.55	346.01	375.43	527.52	537.90	591.20	654.82
H ₂ ¹² C ¹⁸ O ¹⁶ O ¹⁸ O	12.86	50.87	81.90	96.61	158.22	188.60	234.66	252.34	324.88	346.25	375.53	528.89	540.62	588.02	654.78
H ₂ ¹² C ¹⁸ O ¹⁸ O ¹⁶ O	14.46	51.32	81.45	97.02	158.24	188.67	235.25	252.96	324.67	346.01	375.81	527.85	538.33	589.02	656.58
H ₂ ¹² C ¹⁷ O ¹⁷ O ¹⁷ O	13.75	51.09	81.68	96.75	158.23	188.63	234.96	252.64	324.77	346.12	375.65	528.16	539.26	588.33	655.60
H ₂ ¹² C ¹⁷ O ¹⁸ O ¹⁷ O	15.34	51.13	81.44	96.07	158.24	188.65	235.01	252.94	324.61	346.00	375.61	527.70	538.14	589.35	655.59
H ₂ ¹² C ¹⁷ O ¹⁷ O ¹⁸ O	14.68	50.92	81.67	95.87	158.23	188.61	234.71	252.62	324.71	346.12	375.48	528.05	539.12	589.21	654.79
H ₂ ¹² C ¹⁶ O ¹⁷ O ¹⁷ O	15.10	51.36	81.88	96.86	158.25	188.67	235.42	253.37	324.79	346.19	375.69	531.14	543.49	599.01	656.35
H ₂ ¹² C ¹⁷ O ¹⁶ O ¹⁷ O	13.33	51.31	82.12	97.60	158.24	188.66	235.37	253.05	324.97	346.32	375.74	531.86	544.79	597.41	656.32
H ₂ ¹² C ¹⁷ O ¹⁷ O ¹⁶ O	14.15	51.54	81.89	97.80	158.24	188.69	235.67	253.41	324.86	346.19	375.89	531.29	543.66	597.78	657.35
H ₂ ¹² C ¹⁶ O ¹⁷ O ¹⁸ O	15.33	51.06	81.77	95.92	158.24	188.63	234.95	252.97	324.72	346.16	375.50	529.76	540.92	595.14	655.15
H ₂ ¹² C ¹⁶ O ¹⁸ O ¹⁷ O	15.94	51.27	81.54	96.12	158.25	188.67	235.25	253.32	324.62	346.04	375.63	529.41	540.06	595.06	655.95

Sub-table (a) Continued

Isotopologue ^a		ϖ_1	ϖ_2	ϖ_3	ϖ_4	ϖ_5	ϖ_6	ϖ_7	ϖ_8	ϖ_9	ϖ_{10}	ϖ_{11}	ϖ_{12}	ϖ_{13}	ϖ_{14}	ϖ_{15}
H ₂ ¹² C ¹⁷ O ¹⁶ O ¹⁸ O	13.61	51.00	82.00	96.66	158.23	188.62	234.89	252.67	324.90	346.28	375.54	530.52	542.42	593.26	655.10	
H ₂ ¹² C ¹⁷ O ¹⁸ O ¹⁶ O	15.09	51.45	81.54	97.07	158.24	188.69	235.49	253.34	324.68	346.04	375.83	529.59	540.32	593.78	656.92	
H ₂ ¹² C ¹⁸ O ¹⁶ O ¹⁷ O	12.55	51.18	82.02	97.54	158.23	188.64	235.15	252.69	324.96	346.28	375.72	530.61	542.48	592.41	655.92	
H ₂ ¹² C ¹⁸ O ¹⁷ O ¹⁶ O	13.44	51.42	81.79	97.75	158.23	188.67	235.44	253.02	324.85	346.16	375.87	530.02	541.22	593.03	656.94	
H ₂ ¹² C ¹⁷ O ¹⁷ O ¹⁷ O	14.43	51.22	81.78	96.80	158.24	188.65	235.19	252.99	324.78	346.16	375.67	529.88	541.09	593.35	655.93	
H ₂ ¹² C ¹⁸ O ¹⁸ O ¹⁸ O	14.99	50.71	81.25	95.10	158.22	188.59	234.31	252.25	324.52	345.94	375.40	522.75	535.77	579.97	654.28	
H ₂ ¹³ C ¹⁷ O ¹⁶ O ¹⁸ O	13.07	51.63	82.10	98.48	158.24	188.68	235.69	253.23	325.03	346.31	375.95	532.46	546.19	600.09	657.49	
H ₂ ¹³ C ¹⁶ O ¹⁷ O ¹⁶ O	14.87	51.67	81.86	97.74	158.25	188.70	235.73	253.57	324.85	346.19	375.90	531.76	545.08	601.61	657.53	
H ₂ ¹³ C ¹⁶ O ¹⁶ O ¹⁷ O	14.11	51.44	82.08	97.54	158.24	188.67	235.43	253.20	324.96	346.31	375.75	532.31	546.13	601.31	656.47	
H ₂ ¹³ C ¹⁷ O ¹⁸ O ¹⁸ O	15.59	50.83	81.22	95.04	158.23	188.60	234.38	252.38	324.51	345.93	375.42	524.04	536.13	583.75	654.23	
H ₂ ¹³ C ¹⁸ O ¹⁷ O ¹⁸ O	14.08	50.78	81.45	95.71	158.22	188.58	234.31	252.11	324.67	346.04	375.46	524.70	537.35	582.28	654.21	
H ₂ ¹³ C ¹⁸ O ¹⁸ O ¹⁷ O	14.77	51.00	81.23	95.92	158.23	188.61	234.60	252.38	324.57	345.93	375.59	524.18	536.31	582.83	655.03	
H ₂ ¹³ C ¹⁶ O ¹⁸ O ¹⁸ O	16.15	50.97	81.31	95.10	158.24	188.62	234.62	252.71	324.52	345.96	375.43	526.43	537.15	589.77	654.53	
H ₂ ¹³ C ¹⁸ O ¹⁶ O ¹⁸ O	12.93	50.86	81.78	96.49	158.22	188.59	234.49	252.15	324.86	346.20	375.53	527.92	539.90	586.18	654.46	
H ₂ ¹³ C ¹⁸ O ¹⁸ O ¹⁶ O	14.50	51.31	81.32	96.91	158.23	188.65	235.08	252.74	324.65	345.96	375.81	526.75	537.57	587.57	656.31	
H ₂ ¹³ C ¹⁷ O ¹⁷ O ¹⁸ O	13.81	51.08	81.56	96.64	158.22	188.62	234.79	252.43	324.74	346.08	375.65	527.10	538.55	586.68	655.30	
H ₂ ¹³ C ¹⁸ O ¹⁶ O ¹⁷ O	15.36	51.12	81.32	95.97	158.23	188.63	234.84	252.73	324.58	345.96	375.61	526.62	537.39	587.89	655.31	
H ₂ ¹³ C ¹⁷ O ¹⁷ O ¹⁸ O	14.71	50.91	81.55	95.76	158.23	188.60	234.55	252.42	324.68	346.08	375.48	527.01	538.40	587.57	654.49	
H ₂ ¹³ C ¹⁸ O ¹⁷ O ¹⁷ O	15.11	51.35	81.75	96.75	158.24	188.66	235.25	253.14	324.77	346.15	375.69	530.54	542.21	597.45	656.04	
H ₂ ¹³ C ¹⁷ O ¹⁶ O ¹⁷ O	14.19	51.53	81.76	97.69	158.24	188.68	235.50	253.17	324.83	346.15	375.89	530.69	542.37	596.20	657.04	
H ₂ ¹³ C ¹⁷ O ¹⁷ O ¹⁶ O	13.38	51.30	81.99	97.48	158.23	188.64	235.21	252.83	324.94	346.27	375.74	531.26	543.58	595.64	655.98	
H ₂ ¹³ C ¹⁶ O ¹⁷ O ¹⁸ O	15.34	51.05	81.64	95.82	158.24	188.62	234.78	252.76	324.70	346.11	375.49	528.94	539.92	593.56	654.84	
H ₂ ¹³ C ¹⁶ O ¹⁸ O ¹⁷ O	15.95	51.26	81.41	96.02	158.24	188.65	235.08	253.09	324.60	346.00	375.63	528.60	538.99	593.64	655.66	
H ₂ ¹³ C ¹⁷ O ¹⁶ O ¹⁸ O	13.66	50.99	81.87	96.55	158.23	188.61	234.72	252.46	324.87	346.24	375.54	529.74	541.45	591.46	654.78	
H ₂ ¹³ C ¹⁷ O ¹⁸ O ¹⁶ O	15.12	51.44	81.41	96.96	158.24	188.67	235.32	253.11	324.66	346.00	375.82	528.77	539.23	592.36	656.64	
H ₂ ¹³ C ¹⁸ O ¹⁶ O ¹⁷ O	12.63	51.17	81.89	97.42	158.22	188.62	234.98	252.48	324.93	346.24	375.72	529.82	541.52	590.60	655.60	
H ₂ ¹³ C ¹⁸ O ¹⁷ O ¹⁶ O	13.50	51.41	81.66	97.64	158.23	188.66	235.27	252.80	324.82	346.11	375.87	529.18	540.22	591.43	656.65	
H ₂ ¹³ C ¹⁷ O ¹⁷ O ¹⁷ O	14.47	51.21	81.65	96.69	158.23	188.64	235.02	252.77	324.76	346.11	375.67	529.07	540.10	591.73	655.63	
H ₂ ¹³ C ¹⁸ O ¹⁸ O ¹⁷ O	15.02	50.70	81.13	94.99	158.22	188.58	234.14	252.06	324.50	345.89	375.40	521.36	535.44	578.45	653.99	

Sub-table (b)

Isotopologue &	ϖ_{16}	ϖ_{17}	ϖ_{18}	ϖ_{19}	ϖ_{20}	ϖ_{21}	ϖ_{22}	ϖ_{23}	ϖ_{24}	ϖ_{25}	ϖ_{26}	ϖ_{27}	ϖ_{28}	ϖ_{29}	ϖ_{30}
$H_2^{12}C^{16}O^{16}O^{16}O$	761.70	955.08	1009.89	1136.78	1270.97	1349.42	1545.64	1550.84	1695.64	2748.56	3394.43	3566.40	3598.23	3657.10	3672.46
$H_2^{13}C^{16}O^{16}O^{16}O$	738.07	951.37	1009.73	1126.88	1267.26	1328.45	1545.49	1550.83	1653.31	2748.32	3394.43	3566.38	3598.22	3657.10	3672.45
$H_2^{12}C^{18}O^{16}O^{16}O$	758.02	943.37	1009.74	1136.39	1263.17	1347.78	1545.50	1550.83	1671.09	2748.42	3394.43	3566.39	3598.23	3657.10	3672.46
$H_2^{12}C^{16}O^{18}O^{16}O$	759.44	937.08	1009.14	1128.93	1268.39	1340.27	1545.61	1550.83	1694.35	2737.40	3394.39	3566.39	3598.23	3657.10	3672.46
$H_2^{12}C^{16}O^{16}O^{18}O$	759.32	935.81	1009.86	1126.00	1269.83	1346.91	1545.64	1550.83	1694.94	2748.55	3394.43	3555.16	3598.21	3657.10	3672.45
$H_2^{13}C^{18}O^{16}O^{16}O$	734.27	940.46	1009.59	1126.72	1258.03	1327.43	1545.22	1550.82	1628.09	2748.18	3394.43	3566.38	3598.22	3657.10	3672.45
$H_2^{13}C^{16}O^{18}O^{16}O$	735.81	933.97	1008.96	1117.21	1265.07	1319.60	1545.47	1550.82	1652.08	2737.14	3394.39	3566.38	3598.22	3657.10	3672.45
$H_2^{13}C^{16}O^{16}O^{18}O$	735.61	931.14	1009.70	1116.74	1265.60	1326.18	1545.49	1550.83	1652.63	2748.31	3394.43	3555.14	3598.20	3657.10	3672.45
$H_2^{12}C^{17}O^{16}O^{16}O$	759.75	949.08	1009.81	1136.58	1266.92	1348.54	1545.57	1550.83	1682.45	2748.48	3394.43	3566.39	3598.23	3657.10	3672.46
$H_2^{12}C^{16}O^{17}O^{16}O$	760.50	945.86	1009.49	1132.54	1269.61	1344.40	1545.63	1550.83	1694.95	2742.63	3394.41	3566.39	3598.23	3657.10	3672.46
$H_2^{12}C^{16}O^{16}O^{17}O$	760.43	945.01	1009.87	1130.89	1270.37	1348.08	1545.64	1550.84	1695.27	2748.55	3394.43	3560.43	3598.21	3657.10	3672.45
$H_2^{12}C^{17}O^{18}O^{18}O$	755.10	912.69	1009.02	1116.74	1263.40	1336.54	1545.54	1550.83	1680.26	2737.32	3394.39	3555.15	3598.21	3657.10	3672.45
$H_2^{12}C^{18}O^{17}O^{18}O$	754.43	914.98	1009.29	1120.84	1260.72	1340.16	1545.48	1550.83	1669.42	2742.48	3394.41	3555.15	3598.20	3657.10	3672.45
$H_2^{12}C^{18}O^{18}O^{17}O$	754.49	915.71	1008.96	1121.88	1260.23	1337.11	1545.47	1550.83	1669.11	2737.26	3394.39	3560.42	3598.21	3657.10	3672.45
$H_2^{12}C^{16}O^{18}O^{18}O$	757.05	918.96	1009.10	1116.94	1267.39	1337.37	1545.61	1550.83	1693.65	2737.39	3394.39	3555.16	3598.21	3657.10	3672.45
$H_2^{12}C^{18}O^{16}O^{18}O$	755.64	923.61	1009.69	1125.81	1261.87	1345.41	1545.49	1550.83	1670.22	2748.41	3394.43	3555.15	3598.20	3657.10	3672.45
$H_2^{12}C^{18}O^{18}O^{16}O$	755.76	925.47	1008.98	1128.26	1260.84	1338.58	1545.47	1550.83	1669.57	2737.27	3394.39	3566.39	3598.23	3657.10	3672.45
$H_2^{12}C^{18}O^{17}O^{17}O$	755.55	924.16	1009.31	1125.92	1261.30	1341.36	1545.48	1550.83	1669.82	2742.49	3394.41	3560.43	3598.21	3657.10	3672.45
$H_2^{12}C^{17}O^{18}O^{17}O$	756.22	921.51	1009.03	1122.13	1263.92	1337.85	1545.54	1550.83	1680.62	2737.32	3394.39	3560.43	3598.21	3657.10	3672.45
$H_2^{12}C^{17}O^{17}O^{18}O$	756.17	920.92	1009.37	1120.98	1264.49	1340.86	1545.55	1550.83	1680.92	2742.55	3394.41	3555.15	3598.21	3657.10	3672.45
$H_2^{12}C^{16}O^{17}O^{17}O$	759.23	936.12	1009.47	1126.31	1269.05	1342.94	1545.63	1550.83	1694.58	2742.63	3394.41	3560.43	3598.21	3657.10	3672.45
$H_2^{12}C^{17}O^{16}O^{17}O$	758.49	938.87	1009.79	1130.75	1266.28	1347.23	1545.57	1550.83	1682.03	2748.48	3394.41	3566.39	3598.23	3657.10	3672.46
$H_2^{12}C^{17}O^{17}O^{16}O$	758.55	939.88	1009.41	1132.27	1265.64	1343.50	1545.55	1550.83	1681.70	2742.56	3394.41	3566.39	3598.23	3657.10	3672.46
$H_2^{12}C^{16}O^{17}O^{18}O$	758.12	927.19	1009.46	1121.13	1268.55	1341.68	1545.62	1550.83	1694.25	2742.62	3394.41	3555.16	3598.21	3657.10	3672.45
$H_2^{12}C^{16}O^{18}O^{17}O$	758.17	927.63	1009.12	1122.39	1267.87	1338.72	1545.61	1550.83	1693.98	2737.40	3394.39	3560.43	3598.21	3657.10	3672.45
$H_2^{12}C^{17}O^{16}O^{18}O$	757.37	929.55	1009.77	1125.90	1265.71	1346.10	1545.57	1550.83	1681.67	2748.47	3394.43	3555.16	3598.21	3657.10	3672.45
$H_2^{12}C^{17}O^{18}O^{16}O$	757.49	931.12	1009.06	1128.58	1264.48	1339.36	1545.54	1550.83	1681.05	2737.33	3394.39	3566.39	3598.23	3657.10	3672.46
$H_2^{12}C^{18}O^{16}O^{17}O$	756.76	933.04	1009.71	1130.62	1262.48	1346.51	1545.49	1550.83	1670.62	2748.41	3394.43	3560.43	3598.21	3657.10	3672.45
$H_2^{12}C^{18}O^{17}O^{16}O$	756.82	934.19	1009.34	1132.01	1261.94	1342.73	1545.48	1550.83	1670.28	2742.49	3394.41	3566.39	3598.23	3657.10	3672.46

Sub-table (b) Continued

Isotopologue ^{&}	ϖ_{16}	ϖ_{17}	ϖ_{18}	ϖ_{19}	ϖ_{20}	ϖ_{21}	ϖ_{22}	ϖ_{23}	ϖ_{24}	ϖ_{25}	ϖ_{26}	ϖ_{27}	ϖ_{28}	ϖ_{29}	ϖ_{30}
$H_2^{12}C^{17}O^{17}O^{17}\underline{O}$	757.28	929.98	1009.39	1126.11	1265.04	1342.09	1545.55	1550.83	1681.28	2742.55	3394.41	3560.43	3598.21	3657.10	3672.45
$H_2^{12}C^{18}O^{18}O^{18}\underline{O}$	753.36	906.75	1008.94	1116.55	1259.68	1335.84	1545.47	1550.83	1668.71	2737.25	3394.39	3555.15	3598.20	3657.10	3672.45
$H_2^{13}C^{17}O^{16}O^{16}\underline{O}$	736.06	945.79	1009.65	1126.80	1262.49	1327.89	1545.36	1550.83	1639.73	2748.25	3394.43	3566.38	3598.22	3657.10	3672.45
$H_2^{13}C^{16}O^{17}O^{16}\underline{O}$	736.87	942.51	1009.32	1121.65	1266.11	1323.57	1545.48	1550.83	1652.65	2742.38	3394.41	3566.38	3598.22	3657.10	3672.45
$H_2^{13}C^{16}O^{16}O^{17}\underline{O}$	736.76	940.80	1009.71	1121.33	1266.39	1327.23	1545.49	1550.83	1652.94	2748.31	3394.43	3560.42	3598.21	3657.10	3672.45
$H_2^{13}C^{17}O^{18}O^{18}\underline{O}$	731.30	909.24	1008.84	1105.63	1258.84	1316.45	1545.33	1550.82	1637.62	2737.06	3394.39	3555.14	3598.20	3657.10	3672.45
$H_2^{13}C^{18}O^{17}O^{18}\underline{O}$	730.59	911.60	1009.13	1110.71	1255.29	1320.22	1545.20	1550.82	1626.46	2742.24	3394.41	3555.14	3598.20	3657.10	3672.45
$H_2^{13}C^{18}O^{18}O^{17}\underline{O}$	730.68	912.99	1008.79	1110.67	1255.22	1317.19	1545.19	1550.82	1626.17	2737.00	3394.39	3560.41	3598.21	3657.10	3672.45
$H_2^{13}C^{16}O^{18}O^{18}\underline{O}$	733.32	915.07	1008.93	1105.72	1263.54	1316.93	1545.46	1550.82	1651.40	2737.13	3394.39	3555.14	3598.20	3657.10	3672.45
$H_2^{13}C^{18}O^{16}O^{18}\underline{O}$	731.80	919.81	1009.54	1116.70	1256.25	1325.31	1545.21	1550.82	1627.23	2748.17	3394.43	3555.14	3598.20	3657.10	3672.45
$H_2^{13}C^{18}O^{18}O^{16}\underline{O}$	732.00	923.11	1008.82	1116.85	1256.10	1318.53	1545.20	1550.82	1626.63	2737.01	3394.39	3566.37	3598.22	3657.10	3672.45
$H_2^{13}C^{18}O^{17}O^{17}\underline{O}$	731.75	921.17	1009.15	1115.55	1256.11	1321.29	1545.20	1550.82	1626.85	2742.24	3394.41	3560.41	3598.21	3657.10	3672.45
$H_2^{13}C^{17}O^{18}O^{17}\underline{O}$	732.47	918.43	1008.86	1110.79	1259.60	1317.63	1545.34	1550.82	1637.97	2737.07	3394.39	3560.41	3598.21	3657.10	3672.45
$H_2^{13}C^{17}O^{17}O^{18}\underline{O}$	732.38	917.14	1009.20	1110.76	1259.75	1320.62	1545.34	1550.82	1638.24	2742.30	3394.41	3555.14	3598.20	3657.10	3672.45
$H_2^{13}C^{16}O^{17}O^{17}\underline{O}$	735.55	932.32	1009.30	1115.71	1265.27	1322.24	1545.47	1550.83	1652.29	2742.38	3394.41	3560.42	3598.21	3657.10	3672.45
$H_2^{13}C^{17}O^{16}O^{17}\underline{O}$	734.86	936.93	1009.25	1121.52	1261.41	1323.00	1545.35	1550.82	1639.01	2742.31	3394.41	3566.38	3598.22	3657.10	3672.45
$H_2^{13}C^{17}O^{17}O^{16}\underline{O}$	734.74	935.11	1009.63	1121.28	1261.59	1326.72	1545.36	1550.83	1639.32	2748.24	3394.43	3560.42	3598.21	3657.10	3672.45
$H_2^{13}C^{16}O^{17}O^{18}\underline{O}$	734.39	922.97	1009.29	1110.81	1264.51	1321.09	1545.47	1550.83	1651.97	2742.37	3394.41	3555.14	3598.20	3657.10	3672.45
$H_2^{13}C^{16}O^{18}O^{17}\underline{O}$	734.49	924.14	1008.94	1110.92	1264.27	1318.16	1545.46	1550.82	1651.72	2737.14	3394.39	3560.42	3598.21	3657.10	3672.45
$H_2^{13}C^{17}O^{16}O^{18}\underline{O}$	733.59	925.34	1009.61	1116.72	1260.77	1325.71	1545.36	1550.83	1638.96	2748.23	3394.43	3555.14	3598.20	3657.10	3672.45
$H_2^{13}C^{17}O^{18}O^{16}\underline{O}$	733.79	928.42	1008.89	1117.03	1260.44	1319.01	1545.34	1550.82	1638.39	2737.07	3394.39	3566.38	3598.22	3657.10	3672.45
$H_2^{13}C^{18}O^{16}O^{17}\underline{O}$	732.96	929.67	1009.56	1121.24	1257.09	1326.29	1545.22	1550.82	1627.63	2748.18	3394.43	3560.41	3598.21	3657.10	3672.45
$H_2^{13}C^{18}O^{17}O^{16}\underline{O}$	733.07	931.61	1009.18	1121.40	1257.01	1322.53	1545.21	1550.82	1627.31	2742.25	3394.41	3566.37	3598.22	3657.10	3672.45
$H_2^{13}C^{17}O^{17}O^{17}\underline{O}$	733.54	926.62	1009.22	1115.63	1260.54	1321.72	1545.35	1550.82	1638.60	2742.30	3394.41	3560.41	3598.21	3657.10	3672.45
$H_2^{13}C^{18}O^{18}O^{18}\underline{O}$	729.51	903.68	1008.77	1105.55	1254.43	1316.05	1545.19	1550.82	1625.78	2737.00	3394.39	3555.13	3598.20	3657.10	3672.45

[&] Oxygen atoms here are expressed in the order of atoms 1, 2, 3 as denoted in Fig. 4-2(a). The underlined oxygen atoms (atom 3) are the ones to be abstracted during HCO_3^- dehydration reaction.

Table 4-A2 Scaled vibration frequencies (unit: cm⁻¹) for all 54 isotopologues of our modeled transition state during HCO₃⁻ dehydration reaction in aqueous solution (Fig. 4-2b; DFT-B3LYP/cc-pvtz(-f) with a frequency scaling factor of 0.9614; see sections 2.2 and 2.4 for details). The frequency set contains 30 modes of vibration frequencies for each isotopologue. Due to space limitation, they are presented as here two sub-tables (a) ω_1 to ω_{15} ; (b) ω_{16} to ω_{30} .

Sub-table (a)

Isotopologue &	ω_1	ω_2	ω_3	ω_4	ω_5	ω_6	ω_7	ω_8	ω_9	ω_{10}	ω_{11}	ω_{12}	ω_{13}	ω_{14}	ω_{15}
H ₂ ¹² C ¹⁶ O ¹⁶ O ¹⁶ O	-553.91	49.61	64.27	117.31	175.76	224.62	271.11	332.42	418.22	503.84	519.20	544.32	567.01	621.84	646.26
H ₂ ¹³ C ¹⁶ O ¹⁶ O ¹⁶ O	-548.72	49.65	64.26	117.03	175.43	224.56	270.99	332.40	416.77	503.82	519.11	544.14	566.83	618.07	645.42
H ₂ ¹² C ¹⁸ O ¹⁶ O ¹⁶ O	-553.82	47.58	64.35	117.39	173.84	224.43	271.02	332.41	410.19	503.66	515.52	543.74	566.45	621.11	644.88
H ₂ ¹² C ¹⁶ O ¹⁸ O ¹⁶ O	-553.88	51.11	63.19	114.58	172.74	224.39	270.93	332.42	414.68	503.47	517.47	543.80	565.89	620.85	638.99
H ₂ ¹² C ¹⁶ O ¹⁶ O ¹⁸ O	-550.15	49.00	64.16	116.32	175.23	224.42	270.95	332.18	416.62	503.46	508.36	540.48	563.73	612.86	641.07
H ₂ ¹³ C ¹⁸ O ¹⁶ O ¹⁶ O	-548.63	47.65	64.35	117.11	173.53	224.37	270.90	332.40	408.80	503.64	515.44	543.56	566.28	617.20	644.05
H ₂ ¹³ C ¹⁶ O ¹⁸ O ¹⁶ O	-548.69	51.13	63.19	114.33	172.45	224.34	270.81	332.40	413.31	503.45	517.37	543.64	565.70	616.81	638.15
H ₂ ¹³ C ¹⁶ O ¹⁶ O ¹⁸ O	-544.91	49.03	64.14	116.06	174.90	224.36	270.82	332.15	415.15	503.45	508.26	540.23	563.58	609.36	640.49
H ₂ ¹² C ¹⁷ O ¹⁶ O ¹⁶ O	-553.86	48.56	64.31	117.35	174.77	224.52	271.06	332.42	414.11	503.75	517.23	544.00	566.70	621.47	645.55
H ₂ ¹² C ¹⁶ O ¹⁷ O ¹⁶ O	-553.89	50.40	63.72	115.90	174.20	224.50	271.02	332.42	416.41	503.66	518.32	544.05	566.43	621.35	642.34
H ₂ ¹² C ¹⁶ O ¹⁶ O ¹⁷ O	-551.95	49.29	64.20	116.81	175.49	224.52	271.03	332.30	417.41	503.69	513.88	542.16	565.17	617.21	643.41
H ₂ ¹² C ¹⁷ O ¹⁸ O ¹⁸ O	-550.08	49.47	63.19	113.67	171.37	224.10	270.72	332.17	408.91	501.23	505.32	540.04	562.84	610.41	634.30
H ₂ ¹² C ¹⁸ O ¹⁷ O ¹⁸ O	-550.05	47.77	63.73	115.01	171.86	224.11	270.76	332.17	406.90	500.81	504.86	540.07	563.06	610.86	636.69
H ₂ ¹² C ¹⁸ O ¹⁸ O ¹⁷ O	-551.84	48.86	63.24	114.18	170.73	224.11	270.76	332.29	405.98	502.36	508.12	541.38	563.90	614.69	635.61
H ₂ ¹² C ¹⁶ O ¹⁸ O ¹⁸ O	-550.12	50.48	63.14	113.62	172.28	224.19	270.77	332.17	412.83	502.52	506.74	540.16	562.99	611.03	634.73
H ₂ ¹² C ¹⁸ O ¹⁶ O ¹⁸ O	-550.07	46.93	64.25	116.41	173.30	224.23	270.85	332.17	408.73	502.06	505.10	540.23	563.42	611.88	640.07
H ₂ ¹² C ¹⁸ O ¹⁸ O ¹⁶ O	-553.79	49.21	63.28	114.66	170.97	224.22	270.84	332.41	406.84	503.11	513.57	543.21	565.39	619.90	637.74
H ₂ ¹² C ¹⁷ O ¹⁸ O ¹⁷ O	-551.85	48.09	63.75	115.49	172.10	224.21	270.84	332.29	407.67	502.92	508.93	541.57	564.32	615.54	638.63
H ₂ ¹² C ¹⁸ O ¹⁶ O ¹⁷ O	-551.88	49.79	63.20	114.14	171.59	224.20	270.80	332.29	409.77	502.86	509.81	541.55	564.07	615.24	636.10
H ₂ ¹² C ¹⁷ O ¹⁷ O ¹⁸ O	-550.09	48.74	63.68	114.97	172.76	224.20	270.81	332.17	410.72	502.22	505.69	540.19	563.19	611.41	637.14
H ₂ ¹² C ¹⁶ O ¹⁷ O ¹⁷ O	-551.94	50.08	63.66	115.40	173.95	224.40	270.93	332.30	415.54	503.46	512.91	541.95	564.70	616.53	639.73
H ₂ ¹² C ¹⁷ O ¹⁶ O ¹⁷ O	-551.91	48.24	64.24	116.85	174.50	224.42	270.98	332.29	413.33	503.55	511.71	541.95	564.94	616.77	642.82
H ₂ ¹² C ¹⁷ O ¹⁷ O ¹⁶ O	-553.85	49.38	63.76	115.94	173.26	224.41	270.97	332.42	412.35	503.54	516.28	543.74	566.14	620.94	641.66
H ₂ ¹² C ¹⁶ O ¹⁷ O ¹⁸ O	-550.14	49.78	63.64	114.93	173.71	224.30	270.86	332.18	414.69	503.06	507.46	540.31	563.35	611.96	637.61
H ₂ ¹² C ¹⁶ O ¹⁸ O ¹⁷ O	-551.92	50.78	63.15	114.09	172.50	224.29	270.85	332.29	413.74	503.20	511.99	541.75	564.27	615.81	636.62

Sub-table (a) Continued

Isotopologue [§]	ϖ_1	ϖ_2	ϖ_3	ϖ_4	ϖ_5	ϖ_6	ϖ_7	ϖ_8	ϖ_9	ϖ_{10}	ϖ_{11}	ϖ_{12}	ϖ_{13}	ϖ_{14}	ϖ_{15}
$H_2^{12}C^{17}O^{16}O^{18}O$	-550.11	47.93	64.20	116.37	174.24	224.32	270.90	332.17	412.59	503.02	506.30	540.35	563.56	612.36	640.56
$H_2^{12}C^{17}O^{18}O^{16}O$	-553.83	50.13	63.23	114.62	171.83	224.30	270.89	332.41	410.66	503.30	515.37	543.48	565.61	620.38	638.35
$H_2^{12}C^{18}O^{16}O^{17}O$	-551.87	47.25	64.29	116.89	173.57	224.32	270.93	332.29	409.44	503.36	509.89	541.78	564.76	616.35	642.24
$H_2^{12}C^{18}O^{17}O^{16}O$	-553.81	48.44	63.81	115.98	172.36	224.32	270.93	332.41	408.48	503.40	514.52	543.47	565.90	620.52	641.01
$H_2^{12}C^{17}O^{17}O^{17}O$	-551.89	49.05	63.71	115.45	173.00	224.30	270.89	332.29	411.52	503.24	510.71	541.74	564.49	616.03	639.16
$H_2^{12}C^{18}O^{18}O^{18}O$	-550.04	48.53	63.23	113.71	170.50	224.01	270.68	332.17	405.16	499.49	504.73	539.92	562.71	609.80	633.90
$H_2^{13}C^{17}O^{16}O^{18}O$	-548.67	48.61	64.30	117.07	174.45	224.46	270.94	332.40	412.68	503.73	517.15	543.83	566.52	617.63	644.72
$H_2^{13}C^{16}O^{17}O^{16}O$	-548.70	50.43	63.71	115.64	173.89	224.44	270.89	332.40	415.00	503.64	518.23	543.88	566.24	617.45	641.50
$H_2^{13}C^{16}O^{16}O^{17}O$	-546.73	49.33	64.19	116.54	175.16	224.45	270.90	332.28	415.94	503.67	513.80	541.94	565.00	613.56	642.73
$H_2^{13}C^{17}O^{18}O^{18}O$	-544.84	49.50	63.18	113.43	171.08	224.04	270.60	332.15	407.55	501.21	505.26	539.81	562.69	606.63	633.67
$H_2^{13}C^{18}O^{17}O^{18}O$	-544.81	47.81	63.72	114.76	171.56	224.06	270.63	332.15	405.53	500.79	504.81	539.85	562.92	607.14	636.07
$H_2^{13}C^{18}O^{18}O^{17}O$	-546.62	48.89	63.24	113.93	170.45	224.06	270.63	332.27	404.66	502.35	508.06	541.19	563.74	610.68	634.89
$H_2^{13}C^{16}O^{18}O^{18}O$	-544.88	50.50	63.13	113.39	171.98	224.13	270.64	332.15	411.43	502.51	506.65	539.93	562.83	607.30	634.12
$H_2^{13}C^{18}O^{16}O^{18}O$	-544.82	46.99	64.23	116.14	172.99	224.17	270.73	332.15	407.31	502.06	505.04	540.00	563.29	608.29	639.48
$H_2^{13}C^{18}O^{18}O^{16}O$	-548.60	49.25	63.28	114.41	170.69	224.17	270.72	332.39	405.53	503.08	513.49	543.05	565.20	615.73	636.90
$H_2^{13}C^{17}O^{17}O^{18}O$	-546.63	48.14	63.75	115.23	171.81	224.16	270.72	332.27	406.31	502.91	508.87	541.37	564.16	611.65	637.93
$H_2^{13}C^{17}O^{18}O^{17}O$	-546.66	49.82	63.19	113.89	171.31	224.14	270.68	332.27	408.42	502.85	509.74	541.35	563.90	611.28	635.40
$H_2^{13}C^{17}O^{17}O^{18}O$	-544.85	48.77	63.67	114.72	172.46	224.15	270.68	332.15	409.31	502.21	505.62	539.95	563.04	607.73	636.53
$H_2^{13}C^{18}O^{17}O^{17}O$	-546.72	50.10	63.66	115.15	173.64	224.34	270.81	332.28	414.11	503.44	512.82	541.74	564.54	612.74	639.04
$H_2^{13}C^{17}O^{16}O^{17}O$	-546.69	48.28	64.23	116.58	174.18	224.36	270.86	332.27	411.90	503.53	511.64	541.74	564.79	613.07	642.13
$H_2^{13}C^{17}O^{17}O^{16}O$	-548.66	49.42	63.76	115.68	172.96	224.35	270.85	332.40	410.97	503.52	516.19	543.57	565.95	616.96	640.82
$H_2^{13}C^{16}O^{17}O^{18}O$	-544.89	49.80	63.63	114.68	173.40	224.24	270.73	332.15	413.25	503.05	507.37	540.08	563.20	608.33	637.02
$H_2^{13}C^{16}O^{18}O^{17}O$	-546.71	50.80	63.15	113.85	172.21	224.23	270.73	332.27	412.36	503.18	511.91	541.55	564.09	611.90	635.93
$H_2^{13}C^{17}O^{16}O^{18}O$	-544.86	47.97	64.19	116.10	173.92	224.26	270.77	332.15	411.15	503.01	506.22	540.11	563.42	608.81	639.97
$H_2^{13}C^{17}O^{18}O^{16}O$	-548.64	50.16	63.23	114.37	171.55	224.25	270.76	332.40	409.32	503.28	515.28	543.32	565.42	616.27	637.51
$H_2^{13}C^{18}O^{16}O^{17}O$	-546.65	47.30	64.28	116.62	173.25	224.27	270.81	332.27	408.04	503.35	509.83	541.57	564.61	612.59	641.56
$H_2^{13}C^{17}O^{16}O^{17}O$	-548.62	48.49	63.80	115.72	172.07	224.26	270.80	332.40	407.13	503.38	514.44	543.30	565.73	616.48	640.17
$H_2^{13}C^{17}O^{17}O^{17}O$	-546.68	49.09	63.70	115.19	172.70	224.24	270.76	332.27	410.12	503.23	510.64	541.54	564.33	612.19	638.47
$H_2^{13}C^{18}O^{18}O^{17}O$	-544.80	48.56	63.23	113.47	170.22	223.96	270.55	332.15	403.82	499.47	504.68	539.70	562.57	605.99	633.25

Sub-table (b)

Isotopologue*	Φ_{16}	Φ_{17}	Φ_{18}	Φ_{19}	Φ_{20}	Φ_{21}	Φ_{22}	Φ_{23}	Φ_{24}	Φ_{25}	Φ_{26}	Φ_{27}	Φ_{28}	Φ_{29}	Φ_{30}
$H_2^{12}C^{16}O^{16}O^{16}O$	739.40	820.93	912.60	1128.00	1279.44	1306.29	1533.53	1585.57	1650.24	1785.13	3047.93	3339.73	3579.72	3625.32	3648.52
$H_2^{13}C^{16}O^{16}O^{16}O$	718.20	814.42	911.90	1127.83	1272.17	1302.18	1533.29	1585.56	1649.90	1735.88	3047.92	3339.65	3579.70	3625.32	3648.51
$H_2^{12}C^{18}O^{16}O^{16}O$	735.51	813.85	911.92	1126.91	1263.27	1298.51	1533.50	1585.57	1650.16	1770.18	3047.93	3339.71	3579.71	3625.32	3648.51
$H_2^{12}C^{16}O^{18}O^{16}O$	735.87	814.94	910.79	1118.34	1264.19	1302.09	1533.47	1585.56	1650.23	1774.68	3047.92	3339.69	3579.71	3625.32	3648.51
$H_2^{12}C^{16}O^{16}O^{18}O$	737.55	818.48	909.67	1121.10	1277.82	1303.61	1533.16	1585.46	1647.49	1784.85	3047.91	3339.73	3568.12	3625.30	3648.51
$H_2^{13}C^{18}O^{16}O^{16}O$	714.40	807.67	911.32	1126.66	1252.71	1297.21	1533.22	1585.55	1649.69	1720.61	3047.92	3339.62	3579.70	3625.32	3648.51
$H_2^{13}C^{16}O^{18}O^{16}O$	714.78	808.68	910.31	1117.68	1254.62	1300.01	1533.20	1585.55	1649.83	1725.31	3047.92	3339.60	3579.70	3625.32	3648.51
$H_2^{13}C^{16}O^{16}O^{18}O$	716.07	811.75	908.98	1120.98	1270.10	1299.86	1532.92	1585.44	1647.14	1735.61	3047.91	3339.65	3568.11	3625.30	3648.51
$H_2^{12}C^{17}O^{16}O^{16}O$	737.34	817.26	912.23	1127.45	1272.00	1301.19	1533.51	1585.57	1650.20	1777.04	3047.93	3339.72	3579.72	3625.32	3648.51
$H_2^{12}C^{16}O^{17}O^{16}O$	737.54	817.83	911.66	1123.21	1271.69	1303.54	1533.50	1585.57	1650.24	1779.46	3047.93	3339.71	3579.71	3625.32	3648.51
$H_2^{12}C^{16}O^{16}O^{17}O$	738.41	819.62	911.04	1124.33	1278.58	1304.83	1533.34	1585.51	1648.77	1784.98	3047.92	3339.73	3573.56	3625.31	3648.51
$H_2^{12}C^{17}O^{18}O^{18}O$	731.92	808.10	907.56	1111.67	1252.13	1297.38	1533.06	1585.44	1647.41	1765.68	3047.91	3339.68	3568.12	3625.30	3648.51
$H_2^{12}C^{18}O^{17}O^{18}O$	731.75	807.62	908.11	1115.66	1251.19	1296.18	1533.08	1585.44	1647.37	1763.59	3047.91	3339.69	3568.12	3625.30	3648.51
$H_2^{12}C^{18}O^{18}O^{17}O$	730.90	805.82	908.63	1113.64	1244.56	1296.82	1533.22	1585.49	1648.65	1758.43	3047.91	3339.67	3573.56	3625.31	3648.51
$H_2^{12}C^{16}O^{18}O^{18}O$	734.01	812.12	907.88	1112.36	1261.46	1299.71	1533.09	1585.44	1647.47	1774.39	3047.91	3339.69	3568.12	3625.30	3648.51
$H_2^{12}C^{18}O^{16}O^{18}O$	733.65	811.11	909.01	1120.22	1260.79	1296.56	1533.13	1585.45	1647.39	1769.86	3047.91	3339.71	3568.12	3625.30	3648.51
$H_2^{12}C^{18}O^{18}O^{16}O$	731.90	807.50	910.16	1116.62	1246.45	1297.83	1533.42	1585.55	1650.13	1758.60	3047.92	3339.67	3579.71	3625.32	3648.51
$H_2^{12}C^{18}O^{17}O^{17}O$	732.62	809.00	909.47	1118.56	1252.57	1297.05	1533.26	1585.50	1648.66	1763.74	3047.92	3339.69	3573.56	3625.31	3648.51
$H_2^{12}C^{17}O^{18}O^{17}O$	732.78	809.49	908.91	1114.41	1253.60	1298.32	1533.24	1585.49	1648.70	1765.83	3047.91	3339.68	3573.56	3625.31	3648.51
$H_2^{12}C^{17}O^{17}O^{18}O$	733.61	811.27	908.40	1116.21	1260.49	1297.92	1533.10	1585.44	1647.42	1770.75	3047.91	3339.70	3568.12	3625.30	3648.51
$H_2^{12}C^{16}O^{17}O^{17}O$	736.55	816.43	910.11	1119.79	1270.52	1302.17	1533.30	1585.50	1648.76	1779.31	3047.92	3339.71	3573.56	3625.31	3648.51
$H_2^{12}C^{17}O^{16}O^{17}O$	736.35	815.87	910.68	1123.84	1270.88	1299.96	1533.32	1585.51	1648.72	1776.88	3047.92	3339.72	3573.56	3625.31	3648.51
$H_2^{12}C^{17}O^{17}O^{16}O$	735.47	814.07	911.31	1122.51	1263.15	1300.05	1533.47	1585.56	1650.19	1771.06	3047.93	3339.70	3579.71	3625.32	3648.51
$H_2^{12}C^{16}O^{17}O^{18}O$	735.69	815.20	908.74	1116.77	1269.50	1301.03	1533.12	1585.45	1647.48	1779.18	3047.91	3339.71	3568.12	3625.30	3648.51
$H_2^{12}C^{16}O^{18}O^{17}O$	734.88	813.44	909.24	1115.17	1262.73	1300.79	1533.27	1585.50	1648.76	1774.52	3047.91	3339.69	3573.56	3625.31	3648.51
$H_2^{12}C^{17}O^{16}O^{18}O$	735.49	814.66	909.31	1120.65	1269.90	1298.93	1533.14	1585.45	1647.44	1776.74	3047.91	3339.72	3568.12	3625.30	3648.51
$H_2^{12}C^{17}O^{18}O^{16}O$	733.78	811.08	910.45	1117.48	1255.30	1299.44	1533.44	1585.56	1650.18	1765.99	3047.92	3339.68	3579.71	3625.32	3648.51
$H_2^{12}C^{18}O^{16}O^{17}O$	734.51	812.39	910.37	1123.37	1261.94	1297.45	1533.30	1585.50	1648.68	1770.01	3047.92	3339.71	3573.56	3625.31	3648.51
$H_2^{12}C^{18}O^{17}O^{16}O$	733.61	810.57	911.01	1121.82	1254.19	1298.08	1533.45	1585.56	1650.14	1763.91	3047.93	3339.69	3579.71	3625.32	3648.51

Sub-table (b) Continued

Isotopologue ^{&}	ω_{16}	ω_{17}	ω_{18}	ω_{19}	ω_{20}	ω_{21}	ω_{22}	ω_{23}	ω_{24}	ω_{25}	ω_{26}	ω_{27}	ω_{28}	ω_{29}
$H_2^{12}C^{17}O^{17}O^{17}O$	734.47	812.58	909.77	1119.17	1261.72	1298.89	1533.28	1585.50	1648.71	1770.89	3047.92	3339.70	3573.56	3625.31
$H_2^{12}C^{18}O^{18}O^{18}O$	730.04	804.35	907.28	1110.98	1242.94	1295.97	1533.04	1585.44	1647.36	1758.27	3047.91	3339.67	3568.12	3625.30
$H_2^{13}C^{17}O^{16}O^{16}O$	716.19	810.92	911.59	1127.24	1262.65	1298.94	1533.25	1585.55	1649.80	1727.59	3047.92	3339.63	3579.70	3625.32
$H_2^{13}C^{16}O^{17}O^{16}O$	716.40	811.46	911.08	1122.84	1262.91	1300.77	1533.24	1585.55	1649.86	1730.14	3047.92	3339.62	3579.70	3625.32
$H_2^{13}C^{16}O^{16}O^{17}O$	717.06	813.00	910.35	1124.20	1271.07	1300.91	1533.09	1585.49	1648.42	1735.74	3047.92	3339.65	3573.55	3625.31
$H_2^{13}C^{17}O^{18}O^{18}O$	710.56	801.80	907.14	1111.08	1241.30	1296.25	1532.77	1585.42	1646.93	1716.05	3047.90	3339.59	3568.10	3625.30
$H_2^{13}C^{18}O^{17}O^{18}O$	710.39	801.36	907.64	1115.28	1240.00	1295.28	1532.79	1585.42	1646.85	1713.87	3047.90	3339.60	3568.11	3625.30
$H_2^{13}C^{18}O^{18}O^{17}O$	709.76	799.81	908.24	1112.86	1233.40	1295.98	1532.91	1585.47	1648.07	1708.63	3047.91	3339.58	3573.54	3625.31
$H_2^{13}C^{16}O^{18}O^{18}O$	712.61	805.63	907.41	1111.86	1251.41	1297.91	1532.82	1585.43	1647.08	1725.02	3047.90	3339.60	3568.11	3625.30
$H_2^{13}C^{18}O^{16}O^{18}O$	712.23	804.70	908.42	1120.06	1249.92	1295.43	1532.85	1585.43	1646.91	1720.28	3047.91	3339.62	3568.11	3625.30
$H_2^{13}C^{18}O^{18}O^{16}O$	710.95	801.61	909.77	1115.72	1235.51	1296.92	1533.10	1585.54	1649.55	1708.81	3047.92	3339.58	3579.70	3625.32
$H_2^{13}C^{18}O^{17}O^{17}O$	711.40	802.84	908.99	1118.12	1241.54	1296.08	1532.96	1585.48	1648.14	1714.03	3047.91	3339.60	3573.55	3625.31
$H_2^{13}C^{17}O^{18}O^{18}O$	711.58	803.30	908.49	1113.74	1242.95	1297.11	1532.95	1585.48	1648.22	1716.20	3047.91	3339.59	3573.55	3625.31
$H_2^{13}C^{17}O^{17}O^{18}O$	712.20	804.84	907.88	1115.89	1250.02	1296.51	1532.82	1585.43	1646.98	1721.19	3047.90	3339.61	3568.11	3625.30
$H_2^{13}C^{16}O^{17}O^{17}O$	715.24	809.93	909.53	1119.48	1261.49	1299.58	1533.04	1585.49	1648.39	1729.99	3047.91	3339.62	3573.55	3625.31
$H_2^{13}C^{17}O^{16}O^{17}O$	715.04	809.41	910.04	1123.68	1261.31	1297.86	1533.06	1585.49	1648.31	1727.43	3047.91	3339.63	3573.55	3625.31
$H_2^{13}C^{17}O^{17}O^{16}O$	714.38	807.87	910.78	1122.07	1253.07	1298.42	1533.20	1585.55	1649.74	1721.49	3047.92	3339.61	3579.70	3625.32
$H_2^{13}C^{16}O^{17}O^{18}O$	714.24	808.59	908.17	1116.50	1260.25	1298.58	1532.87	1585.43	1647.11	1729.85	3047.90	3339.62	3568.11	3625.30
$H_2^{13}C^{16}O^{18}O^{17}O$	713.62	807.06	908.77	1114.60	1252.90	1298.87	1533.00	1585.48	1648.36	1725.15	3047.91	3339.60	3573.55	3625.31
$H_2^{13}C^{17}O^{16}O^{18}O$	714.04	808.09	908.68	1120.51	1260.16	1296.96	1532.88	1585.43	1647.02	1727.29	3047.91	3339.63	3568.11	3625.30
$H_2^{13}C^{17}O^{18}O^{16}O$	712.75	805.02	910.02	1116.71	1244.88	1298.13	1533.15	1585.54	1649.69	1716.36	3047.92	3339.59	3579.70	3625.32
$H_2^{13}C^{18}O^{16}O^{17}O$	713.24	806.08	909.78	1123.16	1251.20	1296.24	1533.03	1585.48	1648.21	1720.43	3047.91	3339.62	3573.55	3625.31
$H_2^{13}C^{18}O^{17}O^{16}O$	712.58	804.54	910.53	1121.29	1243.35	1297.03	1533.16	1585.54	1649.62	1714.20	3047.92	3339.60	3579.70	3625.32
$H_2^{13}C^{17}O^{17}O^{17}O$	713.21	806.26	909.24	1118.80	1251.43	1297.38	1533.00	1585.48	1648.27	1721.33	3047.91	3339.61	3573.55	3625.31
$H_2^{13}C^{18}O^{18}O^{18}O$	708.74	798.23	906.90	1110.29	1231.61	1295.19	1532.73	1585.42	1646.78	1708.48	3047.90	3339.58	3568.10	3625.30

[&] Oxygen atoms here are expressed in the order of atoms 1, 2, 3 as denoted in Fig. 4-2(b). The underlined oxygen atoms (atom 3) are the ones to be abstracted during HCO_3^- dehydration reaction.

Table 4-A3 Scaled vibration frequencies (unit: cm⁻¹) for all 54 isotopologues of our modeled reactant during HCO₃⁻ dehydroxylation reaction in aqueous solution (Fig. 4-2c; DFT-B3LYP/cc-pvtz(-f) with a frequency scaling factor of 0.9614; see sections 2.2 and 2.4 for details). The frequency set contains 9 modes of vibration frequencies for each isotopologue.

Isotopologue ^{&}	ω_1	ω_2	ω_3	ω_4	ω_5	ω_6	ω_7	ω_8	ω_9
H ¹² C ¹⁶ O ¹⁶ O ¹⁶ O ⁻	456.58	547.13	636.71	771.76	887.63	1170.90	1277.82	1637.48	3631.44
H ¹³ C ¹⁶ O ¹⁶ O ¹⁶ O ⁻	456.58	545.12	635.56	747.69	875.89	1170.35	1257.23	1592.93	3631.42
H ¹² C ¹⁸ O ¹⁶ O ¹⁶ O ⁻	456.05	540.39	625.06	768.31	879.25	1163.14	1261.46	1626.75	3631.44
H ¹² C ¹⁶ O ¹⁸ O ¹⁶ O ⁻	453.87	538.65	623.04	769.92	870.39	1162.86	1277.66	1636.62	3619.92
H ¹² C ¹⁶ O ¹⁶ O ¹⁸ O ⁻	456.35	537.82	627.13	768.38	879.28	1169.80	1255.23	1626.72	3631.44
H ¹³ C ¹⁸ O ¹⁶ O ¹⁶ O ⁻	456.04	538.50	623.79	744.13	868.66	1161.32	1240.75	1582.01	3631.42
H ¹³ C ¹⁶ O ¹⁸ O ¹⁶ O ⁻	453.87	536.56	622.36	745.79	858.03	1162.43	1257.03	1592.02	3619.90
H ¹³ C ¹⁶ O ¹⁶ O ¹⁸ O ⁻	456.35	535.96	625.87	744.20	868.71	1169.32	1233.12	1581.98	3631.42
H ¹² C ¹⁷ O ¹⁶ O ¹⁶ O ⁻	456.30	543.70	630.54	769.93	883.35	1167.11	1268.92	1631.63	3631.44
H ¹² C ¹⁶ O ¹⁷ O ¹⁶ O ⁻	455.15	542.70	629.78	770.78	878.37	1166.61	1277.73	1637.02	3625.33
H ¹² C ¹⁶ O ¹⁶ O ¹⁷ O ⁻	456.46	542.34	631.66	769.97	883.34	1170.38	1265.90	1631.61	3631.44
H ¹² C ¹⁷ O ¹⁸ O ¹⁸ O ⁻	453.36	525.93	607.70	764.68	856.57	1158.52	1246.45	1619.27	3619.91
H ¹² C ¹⁸ O ¹⁷ O ¹⁸ O ⁻	454.40	527.02	608.29	763.91	860.65	1158.59	1239.33	1614.30	3625.32
H ¹² C ¹⁸ O ¹⁸ O ¹⁷ O ⁻	453.23	527.07	606.73	764.64	856.74	1155.12	1249.52	1619.29	3619.91
H ¹² C ¹⁶ O ¹⁸ O ¹⁸ O ⁻	453.62	529.17	614.04	766.53	861.26	1161.86	1255.14	1625.77	3619.91
H ¹² C ¹⁸ O ¹⁶ O ¹⁸ O ⁻	455.83	531.68	614.66	764.90	870.50	1162.78	1239.52	1614.84	3631.43
H ¹² C ¹⁸ O ¹⁸ O ¹⁶ O ⁻	453.35	531.56	611.97	766.44	861.65	1155.29	1260.97	1625.84	3619.91
H ¹² C ¹⁸ O ¹⁷ O ¹⁷ O ⁻	454.51	531.29	613.07	765.51	865.10	1158.78	1249.70	1619.75	3625.32
H ¹² C ¹⁷ O ¹⁸ O ¹⁷ O ⁻	453.47	530.38	612.16	766.27	861.10	1158.85	1256.96	1624.49	3619.91
H ¹² C ¹⁷ O ¹⁷ O ¹⁸ O ⁻	454.64	530.11	614.04	765.55	865.03	1162.21	1246.54	1619.73	3625.32
H ¹² C ¹⁶ O ¹⁷ O ¹⁷ O ⁻	455.02	537.87	624.88	768.99	873.86	1166.11	1265.84	1631.12	3625.32
H ¹² C ¹⁷ O ¹⁶ O ¹⁷ O ⁻	456.18	539.08	625.27	768.13	878.95	1166.79	1257.19	1625.43	3631.44
H ¹² C ¹⁷ O ¹⁷ O ¹⁶ O ⁻	454.87	539.18	623.77	768.94	873.99	1162.86	1268.76	1631.16	3625.32
H ¹² C ¹⁶ O ¹⁷ O ¹⁸ O ⁻	454.91	533.30	620.50	767.40	869.61	1165.57	1255.18	1626.21	3625.32
H ¹² C ¹⁶ O ¹⁸ O ¹⁷ O ⁻	453.74	533.78	618.28	768.12	865.69	1162.38	1265.79	1630.70	3619.92
H ¹² C ¹⁷ O ¹⁶ O ¹⁸ O ⁻	456.08	534.70	620.54	766.53	874.79	1166.44	1246.64	1620.26	3631.44
H ¹² C ¹⁷ O ¹⁸ O ¹⁶ O ⁻	453.60	535.05	617.17	768.07	865.91	1159.15	1268.62	1630.74	3619.92
H ¹² C ¹⁸ O ¹⁶ O ¹⁷ O ⁻	455.93	535.92	619.58	766.50	874.76	1162.97	1249.92	1620.26	3631.43
H ¹² C ¹⁸ O ¹⁷ O ¹⁶ O ⁻	454.63	535.78	618.43	767.31	869.81	1158.95	1261.19	1626.26	3625.32
H ¹² C ¹⁷ O ¹⁷ O ¹⁷ O ⁻	454.75	534.53	618.63	767.14	869.38	1162.55	1257.07	1624.93	3625.32
H ¹² C ¹⁸ O ¹⁸ O ¹⁸ O ⁻	453.12	522.77	602.06	763.03	852.12	1154.94	1239.17	1613.82	3619.91
H ¹³ C ¹⁷ O ¹⁶ O ¹⁶ O ⁻	456.30	541.75	629.33	745.81	872.20	1166.04	1248.15	1586.96	3631.42
H ¹³ C ¹⁶ O ¹⁷ O ¹⁶ O ⁻	455.15	540.64	628.89	746.68	866.29	1166.12	1257.12	1592.44	3625.31
H ¹³ C ¹⁶ O ¹⁶ O ¹⁷ O ⁻	456.46	540.41	630.44	745.84	872.21	1169.88	1244.53	1586.93	3631.42
H ¹³ C ¹⁷ O ¹⁸ O ¹⁸ O ⁻	453.36	524.06	606.83	740.38	845.95	1157.83	1224.06	1574.26	3619.90
H ¹³ C ¹⁸ O ¹⁷ O ¹⁸ O ⁻	454.40	525.26	607.14	739.59	850.89	1157.17	1216.98	1569.18	3625.30
H ¹³ C ¹⁸ O ¹⁸ O ¹⁷ O ⁻	453.23	525.19	605.86	740.34	846.09	1153.75	1227.84	1574.29	3619.90
H ¹³ C ¹⁶ O ¹⁸ O ¹⁸ O ⁻	453.62	527.24	613.25	742.30	850.05	1161.45	1233.06	1580.97	3619.90
H ¹³ C ¹⁸ O ¹⁶ O ¹⁸ O ⁻	455.83	529.95	613.26	740.61	861.11	1161.17	1217.26	1569.76	3631.42

Table 4-A3 (Continued)

Isotopologue^{&}	ω_1	ω_2	ω_3	ω_4	ω_5	ω_6	ω_7	ω_8	ω_9
H ¹³ C ¹⁸ O ¹⁸ O ¹⁶ <u>O⁻</u>	453.35	529.60	611.18	742.20	850.37	1153.84	1240.01	1581.05	3619.90
H ¹³ C ¹⁸ O ¹⁷ O ¹⁷ <u>O⁻</u>	454.50	529.45	611.99	741.24	854.77	1157.26	1228.11	1574.77	3625.30
H ¹³ C ¹⁷ O ¹⁸ O ¹⁷ <u>O⁻</u>	453.47	528.44	611.35	742.03	849.91	1158.09	1235.31	1579.59	3619.90
H ¹³ C ¹⁷ O ¹⁷ O ¹⁸ <u>O⁻</u>	454.64	528.28	612.96	741.28	854.71	1161.45	1224.16	1574.75	3625.31
H ¹³ C ¹⁶ O ¹⁷ O ¹⁷ <u>O⁻</u>	455.02	535.89	623.93	744.83	862.39	1165.66	1244.47	1586.42	3625.31
H ¹³ C ¹⁷ O ¹⁶ O ¹⁷ <u>O⁻</u>	456.18	537.21	623.98	743.95	868.43	1165.83	1235.62	1580.59	3631.42
H ¹³ C ¹⁷ O ¹⁷ O ¹⁶ <u>O⁻</u>	454.87	537.19	622.81	744.78	862.49	1161.92	1247.92	1586.46	3625.31
H ¹³ C ¹⁶ O ¹⁷ O ¹⁸ <u>O⁻</u>	454.91	531.40	619.50	743.19	858.70	1165.12	1233.09	1581.44	3625.31
H ¹³ C ¹⁶ O ¹⁸ O ¹⁷ <u>O⁻</u>	453.74	531.78	617.54	743.94	853.92	1161.97	1244.42	1585.97	3619.90
H ¹³ C ¹⁷ O ¹⁶ O ¹⁸ <u>O⁻</u>	456.08	532.91	619.20	742.30	864.84	1165.58	1224.28	1575.31	3631.42
H ¹³ C ¹⁷ O ¹⁸ O ¹⁶ <u>O⁻</u>	453.60	533.03	616.43	743.89	854.10	1158.31	1247.72	1586.02	3619.90
H ¹³ C ¹⁸ O ¹⁶ O ¹⁷ <u>O⁻</u>	455.93	534.12	618.23	742.27	864.79	1161.25	1228.45	1575.32	3631.42
H ¹³ C ¹⁸ O ¹⁷ O ¹⁶ <u>O⁻</u>	454.62	533.85	617.42	743.10	858.85	1157.34	1240.34	1581.49	3625.31
H ¹³ C ¹⁷ O ¹⁷ O ¹⁷ <u>O⁻</u>	454.75	532.62	617.60	742.93	858.49	1161.70	1235.45	1580.06	3625.31
H ¹³ C ¹⁸ O ¹⁸ O ¹⁸ <u>O⁻</u>	453.12	520.97	601.14	738.68	842.04	1153.66	1216.75	1568.68	3619.89

[&] Oxygen atoms here are expressed in the order of atoms 1, 2, 3 as denoted in Fig. 4-2c. The underlined oxygen atoms (atom 3) are the ones to be abstracted during HCO₃⁻ dehydroxylation reaction.

Table 4-A4 Scaled vibration frequencies (unit: cm⁻¹) for all 54 isotopologues of our modeled transition state during HCO₃⁻ dehydroxylation reaction in aqueous solution (Fig. 4-2d; DFT-B3LYP/cc-pvtz(-f) with a frequency scaling factor of 0.9614; see sections 2.2 and 2.4 for details). The frequency set contains 9 modes of vibration frequencies for each isotopologue.

Isotopologue^{&}	ω_1	ω_2	ω_3	ω_4	ω_5	ω_6	ω_7	ω_8	ω_9
H ¹² C ¹⁶ O ¹⁶ O ¹⁶ <u>O⁻</u>	-236.49	183.29	232.84	390.20	593.56	634.20	1300.65	2225.08	3593.01
H ¹³ C ¹⁶ O ¹⁶ O ¹⁶ <u>O⁻</u>	-233.16	183.33	232.36	389.76	584.06	615.95	1299.98	2161.68	3593.01
H ¹² C ¹⁸ O ¹⁶ O ¹⁶ <u>O⁻</u>	-236.29	183.09	228.17	388.10	588.52	629.74	1263.61	2208.60	3593.01
H ¹² C ¹⁶ O ¹⁸ O ¹⁶ <u>O⁻</u>	-231.58	178.82	229.91	381.54	592.45	634.19	1300.62	2225.07	3581.27
H ¹² C ¹⁶ O ¹⁶ O ¹⁸ <u>O⁻</u>	-236.41	182.06	229.13	387.96	589.15	629.76	1263.76	2208.74	3593.01
H ¹³ C ¹⁸ O ¹⁶ O ¹⁶ <u>O⁻</u>	-232.99	183.12	227.74	387.57	579.02	611.36	1262.84	2144.75	3593.01
H ¹³ C ¹⁶ O ¹⁸ O ¹⁶ <u>O⁻</u>	-228.25	178.85	229.42	381.13	582.94	615.93	1299.95	2161.67	3581.27
H ¹³ C ¹⁶ O ¹⁶ O ¹⁸ <u>O⁻</u>	-233.10	182.09	228.67	387.45	579.67	611.38	1262.97	2144.90	3593.01
H ¹² C ¹⁷ O ¹⁶ O ¹⁶ <u>O⁻</u>	-236.38	183.19	230.41	389.09	590.88	631.84	1281.34	2216.23	3593.01
H ¹² C ¹⁶ O ¹⁷ O ¹⁶ <u>O⁻</u>	-233.93	180.93	231.29	385.65	592.97	634.20	1300.64	2225.07	3586.79
H ¹² C ¹⁶ O ¹⁶ O ¹⁷ <u>O⁻</u>	-236.45	182.67	230.90	389.02	591.22	631.85	1281.41	2216.31	3593.01
H ¹² C ¹⁷ O ¹⁸ O ¹⁸ <u>O⁻</u>	-231.34	177.54	223.75	378.04	585.31	627.36	1244.73	2199.31	3581.27
H ¹² C ¹⁸ O ¹⁷ O ¹⁸ <u>O⁻</u>	-233.61	179.49	223.10	381.06	583.48	625.26	1227.30	2191.17	3586.79
H ¹² C ¹⁸ O ¹⁸ O ¹⁷ <u>O⁻</u>	-231.27	178.04	223.28	378.06	585.04	627.36	1244.66	2199.24	3581.27

Table 4-A4 (Continued)

Isotopologue^{&}	w₁	w₂	w₃	w₄	w₅	w₆	w₇	w₈	w₉
H ¹² C ¹⁶ O ¹⁸ O ¹⁸ <u>O⁻</u>	-231.47	177.65	226.07	379.31	588.01	629.74	1263.72	2208.73	3581.27
H ¹² C ¹⁸ O ¹⁶ O ¹⁸ <u>O⁻</u>	-236.21	181.79	224.77	385.66	584.09	625.27	1227.31	2191.17	3593.01
H ¹² C ¹⁸ O ¹⁸ O ¹⁶ <u>O⁻</u>	-231.33	178.66	225.13	379.36	587.41	629.73	1263.58	2208.59	3581.27
H ¹² C ¹⁸ O ¹⁷ O ¹⁷ <u>O⁻</u>	-233.66	180.12	224.75	382.22	585.57	627.36	1244.67	2199.25	3586.79
H ¹² C ¹⁷ O ¹⁸ O ¹⁷ <u>O⁻</u>	-231.39	178.14	225.51	379.15	587.40	629.46	1262.24	2207.15	3581.27
H ¹² C ¹⁷ O ¹⁷ O ¹⁸ <u>O⁻</u>	-233.72	179.61	225.23	382.18	585.85	627.37	1244.75	2199.31	3586.79
H ¹² C ¹⁶ O ¹⁷ O ¹⁷ <u>O⁻</u>	-233.88	180.33	229.32	384.47	590.62	631.84	1281.39	2216.30	3586.79
H ¹² C ¹⁷ O ¹⁶ O ¹⁷ <u>O⁻</u>	-236.34	182.56	228.56	387.86	588.53	629.48	1262.27	2207.15	3593.01
H ¹² C ¹⁷ O ¹⁷ O ¹⁶ <u>O⁻</u>	-233.82	180.85	228.84	384.53	590.29	631.83	1281.32	2216.23	3586.79
H ¹² C ¹⁶ O ¹⁷ O ¹⁸ <u>O⁻</u>	-233.84	179.73	227.52	383.42	588.54	629.75	1263.74	2208.74	3586.79
H ¹² C ¹⁶ O ¹⁸ O ¹⁷ <u>O⁻</u>	-231.52	178.23	227.90	380.36	590.09	631.83	1281.38	2216.30	3581.27
H ¹² C ¹⁷ O ¹⁶ O ¹⁸ <u>O⁻</u>	-236.30	181.92	226.87	386.75	586.46	627.38	1244.77	2199.32	3593.01
H ¹² C ¹⁷ O ¹⁸ O ¹⁶ <u>O⁻</u>	-231.45	178.74	227.43	380.39	589.77	631.83	1281.31	2216.22	3581.27
H ¹² C ¹⁸ O ¹⁶ O ¹⁷ <u>O⁻</u>	-236.25	182.44	226.39	386.81	586.17	627.37	1244.69	2199.25	3593.01
H ¹² C ¹⁸ O ¹⁷ O ¹⁶ <u>O⁻</u>	-233.71	180.76	226.57	383.51	587.93	629.73	1263.59	2208.59	3586.79
H ¹² C ¹⁷ O ¹⁷ O ¹⁷ <u>O⁻</u>	-233.77	180.23	226.95	383.29	587.93	629.47	1262.25	2207.15	3586.79
H ¹² C ¹⁸ O ¹⁸ O ¹⁸ <u>O⁻</u>	-231.22	177.42	221.60	376.91	582.94	625.25	1227.28	2191.16	3581.27
H ¹³ C ¹⁷ O ¹⁶ O ¹⁶ <u>O⁻</u>	-233.07	183.23	229.96	388.61	581.38	613.52	1280.63	2152.58	3593.01
H ¹³ C ¹⁶ O ¹⁷ O ¹⁶ <u>O⁻</u>	-230.61	180.97	230.81	385.23	583.47	615.94	1299.97	2161.68	3586.78
H ¹³ C ¹⁶ O ¹⁶ O ¹⁷ <u>O⁻</u>	-233.13	182.71	230.43	388.54	581.73	613.53	1280.70	2152.66	3593.01
H ¹³ C ¹⁷ O ¹⁸ O ¹⁸ <u>O⁻</u>	-228.06	177.57	223.31	377.52	575.81	608.90	1243.99	2135.15	3581.27
H ¹³ C ¹⁸ O ¹⁷ O ¹⁸ <u>O⁻</u>	-230.35	179.51	222.68	380.47	573.99	606.74	1226.56	2126.75	3586.78
H ¹³ C ¹⁸ O ¹⁸ O ¹⁷ <u>O⁻</u>	-228.00	178.07	222.86	377.53	575.53	608.90	1243.93	2135.08	3581.27
H ¹³ C ¹⁶ O ¹⁸ O ¹⁸ <u>O⁻</u>	-228.17	177.68	225.60	378.83	578.51	611.35	1262.93	2144.90	3581.27
H ¹³ C ¹⁸ O ¹⁶ O ¹⁸ <u>O⁻</u>	-232.94	181.81	224.36	385.04	574.61	606.75	1226.58	2126.75	3593.01
H ¹³ C ¹⁸ O ¹⁸ O ¹⁶ <u>O⁻</u>	-228.04	178.69	224.70	378.87	577.89	611.33	1262.81	2144.74	3581.27
H ¹³ C ¹⁸ O ¹⁷ O ¹⁷ <u>O⁻</u>	-230.38	180.15	224.33	381.67	576.07	608.91	1243.94	2135.08	3586.78
H ¹³ C ¹⁷ O ¹⁸ O ¹⁷ <u>O⁻</u>	-228.10	178.17	225.06	378.66	577.89	611.06	1261.54	2143.22	3581.27
H ¹³ C ¹⁷ O ¹⁷ O ¹⁸ <u>O⁻</u>	-230.44	179.64	224.79	381.64	576.36	608.92	1244.01	2135.16	3586.78
H ¹³ C ¹⁶ O ¹⁷ O ¹⁷ <u>O⁻</u>	-230.57	180.37	228.85	384.01	581.12	613.52	1280.68	2152.66	3586.78
H ¹³ C ¹⁷ O ¹⁶ O ¹⁷ <u>O⁻</u>	-233.04	182.59	228.12	387.33	579.04	611.09	1261.57	2143.22	3593.01
H ¹³ C ¹⁷ O ¹⁷ O ¹⁶ <u>O⁻</u>	-230.51	180.88	228.39	384.06	580.78	613.51	1280.62	2152.58	3586.78
H ¹³ C ¹⁶ O ¹⁷ O ¹⁸ <u>O⁻</u>	-230.54	179.77	227.05	382.92	579.06	611.36	1262.95	2144.90	3586.78
H ¹³ C ¹⁶ O ¹⁸ O ¹⁷ <u>O⁻</u>	-228.21	178.27	227.42	379.92	580.59	613.50	1280.67	2152.66	3581.27
H ¹³ C ¹⁷ O ¹⁶ O ¹⁸ <u>O⁻</u>	-233.02	181.96	226.43	386.19	576.98	608.93	1244.03	2135.16	3593.01
H ¹³ C ¹⁷ O ¹⁸ O ¹⁶ <u>O⁻</u>	-228.14	178.77	226.97	379.94	580.25	613.50	1280.60	2152.57	3581.27
H ¹³ C ¹⁸ O ¹⁶ O ¹⁷ <u>O⁻</u>	-232.97	182.47	225.97	386.24	576.68	608.92	1243.96	2135.09	3593.01
H ¹³ C ¹⁸ O ¹⁷ O ¹⁶ <u>O⁻</u>	-230.42	180.79	226.14	383.00	578.42	611.35	1262.82	2144.74	3586.78
H ¹³ C ¹⁷ O ¹⁷ O ¹⁷ <u>O⁻</u>	-230.47	180.26	226.51	382.78	578.43	611.08	1261.55	2143.22	3586.78
H ¹³ C ¹⁸ O ¹⁸ O ¹⁸ <u>O⁻</u>	-227.96	177.45	221.18	376.34	573.45	606.73	1226.55	2126.75	3581.27

[&] Oxygen atoms here are expressed in the order of atoms 1, 2, 3 as denoted in Fig. 4-2(d). The underlined oxygen atoms (atom 3) are the ones to be abstracted during HCO₃⁻ dehydration reaction.

Table 4-A5 Model predicted kinetic isotope fractionations (unit: ‰) for all isotopologues during HCO_3^- dehydration reaction in aqueous solution at 25°C. For isotopologues comprising more than one isotopomers, ‘Average’ denotes the average isotopic fractionation of its all comprising isotopomers.

Temperature (°C)	0	5	15	25	35	45	55	65	75	85	95	100
$\text{H}_2^{12}\text{C}^{16}\text{O}^{16}\text{O}^{16}\text{O}$												
$\text{H}_2^{13}\text{C}^{16}\text{O}^{16}\text{O}^{16}\text{O}$	-32.5	-31.9	-30.8	-29.7	-28.7	-27.7	-26.8	-26.0	-25.2	-24.5	-23.8	-23.5
$\text{H}_2^{12}\text{C}^{18}\text{O}^{16}\text{O}^{16}\text{O}$	-5.3	-5.2	-4.9	-4.7	-4.5	-4.3	-4.1	-4.0	-3.8	-3.6	-3.5	-3.4
$\text{H}_2^{12}\text{C}^{16}\text{O}^{18}\text{O}^{16}\text{O}$	-10.3	-10.1	-9.7	-9.3	-8.9	-8.5	-8.2	-7.9	-7.6	-7.4	-7.1	-7.0
$\text{H}_2^{12}\text{C}^{16}\text{O}^{16}\text{O}^{18}\text{O}$	-13.8	-13.7	-13.4	-13.1	-12.9	-12.6	-12.4	-12.1	-11.9	-11.7	-11.5	-11.4
Average	-9.8	-9.7	-9.3	-9.0	-8.7	-8.5	-8.2	-8.0	-7.8	-7.6	-7.4	-7.3
$\text{H}_2^{13}\text{C}^{18}\text{O}^{16}\text{O}^{16}\text{O}$	-37.9	-37.2	-35.8	-34.4	-33.2	-32.1	-31.0	-30.0	-29.1	-28.2	-27.4	-27.0
$\text{H}_2^{13}\text{C}^{16}\text{O}^{18}\text{O}^{16}\text{O}$	-42.6	-41.8	-40.2	-38.7	-37.3	-36.0	-34.8	-33.7	-32.7	-31.7	-30.8	-30.3
$\text{H}_2^{13}\text{C}^{16}\text{O}^{16}\text{O}^{18}\text{O}$	-46.8	-46.0	-44.5	-43.1	-41.8	-40.6	-39.5	-38.4	-37.4	-36.5	-35.6	-35.2
Average	-42.4	-41.6	-40.1	-38.8	-37.5	-36.2	-35.1	-34.0	-33.1	-32.1	-31.2	-30.8
$\text{H}_2^{12}\text{C}^{17}\text{O}^{16}\text{O}^{16}\text{O}$	-2.8	-2.7	-2.6	-2.5	-2.4	-2.3	-2.2	-2.1	-2.0	-1.9	-1.8	-1.8
$\text{H}_2^{12}\text{C}^{16}\text{O}^{17}\text{O}^{16}\text{O}$	-5.5	-5.4	-5.2	-4.9	-4.7	-4.5	-4.4	-4.2	-4.1	-3.9	-3.8	-3.7
$\text{H}_2^{12}\text{C}^{16}\text{O}^{16}\text{O}^{17}\text{O}$	-7.3	-7.2	-7.0	-6.9	-6.7	-6.6	-6.5	-6.4	-6.2	-6.1	-6.0	-6.0
Average	-5.2	-5.1	-4.9	-4.8	-4.6	-4.5	-4.3	-4.2	-4.1	-4.0	-3.9	-3.8
$\text{H}_2^{12}\text{C}^{17}\text{O}^{18}\text{O}^{18}\text{O}$	-27.0	-26.5	-25.7	-24.9	-24.1	-23.4	-22.8	-22.1	-21.5	-21.0	-20.5	-20.2
$\text{H}_2^{12}\text{C}^{18}\text{O}^{17}\text{O}^{18}\text{O}$	-24.7	-24.3	-23.5	-22.8	-22.1	-21.5	-20.9	-20.3	-19.8	-19.3	-18.8	-18.6
$\text{H}_2^{12}\text{C}^{18}\text{O}^{18}\text{O}^{17}\text{O}$	-22.9	-22.4	-21.6	-20.8	-20.1	-19.4	-18.8	-18.2	-17.6	-17.1	-16.6	-16.4
Average	-24.8	-24.4	-23.6	-22.8	-22.1	-21.4	-20.8	-20.2	-19.7	-19.1	-18.6	-18.4
$\text{H}_2^{12}\text{C}^{16}\text{O}^{18}\text{O}^{18}\text{O}$	-24.2	-23.8	-23.1	-22.4	-21.8	-21.2	-20.6	-20.1	-19.6	-19.1	-18.6	-18.4
$\text{H}_2^{12}\text{C}^{18}\text{O}^{16}\text{O}^{18}\text{O}$	-19.2	-18.9	-18.4	-17.9	-17.4	-16.9	-16.5	-16.1	-15.7	-15.4	-15.0	-14.9
$\text{H}_2^{12}\text{C}^{18}\text{O}^{18}\text{O}^{16}\text{O}$	-15.6	-15.2	-14.5	-13.9	-13.3	-12.8	-12.3	-11.8	-11.4	-11.0	-10.6	-10.4
Average	-19.7	-19.3	-18.7	-18.1	-17.5	-17.0	-16.5	-16.0	-15.6	-15.1	-14.7	-14.6
$\text{H}_2^{12}\text{C}^{18}\text{O}^{17}\text{O}^{17}\text{O}$	-18.1	-17.7	-17.1	-16.5	-16.0	-15.5	-15.0	-14.5	-14.1	-13.7	-13.3	-13.1
$\text{H}_2^{12}\text{C}^{17}\text{O}^{18}\text{O}^{17}\text{O}$	-20.4	-20.0	-19.3	-18.6	-18.0	-17.4	-16.9	-16.3	-15.9	-15.4	-15.0	-14.8
$\text{H}_2^{12}\text{C}^{17}\text{O}^{17}\text{O}^{18}\text{O}$	-22.2	-21.8	-21.2	-20.6	-20.0	-19.4	-18.9	-18.4	-18.0	-17.6	-17.2	-17.0
Average	-20.2	-19.9	-19.2	-18.6	-18.0	-17.4	-16.9	-16.4	-16.0	-15.6	-15.2	-15.0
$\text{H}_2^{12}\text{C}^{16}\text{O}^{17}\text{O}^{17}\text{O}$	-12.8	-12.6	-12.2	-11.8	-11.5	-11.2	-10.9	-10.6	-10.3	-10.1	-9.8	-9.7
$\text{H}_2^{12}\text{C}^{17}\text{O}^{16}\text{O}^{17}\text{O}$	-10.1	-9.9	-9.6	-9.4	-9.1	-8.9	-8.7	-8.5	-8.3	-8.1	-7.9	-7.8
$\text{H}_2^{12}\text{C}^{17}\text{O}^{17}\text{O}^{16}\text{O}$	-8.3	-8.1	-7.7	-7.4	-7.1	-6.8	-6.5	-6.3	-6.1	-5.8	-5.6	-5.5
Average	-10.4	-10.2	-9.9	-9.5	-9.2	-9.0	-8.7	-8.4	-8.2	-8.0	-7.8	-7.7
$\text{H}_2^{12}\text{C}^{16}\text{O}^{17}\text{O}^{18}\text{O}$	-19.4	-19.1	-18.6	-18.1	-17.6	-17.2	-16.7	-16.4	-16.0	-15.6	-15.3	-15.1
$\text{H}_2^{12}\text{C}^{16}\text{O}^{18}\text{O}^{17}\text{O}$	-17.6	-17.3	-16.7	-16.1	-15.6	-15.1	-14.7	-14.3	-13.9	-13.5	-13.2	-13.0
$\text{H}_2^{12}\text{C}^{17}\text{O}^{16}\text{O}^{18}\text{O}$	-16.7	-16.4	-16.0	-15.6	-15.2	-14.9	-14.6	-14.2	-13.9	-13.6	-13.4	-13.2
$\text{H}_2^{12}\text{C}^{17}\text{O}^{18}\text{O}^{16}\text{O}$	-13.1	-12.8	-12.2	-11.7	-11.2	-10.8	-10.4	-10.0	-9.6	-9.3	-9.0	-8.8
$\text{H}_2^{12}\text{C}^{18}\text{O}^{16}\text{O}^{17}\text{O}$	-12.6	-12.4	-12.0	-11.6	-11.3	-10.9	-10.6	-10.3	-10.1	-9.8	-9.5	-9.4
$\text{H}_2^{12}\text{C}^{18}\text{O}^{17}\text{O}^{16}\text{O}$	-10.8	-10.5	-10.0	-9.6	-9.2	-8.8	-8.5	-8.1	-7.8	-7.6	-7.3	-7.2
Average	-15.0	-14.8	-14.3	-13.8	-13.4	-13.0	-12.6	-12.2	-11.9	-11.6	-11.3	-11.1
$\text{H}_2^{12}\text{C}^{17}\text{O}^{17}\text{O}^{17}\text{O}$	-15.6	-15.3	-14.8	-14.3	-13.8	-13.4	-13.0	-12.7	-12.3	-12.0	-11.7	-11.5
$\text{H}_2^{12}\text{C}^{18}\text{O}^{18}\text{O}^{18}\text{O}$	-29.5	-29.0	-28.0	-27.1	-26.2	-25.4	-24.7	-24.0	-23.3	-22.7	-22.1	-21.8

Table 4-A5 (Continued)

Temperature (°C)	0	5	15	25	35	45	55	65	75	85	95	100
$\text{H}_2^{13}\text{C}^{17}\text{O}^{16}\text{O}^{16}$	-35.4	-34.7	-33.4	-32.2	-31.1	-30.0	-29.0	-28.1	-27.3	-26.4	-25.7	-25.3
$\text{H}_2^{13}\text{C}^{16}\text{O}^{17}\text{O}^{16}$	-37.9	-37.2	-35.8	-34.5	-33.3	-32.1	-31.1	-30.1	-29.2	-28.3	-27.5	-27.1
$\text{H}_2^{13}\text{C}^{16}\text{O}^{16}\text{O}^{17}$	-40.0	-39.3	-38.0	-36.7	-35.6	-34.5	-33.5	-32.5	-31.6	-30.8	-30.0	-29.6
Average	-37.8	-37.1	-35.7	-34.5	-33.3	-32.2	-31.2	-30.2	-29.4	-28.5	-27.7	-27.4
$\text{H}_2^{13}\text{C}^{17}\text{O}^{18}\text{O}^{18}$	-59.7	-58.6	-56.6	-54.7	-52.9	-51.3	-49.7	-48.3	-46.9	-45.6	-44.4	-43.8
$\text{H}_2^{13}\text{C}^{18}\text{O}^{17}\text{O}^{18}$	-57.5	-56.5	-54.6	-52.7	-51.0	-49.4	-47.9	-46.5	-45.2	-44.0	-42.8	-42.3
$\text{H}_2^{13}\text{C}^{18}\text{O}^{18}\text{O}^{17}$	-55.4	-54.3	-52.3	-50.5	-48.8	-47.1	-45.6	-44.2	-42.9	-41.6	-40.5	-39.9
Average	-57.5	-56.5	-54.5	-52.6	-50.9	-49.3	-47.8	-46.3	-45.0	-43.7	-42.6	-42.0
$\text{H}_2^{13}\text{C}^{16}\text{O}^{18}\text{O}^{18}$	-56.8	-55.8	-53.9	-52.2	-50.5	-49.0	-47.5	-46.1	-44.9	-43.7	-42.5	-42.0
$\text{H}_2^{13}\text{C}^{18}\text{O}^{16}\text{O}^{18}$	-52.2	-51.3	-49.6	-47.9	-46.4	-45.0	-43.7	-42.5	-41.3	-40.2	-39.1	-38.7
$\text{H}_2^{13}\text{C}^{18}\text{O}^{18}\text{O}^{16}$	-47.9	-46.9	-45.1	-43.4	-41.8	-40.3	-39.0	-37.7	-36.5	-35.3	-34.3	-33.8
Average	-52.3	-51.4	-49.5	-47.8	-46.3	-44.8	-43.4	-42.1	-40.9	-39.7	-38.7	-38.1
$\text{H}_2^{13}\text{C}^{18}\text{O}^{17}\text{O}^{17}$	-50.7	-49.8	-48.0	-46.3	-44.7	-43.3	-41.9	-40.6	-39.4	-38.3	-37.2	-36.7
$\text{H}_2^{13}\text{C}^{17}\text{O}^{18}\text{O}^{17}$	-52.9	-51.9	-50.0	-48.2	-46.6	-45.1	-43.7	-42.3	-41.1	-39.9	-38.8	-38.3
$\text{H}_2^{13}\text{C}^{17}\text{O}^{17}\text{O}^{18}$	-55.0	-54.0	-52.2	-50.5	-48.9	-47.4	-46.0	-44.7	-43.4	-42.3	-41.2	-40.6
Average	-52.9	-51.9	-50.1	-48.3	-46.7	-45.2	-43.8	-42.5	-41.3	-40.2	-39.1	-38.5
$\text{H}_2^{13}\text{C}^{16}\text{O}^{17}\text{O}^{17}$	-45.4	-44.6	-43.0	-41.5	-40.2	-38.9	-37.7	-36.6	-35.6	-34.6	-33.7	-33.3
$\text{H}_2^{13}\text{C}^{17}\text{O}^{16}\text{O}^{17}$	-47.8	-46.9	-45.2	-43.6	-42.2	-40.8	-39.5	-38.2	-37.1	-36.0	-35.0	-34.5
$\text{H}_2^{13}\text{C}^{17}\text{O}^{17}\text{O}^{16}$	-35.7	-35.1	-33.8	-32.6	-31.5	-30.5	-29.5	-28.6	-27.8	-27.0	-26.2	-25.9
Average	-43.0	-42.2	-40.7	-39.3	-37.9	-36.7	-35.6	-34.5	-33.5	-32.5	-31.6	-31.2
$\text{H}_2^{13}\text{C}^{16}\text{O}^{17}\text{O}^{18}$	-52.1	-51.2	-49.5	-48.0	-46.5	-45.1	-43.8	-42.5	-41.4	-40.3	-39.3	-38.8
$\text{H}_2^{13}\text{C}^{16}\text{O}^{18}\text{O}^{17}$	-50.1	-49.1	-47.4	-45.8	-44.2	-42.8	-41.5	-40.2	-39.1	-38.0	-36.9	-36.4
$\text{H}_2^{13}\text{C}^{17}\text{O}^{16}\text{O}^{18}$	-49.6	-48.8	-47.2	-45.7	-44.3	-43.0	-41.7	-40.6	-39.5	-38.4	-37.5	-37.0
$\text{H}_2^{13}\text{C}^{17}\text{O}^{18}\text{O}^{16}$	-45.4	-44.5	-42.8	-41.2	-39.7	-38.3	-37.0	-35.8	-34.7	-33.6	-32.6	-32.1
$\text{H}_2^{13}\text{C}^{18}\text{O}^{16}\text{O}^{17}$	-45.4	-44.6	-43.0	-41.5	-40.1	-38.9	-37.7	-36.5	-35.5	-34.5	-33.5	-33.1
$\text{H}_2^{13}\text{C}^{18}\text{O}^{17}\text{O}^{16}$	-43.2	-42.4	-40.7	-39.2	-37.8	-36.5	-35.2	-34.1	-33.0	-32.0	-31.1	-30.6
Average	-44.7	-43.8	-42.2	-40.6	-39.2	-37.9	-36.6	-35.5	-34.4	-33.4	-32.4	-31.9
$\text{H}_2^{13}\text{C}^{17}\text{O}^{17}\text{O}^{17}$	-48.2	-47.3	-45.6	-44.1	-42.6	-41.2	-39.9	-38.7	-37.6	-36.6	-35.6	-35.1
$\text{H}_2^{13}\text{C}^{18}\text{O}^{18}\text{O}^{18}$	-62.2	-61.1	-58.9	-56.9	-55.0	-53.3	-51.7	-50.1	-48.7	-47.3	-46.1	-45.5

Table 4-A6 Model predicted kinetic isotope fractionations (unit: ‰) for all isotopologues during HCO_3^- dehydroxylation reaction in aqueous solution at 25°C. For isotopologues comprising more than one isotopomers, ‘Average’ denotes the average isotopic fractionation of its all comprising isotopomers.

Temperature (°C)	0	5	15	25	35	45	55	65	75	85	95	100
$\text{H}^{12}\text{C}^{16}\text{O}^{16}\text{O}^{16}\text{O}^-$												
$\text{H}^{13}\text{C}^{16}\text{O}^{16}\text{O}^{16}\text{O}^-$	-25.3	-24.7	-23.5	-22.5	-21.5	-20.5	-19.7	-18.9	-18.2	-17.5	-16.9	-16.6
$\text{H}^{12}\text{C}^{18}\text{O}^{16}\text{O}^{16}\text{O}^-$	13.5	13.3	13.0	12.7	12.4	12.1	11.8	11.5	11.2	10.9	10.6	10.5
$\text{H}^{12}\text{C}^{16}\text{O}^{18}\text{O}^{16}\text{O}^-$	-83.2	-81.5	-78.2	-75.2	-72.3	-69.7	-67.3	-65.1	-63.0	-61.0	-59.2	-58.3
$\text{H}^{12}\text{C}^{16}\text{O}^{16}\text{O}^{18}\text{O}^-$	13.2	13.1	12.8	12.5	12.2	11.9	11.6	11.4	11.1	10.8	10.6	10.5
Average	-18.8	-18.4	-17.5	-16.7	-15.9	-15.3	-14.6	-14.1	-13.6	-13.1	-12.7	-12.4
$\text{H}^{13}\text{C}^{18}\text{O}^{16}\text{O}^{16}\text{O}^-$	-11.4	-10.9	-10.1	-9.4	-8.7	-8.1	-7.6	-7.1	-6.6	-6.3	-5.9	-5.8
$\text{H}^{13}\text{C}^{16}\text{O}^{18}\text{O}^{16}\text{O}^-$	-109.1	-106.7	-102.2	-98.1	-94.2	-90.7	-87.4	-84.4	-81.6	-78.9	-76.5	-75.3
$\text{H}^{13}\text{C}^{16}\text{O}^{16}\text{O}^{18}\text{O}^-$	-11.7	-11.3	-10.4	-9.6	-8.9	-8.3	-7.7	-7.2	-6.8	-6.4	-6.0	-5.9
Average	-44.1	-43.0	-40.9	-39.0	-37.3	-35.7	-34.2	-32.9	-31.7	-30.5	-29.5	-29.0
$\text{H}^{12}\text{C}^{17}\text{O}^{16}\text{O}^{16}\text{O}^-$	7.1	7.0	6.8	6.7	6.5	6.3	6.2	6.0	5.9	5.7	5.6	5.5
$\text{H}^{12}\text{C}^{16}\text{O}^{17}\text{O}^{16}\text{O}^-$	-43.8	-42.9	-41.1	-39.5	-38.0	-36.7	-35.4	-34.2	-33.1	-32.1	-31.1	-30.6
$\text{H}^{12}\text{C}^{16}\text{O}^{16}\text{O}^{17}\text{O}^-$	6.9	6.9	6.7	6.5	6.4	6.3	6.1	6.0	5.8	5.7	5.6	5.5
Average	-9.9	-9.7	-9.2	-8.8	-8.4	-8.0	-7.7	-7.4	-7.1	-6.9	-6.6	-6.5
$\text{H}^{12}\text{C}^{17}\text{O}^{18}\text{O}^{18}\text{O}^-$	-63.2	-61.7	-58.9	-56.3	-53.9	-51.8	-49.8	-47.9	-46.3	-44.7	-43.3	-42.6
$\text{H}^{12}\text{C}^{18}\text{O}^{17}\text{O}^{18}\text{O}^-$	-17.1	-16.5	-15.4	-14.5	-13.6	-12.8	-12.1	-11.5	-10.9	-10.4	-10.0	-9.8
$\text{H}^{12}\text{C}^{18}\text{O}^{18}\text{O}^{17}\text{O}^-$	-63.1	-61.6	-58.8	-56.2	-53.9	-51.7	-49.7	-47.9	-46.3	-44.7	-43.3	-42.6
Average	-47.8	-46.6	-44.4	-42.3	-40.5	-38.8	-37.2	-35.8	-34.5	-33.3	-32.2	-31.7
$\text{H}^{12}\text{C}^{16}\text{O}^{18}\text{O}^{18}\text{O}^-$	-70.3	-68.7	-65.7	-62.9	-60.4	-58.0	-55.9	-53.9	-52.1	-50.3	-48.8	-48.0
$\text{H}^{12}\text{C}^{18}\text{O}^{16}\text{O}^{18}\text{O}^-$	26.9	26.6	26.0	25.3	24.7	24.1	23.5	22.9	22.4	21.8	21.3	21.1
$\text{H}^{12}\text{C}^{18}\text{O}^{18}\text{O}^{16}\text{O}^-$	-70.0	-68.5	-65.5	-62.8	-60.3	-58.0	-55.8	-53.9	-52.0	-50.4	-48.8	-48.1
Average	-37.8	-36.8	-35.1	-33.4	-32.0	-30.6	-29.4	-28.3	-27.2	-26.3	-25.4	-25.0
$\text{H}^{12}\text{C}^{18}\text{O}^{17}\text{O}^{17}\text{O}^-$	-23.4	-22.8	-21.5	-20.4	-19.4	-18.5	-17.6	-16.9	-16.2	-15.6	-15.0	-14.7
$\text{H}^{12}\text{C}^{17}\text{O}^{18}\text{O}^{17}\text{O}^-$	-69.4	-67.9	-64.9	-62.2	-59.7	-57.4	-55.2	-53.3	-51.5	-49.8	-48.2	-47.5
$\text{H}^{12}\text{C}^{17}\text{O}^{17}\text{O}^{18}\text{O}^-$	-23.6	-22.9	-21.6	-20.5	-19.5	-18.5	-17.7	-16.9	-16.2	-15.6	-15.0	-14.7
Average	-38.8	-37.8	-36.0	-34.3	-32.8	-31.4	-30.2	-29.0	-28.0	-27.0	-26.1	-25.7
$\text{H}^{12}\text{C}^{16}\text{O}^{17}\text{O}^{17}\text{O}^-$	-36.9	-36.1	-34.5	-33.0	-31.7	-30.5	-29.3	-28.3	-27.3	-26.4	-25.6	-25.2
$\text{H}^{12}\text{C}^{17}\text{O}^{16}\text{O}^{17}\text{O}^-$	14.1	13.9	13.6	13.3	12.9	12.6	12.3	12.0	11.7	11.5	11.2	11.1
$\text{H}^{12}\text{C}^{17}\text{O}^{17}\text{O}^{16}\text{O}^-$	-36.8	-35.9	-34.4	-32.9	-31.6	-30.4	-29.3	-28.2	-27.3	-26.4	-25.6	-25.2
Average	-19.9	-19.4	-18.4	-17.6	-16.8	-16.1	-15.4	-14.8	-14.3	-13.8	-13.3	-13.1
$\text{H}^{12}\text{C}^{16}\text{O}^{17}\text{O}^{18}\text{O}^-$	-30.7	-29.9	-28.5	-27.2	-26.0	-24.9	-23.8	-22.9	-22.1	-21.3	-20.6	-20.2
$\text{H}^{12}\text{C}^{16}\text{O}^{18}\text{O}^{17}\text{O}^-$	-76.4	-74.8	-71.6	-68.7	-66.1	-63.6	-61.3	-59.2	-57.2	-55.4	-53.7	-52.9
$\text{H}^{12}\text{C}^{17}\text{O}^{16}\text{O}^{18}\text{O}^-$	20.4	20.2	19.7	19.2	18.8	18.3	17.9	17.5	17.0	16.6	16.2	16.0
$\text{H}^{12}\text{C}^{17}\text{O}^{18}\text{O}^{16}\text{O}^-$	-76.3	-74.6	-71.5	-68.6	-66.0	-63.5	-61.3	-59.2	-57.2	-55.4	-53.7	-52.9
$\text{H}^{12}\text{C}^{18}\text{O}^{16}\text{O}^{17}\text{O}^-$	20.6	20.3	19.8	19.3	18.8	18.4	17.9	17.5	17.1	16.7	16.3	16.1
$\text{H}^{12}\text{C}^{18}\text{O}^{17}\text{O}^{16}\text{O}^-$	-30.4	-29.7	-28.3	-27.0	-25.8	-24.7	-23.8	-22.9	-22.0	-21.3	-20.6	-20.2
Average	-28.8	-28.1	-26.7	-25.5	-24.4	-23.3	-22.4	-21.5	-20.7	-20.0	-19.4	-19.0
$\text{H}^{12}\text{C}^{17}\text{O}^{17}\text{O}^{17}\text{O}^-$	-29.8	-29.1	-27.7	-26.4	-25.2	-24.2	-23.2	-22.3	-21.5	-20.7	-20.0	-19.7
$\text{H}^{12}\text{C}^{18}\text{O}^{18}\text{O}^{18}\text{O}^-$	-56.9	-55.4	-52.8	-50.3	-48.1	-46.1	-44.3	-42.6	-41.0	-39.6	-38.3	-37.7

Table 4-A6 (Continued)

Temperature (°C)	0	5	15	25	35	45	55	65	75	85	95	100
H ¹³ C ¹⁷ O ¹⁶ O ¹⁶ O ⁻	-18.0	-17.5	-16.5	-15.6	-14.8	-14.0	-13.3	-12.7	-12.1	-11.6	-11.1	-10.9
H ¹³ C ¹⁶ O ¹⁷ O ¹⁶ O ⁻	-69.4	-67.8	-64.9	-62.2	-59.7	-57.4	-55.3	-53.3	-51.5	-49.8	-48.2	-47.4
H ¹³ C ¹⁶ O ¹⁶ O ¹⁷ O ⁻	-18.2	-17.6	-16.6	-15.7	-14.9	-14.1	-13.4	-12.8	-12.2	-11.7	-11.2	-11.0
Average	-35.2	-34.3	-32.7	-31.2	-29.8	-28.5	-27.3	-26.3	-25.3	-24.3	-23.5	-23.1
H ¹³ C ¹⁷ O ¹⁸ O ¹⁸ O ⁻	-88.4	-86.3	-82.3	-78.6	-75.3	-72.2	-69.3	-66.7	-64.3	-62.1	-60.1	-59.1
H ¹³ C ¹⁸ O ¹⁷ O ¹⁸ O ⁻	-41.9	-40.7	-38.4	-36.4	-34.5	-32.8	-31.3	-29.9	-28.6	-27.5	-26.4	-26.0
H ¹³ C ¹⁸ O ¹⁸ O ¹⁷ O ⁻	-88.3	-86.2	-82.2	-78.5	-75.2	-72.1	-69.3	-66.7	-64.3	-62.1	-60.1	-59.1
Average	-72.9	-71.1	-67.6	-64.5	-61.7	-59.0	-56.6	-54.4	-52.4	-50.6	-48.8	-48.0
H ¹³ C ¹⁶ O ¹⁸ O ¹⁸ O ⁻	-95.7	-93.5	-89.3	-85.4	-81.9	-78.6	-75.6	-72.9	-70.3	-67.9	-65.7	-64.7
H ¹³ C ¹⁸ O ¹⁶ O ¹⁸ O ⁻	2.4	2.7	3.2	3.6	4.0	4.3	4.5	4.7	4.9	5.0	5.0	5.1
H ¹³ C ¹⁸ O ¹⁸ O ¹⁶ O ⁻	-95.4	-93.2	-89.1	-85.3	-81.8	-78.5	-75.5	-72.8	-70.3	-67.9	-65.7	-64.7
Average	-62.9	-61.3	-58.4	-55.7	-53.2	-51.0	-48.9	-47.0	-45.2	-43.6	-42.1	-41.5
H ¹³ C ¹⁸ O ¹⁷ O ¹⁷ O ⁻	-48.4	-47.1	-44.7	-42.5	-40.5	-38.7	-37.0	-35.5	-34.1	-32.8	-31.6	-31.1
H ¹³ C ¹⁷ O ¹⁸ O ¹⁷ O ⁻	-94.8	-92.6	-88.5	-84.7	-81.2	-77.9	-75.0	-72.2	-69.7	-67.3	-65.2	-64.1
H ¹³ C ¹⁷ O ¹⁷ O ¹⁸ O ⁻	-48.5	-47.2	-44.8	-42.6	-40.6	-38.7	-37.1	-35.5	-34.1	-32.8	-31.6	-31.1
Average	-63.9	-62.3	-59.3	-56.6	-54.1	-51.8	-49.7	-47.7	-45.9	-44.3	-42.8	-42.1
H ¹³ C ¹⁶ O ¹⁷ O ¹⁷ O ⁻	-62.3	-60.8	-58.1	-55.5	-53.2	-51.0	-49.1	-47.2	-45.5	-44.0	-42.5	-41.8
H ¹³ C ¹⁷ O ¹⁶ O ¹⁷ O ⁻	-10.8	-10.4	-9.6	-8.8	-8.1	-7.5	-7.0	-6.5	-6.1	-5.7	-5.4	-5.2
H ¹³ C ¹⁷ O ¹⁷ O ¹⁶ O ⁻	-62.1	-60.7	-57.9	-55.4	-53.1	-51.0	-49.0	-47.2	-45.5	-43.9	-42.5	-41.8
Average	-45.1	-44.0	-41.8	-39.9	-38.1	-36.5	-35.0	-33.6	-32.4	-31.2	-30.1	-29.6
H ¹³ C ¹⁶ O ¹⁷ O ¹⁸ O ⁻	-55.9	-54.5	-51.9	-49.5	-47.3	-45.3	-43.4	-41.7	-40.2	-38.7	-37.4	-36.8
H ¹³ C ¹⁶ O ¹⁸ O ¹⁷ O ⁻	-102.0	-99.7	-95.4	-91.4	-87.8	-84.4	-81.2	-78.3	-75.6	-73.2	-70.8	-69.7
H ¹³ C ¹⁷ O ¹⁶ O ¹⁸ O ⁻	-4.3	-3.9	-3.3	-2.7	-2.2	-1.7	-1.3	-1.0	-0.7	-0.4	-0.2	-0.1
H ¹³ C ¹⁷ O ¹⁸ O ¹⁶ O ⁻	-101.9	-99.6	-95.3	-91.3	-87.7	-84.3	-81.2	-78.3	-75.6	-73.1	-70.8	-69.7
H ¹³ C ¹⁸ O ¹⁶ O ¹⁷ O ⁻	-4.2	-3.8	-3.1	-2.6	-2.1	-1.6	-1.2	-0.9	-0.6	-0.4	-0.2	-0.1
H ¹³ C ¹⁸ O ¹⁷ O ¹⁶ O ⁻	-55.6	-54.2	-51.6	-49.3	-47.1	-45.1	-43.3	-41.6	-40.1	-38.6	-37.3	-36.7
Average	-54.0	-52.6	-50.1	-47.8	-45.7	-43.7	-41.9	-40.3	-38.8	-37.4	-36.1	-35.5
H ¹³ C ¹⁷ O ¹⁷ O ¹⁷ O ⁻	-55.0	-53.6	-51.0	-48.7	-46.5	-44.5	-42.7	-41.0	-39.5	-38.1	-36.8	-36.2
H ¹³ C ¹⁸ O ¹⁸ O ¹⁸ O ⁻	-81.9	-79.8	-76.0	-72.5	-69.3	-66.3	-63.7	-61.2	-58.9	-56.8	-54.9	-54.0